Structure-properties relationship in dense collagen gels produced by injection of spray-dried collagen

Miléna Lama

Sorbonne Université

Ecole Doctorale 397 : Physique et Chimie des Matériaux

Laboratoire de Chimie de la Matière Condensée de Paris

Laboratoire Science et Ingénierie de la Matière Molle

Structure-properties relationship in dense collagen gels produced by injection of spray-dried collagen

Par **Miléna Lama**

Thèse de doctorat de Chimie des Matériaux

Dirigée par Nadine Nassif et Alba Marcellan

Présentée et soutenue publiquement le 16 septembre 2019

Devant un jury composé de :

M. P. Guégan	Professeur, SU	Président du Jury
Mme A. Pellé	Professeure, Université Paris 13	Examinatrice
M. S. Banzet	Directeur de Recherche INSERM, CTSA	Examinateur
M. R. Weinkamer	Professeur, Max Planck Institute (Potsdam, Allemagne)	Rapporteur
M. F. Pignon	Directeur de Recherche CNRS, Université Grenoble-Alpes	Rapporteur
Mme N. Nassif	Chargée de Recherche CNRS, SU	Directrice de thèse
Mme A. Marcellan	Maître de Conférences, SU	Co-directrice de thèse
M. F.M. Fernandes	Maître de Conférences, SU	Co-encadrant, invité
M. C. Boissière	Directeur de Recherche CNRS, SU	Co-encadrant, invité
Mme M-M. Giraud-Guille	Directrice d'Etudes, EPHE	Invitée

Remerciements

Je ne serais jamais arrivée jusque là sans une suite de bonnes rencontres et de hasards heureux. Lors de mon stage de fin d'études chez EVESA (en dernière année d'école d'ingénieurs en génie urbain, EIVP), dont l'objectif était de créer un guide d'éclairage respecteux de l'environnement dans les parcs et jardins de Paris, je me suis rendue compte que le métier d'ingénieure vers lequel je me dirigeais allait m'apporter des frustrations sur le plan intellectuel. De plus, ayant adoré la chimie en classe préparatoire, l'idée d'y revenir m'avait trotté dans la tête. J'ai donc décidé de postuler à deux master 2 de chimie, l'un à l'université Paris 6 et l'autre à l'université Paris 7. Paris 7 m'a refusée, et quelle ne fut pas ma surprise de voir que Paris 6 m'avait acceptée ! Corinne Chanéac et Dominique Hourdet étant les responsables du master de chimie, je leur suis reconnaissante ainsi qu'à l'université pour m'avoir donné ma chance alors que je n'avais pas fait de chimie depuis la prépa (donc depuis un équivalent de la 2e année de licence)...

Ayant choisi un enseignement de mécanique des matériaux, j'ai eu la chance de suivre des TD avec Alba (que j'étais l'une des rares à pouvoir préparer, ayant plutôt étudié la mécanique des matériaux de par ma formation que la chimie !). Alba m'a ensuite proposé un sujet de stage de M2, que j'ai accepté. Ce stage de six mois au sein du laboratoire SIMM s'est très bien passé, Alba m'a donc parlé du financement de thèse MATISSE qu'elle venait d'obtenir avec d'autres chercheurs du LCMCP (Nadine, Francisco et Cédric). Le sujet de thèse était similaire à mon sujet de stage M2 dans le sens où il fallait étudier le lien entre la microstructure et les propriétés macroscopiques (mécaniques) du matériau, ce qui m'a plu. J'ai ensuite été acceptée pour commencer cette thèse entre les deux laboratoires, encadrée par une équipe de chocs : Alba, Nadine, Francisco et Cédric.

Alba, tu es la première personne qui m'a guidée dans le monde de la recherche, qui a donné sa chance à une étudiante qui n'avait pas fait de chimie depuis presque 4 ans. Tu as toujours été présente, même dans les moments difficiles, tu m'as soutenue et tu as cru en moi. Je te suis extrêmement reconnaissante pour tout ce que tu m'as appris, scientifiquement et humainement, lors de cette aventure de presque quatre ans qui a fait prendre un autre tournant à ma vie. Je me considère comme très chanceuse de t'avoir rencontrée et d'avoir pu travailler avec toi. Même si je ne suis pas du matin, je me souviendrai des petits déjeuners du lundi matin avec la "team Alba", des restaurants d'équipe à la fin du mois de juin pour célébrer la fin des stages de M2. Ma fin de thèse a été difficile et compliquée, tant sur le plan professionnel que personnel, et j'aimerais aussi te dire un grand merci pour avoir été une oreille attentive et pour m'avoir remonté le moral à chaque fois que je craquais dans ton bureau (et j'en suis désolée, je pense que ça n'a pas dû être facile pour toi !).

Nadine, je ne te cacherai pas que mes débuts de thèse ont été difficiles (mais tu le sais), j'avais l'impression de devoir faire mes preuves en permanence pour que tu m'accordes ta confiance. Petit à petit, nous avons appris à nous connaître et à travailler ensemble, j'ai développé le Nadine-translate (comme Google translate mais version Nadine) et nous avons pu commencer à nous comprendre au bout d'environ six mois. Cela a été un vrai bonheur de travailler à tes côtés, j'ai tellement appris ! Je pense que tu fais partie de ces rencontres qui changent la vie, et la vision que l'on a de la vie. Je n'ai pas assez de mots pour te remercier - merci pour ton soutien indéfectible, pour m'avoir fait confiance, pour ta reconnaissance, pour ces heures (indues) passées à plancher pour écrire un papier dans ton salon, pour le meilleur baba au rhum du monde, le thé, les crêpes au sirop d'érable du Canada, ta disponibilité hors normes le soir et le weekend, ta philosophie, tes conseils, ton savoir, ton enthousiasme. Vive la science, et vive la vie ! Plaisir, confiance et honnêteté (si je me souviens bien).

Francisco, j'aimerais te dire un grand merci pour tous ces moments partagés avec toi, et les échanges

que nous avons eus tant sur le plan humain que professionnel. Merci pour ta disponibilité, pour le chocolat qui remonte le moral en cas de coup dur, pour ton oreille attentive, tes conseils, nos échanges scientifiques. Merci aussi pour ces moments sympathiques autour des ptit dej biblio à discuter science. Je tiens également à souligner ton talent pour le bricolage de manips, j'ai beaucoup appris et je pense que l'on peut dire que nous sommes les rois du système D (mais cela fonctionne !).

Cédric, tu es celui que je suis allée le moins souvent voir au cours de ces trois années. Cependant, comme je te l'avais dit, je préfère un encadrement de qualité plutôt qu'en quantité ! Je tiens à te remercier pour les discussion que nous avons eues, pour ton enthousiasme et tes idées, pour ton soutien, pour ta façon de voir les choses qui je pense ont été indispensables dans l'équipe de ma thèse.

Cette aventure s'est finie - du moins pour moi - en apothéose grâce aux membres du jury qui ont chacun apporté un éclairage sur des aspects différents de ma thèse lors d'une discussion intense mais passionnante. Je tiens donc à remercier chaleureusement Philippe Guégan, Anne Pellé, Sébastien Banzet avec qui nous sommes maintenant en contact, Richard Weinkamer et Frédéric Pignon pour leur relecture attentive de mon manuscrit et leur retour non moins précis et enrichissant, ainsi que Marie-Madeleine Giraud-Guille que j'ai déjà eu l'occasion de rencontrer grâce à Nadine et qui possède un savoir si précieux.

Je souhaite également remercier les anciens directeurs des deux laboratoires, Christian Fretigny (SIMM) et Florence Babonneau (LCMCP) pour m'avoir acceptée au sein de leur unité, ainsi que les directeurs actuels Etienne Barthel (SIMM), Christian Bonhomme (LCMCP) et François Ribot (adjoint, LCMCP).

Je remercie très chaleureusement les gestionnaires du LCMCP, Corinne Pozzo di Borgo et Hélène Gervais, tant pour leur disponibilité et leur bonne humeur que pour leur travail indispensable au bon fonctionnement du laboratoire. Merci de nous permettre de travailler dans les meilleures conditions possibles, d'accepter parfois de passer des commandes un peu farfelues, quelques fois en urgence... Merci également aux gestionnaires du SIMM, Mayu Hiranot-Courcot, Fabienne Decuq et Marie-Theresa Mendy. Je remercie aussi ici Nora Abdoul et Diana Lesueur pour les commandes, leur sourire et leur gentillesse, ainsi que Simon Dadoun. Merci à Armand Hakopian pour sa sympathie et pour avoir accepté d'augmenter mon espace de stockage quand le besoin s'en est fait sentir. Merci aussi à Freddy Martin et Gilles Garnaud pour leur aide et leur disponibilité.

Ce travail a requis l'usage de divers instruments qui ont nécessité une formation au préalable. Je tiens donc à remercier Isabelle Génois pour la formation sur le MEB, Bruno Bresson pour la formation sur le SEMFEG, Patrick Le Griel pour la formation sur le TEM et sa disponibilité pour faire de beaux clichés quand nécessaire, Bernard Haye pour la formation aux préparations des échantillons TEM, Christophe Helary et Corinne Illoul pour la formation en histologie, Mohamed Hanafi pour la formation ATG. Un grand merci également à l'atelier : Ludo, Alex et Amaury, pour leur disponiblité, leur savoir-faire, leur sympathie. Merci à Damien Brégiroux pour sa formation sur le rhéomètre du LCMCP. Egalement un grand merci à Guylaine pour sa gentillesse, son professionnalisme et pour m'avoir formée à la rhéologie lors de mon stage de M2, même si finalement je n'en ai pas refait en thèse. Merci à Emilie Verneuil pour m'avoir formée sur la DVS.

Un remerciement spécial pour une personne tout aussi spéciale : merci Chakib ! Pour ton humour, ton savoir-faire en microscopie, ta bonne humeur (parfois), les moments passés à discuter de choses et d'autres dans ton labo, ta patience lorsqu'on te mettait à bout avec Camila.

Je tiens également à remercier Biravena Raveendranathan, qui a travaillé pendant six mois avec moi sur les gels de collagène. Merci pour ta gentillesse, ta bonne humeur, ton envie de bien faire. Je remercie aussi Sophie Ramos qui nous a aidées à faire une extraction de collagène.

Je remercie également Juliette Peltzer, Marina Trouillas et Marion Grosbot pour leur motivation, leur efficacité, je suis très contente de pouvoir travailler avec vous.

Dans un registre plus administratif, je remercie le labex MATISSE d'avoir financé cette thèse ainsi que la SATT Lutech qui nous épaule via Laurent David. Merci également à Laurène El Bahhaj et Emilie Maucourt-Bacchi pour leur gestion des relations avec les entreprises.

Enfin, je souhaite remercier tous les membres permanents et non-permanents des deux laboratoires, qui participent à une ambiance de travail épanouissante.

En particulier, je souhaite remercier la team biomin (Thierry, Marie, Elora, Camila, bientôt Julie et Tristan) avec qui j'ai passé et je passe de très bons moments (vive les escape game !), ainsi que la team Alba. Egalement le groupe SoftPolyNet qui nous permet de présenter nos résultats de manière régulière et d'en discuter de façon informelle. Je remercie également Marco, qui a notamment pris un peu de temps pour me coacher pour ma présentation au MIT, ainsi que Nikki avec qui nous avons partagé quelques déjeuners tardifs à la cantine. Je souhaite également remercier Clément S pour ses précieux conseils et ses anecdotes. Merci à Capucine, pour son humour, les discussion informelles que nous avons eues et sa patience lorsque je cherchais Nadine et qu'elle n'était pas dans son bureau. Merci à Ahmed Hamraoui, Gervaise Mosser, Léa Trichet pour leur sympathie et les discussions informelles que nous avons eues. Merci à la team du 3e (Bruno, Matteo, Alba, Artem, Xavier, Mélanie, Raphaëlle, Clotilde, Mehdi, Giorgia, Juliette) pour ces super déjeuners mensuels ! Un grand merci également à tous mes cobureaux des deux labos, passés ou présents, qui donnent envie de venir au labo : Widad, Chrystelle, Clio, Kankan, Chloé, Juliette, Mehdi et Giorgia. En vrac, je remercie également chaleureusement Cécile M, Anne-cha, Antoche, Cyprioche, Heiva, Valoche, Francisco C, Cécile C, Gabo, Paul, Ludo F, Maeva, Julie, Gaelle, Claire, Julien, Sandrine, Pascal, Nassim, Kusina, Souf, Wilbert, Louis, Pierre... ainsi que Alexandra, Mateusz, Alexis, Claudia, Civan, Laetitia, Xavier F, Francisco G, ...

Comme j'ai également travaillé en-dehors du laboratoire, je souhaite remercier mes collègues de l'unité de chimie du Palais de la Découverte.

Je souhaite aussi remercier tous les amis qui m'ont soutenue jusque là: la bande de copains du lycée (Clémence, Soumaya, Megguy, Salomé, Maeva, JL), Oriane de prépa, les filles de l'EIVP (Marie, Karine, Kajin), les Anges du Palais, Silvia et Antoine B du M2, Quentin du labo, Clara,...

Un merci particulier à Nicolas, qui m'a soutenue et supportée pendant ces trois ans - merci également d'avoir relu et corrigé certaines parties de mon manuscrit.

Enfin, je souhaite adresser un immense merci à ma famille qui me soutient depuis toujours : mes parents, ma soeur, Karine et ses filles. Merci d'avoir été là pour partager ce moment avec moi, merci pour votre aide, votre écoute, votre amour en toutes circonstances.

Contents

Introduction and outline of the manuscript

Biological tissues possess a variety of mechanical properties, intimately related to their function. Their stiffness ranges from few kPa to thousands of kPa for soft tissues, and up to few GPa for biomineralized tissues. So, why not take inspiration from Nature to make improved (bio)materials, especially for guided tissue regeneration?

Different strategies can be used for making biomaterials [1]:

- biocompatible non degradable (*e.g.* alloys for orthopaedics, most synthetic polymers as prosthetics, ceramics as dental implants).
- biocompatible biodegradable (*e.g.* synthetic hydrogels as drug carriers, most biopolymers for soft tissue engineering).

By definition, a **biomaterial** is a nonviable material used in a medical device, intended to interact with biological systems [2]. Aside external medical devices, one of the aims in using a biomaterial is to fully replace the organ or to provide a structure for growing a new tissue. Ideally, the biomaterial is a scaffold that is biocompatible and induces after implantation *(i)* colonization by host cells, *(ii)* vascularization and *(iii)* full resorption to allow re-growth of a new host tissue without inflammatory response.

However, none of the previous mentioned strategies has been found satisfactory enough to replace the **gold standard: the autologous transplant**. There are two main reasons. First, it is hard to cross the so-called "death valley" between the results obtained in the research laboratories and the market. For instance, difficulties may arise from the regulations (fast updating rate, become more strict), the non-realistic research project ideas (use of exotic compounds, complicated scale-up, weak quality/price ratio) and the lack of financial resources in public laboratories leading to incomplete validation of the requirements (implantations in model animals are expensive but necessary). Second, none of the biodegradable biomaterials are as efficient as an autologous transplant in terms of integration: inflammatory responses may arise from a non-biomimetic composition, too fast resorption from a lack of density (non-biomimetic architecture and concentration). Nevertheless, using an autologous transplant is challenging because of the limited amount of available tissue, potential infections that may arise from another surgery, potentially implying a worsening of the patient's condition.

Collagen is the major component of the extracellular matrix (about 30% of all the proteins). There exists 28 types of collagen and among them **type I** is the most abundant. It is a structural protein, meaning that it is the major support of cells and by extension organs. Therefore, to build a 3D scaffold as efficient as an autologous tissue, we hypothesize that:

- apart water, type I collagen should be the only/the **major component** of the scaffold (biomimetic composition);
- the scaffold should contain a **high collagen concentration** (biomimetic density);
- **collagen 3D architecture** in the scaffold is as important as the two previous requirements;

(those three requirements were partly validated with pre-formed dense collagen matrices [3])

- the **mechanical behavior** of the collagen scaffold should be close to that of biological tissues;
- the scaffold should be **injectable** to limit invasive procedures on the patient.

To circumvent the high viscosity of collagen when its concentration increases, our strategy is to use **spray-drying** to form dense collagen beads [4]. The beads can be suspended in an injectable fluid to form a highly concentrated collagen suspension. After injection in a mold mimicking a tissue defect, the collagen beads will dissolve and form a collagen gel *in situ*. To assess its relevance for tissue engineering, three main points arise: *(i)* is the architecture of the gel truly biomimetic? *(ii)* does its mechanical behaviour reproduce that of the targeted tissue? *(iii)* how does the gel interact with its environment (*e.g.* swelling, adhesion, cell colonization and vascularization, resorption time)?

The study of the **architecture-mechanical properties relationship in dense collagen gels** is the main problematic of this manuscript. Therefore, this thesis is at the crossroads of different domains:

- physico-chemistry and processing of collagen, specific knowledge of CMCP laboratory;
- design of model systems (especially hydrogels) and characterization of their mechanical behavior, specific knowledge of SIMM laboratory.

The main reference of such relationship in our case is the biological tissue. However, depending on its origin (animal, type of tissue), its processing (frozen, dried, freeze-dried, hydrated, type of solvent), its characterization (microscopy preparation, type of microscope, type of mechanical test) the results may change dramatically. Thus, this relationship in biological tissues is not straightforward. By building pure collagen scaffolds, we also aim at providing model systems to study further and more accurately the properties of such materials, and more specifically the connection between architectural changes at the microscale and the bulk mechanical behaviour.

This multidisciplinary work requires the definition of some terms used throughout the manuscript: the concentration will be given in mg/mL (1 mg/mL = 0.1 wt%); the ultrastructure is the architecture of the material as observed by an electron microscope (10 µm to 100 µm); the microstructure is the architecture of the material at the scale of the cell (1 µm to 10 µm); collagen scaffold, collagen gel/hydrogel, collagen matrix will be used indifferently.

The manuscript is organized as follows:

- the **first chapter** aims at providing a state of the art about collagen properties, architecture and mechanical properties of reference biological tissues and collagen processing for making scaffolds;
- the **second chapter** is a study on spray-dried collagen beads, that can be used as a platform for encapsulating active biomolecules or making anisotropic scaffolds;
- the **third chapter** explores the ultrastructure of collagen gels made with dense collagen beads, depending on the processing conditions;
- the **fourth chapter** links the mechanical properties of the collagen gels to their ultrastructure;
- the **fifth chapter** is confidential;
- finally, all experimental conditions are described in the **experimental part**, before the general conclusion.

Bibliography

1. Ratner, B. D., Hoffman, A. S., Schoen, F. J. & Lemons, J. E. *Biomaterials science: an introduction to materials in medicine* (Elsevier, 2004).
2. Williams, D. F. *Definitions in biomaterials: proceedings of a consensus conference of the European Society for Biomaterials* Volume 4 (Elsevier Ltd, Chester, England, 1987).
3. Giraud-Guille, M.-M., Nassif, N., Wang, Y., Helary, C. & Pellé, A. *Dense fibrillar collagen matrices for tissue repair and the preparation method thereof, Patent US9867902B2* 2010.
4. Nassif, N., Fernandes, F. M., BOISSIERE, C., Sanchez, C. & Giraud-Guille, M.-M. *Injectable collagen suspensions, the preparation method thereof, and the uses thereof, particularly for forming dense collagen matrices, Patent WO2016146954A1* 2015.

1 State of the art

Contents

1.1 Type I collagen protein: from molecule to fibril

Collagen is the most abundant proteins in vertebrates. It represents around 30% of the total protein content in mammals. Collagen is the major component of the extracellular matrix (ECM). There exists 28 types of proteins called "collagen"; type I being the most abundant in human connective tissues such as dermis, tendon, cornea, blood vessels and bone. Type I collagen belongs to the fibrillar collagen family, as well as type II (mainly found in cartilage), type III (found in artery walls for instance), type V (constituent of the cornea) and type XI (found in small quantities with type II). Other collagen families include non-fibrillar, fibril associated collagens with interrupted triple helices (FACITs), and collagen-like proteins [1]. Those families have different protein structures that can form percolating networks, filaments or associate with fibrillar collagens [2]. All collagen proteins are triple helix-based (with possible partial unfolding depending on the type) and have at least one common point: their sequence, which is composed of a repetitive motif of three amino acids *-(Gly-X-Y)$_n$-*, *Gly* being Glycine, X and Y other amino acids *e.g.* Proline, Hydroxyproline, Hydroxylysine, Alanine (see **Figure 1.1**).

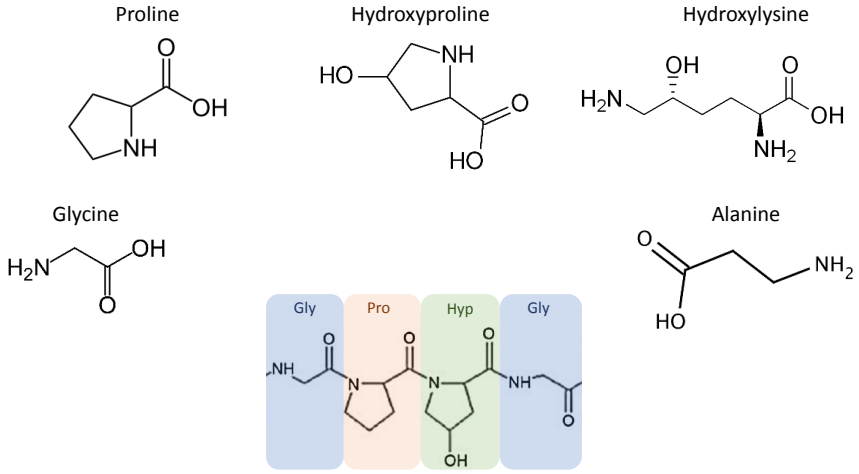

Figure 1.1: Chemical formula of the most frequently found amino acids in collagen molecules together with a short collagen polypeptide sequence as an example. Reproduced and modified from Jang 2016 [3].

1.1.1 *In vivo* synthesis

The α-chains of the procollagen molecule are synthesized inside the cells, on the ribosome (see **Figure 1.2, step 1**). Each chain is a left-handed helix. The assembly of the peptides in each chain follows the typical collagen sequence as described above with X being Proline with 0.22 probability and Y being Hydroxyproline with 0.11 probability for type I collagen [4, 5] and the values have a low dependency on the species. The α-chains are then exported to the endoplasmic reticulum of the cells. Here collagen strands undergo a series of post-translational modifications *e.g.* hydroxylation of some Proline and Lysine residues to Hydroxyproline and Hydroxylysine (steps 2 and 3 in **Figure 1.2**). Those modifications are necessary to enhance the thermal stability of the collagen molecule [7]. The collagen strands then assemble to form a triple-helix called procollagen molecule (steps 4 and 5 in **Figure 1.2**). Glycine is required to be at the center of the triple helix because of its small size compared to the other amino acids (no side chain in Glycine), thus provinding additional hydrogen

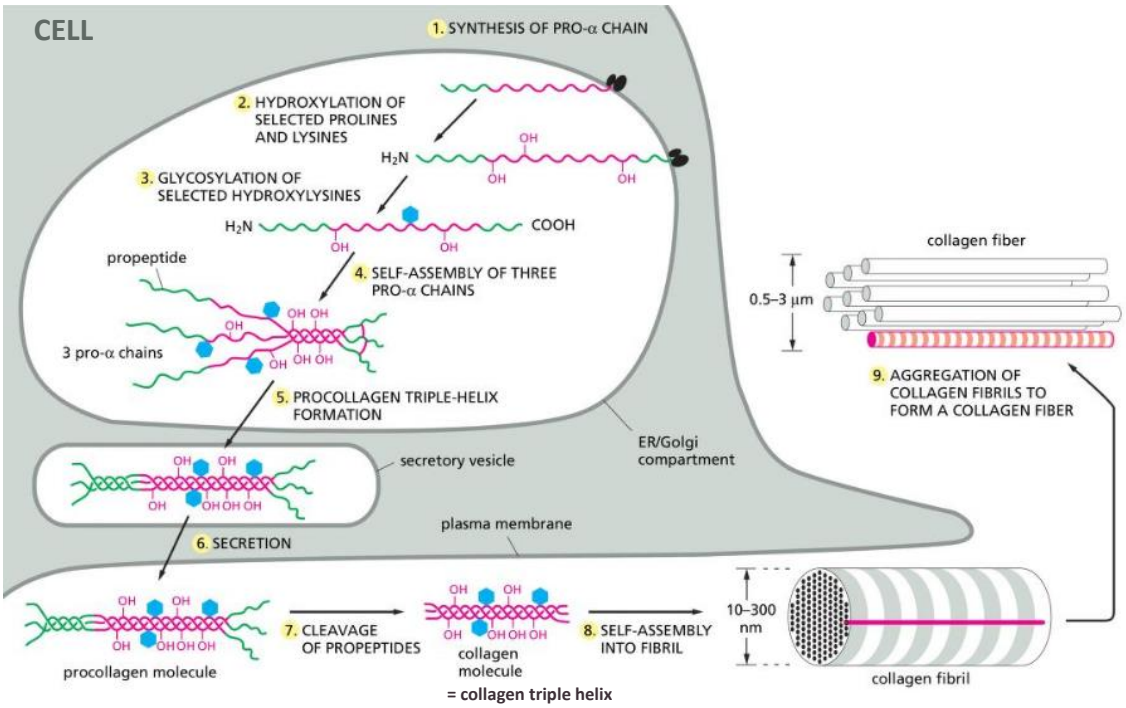

Figure 1.2: *In vivo* synthesis of collagen. Reproduced and modified from Alberts 2002 [6].

bonding sites to further stabilize the triple helix [8]. Voluminous amino acids occupy the periphery of the helix, enabling interactions with other molecules and fluids [9]. The triple helix is right-handed (see **Figure 1.3, left**) and is stabilized by inner hydrogen bonds (see **Figure 1.3, right**).

This precursor molecule has loose ends named C- and N-terminal propeptides due to their difference in chemical composition. Those extremities enable the procollagen molecule to be soluble at physiological pH *i.e.* about 7.4, thanks to their negative charge. Procollagen molecules are then transported to the Golgi apparatus where they are packed into secretory vesicles [11]. Immediately after secretion in the extracellular space the procollagen molecule undergoes an enzymatic cleavage: N and C propeptides are removed, leaving smaller (compared to the size of the triple-helix) non-helical ends called telopeptides (steps 6 and 7 in **Figure 1.2**). This newly formed molecule is called tropocollagen or collagen molecule. It is not soluble at physiological pH [12]. The size of this molecule is about 300 nm long and 1.5 nm in diameter [9].

Right after the enzymatic cleavage, collagen molecules self-assemble into fibrils, supramolecular units that are stabilized by covalent crosslinks. Those are induced by lysyl oxidase enzymes which transforms Lysine or Hydroxylysine residues into their aldehyde equivalents in the telopeptide regions; these aldehyde functions react with other aldehydes, Lysine or Hydroxylysine residues present in the neighbouring molecules thus forming imine bonds [1]. The type of chemical crosslinks depends on the age of the tissue, the type of the tissue (mineralized or not) and even on the type of collagen with the formation of disulfide bonds for non-fibrillar collagens for example [13].

The self-assembly process of collagen molecules into fibrils is called fibrillogenesis. A typical intermolecular (longitudinal) spacing is observed in fibrils, called D-period and commonly described as being equal to 67 nm. This periodic arrangement consists in a region containing only stacked collagen molecules (called overlap region) next to a gap region containing the telopeptides of two successive collagen molecules [14] as shown in **Figure 1.4**. However it was recently demonstrated that, indepen-

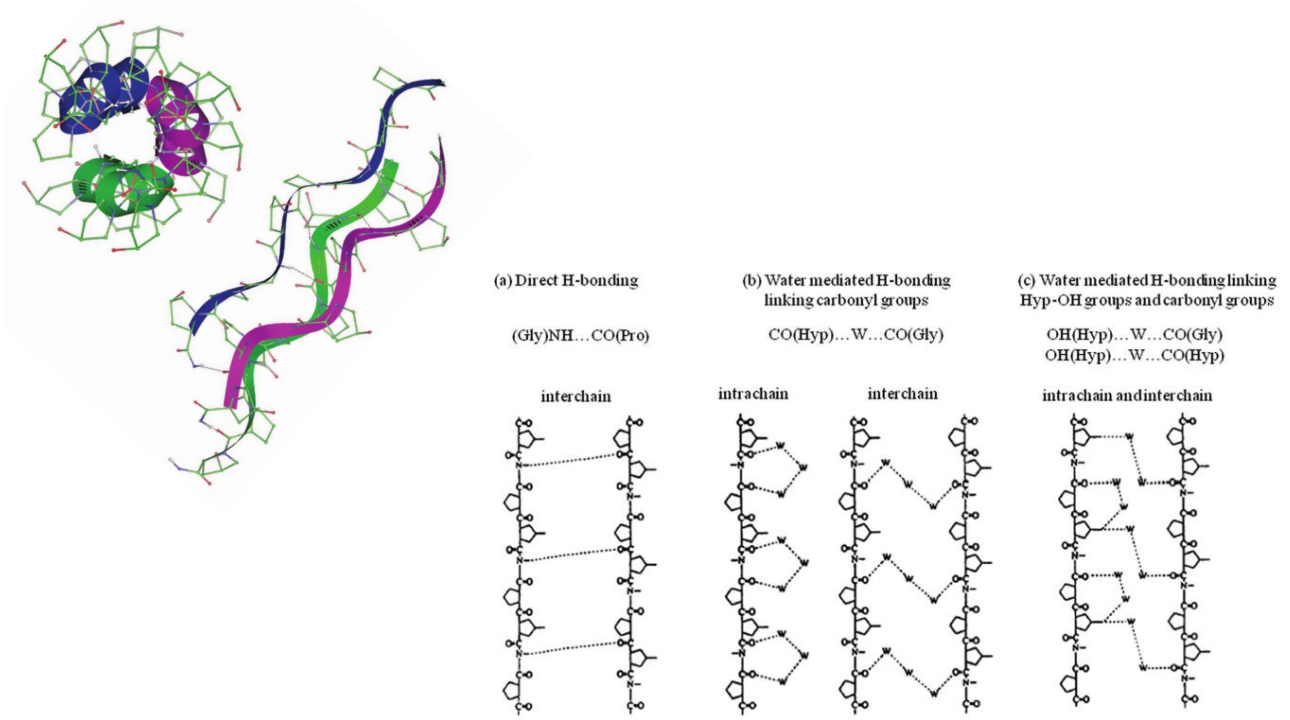

Figure 1.3: Top left: Collagen triple helix, top view on the left, side view on the right. Reproduced from Bhattacharjee 2005 [8]; bottom right: hydrogen bonding possibilities between neighbouring amino acids in the triple helix. Reproduced from Nguyen 2013 [10].

dently of tissue types or mammals, this D-spacing varies from 58 nm to 67 nm and can be different in each bundle of fibrils [15]. Collagen fibril diameter range from 30 nm (in the cornea [16]) to 300 nm (in tendons [17]). Their length is around 1μm. The supramolecular collagen self-assembly continues beyond the fibril scale to form fibers that further assemble into bundles, until the tissue scale is reached; an example for tendons [18] is in **Figure 1.5**.

1.1.2 *In vitro* self-assembly

Even if the synthesis of collagen-like molecules has progressed in the past years [19], it is still not yet possible to perfectly mimick the native features of collagen triple helix and their self-assembly into fibrils [20]. Thus collagen molecules have to be extracted *in vitro* from living tissues such as rat tail tendon or pig dermis. The collagen-rich tissues are dissolved at acidic pH to obtain *in vitro* acid-soluble collagen [21] thanks to the positive charge of the collagen molecule which makes it soluble *in vitro* at low pH (the isoelectric point of collagen being at pH=7.4 [22, 23]; it is dependent on the ionic strength of the medium hence its isoionic point at pH=9.3 [23]). Common laboratory procedures use acetic acid or hydrochloric acid to solubilize the tissue. Then, the solution is purified through different steps (centrifugation, precipitation, dialysis) to remove blood cells, other cells and proteins to finally obtain a diluted (about 3 mg/mL or 0.3 wt%) stock solution made of collagen molecules at acidic pH (about 2.5). Commercially available pure collagen solutions are rather obtained from bovine or porcine skin (clinical grade) and sold at an expensive price due to the sensitive process and their degree of purity.

To reproduce the *in vivo* collagen self-assembly, the precipitation of fibrils in solution can be induced *in vitro* by changing several parameters such as ionic strength, temperature or pH. Acid-

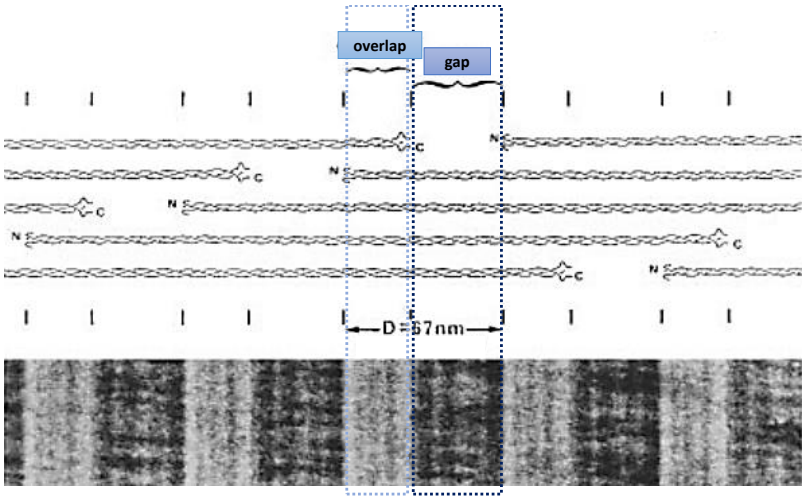

Figure 1.4: Stacking of collagen molecules in a fibril and striations as observed by TEM. The staining molecules (*e.g.* uranyl acetate) are mostly found in gap zones hence providing contrast. Reproduced and modified from Kadler 1996 [14].

soluble collagen tends to precipitate into fibrils at physiological temperature (37 celsius degrees) and/or neutral pH [24]. A study performed on collagen solutions at 10 mg/mL [25] showed that when the fibrillogenesis pH of Tris buffer decreases from 7 to 5 at room temperature, the fibril diameter tends to increase. The use of phosphate buffers inherently induces a certain ionic strength that is more or less controlled thus potentially interfering with the pH effects which can produce fibrils with different sizes. Typically, ammonia vapours are used to increase the pH of the collagen solution [26] thus avoiding addition of alkali salts that tend to form more heterogeneous fibrils in terms of size. Such conditions lead to the association of collagen molecules *via* electrostatic, hydrophobic and hydrogen interactions inducing the formation of native-like fibrils (see **Figure 1.6**).

The formation of a fibril precursor, called microfibril, has been evidenced *in vitro* [28, 29] but its presence *in vivo* is still under discussion. More exotic fibril morphologies can be precipitated *in vitro* depending on the conditions (temperature, type of ions, ionic strength) *e.g.* toroidal fibrils [30], smaller aggregates called segmental long spacing (SLS) [31, 32]. The concentration of collagen solutions or gels precipitated *in vitro* is classically assessed by Hydroxyproline titration. It is worth noticing that the collagen concentration in living tissues is not known for the moment due to the complexity of the extracellular matrix.

1.1.3 Collagen stability

Collagen molecules are highly sensitive to temperature *in vitro* (see **Figure 1.7**). They irreversibly denature into gelatin (unfolding of the triple helix) above 37°C even though this temperature has been shown to depend on the collagen source, the solvent and even the heating rate [33] and can thus be lower. It is worth noticing that the thermal stability of collagen gels can be tuned by changing the collagen source [34].

It was proposed that the stability of the collagen molecule is due to the presence of Hydroxyproline residues in the triple helix [35]. Water molecules are able to form bridges between two adjacent chains inside the triple helix [36], and especially on Hydroxyproline binding sites. There are evidences supporting the hypothesis that water actually plays a crucial role in stabilizing the collagen triple helix

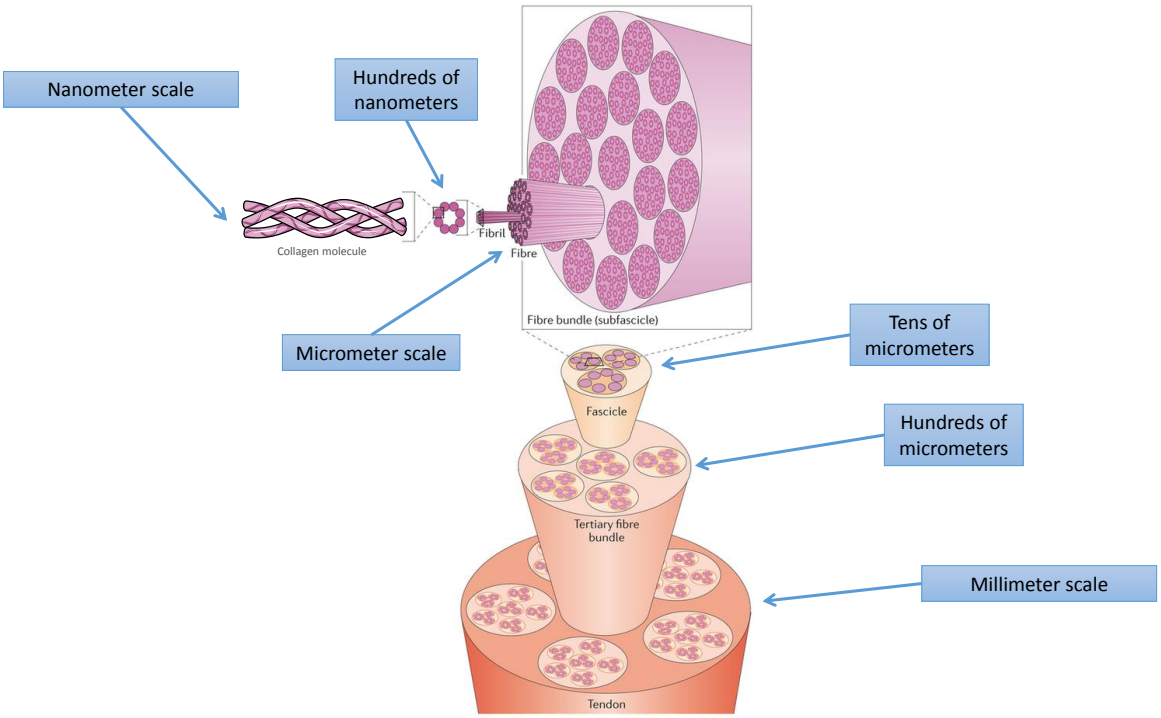

Figure 1.5: Supramolecular assembly of collagen *in vivo* in the case of a tendon. Typical cross-section scales are indicated. Reproduced and modified from Mouw 2014 [18].

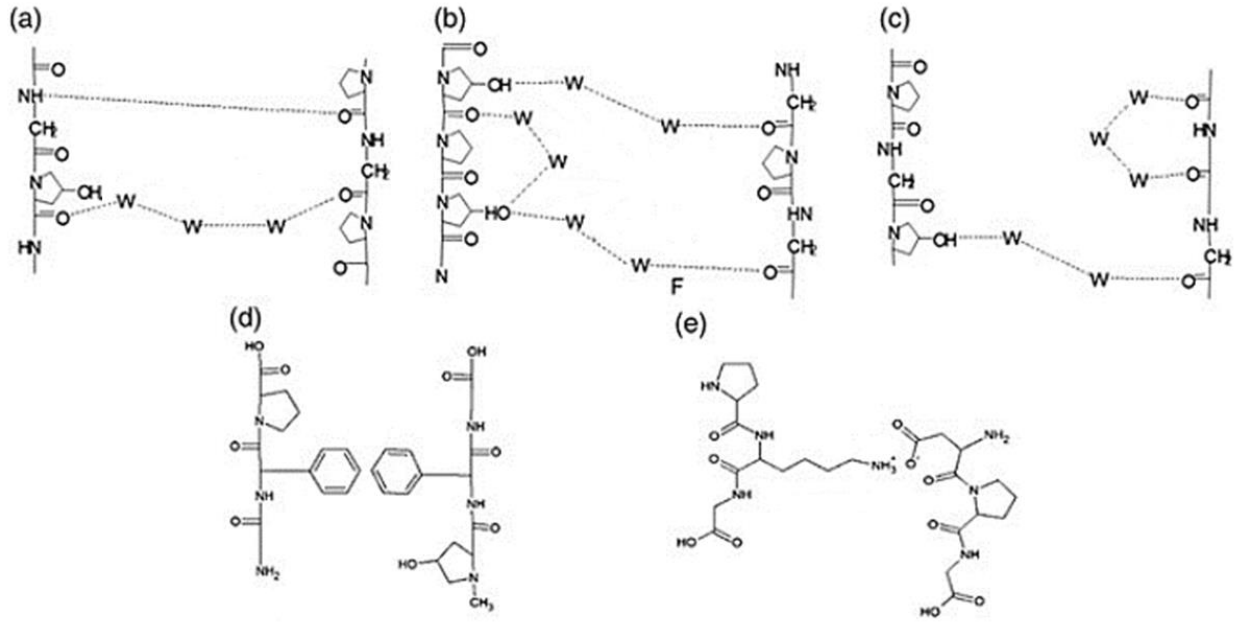

Figure 1.6: Different types of physical interactions during collagen molecules self-assembly: (a), (b) and (c) represent hydrogen and water-mediated hydrogen bonding, (d) hydrophobic interactions and (e) electrostatic interactions. Reproduced from Sriramoju 2015 [27].

[37, 38]. When forming hierarchical organizations by self-assembly, more water molecules are recruited to form bridges between adjacent triple helices. This phenomenon can partially explain the increased stability of collagen fibrils, that have a denaturation temperature around 55°C [39]. Collagen fibers are even more stable: their denaturation temperature is close to 70°C [40]. Supramolecular assemblies together with other components of the ECM thus enable collagen molecules to perform their function without denaturation at body temperature *in vivo*.

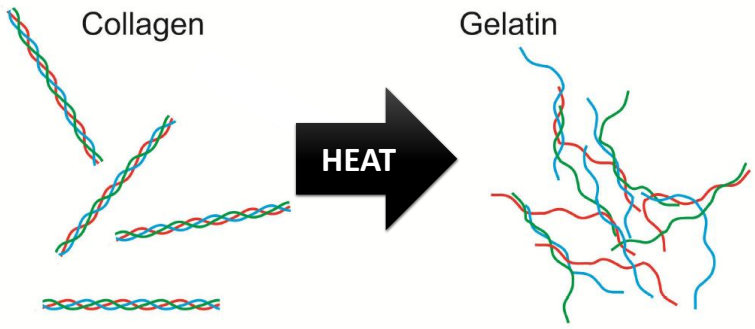

Figure 1.7: Collagen molecules irreversibly denature into gelatin when heated above 37°C. Reproduced and modified from Shayegan 2013 [41].

1.2 Lyotropic properties of collagen

1.2.1 Collagen phase diagram and tissue analogs

Yves Bouligand was the first to make a link between certain biopolymers organizations in diverse ECM *e.g.* chitin, collagen, and liquid crystal phases (especially the cholesteric phase, or well-known Bouligand's twisted plywood model in **Figure 1.8**) [42]. He demonstrated that the arches appearing in electron micrographs (see **Figure 1.9** for an example in compact bone [44], and its equivalent highlighted in orange in **Figure 1.8**) were not formed by long molecular strands but by discrete molecules aligned in superimposed planes possessing different orientations. Therefore, arched patterns are revealed thanks to an oblique section performed in the twisted plywood. Such organized tissues were named as analogs of liquid cystals, because of the similarities in their architecture even if they are not liquid at all.

Later, Marie-Madeleine Giraud-Guille worked on acidic collagen solutions *in vitro* to reproduce the twisted plywood observed in bone [45]. She further proved that collagen has lyotropic properties *in vitro* [46] *i.e.* at acidic conditions. She showed that collagen molecules self-assemble to form different liquid crystal phases (not only cholesteric) depending on their concentration.

Finally, a more precise phase diagram of collagen in solution *in vitro* was proposed over a large range of concentrations at acidic conditions [47] (see **Figure 1.10**). The nematic phase, characterized by alignments, is reached in acidic solutions just above 40 mg/mL (or 4 wt%). The precholesteric phase, characterized by crimped patterns, is obtained between 50 and 70 mg/mL (or 5 wt% to 7 wt%). Finally, a twisted-plywood organization, typical of a cholesteric phase is reached *in vitro* above 80 mg/mL (or 8 wt%).

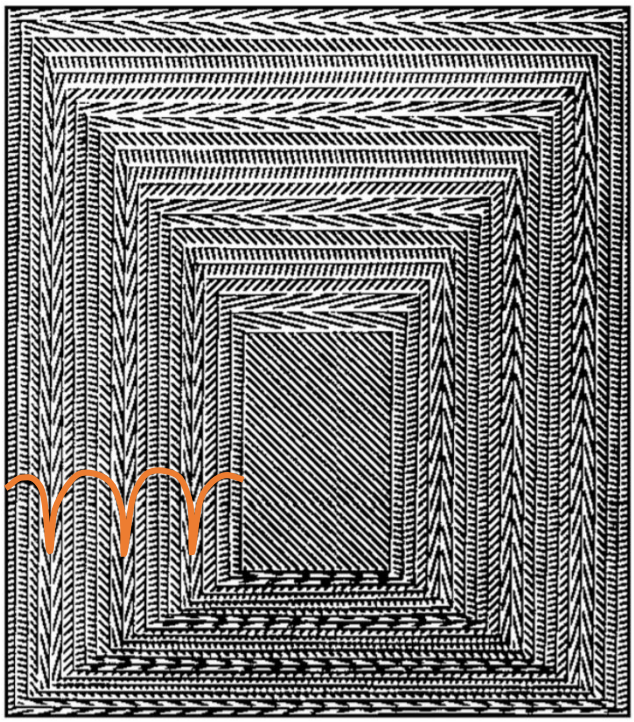

Figure 1.8: Bouligand's drawing of the cholesteric organization. Reproduced and modified from Bouligand 2008 [43].

After reaching a desired liquid crystal phase in solution, it was proven that inducing fibrillogenesis by ammonia vapours *in vitro* preserves the organization [48] by transforming a continuous molecular twist in a discrete fibrillar twist in the case of the cholesteric phase for example (see **Figure 1.11**). Trying to reproduce such hierarchical organizations *in vitro* can induce long range anisotropy at macromolecular scale, which is a desired feature for mimicking collagen-rich tissues.

1.2.2 Multiscale characterization of the organizations

Thanks to their hierarchical assembly, the ultrastructure of collagen materials can be characterized at different scales. To do so, samples undergo specific preparations to preserve their structure (no shrinkage or burst). It should be kept in mind that even though the protocols are designed to limit the abruptness of the preparation on the sample, small structural modifications remain possible.

- Up to hundreds of microns/tissue scale with Polarized Light Microscopy (PLM)

Liquid crystal phases are typically characterized by PLM. This technique can thus be used to determine collagen organizations in living tissues, concentrated solutions or gels, thanks to their anisotropic properties which modify light polarization (birefringence). Dark regions indicate objects having the same direction as the polarizers or perpendicular to their plane, birefringent (bright) regions indicate objects at 45° from polarizers. Two pictures are required to deduce completely the orientation of the objects: one with polarizers at 0°/90°, another with polarizers at 45°/135°. A lambda plate can be used when the polarizers are positioned at 0°/90°. This plate induces a first order retardation of the light, which shifts the colors towards cyan (second order) when light is polarized along the slow axis of the plate (45°) or towards yellow (first order) when light is polarized along the fast axis of the plate (135°). Samples should be about 4-8 µm thick for optimized observations and are classically prepared with histology protocols.

Figure 1.9: Ultrathin section of human demineralized compact bone displaying typical arched patterns (x2700). Reproduced from Giraud-Guille 1988 [44].

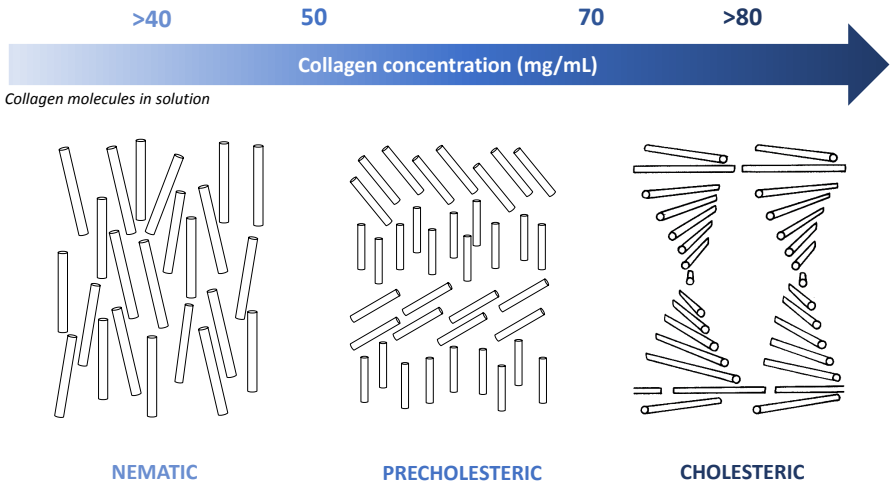

Figure 1.10: Liquid crystal mesophases of the collagen phase diagram. Reproduced and modified from Besseau 1995 [48].

When observed under polarized light, dermis displays large dark and bright birefringent domains which coexist in a disorganized fashion (see **Figure 1.12, top left**). A collagen solution just above 40 mg/mL (4 wt%) *in vitro* shows the same type of birefringence (brightness at the edge of the sample where the concentration locally increases above 40 mg/mL by evaporation, see **Figure 1.12, bottom left**). Tendon exhibits banded-like birefringence, typical of a crimped structure (see **Figure 1.12, top middle**). This kind of birefringent pattern is also found in solution *in vitro* (see **Figure 1.12, bottom middle**). Finally, compact bone also has alternating bands of bright and dark birefringence, but at a smaller scale and more regular, typical of the cholesteric organization (see **Figure 1.12, top right**). This organization is found above 80 mg/mL (8 wt%) in collagen solutions *in vitro* in the form of fingerprint patterns ((see **Figure 1.12, bottom right**). The half-pitch of the cholesteric twist is equal to the distance between two full bright bands (bright-dark-bright) or two full dark bands.

- Up to tens of microns with Scanning Electron Microscopy (SEM)

The organization in collagen materials can also be determined from SEM observations. For example, dermis seems to be organized in sheets with different alignments from one sheet to another and

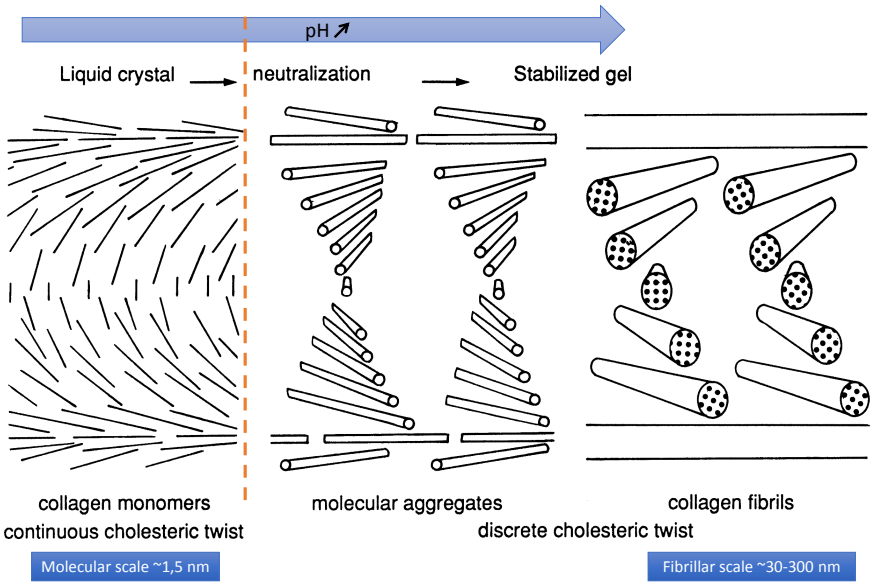

Figure 1.11: *In vitro* stabilization of collagen cholesteric phases. Reproduced from Besseau 1995 [48].

different densities (see **Figure 1.13, top left**). Tendon exhibits crimped organizations also at the SEM scale (see **Figure 1.13, top middle**). Collagen fibrils are organized in a circular fashion in compact bone around haversian channels and in trabecular bone and shows a step-like organization when the sample is cut in oblique way (see **Figure 1.13, top right**). This step-like cholesteric organization has been reproduced *in vitro* in highly concentrated collagen gels (250 mg/mL or 25 wt%) (see **Figure 1.13, bottom right**). Attention should be payed to potential blade-induced alignments or blade-induced crushing of the sample.

- Up to few microns with Transmission Electron Microscopy (TEM)

Finally, TEM can give information at the fibril scale on the tissues. Ultra-thin sections (60-70 nm) are often stained with uranyl acetate and osmium which enhances the contrast. Uranyl acetate actually goes in the gap regions of the collagen fibrils, giving typical banded patterns. Different alignment domains are recognized in dermis (see **Figure 1.14, top left** - white arrow: fibrils perpendicular to the section plane, black arrow: fibrils along the section plane). As well as the crimped fibrils in the tendon (see **Figure 1.14, top middle**). A cholesteric twist is present in bone (see **Figure 1.14, top right**), and was also reproduced in highly concentrated collagen gels (250 mg/mL or 25 wt%) (see **Figure 1.14, bottom right**). It should be kept in mind that the orientation of the diamond blade relatively to the sample may induce artifacts when cutting ultrathin sections [55].

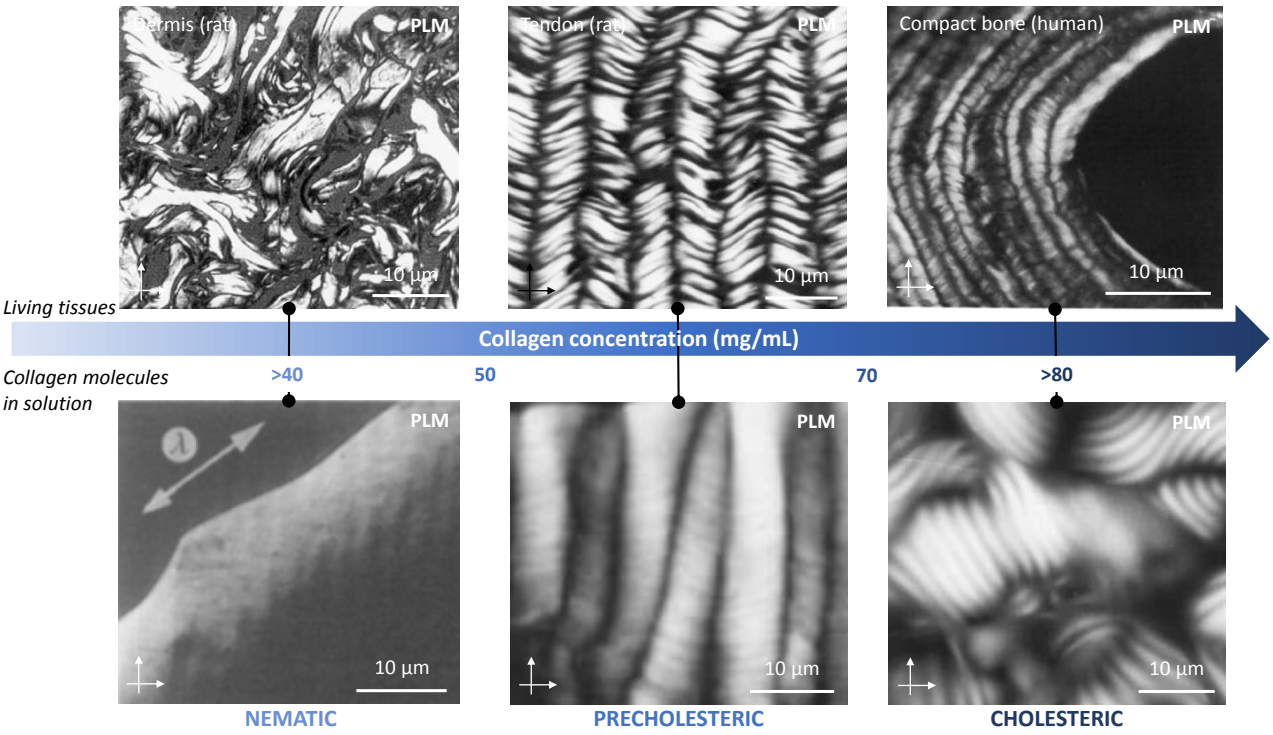

Figure 1.12: Biological tissues observerd under PLM compared with their liquid crystal analog (collagen molecules in solution *in vitro*. Reproduced and modified from Giraud-Guille 1992 [46], 1994 [49], 2003 [50] and 2008 [51].

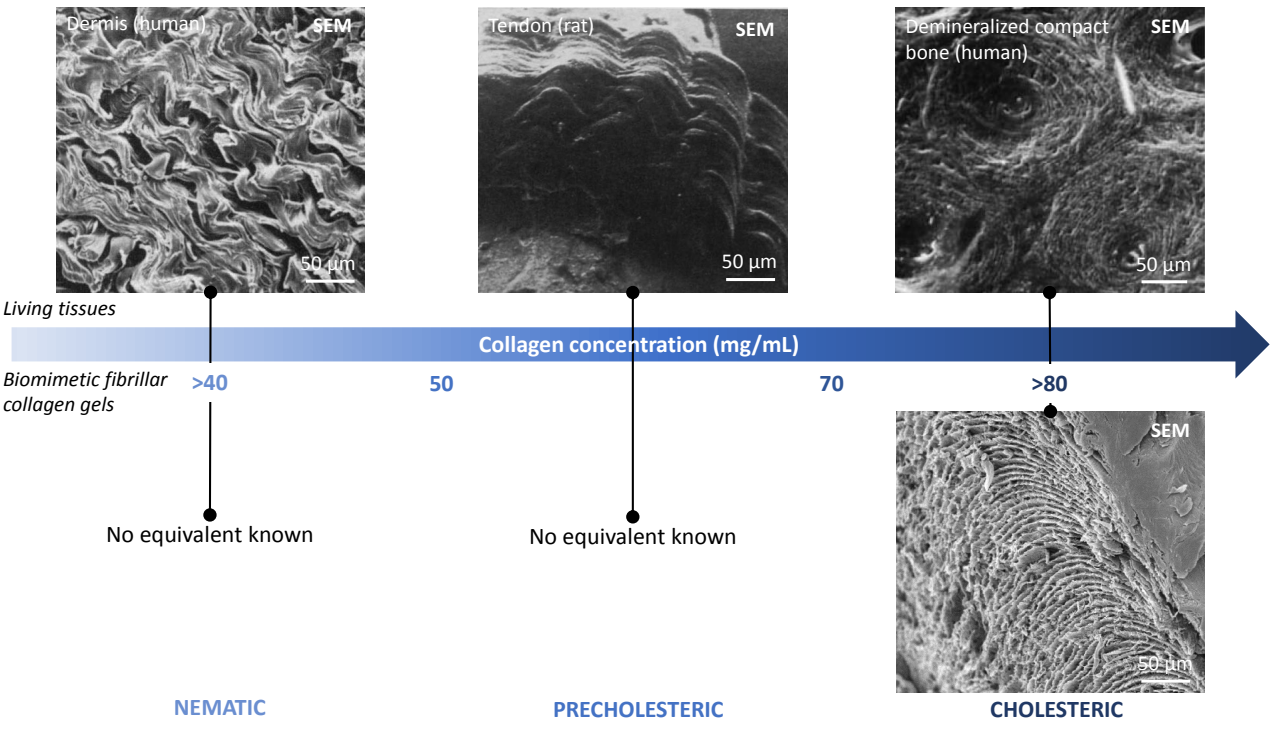

Figure 1.13: Biological tissues observed under SEM compared with up-to-date existing fibrillar matrices *in vitro*. Reproduced and modified from Brown 1972 [52], Gathercole 1978 [53], Giraud-Guille 1994 [49] and Wang 2011 [54].

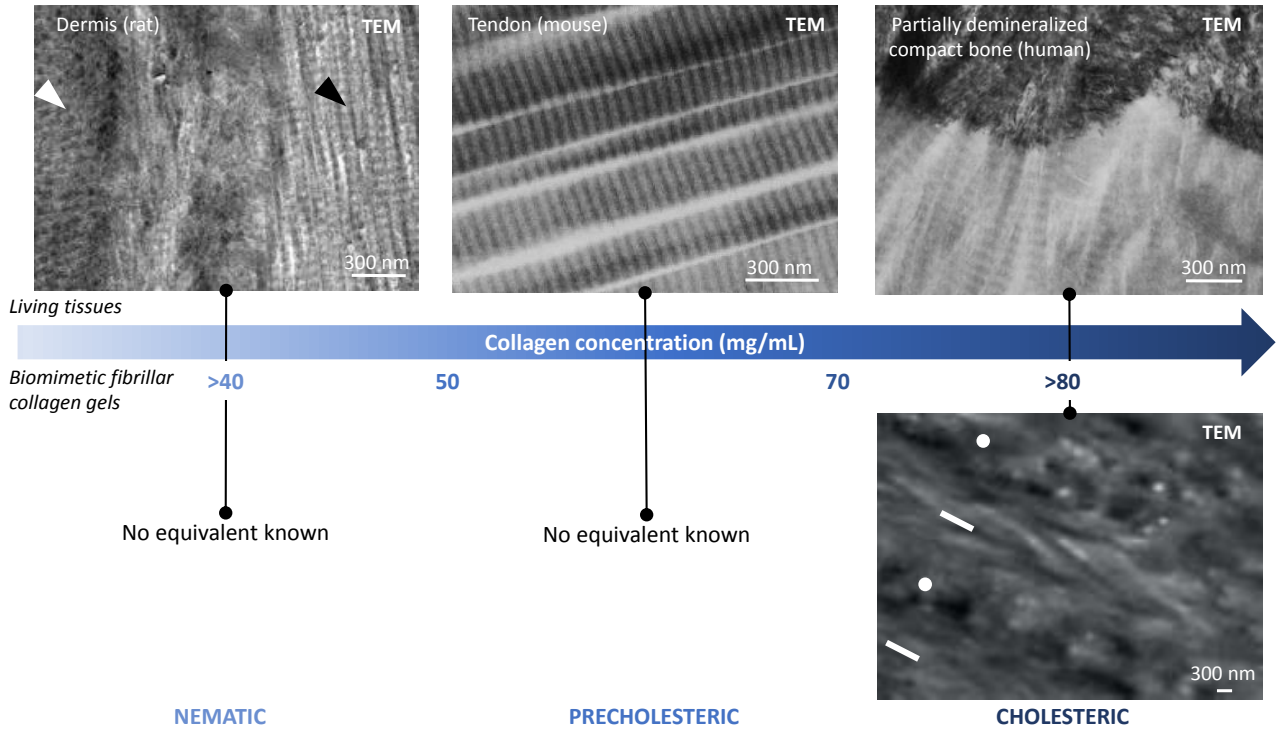

Figure 1.14: Biological tissues observed under TEM compared with up-to-date existing fibrillar matrices *in vitro*. Reproduced and modified from Giraud-Guille 2013 [56] and Wang 2012 [57].

1.3 Structure-mechanical properties relationship in collagen-rich tissues

1.3.1 The origin of mechanical strength in the ECM

From a biological point of view, collagen supports cells in the ECM and helps them differentiate, grow and proliferate [58]. Yet the role of collagen goes well beyond cell raising. It offers a crucial support for all organs and for the body, thanks to its particular supramolecular arrangement. Collagen fibers orientation tends to be highly anisotropic in tissues where high stiffness is needed (in tendons for instance) and less complex in terms of hierarchy levels where elasticity is required (*e.g.* in dermis) [59]. In tissues withstanding uniaxial tensile stress, it was noticed that fibril diameter is larger and there are more crosslinks between collagen molecules [17].

Why is there a need for such hierarchical architectures in collagen? Collagen fibril organization is perfectly balanced between brittle fracture (reached when there are too many intra-fibrillar chemical crosslinks) and energy dissipation with yield (happening with intrafibrillar chemical crosslink deficiency) [60]. The smallest unit in collagen structures is the collagen molecule, about 300 nm long for 1.5 nm diameter. Although no consensus has been made on the persistence length of the collagen molecule (due to the use of different measurement techniques), it is assumed that the molecule is semi-flexible (l_P ranging from 14.5 nm to 150 nm) [61, 62]. Sasaki *et al.* measured by Small Angle X-ray Scattering that the molecule stiffness is higher than that of the collagen fibril (persistence length about $l_P = 10^{11} nm$ [62]), which is higher than that of the tendon [63]. Thus, collagen molecules carry all tensile loads while intermolecular chemical crosslinking enables sliding to dissipate forces by shear: they act as sacrificial bonds [64]. Gliding between chemically crosslinked fibrils also helps energy dissipation [65].

Besides, the supramolecular organization of collagen molecules slows down crack propagation (each level of organization provides a new interface) and enhances tissue elasticity [59]. These mechanisms are crucial for tissue resistance.

1.3.2 Mechanical properties of various ECM: reference behaviors and values

Thanks to the specific know-how developed by SIMM in characterizing the mechanical properties of soft materials (and more specifically hydrogels), we aim at performing mechanical tests on collagen gels with a well defined shape and reproducible testing conditions and results for better comparison with biological tissues and existing collagen matrices. Due to variabilities in collagen-rich tissues (animal type and age, location in the body, composition), experiments (type of test, type of machine, experimental conditions *e.g.* immersion) and analyses, no absolute or standard reference can be inferred either for the mechanical behavior or typical values such as Young's modulus or ultimate tensile stress. Nevertheless, if a structure-mechanical properties relationship is to be studied, reference values are needed for comparison purposes. Therefore a trend can be determined for behaviors in standard mechanical tests and for characteristic values.

1.3.2.1 Tensile behavior

Tensile testing consists in stretching a sample of known dimensions at a given speed (v, typically in mm/min) or strain rate ($\dot{\epsilon}$, typically in s^{-1}) until it breaks. Force and deformation are recorded. Rupture usually happens near the clamps, where additional stress is induced due to tightening. En-

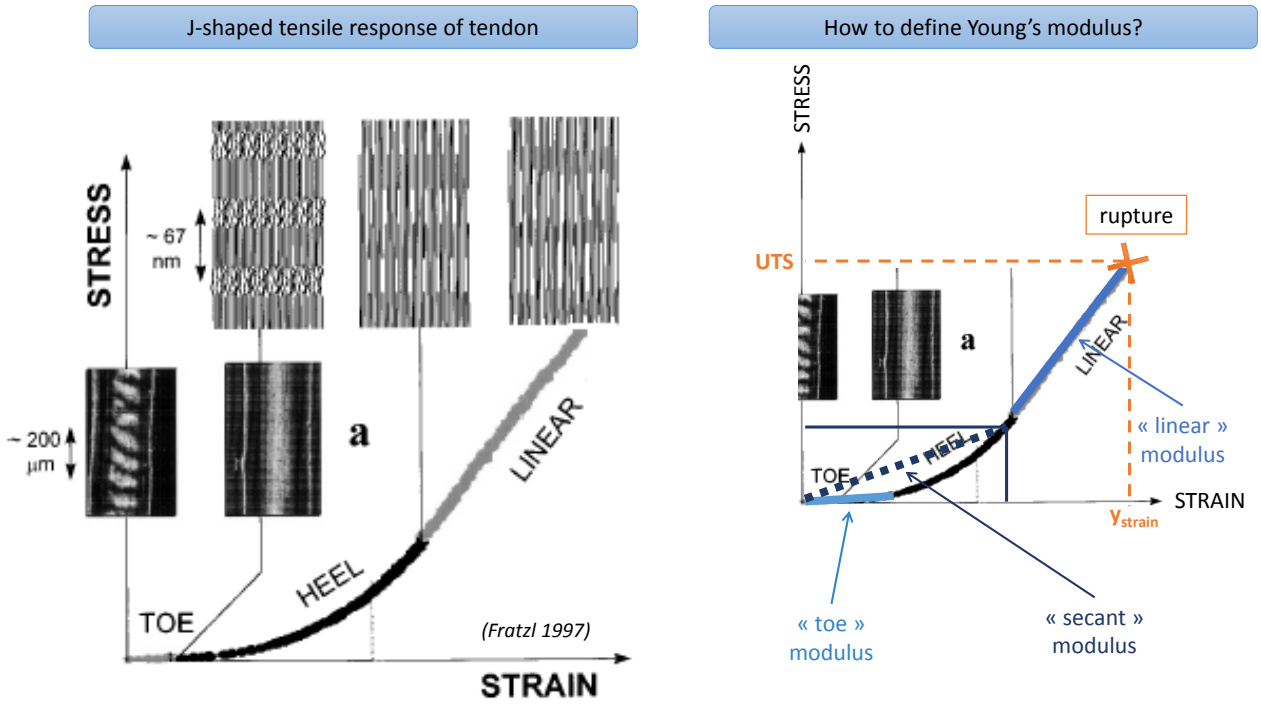

Figure 1.15: Typical J-shaped stress-strain curve of a rat tail tendon (left) and different ways of measuring the Young modulus (right). Reproduced and modified from Fratzl 1997 [66].

gineering or nominal stress (σ, typically in kPa) is defined as the force (F, N) divided by the initial cross-section (A_0, typically in mm^2) of the sample; while true stress (σ_{true}, typically in kPa) is defined as the force divided by the cross-section of the sample at each time point (A_t, typically in mm^2). Thus, engineering stress tends to underestimate the mechanical properties of the sample at large deformations. For practical reasons, only engineering stress will be used in this manuscript. Strain (ϵ, typically in %) is defined as the elongation (L, typically in mm) divided by the initial length of the sample (L_0, typically in mm). Stress-strain curves are typically plotted.

When tendon samples are submitted to tensile tests, a typical J-shaped curve is obtained [66]. The tensile process is divided into three main regions (see **Figure 1.15, left**): a toe region (removal of a macroscopic fold in collagen molecules), a heel region (loss of entropy in gap regions where collagen molecules telopeptides were twisted) and a linear region (extension of collagen molecules and their crosslinks, and sliding of adjacent molecules - this leads to an increase in D-spacing thus enhancing fibril length). Therefore, different Young's moduli can be defined (see **Figure 1.15, right**). A first one in the toe region (linear at small deformations), a second one in the linear region (large deformations) and a last one at a given strain (*e.g.* 20%) also called secant modulus. Ultimate Tensile Stress (UTS) and strain at break (y_{strain}) can also be used to characterize the tensile behavior of collagen materials.

Some reference values from the literature are listed below:

- Human skin: ultimate tensile stress UTS ≈ 12 MPa - strain at break y_{strain} ≈ 100% - Young's modulus E ≈ 0.01 MPa (toe/heel region)- 20-70 MPa (linear region) [17, 67, 68].
- Human tendon: UTS ≈ 25-80 MPa - y_{strain} ≈ 2.5-30% - E ≈ 0.2 GPa (toe region)-1 GPa (linear region) [69–72].

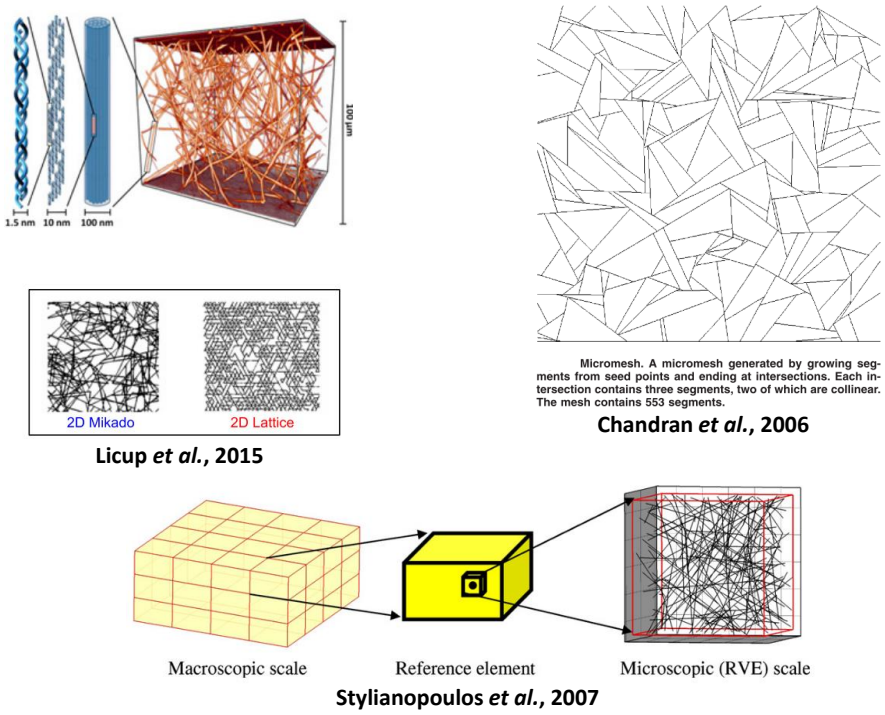

Figure 1.16: Examples of models used for modelling the non-linear response of collagen materials. Reproduced from Licup 2015 [79], Stylianopoulos 2007 [81] and Chandran 2006 [83].

- Human cartilage: UTS ≈ 1-25 MPa - y_{strain} ≈ 10-80% - E ≈ 1-15 GPa (linear region) [73, 74].
- Human ligament: UTS ≈ 25 MPa - y_{strain} ≈ 30% - E ≈ 100 MPa (linear region) [75].

The J-shaped curve is typical of biological tissues. The particular shape of this curve evidences a non-linear mechanical response [76]. After performing mechanical tests on rabbit's mesentery, Fung proposed to fit its non-linear behavior with an exponential dependency of stress on strain [77]:

$$\sigma \propto \exp(\frac{\epsilon}{\epsilon_0}) \tag{1.1}$$

with σ being stress (Pa), ϵ being strain (%), ϵ_0 is a constant. This fitting equation was then used to fit the non-linear response of tendon [71], cornea [78] and dilute collagen gels [79]. Hence showing its relevance when applied to biological tissues or collagen gels.

This simple exponential equation further enabled the elaboration of models to simulate the mechanical behavior of collagen scaffolds, either for rheology [79], biaxial tensile properties [80] or uniaxial tensile tests [81, 82]. When compared to results from the literature, these models are actually quite accurate in reproducing the viscoelastic behavior of collagen-rich tissues or collagen gels. This is surprising since most of the models are based on representations of tissues such as "Mikado model" or branched network that do not mimick the density and organization of collage-rich tissues. Examples of such models are given in **Figure 1.16**. Thus, mechanical testing of living tissues shows that the ability of collagen fibrils to align towards the tensile direction may provide stiffness to the ECM.

Collagen fibrils may play a major role in collagen gels mechanics. Actually, single collagen fibrils themselves exhibit a non-linear behavior in hydrated conditions during tensile testing [84, 85]. And the mechanical behavior of collagen gels or collagen-rich tissues appears to depend on collagen fibril diameter [17] and collagen fibril diameter distribution [59]. In collagen-rich tissues, larger fibrils would

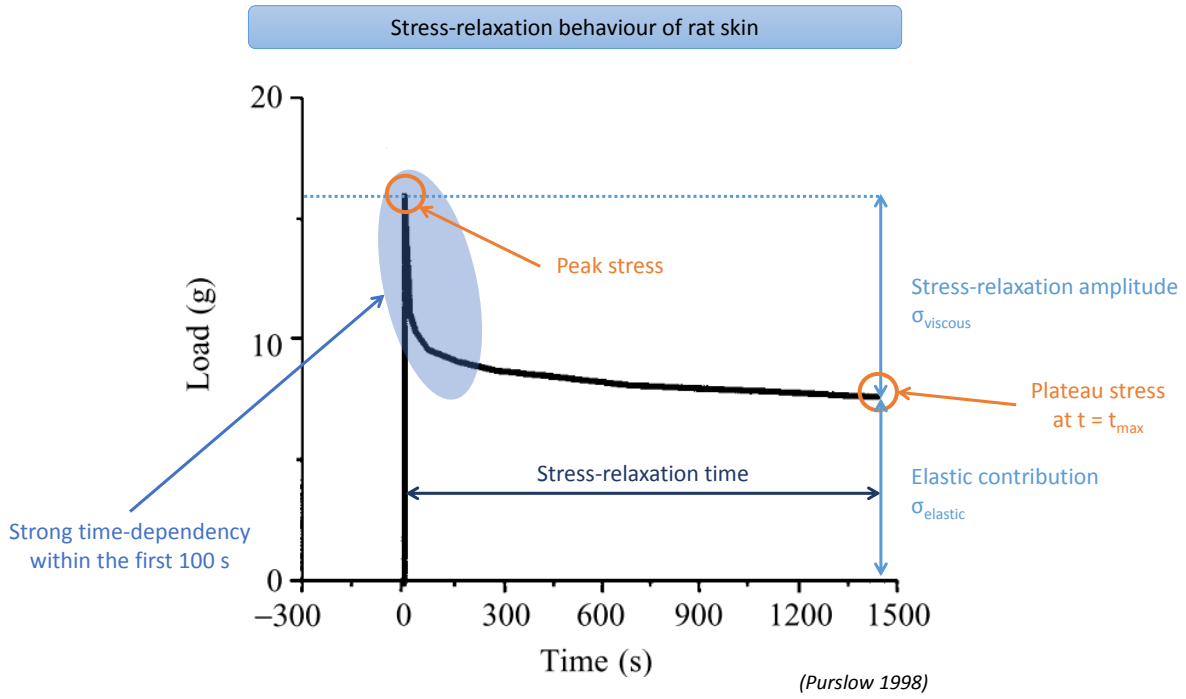

Figure 1.17: Stress-relaxation test: definitions and typical biological tissue behavior.

promote the formation of more intrafibrillar crosslinks thus enhancing tensile strength while smaller fibrils would increase the density of electrostatic interactions thus providing better creep recovering properties. It was observed that fibrils with large and heterogeneous diameter are mostly found in tissues requiring high tensile stresses (*e.g.* tendons) while fibrils with uniform diameter are found in more hydrated tissues (*e.g.* cornea, dermis). Besides, Silver *et al.* found that viscoelastic properties of collagen materials are more dependent on collagen fibril length than diameter [86]. However, it is quite difficult to measure the length of fibrils in a tissue thus it is possible that the mechanical behavior of collagen materials depends on both diameter and length of collagen fibrils.

1.3.2.2 Stress-relaxation behavior

Stress-relaxation testing consists in stretching rapidly a sample until a given deformation and maintaining this deformation during a certain time. Stress-time curves are typically plotted (see **Figure 1.17**). The time-dependent behavior of collagen materials is characterized by a maximum stress at the beginning of the test (σ_{peak}), by a stress-relaxation amplitude ($\sigma_{viscous}$, an elastic contribution ($\sigma_{elastic}$), a stress-relaxation time and a strong dependency of stress on time within the first 100 seconds. This kind of test is particularly interesting for visco-elastic materials because the sample accomodates strain to relax a certain amount of stress. The stress-relaxation proceeds over time by structural reorganizations.

Working with alveolar walls, Fukaya *et al.* showed that the stress-relaxation amplitude depends on [87]:

- the peak stress: when σ_{peak} increases, the elastic contribution is more important. The viscous contribution remains identical.

- the initial loading rate: when $\dot{\epsilon}$ increases, the peak stress increases and the stress-relaxation

amplitude is enhanced.

The strain-relaxation amplitude was also shown to depend on the hydration state of the sample: Chimich *et al.* plotted normalized stress-time plot to compare the different hydration conditions of ligaments [88]. They found that the stress-relaxation amplitude is enhanced when the water content increases. Other biological tissues were investigated by stress-relaxation experiments such as rat tendon [89], rabbit jaw joint disc [90] or rat skin and rat perimysium [91]. Given the absence of structural reorganizations, the hypothesis that stress-relaxation phenomenon seem to be independent on collagen microstructure was proposed [89, 91].

From observations of the viscoelastic response of biological tissues, Fung proposed a quasi-linear viscoelaticity model to explain their behavior [92]. Instead of only being a function of time (linear viscoelasticity), the relaxation function depends on both time and strain. It appeared that this model does not apply to all biological tissues *e.g.* ligaments [93]. Therefore the viscoelastic behavior of biological tissues appears even more complex and requires other constitutive equations [94]. A more simple way to fit the viscoelastic response of biological tissues that accounts for both time and strain dependencies is to use a power-law dependence of stress on strain and time [95, 96]:

$$\sigma(\epsilon, t) = \sigma_0 \times t^{n(\epsilon)} \tag{1.2}$$

with σ_0 the peak stress (depends on the applied strain) and n the strain-dependent rate of relaxation. This equation is used within the 100 first seconds of the stress-relaxation response and gives exponents on the order of magnitude of -0.1.

1.3.2.3 Fatigue behavior

Cyclic loading-unloading tests are used to probe dynamically long-term properties of materials usually until failure. From a practical point of view, it should be ensured that the sample does not slip during the test to provide unaltered data. When the sample is subjected to potential drying, the test should be performed in immersed conditions. As displayed in **Figure 1.18, left**, fatigue tests can be stress controlled (meaning that a maximum stress is applied for the loading curve). They can also be strain controlled (in this case, a maximum strain is applied). The first cycle tends to have a large hysteresis contrary to the following cycles (see **Figure 1.18, right**). Characteristic values are the stress level, strain level, potential stress-relaxation and creep phenomenon during the test, cycle frequency, cycle area and a parameter that can represent the potential ultrastructural damages of the material during cycling such as the secant modulus.

The tendon is the most studied collagen-rich tissue in the literature [97], because tendons support cyclic movements during the lifetime of the vertebrates. When cycled at low stresses, samples are expected to fail earlier than they would during a usual stress-strain experiment [98] due to fatigue effects that induce irreversible changes in the microstructure. The Young modulus was proposed as a relevant characteristic to follow material damage [99] but other studies found it highly variable and sample-dependent [100]. The general fatigue behavior of tendons is that their stiffness is supposed to increase at the beginning of the test due to forced alignment, followed by a slow decrease when damage starts to occur, until a dramatic decrease just before failure [100]. However, this behavior is not always observed depending on the testing conditions or tests analysis [101].

Indeed, different cyclic conditions are used in the literature. Most of the time, collagen-rich tissues are preconditioned to get rid of the strain-memory effect. Starting from the same initial

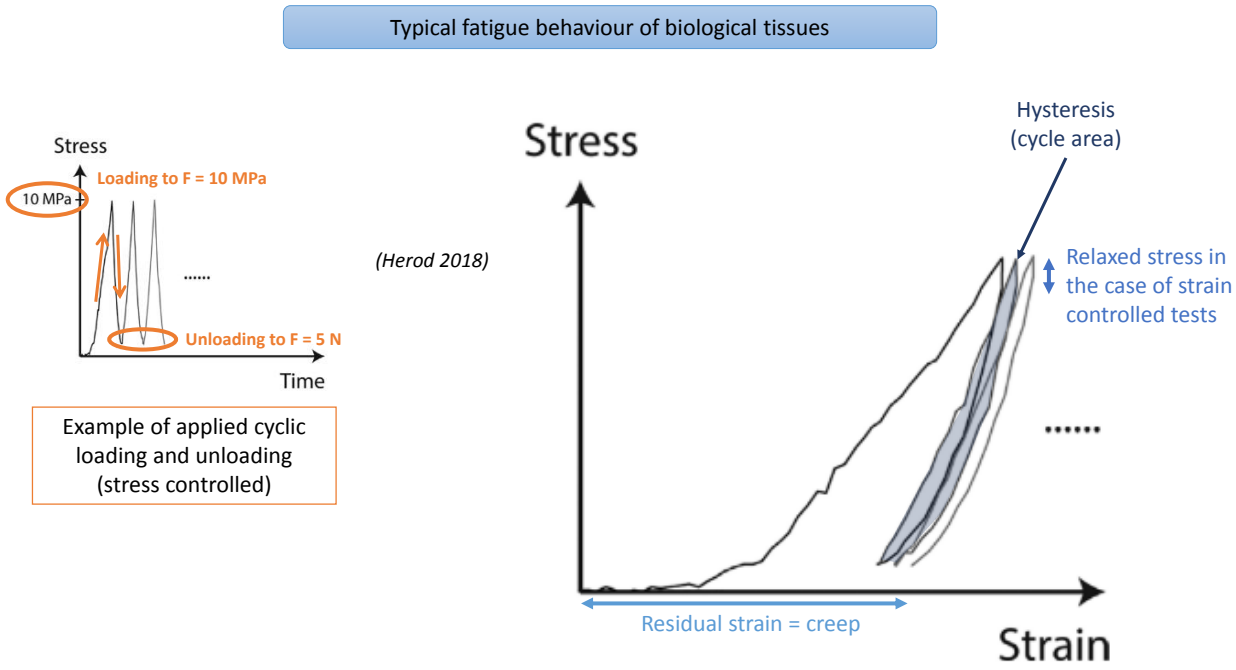

Figure 1.18: Typical fatigue behavior of biological tissues.

conditions enables to improve reproducibility, even though preconditioning conditions themselves are not straightforward [102]. The advantage of using collagen gels is that their history is well known thus no preconditioning should be required to study their fatigue behavior. We chose to perform fatigue tests by imposing a maximum strain (a maximum stress can also be imposed [103]) and a minimum load (a minimum displacement can also be imposed; it was shown that steer tendons tend to fail earlier with the minimum displacement condition [104] due to the bending of the sample). The frequency at which the test is performed may also influence the mechanical response of the material [98]. We chose a frequency of 0.06 Hz due to the limitations of the Instron machine which is normally not dedicated to high frequency fatigue testing. Finally, continuous loading-unloading loops [105] or loading-unloading steps [106] can be performed which may also modify the mechanical behavior of the sample. We chose to perform continuous loops to mimick a repetitive movement.

1.3.2.4 Fracture behavior

The ability of a material to dissipate energy is linked to its fracture properties (resistance to fracture propagation). Typically, single edge notch fracture tests are performed as in **Figure 1.19**. Upon stretching, the crack tends to open widely in the tissue and then propagates until catastrophic failure. Classic stress-strain curves are obtained. A fracture energy density, linked to the ability of the material to dissipate energy to slow down crack propagation, can be calculated using a formula initially defined for rubber materials [107]:

$$G_c = \frac{6 \times c \times W}{\sqrt{\lambda_c}} \tag{1.3}$$

where G_c is the fracture energy density (J/m^2), c the initial notch length (mm), W the strain energy density (area under the loading curve) (kPa), λ_c the stretch ratio at break. By definition, $\lambda = 1 + \epsilon$.

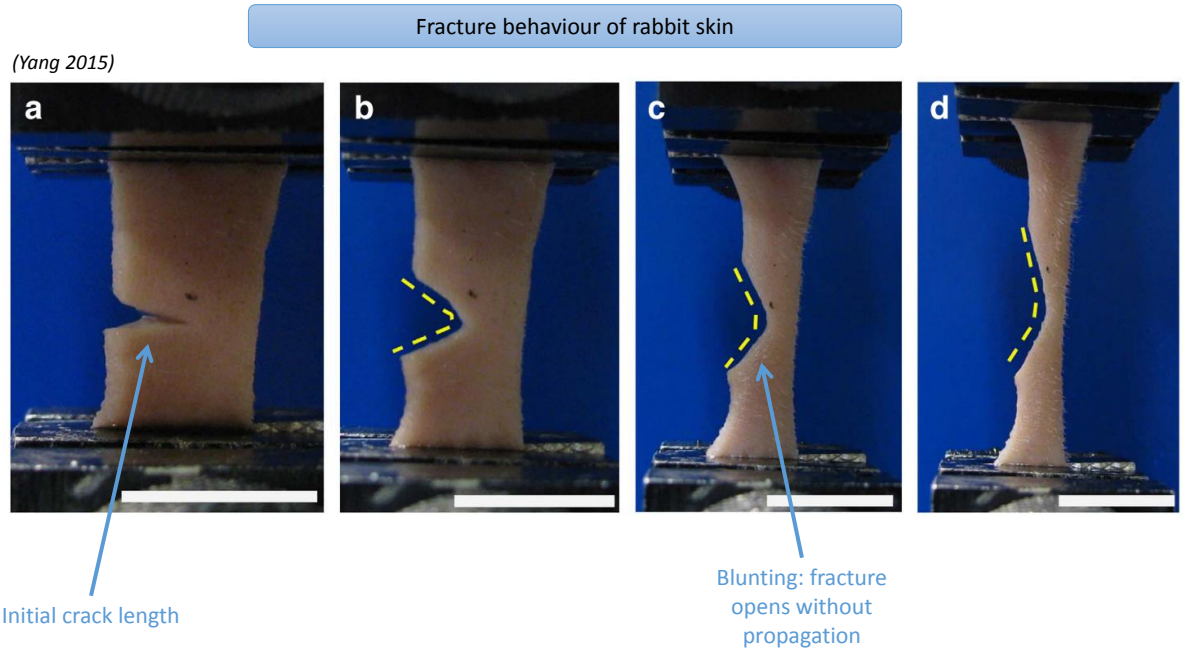

Figure 1.19: Typical fracture behavior of biological tissues.

Different geometries other than single edge notch can be used to perform fracture tests, such as central notch [108]. For the sake of simplicity, we chose to perform single edge notch tests. The fracture propagation observed in rabbit skin [108] and displayed in **Figure 1.19** was also observed in tendon [97]. The fracture energy density of biological tissues is about 200 kJ/m^2 [109]. It appears that stiffer tissues have reduced fracture energies [110]. Finally, the ultrastructural heterogeneities of biological tissues may be one of their strengths to slow down crack propagation [111].

1.3.3 Mechanical testing and data analysis: lack of uniformity in methods

1.3.3.1 Experimental difficulties

A great amount of literature is available about mechanical testing of biological samples. However only few papers really consider biological samples as hydrogels. A hydrogel always interacts with its environment by means of exchanges: solvent or small molecules for instance. It can thus swell or deswell depending on the solvent, that produces osmotic pressure. Hence the definition of preparation conditions, storage and experimental conditions is of high importance. While some papers show results on completely dry samples (*e.g.* [25]) which dramatically enhances mechanical properties due to the loss of water, leading to a collapse of the collagen network, others perform tests on completely immersed samples (*e.g.* [63, 112]) which definitely induces a decrease of mechanical properties in comparison but preserves the water content. In between, some samples are tested while receiving drops of saline solution to prevent them from drying or swelling (e.g. [113, 114]). The latter seems to be the best compromise to keep samples as close as possible to preparation conditions (assuming that storage does not have a high influence on the material) if the test is quick (*e.g.* for tensile tests, stress-relaxation tests).

Other problems can arise during the tests due to the clamps used to maintain the sample at each end. The sample can break in the clamps (if they are too tight or not adapted to fragile

samples), just outside of the clamp (due to stress concentration upon tightening). Hydrated samples also tend to slip during the tests. Besides, samples need to be homogeneous both in composition and shape/size/dimensions to give reproducible and relevant results, which is complicated with biological samples. For example, if the width of a sample is too large compared to its length (as in [112]), hydrostatic tension appears which may artificially increase the stiffness. All these phenomena can produce biased results.

1.3.3.2 Analysis methods

After testing, resulting data is analyzed. There are two mains choices. Let us consider collagen samples submitted to tensile tests. First, one has to chose which definition of stress is the more relevant: true stress or engineering stress? True stress takes into account the diminution of the cross-section of the sample while engineering stress does not which leads to completely different behaviors at large strains. It was shown that true stress is more relevant in the case of skin mechanical testing because it gives more realistic values of the stress [115]. Skin is a collagen-rich tissue; therefore true stress may be relevant for other collagenous materials submitted to uniaxial tensile forces. Nevertheless, measuring the cross-section during the test at each time point can be difficult because biological samples may not have isochoric deformation.

Second, the obtained stress-strain curve is probably J-shaped with three distinct regimes [66] as represented in **Figure 1.15**. How can one define the Young modulus of a biological sample? It is sometimes calculated at fixed strain values (e.g. 4%, 6%, 8% [78]), only from the slope in the linear region of the curve [113, 115, 116]) or from both heel and linear regions [25]. It seems highly relevant to calculate a moduli from the linear region since it is closest to the modulus' definition. However it is also useful to approximate the slope at small strains in order to provide more informations on the behavior of the material. Therefore it would be interesting to define standard strain values at which the Young modulus would be calculated for comparison purposes.

1.4 Towards biomimetism and less invasive surgical procedures: processes for making dense collagen matrices

Since nature is an infinite source of inspiration, biomimetic approaches are a growing trend in research - especially in materials science (combining Biology, Physics and Chemistry) [117]. When it comes to tissue regeneration, biomimetism is of crucial importance: the biomaterial should have characteristics as close as possible to the native tissue (together with its price/quality ratio). LCMCP dedicated their research in the field by forming the hypothesis that aside composition and mechanical properties, the three dimensional organization of the biomaterial is of high importance. Otherwise colonization, vascularization and resorption by host cells cannot happen [118].

It remains difficult to commercialize laboratory-made biomaterials due to strict regulations and their rapid evolution, and numerous tests are needed (*in vitro*, *in vivo* with the relevant animal model, clinical). Those are among the reasons why autologous-transplant remains the gold standard for guided tissue regeneration, even though it increases the number of surgical operations for the patient and it may require a higher amount of tissue than is actually available. Type I collagen being the major component of the ECM, and given its considerable role in it as explained before, some teams are working on collagen-based materials for tissue engineering. In order to bridge the so-called "death valley" between laboratories and the market, simplicity in the composition of the

biomaterial and competitivity are the keys (*i.e.* using already implanted raw materials could be a desirable solution). Injectable biomaterials have a great potential in this field thanks to their easy use and reduced invasiveness in terms of surgical procedures. Nevertheless, injection is not the only solution to all pathologies in the wide field of tissue regeneration. Therefore its use is mostly oriented towards filling small defects in tissues more or less accessible. Still, our approach may provide a basis for other applications: some examples were studied in Chapter 5.

1.4.1 Non-injectable dense collagen matrices

There are several methods to produce dense collagen gels: reverse dialysis [119] (**Figure 1.20, top A**), evaporation [120](**Figure 1.20, top B**), plastic compression [121](**Figure 1.20, top C**), continuous injection [122] (**Figure 1.20, top D**) and combined injection and reverse dialysis [54](**Figure 1.20, bottom**). They all have advantages and drawbacks.

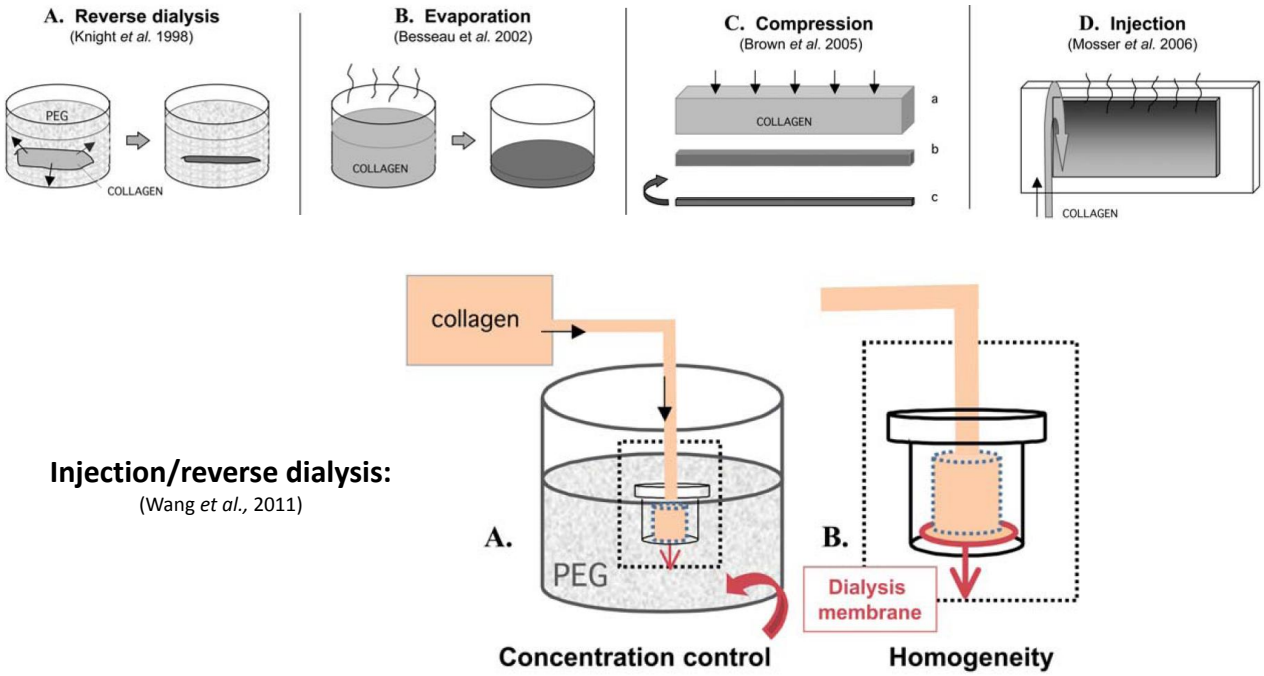

Figure 1.20: Different processes for making concentrated collagen gels. Reproduced and modified from Wang 2011 [54].

Reverse dialysis (**Figure 1.20, top A**) promotes collagen self-assembly because the diffusive process is quite slow. Polyethylene glycol (PEG) is classically used [119]. It is dissolved in the same solvent as the collagen solution but at higher concentration. Water molecules diffuse out of the dialysis membrane containing the collagen solution to equilibrate the difference in polymer concentration because the cut-off is too small to let PEG penetrate the membrane. Thus, the collagen solution is progressively concentrated, enabling mesophases to form if the concentration is high enough. However when reaching high concentrations (*e.g.* about 100 mg/mL, from very dilute solutions, *e.g.* 2 mg/mL) a large collagen solution volume is required. A concentration gradient takes place inside the dialysis membrane (the collagen solution in contact with the membrane equilibrates faster than the collagen solution at the center) which makes it difficult to remove from the membrane and to homogenize afterwards. At high concentrations, the collagen solution actually forms a physical gel (see **Figure 1.21**)

that is quite sticky and hard to remove from dialysis membranes without altering the organization. If the fibrillogenesis *in vitro* is induced before removing the collagen solution, there is no control of the morphology and the dimensions of the gel.

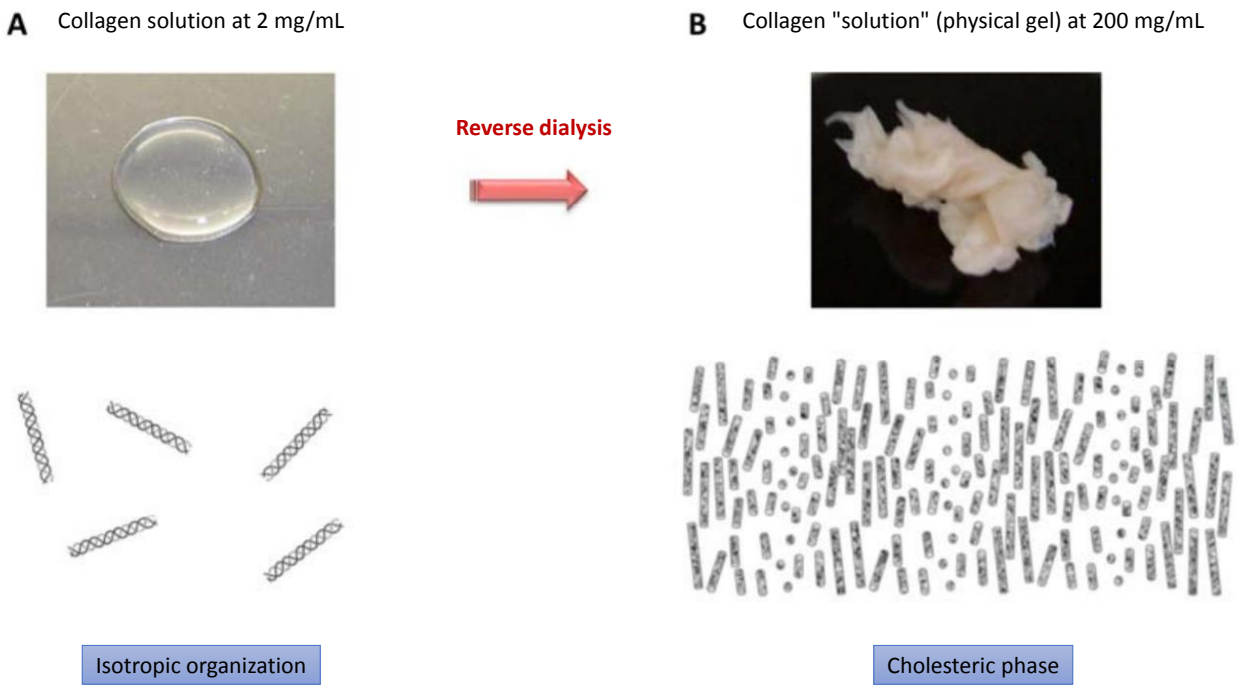

Figure 1.21: From a dilute collagen solution to a highly concentrated physical collagen gel by reverse dialysis. Reproduced and modified from Wang 2012 [123].

Evaporation (**Figure 1.20, top B**) also promotes collagen self-assembly by enabling slow reorganizations upon concentration. Starting from a large volume of dilute collagen solution, the solvent evaporates progressively thus increasing collagen concentration. However, several problems arise:

- it is possible that water molecules evaporate but other molecules may not completely evaporate (*e.g.* acetic acid) thus concentrating the collagen solution both in collagen and in ions, leading to a possible increase of both pH and ionic strength.
- a concentration gradient appears between the upper (in contact with air) and bottom part of the solution. This gradient limits further solvent evaporation by sometimes forming a layer of highly concentrated collagen on the top that acts as a skin, but can be limited by mixing regularly the solution. Nevertheless, this induces shear which perturbates the organization.
- due to the high increase in viscosity upon collagen concentration, it is experimentally difficult to reach concentrations above 60 mg/mL.
- it is difficult to control the 3D shape of the final material.

Compression (**Figure 1.20, top C**) consists in removing water from the gel (which is fibrillar in most cases) by applying a load onto it. The solvent is removed because the fibrillar solution is placed on a fine mesh. This process prevents the self-assembly properties of collagen to occur because collagen fibrils do not self-assemble, contrary to collagen molecules. This process forms gels that can

be dense but not biomimetic (no formation of mesophases prior to concentration, and water content may not be high enough).

Injection coupled with evaporation(**Figure 1.20, top D**) allows collagen molecules to self-assemble, as in the simple evaporation process, and to control the 2D geometry of the sample. A dilute collagen solution is continuously injected between two plates at a slow rate. The loss of volume between the plates, due to collagen concentration by evaporation, is balanced by the flow of dilute collagen solution. However, evaporation only occurs on one side of the solution thus leading to a concentration gradient. The final concentration of the solution is not controlled. Besides, the shape of the material is not three-dimensional.

Finally, the injection coupled with reverse dialysis (**Figure 1.20, bottom**) is a good compromise: it enables collagen molecules to self-assemble by slow diffusive processes thanks to dialysis, to control the volume of the sample thanks to continuous slow injection and the size and shape by using different molds. The sample is homogeneous in terms of concentration. However, such a collagen matrix is not injectable.

Interestingly, few of the mentioned collagen matrices were mechanically characterized. As an example, we chose to describe results of mechanical tests performed on collagen matrices made by plastic compression [121]. The first gels were concentrated up to $\approx$ 20wt%, with a UTS equal to $\approx$ 1.5 MPa, strain at break equal to $\approx$ 55% and Young's modulus around $\approx$ 1.4 MPa. After checking on the provided curve, the Young modulus was calculated in the linear part of the tensile curve. Double compression was then tested, also with different shapes (tubes for instance) giving the same order of magnitude for concentration, UTS, y_{strain} and linear modulus [124]. This technique enables to make collagen hydrogels with characteristics close to human living tissues: linear modulus approaching the value for ligament, UTS and y_{strain} similar to that of cartilage. Even though those gels have similar features with living tissues their structure is not biomimetic (see **Figure 1.22 a)**) as discussed before. Also, the collagen sheets are dense but the distance between the sheets reminds that of porous collagen sponges. Besides, the final material is too viscous to be injected. The implantation would be made by classical surgery procedures *i.e.* opening, putting the material in place, closing the wound which is an additional trauma for the patient. Hence, the need for injectable collagen hydrogels.

1.4.2 Injectable collagen gels with low collagen concentration and poor mechanical properties

Knapp and co-workers succeded in injecting 15 mg/mL collagen matrix through a 30 G needle (inner diameter equal to 0.16 mm, typically used for filler in aesthetic surgery) under human skin for soft tissue regeneration. However, they noticed that the gel lost volume in the day following the injection, leading to repeated injections in order to complete the treatment [125]. This volume reduction is due to the remodeling (contraction) of the injected material by cells, more specifically fibroblasts [126]. When collagen gels are more concentrated, it was shown that cell-induced contraction is slower and reduces less the volume of the gel [127]. The resorption rate may also be slowed down [128]. Therefore, a fast volume reduction of an implanted collagen matrix is probably due to insufficient collagen concentration. Repeated injections for aesthetic surgery are still a standard procedure nowadays, demonstrating that no process is able to make highly concentrated and injectable collagen matrices for the moment.

More recently, attempts to reproduce cartilage were made. A 10 mg/mL injectable collagen hydrogel showed no biomimetic organization after fibrillogenesis as shown by the numerous pores in **Figure**

1.22 b) and has a compressive modulus equal to 7 kPa [129] (no precision given on how it was calculated). This value is lower than the compressive modulus of bovine articular cartilage (around 1 MPa) [130] or than that of human articular cartilage (around 10 MPa) [131]. It is worth noticing that cartilage contains mainly type II collagen and a high amount of proteoglycans [132].

The mechanical properties of injectable hydrogels could be improved by dramatically increasing their collagen concentration. Such injectable hydrogels found in the literature made of 100 % collagen are thus not able to reproduce the architecture and mechanical properties of targeted tissues, due to their low concentration restricted by injectability limits. Solutions have to be found to propose stiffer collagen-based materials that are also injectable.

1.4.3 Non-biomimetic injectable collagen-based materials

Collagen-based materials do not contain collagen only: they can contain organic or inorganic moieties. The risk of using such hydrogels is the potential inflammatory response associated to the non-collagen moiety. Several types of injectable hybrid collagen gels can be found in the literature. An acrylated collagen gel (less than 4 mg/mL collagen) containing rat muscle cells showed little cytotoxicity but had the same volume loss as its 100 % collagen equivalent by cell-mediated contraction. Assessed by rheological measurements, its Young's modulus is about $\approx$ 160 kPa [133]. It is at least one order of magnitude above collagen gels described in the previous subsection. Yet this value is still below the stiffness of living tissues. Besides this hybrid gel might lead to an inflammatory response if animal-tested due to its non-biomimetic composition and its residual cytotoxicity.

Glutaraldehyde crosslinking is a widespread technique for collagen gels reinforcement: it reduces the creeping processes. A collagen-glycosaminoglycan-poly(vinyl alcohol) hybrid gel crosslinked with glutaraldehyde for a final collagen concentration of 3 mg/mL showed an UTS$\approx$ 0.15 MPa, $y_{strain} \approx 10$ % and modulus $\approx$ 1.5 MPa without cytotoxicity [134]. Those values are much closer to non-injectable collagen scaffolds. However the gel composition and structure are not biomimetic as seen in **Figure 1.22 c)**. And it is known that glutaraldehyde leads to an inflammatory response [135] therefore this method is not an ideal solution.

1.4.4 Dense and injectable collagen scaffolds with recent techniques

Recently, Nazhat *et al.* developed an aspiration-ejection system of dilute fibrillar collagen gels [136]. It consists in aspiring dilute fibrillar collagen gels, and removing water upon extrusion which compacts the collagen fibrils. However no mechanical tests were performed. One year later, the technique was improved and collagen gels were submitted to tensile testing [137]. For a 180 mg/mL collagen fibrillar concentration, the gel exhibited an UTS $\approx$ 0.45 MPa and a modulus E $\approx$ 3.1 MPa. Those values are comparable to non-injectable dense collagen matrices. However, it was noticed that there was less fibrillar alignment and more porosity in the gels than in living tissues. Besides, the fibrils are not homogeneous in diameter as shown in **Figure 1.22 d)**. As for plastic compression, collagen self-assembly is avoided because collagen fibrils do not have the ability to self-assemble and form mesophases.

1.4.5 Our strategy for making biomimetic and injectable collagen scaffolds

As mentioned previously, the LCMCP has developed strategies for making biomimetic collagen scaffolds having features close to that of native biological tissues.

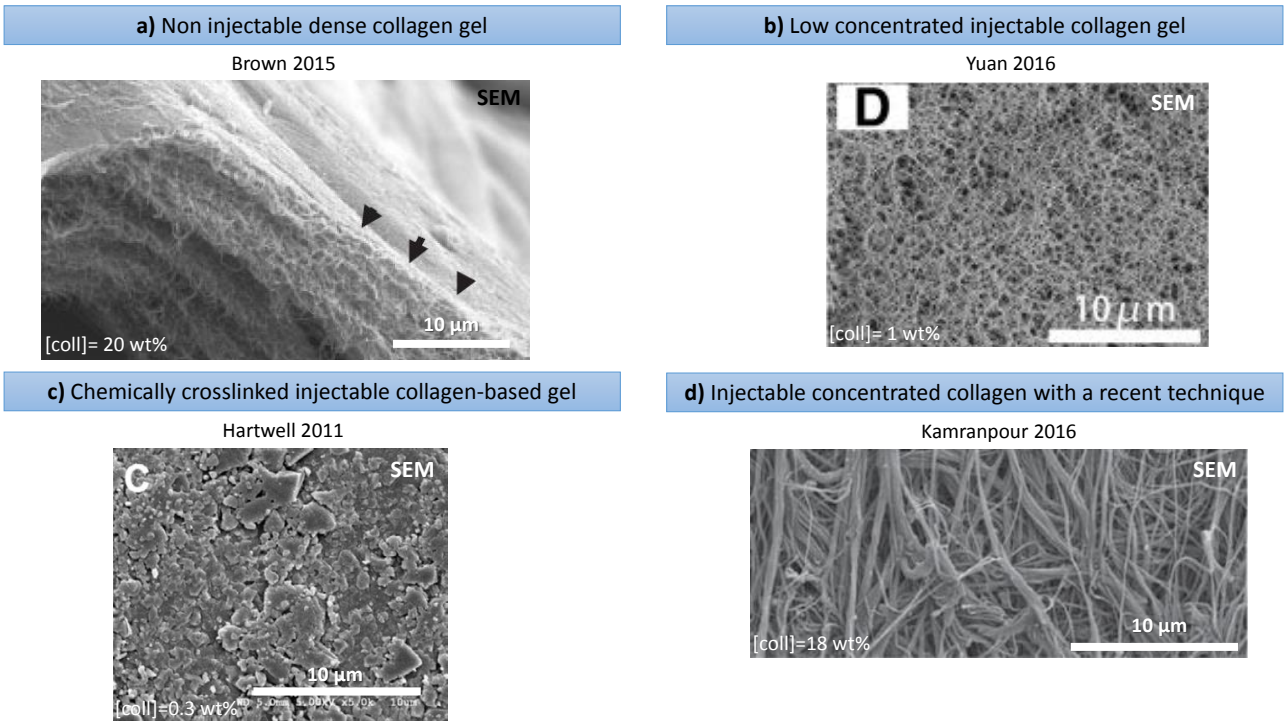

Figure 1.22: SEM micrographs of collagen matrices, injectable or not, obtained by different methods. Reproduced from Brown 2005 [121], Yuan 2016 [129], Hartwell 2011 [134] and Kamranpour 2016 [137].

We chose type I collagen as the building block for our materials because of its abundance in the ECM. The underlying hypothesis of this work is that dense and organized type I collagen (due to its lyotropic properties) is a necessary and sufficient condition for making scaffolds that are biomimetic and that will be integrated by the cells during guided tissue regeneration. Thus, we will be able to make *in vitro* highly concentrated collagen solutions, inject them in a targeted tissue defect, and fibrillogenesis *in situ* would occur to finally form a dense collagen matrix with the required properties (*in situ* formation of a transplant-like material).

To do so, we have to:

- circumvent the high viscosity of collagen solutions upon concentration.
- recover the self-assembly properties of collagen molecules after injection.
- not disturb its organization upon injection.
- control the concentration of the matrix.
- fill the targeted defect.

Therefore, the strategy consists in making highly concentrated (dry) collagen beads by means of a spray-drier (**Figure 1.23**). The collagen beads will be injected through an as thin as possible needle (to match harshest conditions *i.e.* fillers) thanks to an injectable fluid that will act as a vector. After injecting the collagen beads, they will dissolve to form a highly concentrated collagen solution. While collagen molecules self-assemble according to the phase diagram, fibrillogenesis will occur due to the increase of pH (physiological pH in living tissues) thus forming a self-assembled, biomimetic collagen matrix *in situ* that will serve as a support for cell colonization, vascularization and finally remodeling by resorbing the matrix and forming new tissue. The spray-drying process enables to start from a

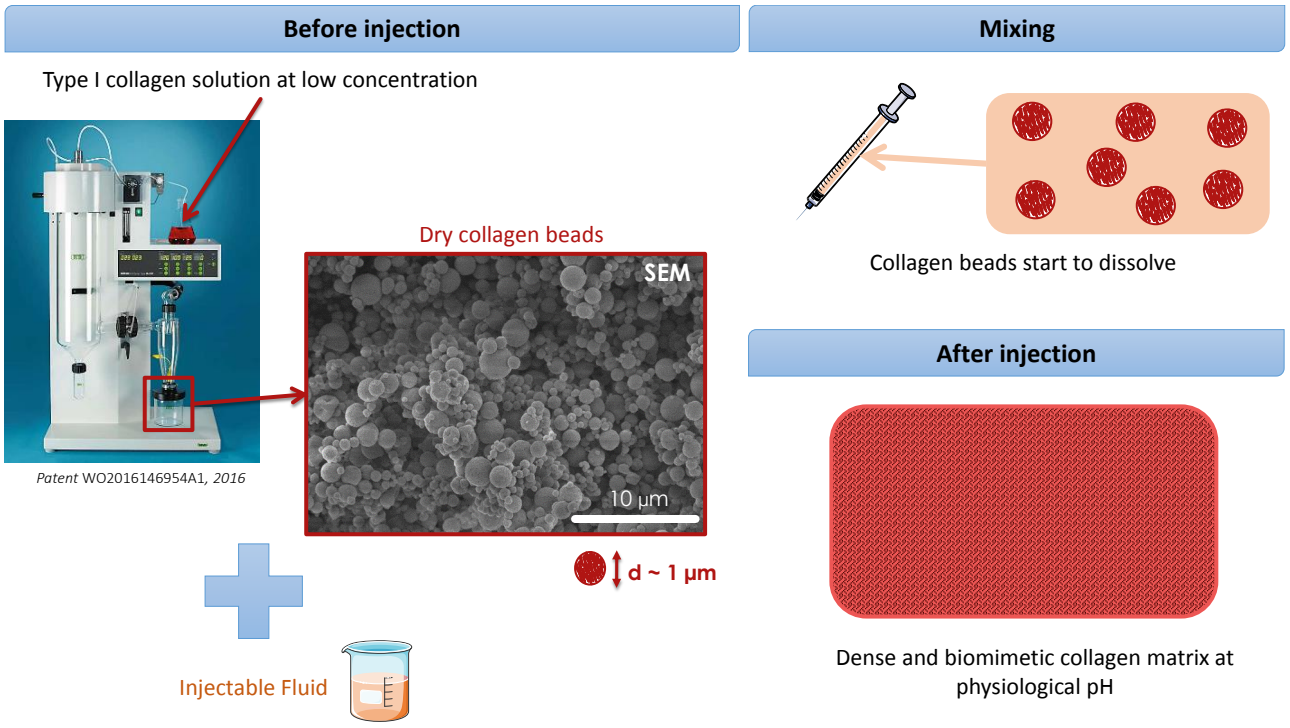

Figure 1.23: Our approach for making dense and injectable collagen scaffolds.

raw material that is already highly concentrated in collagen. Therefore this processing technique does not require the use of crosslinkers. Those are the main strengths of the process. The main challenge will be to adapt a process initially designed for high temperatures and high solution/air flows to thermo-sensitive biomolecules in viscous solutions.

Bibliography

1. Fratzl, P. *Collagen: Structure and Mechanics* (2008).
2. Prockop, D. J. & Kivirikko, K. I. COLLAGENS : Molecular Biology , Diseases , and Potentials. *Annu. Rev. Biochem* **64,** 403–34 (1995).
3. Jang, I. S. & Park, S. J. Hydroxyproline-containing collagen peptide derived from the skin of the Alaska pollack inhibits HIV-1 infection. *Molecular Medicine Reports* **14,** 5489–5494 (2016).
4. Schilb, L., Fiegel, V. & Knighton, D. R. Hydroxyproline measurement by high performance liquid chromatography: An improved method of derivatization. *Journal of Liquid Chromatography* **13,** 557–567 (1990).
5. Cissell, D. D., Link, J. M., Hu, J. C. & Athanasiou, K. A. A Modified Hydroxyproline Assay Based on Hydrochloric Acid in Ehrlich's Solution Accurately Measures Tissue Collagen Content. *Tissue Engineering Part C: Methods* **23,** 243–250 (2017).
6. Alberts, B. *et al. Molecular Biology of the Cell, 4th edition* Garland Sc, 1224 (New York, 2002).
7. Myllyharju, J. Intracellular post-translational modifications of collagens. *Topics in Current Chemistry* **247,** 115–147 (2005).
8. Bhattacharjee, A. & Bansal, M. Collagen Structure: The Madras Triple Helix and the Current Scenario. *IUBMB Life (International Union of Biochemistry and Molecular Biology: Life)* **57,** 161–172 (2005).
9. Gelse, K., Pöschl, E. & Aigner, T. Collagens - Structure, function, and biosynthesis. *Advanced Drug Delivery Reviews* **55,** 1531–1546 (2003).
10. Nguyen, T. T. *et al.* Raman comparison of skin dermis of different ages: Focus on spectral markers of collagen hydration. *Journal of Raman Spectroscopy* **44,** 1230–1237 (2013).
11. Canty, E. G. & Kadler, K. E. Procollagen trafficking, processing and fibrillogenesis. *Journal of cell science* **118,** 1341–1353 (2005).
12. Hulmes, D. J. S. Building Collagen Molecules, Fibrils, and Suprafibrillar Structures. *Journal of structural biology* **137,** 2–10 (2002).
13. Eyre, D. R. & Wu, J. J. Collagen cross-links. *Topics in Current Chemistry* **247,** 207–229 (2005).
14. Kadler, K. E., Holmes, D. F., Trotter, J. A. & Chapman, J. A. Collagen Fibril Formation. *Biochemical Journal* **316,** 1–11 (1996).
15. Fang, M. *et al.* Type I collagen D-spacing in fibril bundles of dermis, tendon, and bone: Bridging between nano- and micro-level tissue hierarchy. *ACS Nano* **6,** 9503–9514 (2012).
16. Meek, K. M. & Fullwood, N. J. Corneal and scleral collagens - A microscopist's perspective. *Micron* **32,** 261–272 (2001).

17. Parry, D. A., Barnes, G. R. & Craig, A. S. A comparison of the size distribution of collagen fibrils in connective tissues as a function of age and a possible relation between fibril size distribution and mechanical properties. *Proceedings of the Royal Society of London - Biological Sciences* **203,** 305–321 (1978).

18. Mouw, J. K., Ou, G. & Weaver, V. M. Extracellular matrix assembly: a multiscale deconstruction. *Nature reviews. Molecular cell biology* **15,** 771–785 (2014).

19. Shoulders, M. D. & Raines, R. T. Collagen Structure and Stability. *Annual Review of Biochemistry* **78,** 929–958 (2009).

20. Tanrikulu, I. C., Forticaux, A., Jin, S. & Raines, R. T. Peptide tessellation yields micrometre-scale collagen triple helices. *Nature Chemistry* **8,** 1008–1014 (2016).

21. Zachariades, P. A. Recherches sur la structure du tissu conjonctif, sensibilité du tendon aux acides. *Cr Séanc. Soc. Biol* **52,** 182–4 (1900).

22. Highberger, J. H. The Isoelectric Point of Collagen. *Journal of the American Chemical Society* **61,** 2302–2303 (1939).

23. Jackson, D. & Neuberger, A. Observations on the isoionic and isoelectric point of acid-processed gelatin from insoluble and citrate-extracted collagen. *Short communications* **26,** 638–639 (1957).

24. GROSS, J. & KIRK, D. The heat precipitation of collagen from neutral salt solutions: some rate-regulating factors. *The Journal of biological chemistry* **233,** 355–360 (1958).

25. Christiansen, D. L., Huang, E. K. & Silver, F. H. Assembly of type I collagen: Fusion of fibril subunits and the influence of fibril diameter on mechanical properties. *Matrix Biology* **19,** 409–420 (2000).

26. Ehrmann, R. L. & Gey, G. O. The growth of cells on a transparent gel of reconstituted rat-tail collagen. **16,** 1375–1403 (1956).

27. Sriramoju, V. & Alfano, R. R. In vivo studies of ultrafast near-infrared laser tissue bonding and wound healing. *Journal of Biomedical Optics* **20,** 108001 (2015).

28. Cisneros, D. A., Hung, C., Franz, C. M. & Muller, D. J. Observing growth steps of collagen self-assembly by time-lapse high-resolution atomic force microscopy. *Journal of Structural Biology* **154,** 232–245 (2006).

29. Yang, L., van der Werf, K. O., Dijkstra, P. J., Feijen, J. & Bennink, M. L. Micromechanical analysis of native and cross-linked collagen type I fibrils supports the existence of microfibrils. *Journal of the Mechanical Behavior of Biomedical Materials* **6,** 148–158 (2012).

30. Cooper, A. The precipitation of toroidal collagen fibrils. *Biochemical Journal* **112,** 515–519 (1968).

31. Schmitt, F. O., Gross, J. & Highberger, J. H. A new particle type in certain connective tissue extracts. *Proceedings of the National Academy of Sciences* **39** (1953).

32. Paige, M. F. & Goh, M. C. Ultrastructure and assembly of segmental long spacing collagen studied by atomic force microscopy. *Micron* **32,** 355–361 (2001).

33. Leikina, E., Mertts, M. V., Kuznetsova, N. & Leikin, S. Type I collagen is thermally unstable at body temperature. *Proceedings of the National Academy of Sciences* **99,** 1314–1318 (2002).

34. Nomura, Y., Toki, S., Ishii, Y. & Shirai, K. The physicochemical property of shark type I collagen gel and membrane. *Journal of Agricultural and Food Chemistry* **48,** 2028–2032 (2000).

35. Rosenbloom, J., Harsch, M. & Jimenez, S. Hydroxyproline content determines the denaturation temperature of chick tendon collagen. *Archives of Biochemistry and Biophysics* **158,** 478–484 (1973).

36. Ramachandran, G. N. & Chandrasekharan, R. Interchain hydrogen bonds via bound water molecules in the collagen triple helix. *Biopolymers* **6,** 1649–1658 (1968).

37. Miles, C. A. & Bailey, A. J. Thermally labile domains in the collagen molecule. *Micron* **32,** 325–332 (2001).

38. Miles, C. A., Avery, N. C., Rodin, V. V. & Bailey, A. J. The increase in denaturation temperature following cross-linking of collagen is caused by dehydration of the fibres. *Journal of Molecular Biology* **346,** 551–556 (2005).

39. Tiktopulo, E. I. & Kajava, A. V. Denaturation of type I collagen fibrils is an endothermic process accompanied by a noticeable change in the partial heat capacity. *Biochemistry* **37,** 8147–8152 (1998).

40. Miles, C. A., Burjanadze, T. V. & Bailey, A. J. The kinetics of the thermal denaturation of collagen in unrestrained rat tail tendon determined by differential scanning calorimetry. *Journal of molecular biology* **245,** 437–46 (1995).

41. Shayegan, M. *et al.* Probing multiscale mechanics of collagen with optical tweezers. *Optical Trapping and Optical Micromanipulation X* **8810,** 88101P (2013).

42. Bouligand, Y. & Giraud-Guille, M.-M. in *Biology of Invertebrate and Lower Vertebrate Collagens* (eds Bairati, A. & Garrone, R.) 115–134 (Springer US, Boston, MA, 1985).

43. Bouligand, Y. Liquid crystals and biological morphogenesis: Ancient and new questions. *Comptes Rendus Chimie* **11,** 281–296 (2008).

44. Tissue, C. 1988 -M. M. Giraud-Guille – Twisted plywood architecture of collagen fibrils in human compact bone osteons, 167–180 (1988).

45. Giraud-Guille, M.-M. Cholesteric Twist of Collagen In Vivo and In Vitro. *Molecular Crystals and Liquid Crystals Incorporating Nonlinear Optics* **153,** 15–30 (1987).

46. Giraud-Guille, M. M. Liquid crystallinity in condensed type I collagen solutions. A clue to the packing of collagen in extracellular matrices. *Journal of Molecular Biology* **224,** 861–873 (1992).

47. Giraud-Guille, M. M. & Besseau, L. Banded patterns in liquid crystalline phases of type I collagen: Relationship with crimp morphology in connective tissue architecture. *Connective Tissue Research* **37,** 183–193 (1998).

48. Besseau, L. & Giraud-Guille, M. M. Stabilization of fluid cholesteric phases of collagen to ordered gelated matrices. *Journal of Molecular Biology* **251,** 197–202 (1995).

49. Giraud-Guille, M. Liquid crystalline order of biopolymers in cuticles and bones. *Microscopy Research and Technique* **27,** 420–428 (1994).

50. Giraud-Guille, M. M., Besseau, L. & Martin, R. Liquid crystalline assemblies of collagen in bone and in vitro systems. *Journal of Biomechanics* **36,** 1571–1579 (2003).

51. Giraud-Guille, M. M., Mosser, G. & Belamie, E. Liquid crystallinity in collagen systems in vitro and in vivo. *Current Opinion in Colloid and Interface Science* **13,** 303–313 (2008).

52. Nilsson, O. & Nygren, K. G. Scanning Electron Microscopy of Human Endometrium. *Upsala Journal of Medical Sciences* **77,** 3–7 (2016).

53. Gathercole, L. J. & Keller, A. Early development of crimping in rat tail tendon collagen: A polarizing optical and SEM study. *Micron (1969)* **9,** 83–89 (1978).

54. Wang, Y. *et al.* Controlled collagen assembly to build dense tissue-like materials for tissue engineering. *Soft Matter* **7,** 9659–9664 (2011).

55. Giraud-Guille, M. M. Direct visualization of microtomy artefacts in sections of twisted fibrous extracellular matrices. *Tissue and Cell* **18,** 603–620 (1986).

56. Giraud Guille, M. M., Nassif, N. & Fernandes, F. M. Collagen-based Materials for Tissue Repair, from Bio-inspired to Biomimetic. *Materials Design Inspired by Nature: Function Through Inner Architecture,* 107–127 (2013).

57. Wang, Y. *Elaboration de modèles collagène/apatite pour l'étude de la biominéralisation du tissu osseux* PhD thesis (2012).

58. Strom, S. & Michalopoulos, G. in *Methods in Enzymology* 544–555 (1982).

59. Ottani, V., Raspanti, M. & Ruggeri, a. Collagen structure and functional implications. *Micron (Oxford, England : 1993)* **32,** 251–260 (2001).

60. Buehler, M. J. Nanomechanics of collagen fibrils under varying cross-link densities: Atomistic and continuum studies. *Journal of the Mechanical Behavior of Biomedical Materials* **1,** 59–67 (2008).

61. Sun, Y. L., Luo, Z. P., Fertala, A. & An, K. N. Direct quantification of the flexibility of type I collagen monomer. *Biochemical and Biophysical Research Communications* **295,** 382–386 (2002).

62. Varma, S., Orgel, J. P. & Schieber, J. D. Nanomechanics of Type I Collagen. *Biophysical Journal* **111,** 50–56 (2016).

63. Sasaki, N. & Odajima, S. Elongation mechanisms of collagen fibrils and force-strain relations of tendons at each level of structural hierarchy. *Journal of Biomechanics* **29,** 1131–1136 (1996).

64. Buehler, M. J. Nature designs tough collagen: explaining the nanostructure of collagen fibrils. *Proceedings of the National Academy of Sciences of the United States of America* **103,** 12285–12290 (2006).

65. Screen, H. R. C., Lee, D. A., Bader, D. L. & Shelton, J. C. An investigation into the effects of the hierarchical structure of tendon fascicles on micromechanical properties. *Proceedings of the Institution of Mechanical Engineers. Part H, Journal of engineering in medicine* **218,** 109–19 (2004).

66. Fratzl, P. *et al.* Fibrillar structure and mechanical properties of collagen. *Journal of Structural Biology* **122,** 119–122 (1997).

67. Shergold, O. A., Fleck, N. A. & Radford, D. The uniaxial stress versus strain response of pig skin and silicone rubber at low and high strain rates. *International Journal of Impact Engineering* **32,** 1384–1402 (2006).

68. Pailler-Mattei, C., Bec, S. & Zahouani, H. In vivo measurements of the elastic mechanical properties of human skin by indentation tests. *Medical Engineering and Physics* **30,** 599–606 (2008).

69. Maganaris, C. N. & Paul, J. P. In vivo human tendon mechanical properties. *J Physiol* **521 Pt 1,** 307–13 (1999).

70. Wren, T. A., Yerby, S. A., Beaupré, G. S. & Carter, D. R. Mechanical properties of the human achilles tendon. *Clinical Biomechanics* **16,** 245–251 (2001).

71. Lewis, G. & Shaw, K. M. Modeling the tensile behavior of human Achilles tendon. *Bio-Medical Materials and Engineering* **7,** 231–244 (1997).

72. Shaw, K. & Lewis, G. Tensile properties of human Achilles tendon, 338–341 (1997).

73. Rains, J. K., Bert, J. L., Roberts, C. R. & Paré, P. D. Mechanical properties of human tracheal cartilage. *Journal of applied physiology (Bethesda, Md. : 1985)* **72,** 219–225 (1992).

74. Kempson, G. E., Muir, H., Pollard, C. & Tuke, M. The tensile properties of the cartilage of human femoral condyles related to the content of collagen and glycosaminoglycans. *BBA - General Subjects* **297,** 456–472 (1973).

75. Chandrashekar, N., Mansouri, H., Slauterbeck, J. & Hashemi, J. Sex-based differences in the tensile properties of the human anterior cruciate ligament. *Journal of Biomechanics* **39,** 2943–2950 (2006).

76. Hoeltzel, D. A. Strip Extensiometry for Comparison of the Mechanical Response of Bovine, Rabbit, and Human Corneas. *Journal of Biomechanical Engineering* **114,** 202 (1992).

77. Fung, Y. Elasticity of soft tissues in simple elongation. *American Journal of Physiology-Legacy Content* **213,** 1532–1544 (1967).

78. Wollensak, G., Spoerl, E. & Seiler, T. Stress-strain measurements of human and porcine corneas after riboflavin-ultraviolet-A-induced cross-linking. *Journal of Cataract and Refractive Surgery* **29,** 1780–1785 (2003).

79. Licup, A. J. *et al.* Stress controls the mechanics of collagen networks. **112** (2015).

80. Billiar, K. L. & Sacks, M. S. Biaxial Mechanical Properties of the Native and Glutaraldehyde-Treated Aortic Valve Cusp: Part II—A Structural Constitutive Model. *Journal of Biomechanical Engineering* **122,** 327 (2002).

81. Stylianopoulos, T. & Barocas, V. H. Volume-averaging theory for the study of the mechanics of collagen networks. *Computer Methods in Applied Mechanics and Engineering* **196,** 2981–2990 (2007).

82. Chandran, P. L. & Barocas, V. H. Microstructural mechanics of collagen gels in confined compression: poroelasticity, viscoelasticity, and collapse. *Journal of biomechanical engineering* **126,** 152–166 (2004).

83. Chandran, P. L. Affine Versus Non-Affine Fibril Kinematics in Collagen Networks: Theoretical Studies of Network Behavior. *Journal of Biomechanical Engineering* **128,** 259 (2006).

84. Van Der Rijt, J. A., Van Der Werf, K. O., Bennink, M. L., Dijkstra, P. J. & Feijen, J. Micromechanical testing of individual collagen fibrils. *Macromolecular Bioscience* **6,** 699–702 (2006).

85. Svensson, R. B., Hassenkam, T., Hansen, P. & Peter Magnusson, S. Viscoelastic behavior of discrete human collagen fibrils. *Journal of the Mechanical Behavior of Biomedical Materials* **3,** 112–115 (2010).

86. Silver, F. H., Christiansen, D. L., Snowhill, P. B. & Chen, Y. Role of storage on changes in the mechanical properties of tendon and self-assembled collagen fibers. *Connective tissue research* **41,** 155–64 (2000).

87. Mechanial properties of alveolar walls. *Journal of applied physiology* **25,** 689–695 (1968).

88. Chimich, D., Shrive, N., Frank, C., Marchuk, L. & Bray, R. Water content alters viscoelastic behaviour of the normal adolescent rabbit medial collateral ligament. *Journal of Biomechanics* **25** (1992).

89. Miller, K. S., Edelstein, L., Connizzo, B. K. & Soslowsky, L. J. Effect of Preconditioning and Stress Relaxation on Local Collagen Fiber Re-Alignment: Inhomogeneous Properties of Rat Supraspinatus Tendon. *Journal of Biomechanical Engineering* **134,** 031007 (2012).

90. Scapino, R. P., Canham, P. B., Finlay, H. M. & Mills, D. K. The behaviour of collagen fibres in stress relaxation and sress distribution in the jaw-joint disc of rabbits (1997).

91. Purslow, P. P., Wess, T. J. & Hukins, D. W. Collagen orientation and molecular spacing during creep and stress-relaxation in soft connective tissues. *The Journal of experimental biology* **201,** 135–42 (1998).

92. Fung, Y., Perrone, N. & Anliker, M. in *Biomechanics: Its Foundations and Objectives* Englewood, 181–208 (1972).

93. Provenzano, P., Lakes, R., Keenan, T. & Vanderby, R. Nonlinear ligament viscoelasticity. *Annals of Biomedical Engineering* **29,** 908–914 (2001).

94. Provenzano, P. P., Lakes, R. S., Corr, D. T. & Vanderby, R. Application of nonlinear viscoelastic models to describe ligament behavior. *Biomechanics and Modeling in Mechanobiology* **1,** 45–57 (2002).

95. Duenwald, S. E., Vanderby, R. & Lakes, R. S. Viscoelastic relaxation and recovery of tendon. *Annals of Biomedical Engineering* **37,** 1131–1140 (2009).

96. Hingorani, R. V., Provenzano, P. P., Lakes, R. S., Escarcega, A. & Vanderby, R. Nonlinear viscoelasticity in rabbit medial collateral ligament. *Annals of Biomedical Engineering* **32,** 306–312 (2004).

97. Ker, R. F. Mechanics of tendon, from an engineering perspective. *International Journal of Fatigue* **29,** 1001–1009 (2007).

98. Wang, X. T., Ker, R. F. & Alexander, R. M. Fatigue rupture of wallaby tail tendons. *The Journal of Experimental Biology* **198,** 847–852 (1995).

99. Schechtman, H. & Bader, D. L. Fatigue damage of human tendons. *Journal of Biomechanics* **35,** 347–353 (2002).

100. Fung, D. T. *et al.* Subrupture tendon fatigue damage. *Journal of Orthopaedic Research* **27,** 264–273 (2009).

101. Wren, T. A., Lindsey, D. P., Beaupré, G. S. & Carter, D. R. Effects of creep and cyclic loading on the mechanical properties and failure of human Achilles tendons. *Annals of Biomedical Engineering* **31,** 710–717 (2003).

102. Carew, E. O., Barber, J. E. & Vesely, I. Role of preconditioning and recovery time in repeated testing of aortic valve tissues: validation through quasilinear viscoelastic theory. *Annals of Biomedical Engineering* **28,** 1093–1100 (2000).

103. Fung, D. T. *et al.* Early response to tendon fatigue damage accumulation in a novel in vivo model. *Journal of Biomechanics* **43,** 274–279. arXiv: NIHMS150003 (2010).

104. Herod, T. W. & Veres, S. P. Development of overuse tendinopathy: A new descriptive model for the initiation of tendon damage during cyclic loading. *Journal of Orthopaedic Research* **36,** 467–476 (2018).

105. Szczesny, S. E., Aeppli, C., David, A. & Mauck, R. L. Fatigue loading of tendon results in collagen kinking and denaturation but does not change local tissue mechanics. *Journal of Biomechanics* **71,** 251–256 (2018).

106. Susilo, M. E., Paten, J. A., Sander, E. A., Nguyen, T. D. & Ruberti, J. W. Collagen network strengthening following cyclic tensile loading. *Interface Focus* **6** (2016).

107. Greensmith, H. W. Rupture of rubber. X. The change in stored energy on making a small cut in a test piece held in simple extension. *Journal of Applied Polymer Science* **7,** 993–1002 (1963).

108. Yang, W. *et al.* On the tear resistance of skin. *Nature Communications* **6,** 1–10 (2015).

109. Pro, J. W. & Barthelat, F. The fracture mechanics of biological and bioinspired materials. *MRS Bulletin* **44,** 46–52 (2019).

110. Purslow, P. P. Measurement of the fracture toughness of extensible connective tissues. *Journal of Materials Science* **18,** 3591–3598 (1983).

111. Fischer, F. D., Kolednik, O., Predan, J., Razi, H. & Fratzl, P. Crack driving force in twisted plywood structures. *Acta Biomaterialia* **55,** 349–359 (2017).

112. Tower, T. T., Neidert, M. R. & Tranquillo, R. T. Fiber alignment imaging during mechanical testing of soft tissues. *Annals of Biomedical Engineering* **30,** 1221–1233 (2002).

113. Pollock, C. M. & Shadwick, R. E. Relationship between body mass and biomechanical properties of limb tendons in adult mammals. *The American journal of physiology* **266,** R1016–R1021 (1994).

114. Akizuki, S. *et al.* Tensile properties of human knee joint cartilage: I. Influence of ionic conditions, weight bearing, and fibrillation on the tensile modulus. *Journal of Orthopaedic Research* **4,** 379–392 (1986).

115. Karimi, A. & Navidbakhsh, M. Measurement of the uniaxial mechanical properties of rat skin using different stress-strain definitions. *Skin Research and Technology* **21,** 149–157 (2015).

116. Roeder, B. A., Kokini, K., Sturgis, J. E., Robinson, J. P. & Voytik-Harbin, S. L. Tensile Mechanical Properties of Three-Dimensional Type I Collagen Extracellular Matrices With Varied Microstructure. *Journal of Biomechanical Engineering* **124,** 214 (2002).

117. Sanchez, C., Arribart, H. & Giraud Guille, M. M. Biomimetism and bioinspiration as tools for the design of innovative materials and systems. *Nature Materials* **4,** 277–288 (2005).

118. Nassif, N. *et al.* Self-assembled collagen-apatite matrix with bone-like hierarchy. *Chemistry of Materials* **22,** 3307–3309 (2010).

119. Knight, D. P., Nash, L., Hu, X. W., Haffegee, J. & Ho, M. W. In vitro formation by reverse dialysis of collagen gels containing highly oriented arrays of fibrils. *Journal of Biomedical Materials Research* **41,** 185–191 (1998).

120. Besseau, L., Coulomb, B., Lebreton-Decoster, C. & Giraud-Guille, M. M. Production of ordered collagen matrices for three-dimensional cell culture. *Biomaterials* **23,** 27–36 (2002).

121. Brown, R. A., Wiseman, M., Chuo, C. B., Cheema, U. & Nazhat, S. N. Ultrarapid engineering of biomimetic materials and tissues: Fabrication of nano- and microstructures by plastic compression. *Advanced Functional Materials* **15,** 1762–1770 (2005).

122. Mosser, G., Anglo, A., Helary, C., Bouligand, Y. & Giraud-Guille, M. M. Dense tissue-like collagen matrices formed in cell-free conditions. *Matrix Biology* **25,** 3–13 (2006).

123. Wang, Y. *et al.* The predominant role of collagen in the nucleation, growth, structure and orientation of bone apatite. *Nature materials* **11,** 724–33 (2012).

124. Abou Neel, E. A., Cheema, U., Knowles, J. C., Brown, R. A. & Nazhat, S. N. Use of multiple unconfined compression for control of collagen gel scaffold density and mechanical properties. *Soft Matter* **2,** 986 (2006).

125. Knapp, T. R., Kaplan, E. N. & Daniels, J. R. *Injectable collagen for soft tissue augmentation* in (1976).

126. Bell, E., Ivarsson, B. & Merrill, C. Production of a tissue-like structure by contraction of collagen lattices by human fibroblasts of different proliferative potential in vitro. *Proceedings of the National Academy of Sciences of the United States of America* **76,** 1274–8 (1979).

127. Helary, C. *et al.* Concentrated collagen hydrogels as dermal substitutes. *Biomaterials* **31,** 481–490 (2010).

128. Helary, C. *et al.* Evaluation of dense collagen matrices as medicated wound dressing for the treatment of cutaneous chronic wounds. *Biomater. Sci.* **3,** 373–382 (2015).

129. Yuan, L. *et al.* Effects of Composition and Mechanical Property of Injectable Collagen I/II Composite Hydrogels on Chondrocyte Behaviors. *Tissue Engineering Part A* **22,** 899–906 (2016).

130. Schinagl, R. M., Gurskis, D., Chen, A. C. & Sah, R. L. Depth-dependent confined compression modulus of full-thickness bovine articular cartilage. *Journal of Orthopaedic Research* **15,** 499–506 (1997).

131. Shepherd, D. E. T. & Seedhom, B. B. Thickness of human articular cartilage in joints of the lower limb. *Annals of the Rheumatic Diseases* **58,** 27–34 (1999).

132. Sophia Fox, A. J., Bedi, A. & Rodeo, S. A. The basic science of articular cartilage: Structure, composition, and function. *Sports Health* **1,** 461–468 (2009).

133. Brinkman, W. T., Nagapudi, K., Thomas, B. S. & Chaikof, E. L. Photo-cross-linking of type I collagen gels in the presence of smooth muscle cells: Mechanical properties, cell viability, and function. *Biomacromolecules* **4,** 890–895 (2003).

134. Hartwell, R. *et al.* A novel hydrogel-collagen composite improves functionality of an injectable extracellular matrix. *Acta Biomaterialia* **7,** 3060–3069 (2011).

135. Chattopadhyay, S. & Raines, R. T. Review collagen-based biomaterials for wound healing. *Biopolymers* **101,** 821–833 (2014).

136. Marelli, B., Ghezzi, C. E., James-Bhasin, M. & Nazhat, S. N. Fabrication of injectable, cellular, anisotropic collagen tissue equivalents with modular fibrillar densities. *Biomaterials* **37,** 183–193 (2015).

137. Kamranpour, N. O., Miri, A. K., James-Bhasin, M. & Nazhat, S. N. A gel aspiration-ejection system for the controlled production and delivery of injectable dense collagen scaffolds. *Biofabrication* **8,** 000000 (2016).

2

Self-assembled collagen microparticles by aerosol as a versatile platform for injectable anisotropic materials

Contents

2.1 Introduction

This project originates from a collaboration that was build-up for an ANR proposal called "CAPSULE" around an original idea. The aim was to encapsulate secretion factors from gingival Mesenchymatous Stem-Cells (gMSCs) inside collagen beads for therapeutic use. Four institutions participated, with their respective assignments:

- Inserm, represented by Jean-Jacques Lataillade: production of secretion factors from gMSCs in hypoxia conditions. Such conditions are actually present in the first stages of wounds. Stimulating gMSCs in these conditions is therefore supposed to enhance the production and quality of secretion factors.
- Collège de France-Laboratoire de Chimie de la Matière Condensée de Paris (LCMCP), represented by Nadine Nassif: production of collagen beads to encapsulate the secretion factors. Optimization of the conditions to tune the release.
- ScarCell Therapeutics, represented by Laetitia Lallement: select relevant gMSCs for immortalization to have a standardize procedure for reproducible production of secretion factors.
- Paris Descartes, represented by Bernard Coulomb: perform *in vitro* assays to follow the life cycle of the secretion products from their production (effects of hypoxia) to their encapsulation and final release for wound healing.

On the LCMCP's side, a postdoc was hired for the project: Francisco M. Fernandes. He was supervised by Nadine Nassif and Cédric Boissière to fulfill their part of the project as described above. Indeed, they successfully encapsulated gMSCs secretion factors into collagen beads. The secretome of the gMSCs being highly complex, there were difficulties in assessing which were the most relevant components and if those components were actually encapsulated. The secretion products were also produced in small quantities due to the challenging conditions which limitated the *in vitro* assays. When put in contact with a cell culture medium, the loaded collagen beads formed a matrix which made it difficult to characterize the release of secretion products and prevented cell culture to be performed.

For these reasons, another ANR proposal was created under the name "CAPSULE-CARE". The same teams had to work on solutions for the encountered problems, and another goal was added to the list:

- Paris Descartes, represented by A. Lafont and X. Jeunemaitre, and ScarCell Therapeutics, represented by L. Lallement: perform *in vitro* and *in vivo* assays on relevant models for a specific patient condition (type 4 Ehlers-Danlos Syndrome).

Unfortunately the project did not get funding this time, it was then stopped.

The idea to use dense collagen beads and inject them in tissue defects to form collagen matrices *in situ* for tissue repair materialized in the form of a patent. It is referenced under WO 2016/146954 Al and has the following title: "Injectable collagen suspensions, the preparation method thereof, and the uses thereof, particularly for forming dense collagen matrices". This process worked well so they decided to carry on the project. The injected collagen material formed a gel, which could possibly be injected in a tissue defect of form a model material for other studies. To be competitive in

tissue regeneration applications (colonization, vascularization, resorption), they hypothesized that the resulting collagen gel should have an ultrastructure highly similar to that of the targeted tissue. The extracellular matrix, the cells, the organs and simply the movements of the body induce mechanical constraints on tissues. Thus another important aspect of the resulting collagen gel is its mechanical properties, that should match that of the targeted tissue. To have robust mechanical studies and analyses, the LCMCP team built a collaboration with Sciences et Ingénierie de la Matière Molle lab, represented by Alba Marcellan. Six month before the beginning of the thesis, Alba hired a master 2 student (myself) for a six months internship on the mechanical properties of synthetic hydrogels. After obtaining a full funding from Labex MATISSE, they hired the M2 student as PhD candidate to work on the project.

My work first consisted in reproducing Francisco's synthesis of collagen microparticles. I set up my own conditions and obtained the collagen powder. I went further in the characterization of the collagen beads: average size on larger quantities, denaturation state, scanning electron microscopy at higher magnification, water content, organizations (collagen self-assembly) within the microparticles, conditions for injecting of the beads in a medium and characterization of the injected material (microscopies).

Alltogether, these two projects led to the publication of an article under the title: "Self-assembled Collagen Microparticles by Aerosol as a Versatile Platform for Injectable Anisotropic Materials". This article was submitted to Small (Wiley) and is still under review. The cover letter is below.

A main signature of biological tissues is their hierarchical organization. In vertebrates, type I collagen, the main component of soft connective tissues, organizes ar different length scales from individual triple helix to fibril, fibers, bundles and finally extracellular matrices. The structural arrangements of the components (cellular, mineral and organic phases) are of primary importance as they govern function and biological design principles in tissues. Finding a synthetic pathway to artificial analogs of extracellular matrices reprensents a fundamental milestone in the development of materials and in the understanding of mechanisms by which tissues form. Indeed, it is still hard to see how insoluble fibrils could spontaneously and specifically arrange in this three-dimensional way.

Here we report on a bioinspired method to form cell-free dense collagen microparticles. This strategy relies on mimicking the release by the cells of dense procollagen vesicles *in vivo*. This mechanism is common in all biological tissues made of type I collagen and is determinant for the elaboration of the resulting three-dimensional extracellular matrix architecture. The anisotropic microparticles are obtained within seconds by a spray-processing approach entirely without requirements of harsh solvents or an abundance of heat/energy typically used by other processing techniques. The innate molecular characteristics/native properties of the protein (sel-assembly, no denaturation into gelatin) being preserved, they were used as raw materials for setting even more advanced materials being:

- 3D dense and organized materials through simple injection circumventing the high increase of viscosity of type I collagen solutions that usually prevents fast processing of this protein thus its use at biological concentration (×100). The alignment along a predominant direction is performed to achieve specific structural anisotropy at the microscale. Unlike other methods (*e.g.* electrospinning) we show that the injection of anisotropic collagen microparticles enables collagen fibrils to retain their native properties while forming ordered, organized structures at higher length-scales;

- tunable collagen microparticles with stem cell-like components. The production of active secretion products in sufficient quantity, with a quality suited to their therapeutic use and their delivery implies to minimize the extent of cell death in the tissues surrounding the injured area but also the preservation of their phenotype against possible mutations or differentiation processes. A fast and easy set-up is of high interest to pass-by such issues. Since secretion products of gMSCs were shown to have similar effects on cell differentiation as gMSCs themselves, they were used instead of the whole cells. This process enables successfully the one-pot encapsulation of such temperature-sensitive bioactive molecules.

More specifically, this article addresses the following issues in different fields:

- Nanotechnology: these materials have great potential in the field of nanotechnology as they enable the production of organized materials at the microscale such as structured nanocomposites, layer-by-layer materials or filament type for desktop 3D printers to be generated using bottom-up approaches.

- Materials science: above the formation of novel pure organic materials, this process may also be a key to the formation of hybrid mineral composite matrials and ultimately, can serve as an ideal model system to study organic-inorganic interactions at various length scales *i.e.* from molecular, to cellular, to tissue scales (see Chapter 5).

- Biology: as nature applies a hierarchical structuring scheme, it is of high interest to understand the mechanisms involved in biological tissue formation. The use of such extracellular matrix-like scaffolds may clarify the understanding of the structure-property relationship.

- Biomaterials: the properties (mechanical, cell response behaviour, etc.) in complex systems are explained based on the hierarchical structures present in the system thus providing a reliable foundation for efficient collagen-based biomaterials. Overall, this innovative approach should pave the way for making hierarchically tissue-like collagen scaffolds with or without bioactive molecules for tissue regeneration (see Chapter 3 and Chapter 4).

- Supramolecular protein chemistry: previous studies have demonstrated the cooperative binding of proteins to form extracellular matrices. In the case of collagen, the macromolecule itself contains recognition sequences resulting in self-assembled complexes. Our observations stregthen the concept that suprafibrillar tissue architecture is determined by the ability of soluble percursor molecules to form liquid crystalline arrays, prior to fibril assembly.

2.2 Article

Self-assembled Collagen Microparticles by Aerosol as a Versatile Platform for Injectable Anisotropic Materials

Milena Lama, Francisco M. Fernandes, Alba Marcellan, Juliette Peltzer, Marina Trouillas, Marion Grosbot, Clément Sanchez, Marie-Madeleine Giraud-Guille, Jean-Jacques Lataillade, Bernard Coulomb, Cédric Boissière, Nadine Nassif**

M. Lama, Dr. F. M. Fernandes, Prof. C. Sanchez, Prof. M-M. Giraux-Guille, Prof. C. Boissière, Dr.

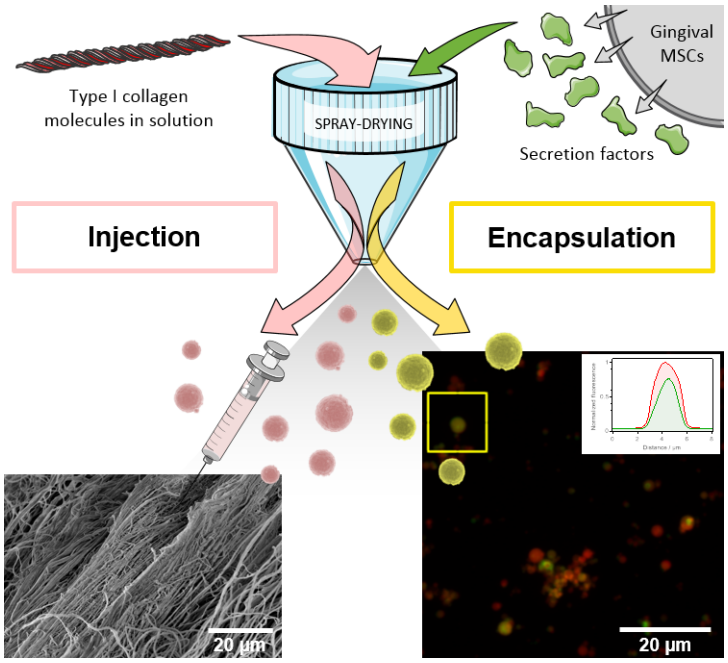

Figure 2.1: An innovative spray-processing approach enables fast and cheap production of anisotropic microparticles containing >90wt % type I collagen. Their injection in a biological medium results in the formation of fibrils retaining innate molecular characteristics while forming ordered, organized structures at higher length-scales. The encapsulation of temperature-sensitive stem-cell products demonstrates the versatility of the approach for tissue regeneration applications.

N. Nassif
Sorbonne Université, CNRS, Collège de France, Laboratoire de Chimie de la Matière Condensée de Paris 4 Place Jussieu, F-75005 Paris, France
E-mail: nadine.nassif@sorbonne-universite.fr

M. Lama, Dr. A. Marcellan
Sciences et Ingénierie de la Matière Molle, ESPCI Paris, PSL University, CNRS, Sorbonne Université 10 rue Vauquelin, 75005 Paris, France

Dr. J. Peltzer, Prof. J-J. Lataillade, Dr. M. Trouillas, M. Grosbot
Unité de thérapie cellulaire, CTS des armées, Hôpital Percy 1, rue du Lieutenant Raoul Batany, 92141 Clamart, France

Prof. B. Coulomb
Paris Research Cardiovascular Center (PARCC), Institut National de la Santé et de la Recherche Médicale (INSERM) U970, Paris-Descartes University 56 rue Leblanc, 75015 Paris, France
E-mail: bernard.coulomb@inserm.fr

Keywords
Biomaterials; Collagen; Spray-drying; Self-assembly; Encapsulation

Abstract

Extracellular matrices (ECM) rich in type I collagen exhibit characteristic anisotropic ultrastruc-

tures. Nevertheless, working in vitro with this biomacromolecule remains challenging. When processed, denaturation of the collagen molecule is easily induced in vitro avoiding proper fibril self-assembly and further hierarchical order. Here, an innovative approach enables the production of highly concentrated injectable collagen microparticles, based on collagen molecules self-assembly thanks to the use of spray-drying process. The versatility of the process is shown by performing encapsulation of secretion products of gingival mesenchymal stem cells (gMSCs), which were chosen as a bio-active therapeutic product for their potential efficiency in stimulating the regeneration of a damaged ECM. The injection of collagen microparticles in a cell culture medium results in a locally organized fibrillar matrix. The efficiency of this approach for making easily handleable collagen microparticles for encapsulation and injection open perspectives in active tissue regeneration and 3D bio-printed scaffolds.

Introduction

Tissue repair is a priority need of any living tissue or organ for recovering functional properties after injury. The repair process is a complex phenomenon that involves soluble mediators, blood cells and components of the extracellular matrix (ECM), especially the cells from the tissue itself such as fibroblasts. Collagen is the major insoluble fibrous protein in the ECM of connective tissue. Type I collagen being one of the most abundant, many methods have been proposed as scaffold for tissue engineering[1] and for its formulation in an attempt to control the release of active molecules[2]. Formulations of beads are mainly based on techniques of emulsion in a water/oil[3] or water/organic solvent mixture[4] under conditions in which proteins are not denatured. However, traces of oil or solvents are associated with the beads formed[5]. An alternative technique is the thermally induced phase separation (TIPS), in which the drops of the solution are introduced into a bath of liquid nitrogen followed by a lyophilization step[6]. Complex coacervation can also be used to produce collagen beads in a controlled manner[7, 8] by taking advantage of the polyelectrolyte nature of the collagen triple helix. In the cited cases, the fragility of collagen beads requires a crosslinking step to reinforce their mechanical properties, by chemical agents (such as aldehydes or carbodiimides) bringing potential toxicity. More recently, the use of microfluidic devices[9], 3D printers[10] and even soft robotics[11] enabled the production of un-crosslinked collagen beads for encapsulation. However, the inner structure of these collagen microparticles remains porous unlike that of the ECM.

Type I collagen solutions are classically obtained in vitro from living tissues (tendons, dermis) placed in acidic media. Dilute dispersions of collagen triple stranded molecules at low concentrations ($\sim$1mg/mL) can be further stabilized in vitro to form hydrated gels used in interaction with cells or tissues[1]. However these loose matrices neglect the fundamental structure-function relationship of connective tissues. Indeed, these conditions lead to a large volume of extrafibrillar space while type I collagen-based ECM are most often dense and organized, forming complex scaffolds providing specific function to the tissue. It was shown that beyond a critical concentration, molecules in solution spontaneously self-organize to form ordered liquid crystalline phases[12]. A sol-gel transition is induced by a rise in pH, stabilizes the mesophase geometries, ending in biomimetic fibrillar organizations[13]. Mechanical properties of these biomaterials allow their use without requiring any additive, rendering their application non-toxic; this shows the interest of working at higher collagen concentrations[1].

Aside the scaffold, another strategy for tissue regeneration is the on-site delivery of bioactive products such as Mesenchymal Stem Cells (MSCs) secretion factors[14]. The secretion of a broad range of bioactive molecules by MSCs, such as growth factors, cytokines and chemokines, constitutes their most biologically significant role under injury conditions. The production of active secretion

products suited to their therapeutic use, and their delivery implies to minimize the extent of cell death in the vicinity of injured areas but also the preservation of their phenotype against possible mutations or differentiation process. Hence, Conditioned Medium (CM) composed of the secretion products of MSCs from gingival connective tissue (gMSCs)[15], instead of the whole cells was used an alternative. CM of gMSCs was previously shown to have a similar effect as gMSCs on cell differentiation[16]. Gingival tissue is known to heal rapidly and without scarring; CM of gMSCs thus appears as a good candidate to promote wound healing.

Based on the cited knowledge, an approach combining both strategies appears as a promising new therapeutic way for efficient tissue regeneration. Herein, we present a one-pot aerosol-assisted processing strategy leading to the easy, cheap and fast continuous production of highly concentrated (>90 wt%) type I collagen microparticles, encapsulating (or not) temperature-sensitive bioactive molecules. The spray-processing approach adopted consists in atomizing a diluted acid-soluble collagen solution in order to form a mist of very thin droplets, immediately dried by evaporation of their solvent in a controlled atmosphere (thanks to the high solution/air interface area of the droplets). The concentration in the collagen drops is high enough to induce the self-assembly of collagen molecules and a subsequent liquid crystal order, i.e. nematic oriented domains. This strategy allows obtaining within seconds highly concentrated collagen microparticles circumventing the high increase of viscosity of type I collagen solutions that usually prevents fast processing of this protein thus its use at biological concentration. A fine control of both formulation and processing parameters as temperature to prevent denaturation of the biomolecules ensure the encapsulation of gMSC secretion products for further injection. The features of the injected material resemble that of living dermis tissue, with local anisotropy and fibrils organized in bundles. The design of such new functional cell-free capsules broadens the range of strategies available for biotherapy and opens perspectives for building anisotropic three-dimensional scaffolds with hierarchical order from the fibril, to bundles, to the material scale.

Collagen microparticles preparation. The spray-drying device available in the laboratory (see Experimental Section) is commonly used for producing organic, inorganic or hybrid (organic/inorganic) microparticles[17]. The spray-drying set up (**Figure 2.2a**) was first optimized to obtain dense type I collagen microparticles; the main drawback being the risk of irreversible thermal denaturation of collagen into gelatin as mentioned above. For this purpose the following parameters: solution flow, air flow, aspiration and temperature were chosen as follows. The spraying step was conducted using initial concentrations of acid soluble collagen between 0.7 and 5 mg/mL to limit the solution viscosity and promote a steady flow. Indeed a high concentration of collagen in solution can even lead to the formation of a physical gel[18] that could hinder both flow and formation of droplets. The drying step is strongly dependent on the solvent evaporation time, which is in turn related to both the temperature of dry air injected in the chamber and the aspiration rate. The dry air and nozzle temperature were fixed at 35±1°C. This temperature range is low enough to prevent protein denaturation but high enough to induce the solvent (acetic acid in water) evaporation in the droplets and reach the cyclone particle collector in dry form. Overall, the drying process takes no more than 4 seconds. **Figure 2.2b and c** illustrates the collected collagen microparticles obtained from different initial concentrations of type I collagen solutions as observed by Scanning Electron Microscopy (SEM) (see also **Figure 2.5**, Supporting Information). The observation shows that the selected processing conditions lead to the precipitation of micron-sized collagen particles. Each droplet of solution leading

to one dry microparticle, the initial concentration of the collagen solution appears to influence the size of the microparticles and the polydispersity, both increasing at higher concentrations. This trend was confirmed by performing laser granulometry (**Figure 2.2d**). The diameter distribution reveals two main populations in counts for the lowest and highest investigated concentrations, the first one at 0.6±0.3µm and 0.6±0.1µm respectively, and the second one at 0.9±0.2 µm and 1.3±0.6 µm respectively. A third population appears at 5.2±0.5 µm for the highest concentration only. This range of diameters is consistent with works in the literature where microparticles were obtained by spray-drying chitosan[19]. We identified the importance of the initial collagen concentration, emphasizing the versatility of the process for targeting different uses where the bead size may play an important role in adjusting release kinetics, as in drug or biomolecules controlled release systems.

Ultrastructure of the collagen beads. Type I collagen possess lyotropic properties in vitro in acidic conditions characterized by the occurrence of mesophases above 40 mg/mL[21]. As a consequence of the collagen concentration during solvent evaporation, self-organization of the molecules may occur in the droplets during the drying step. Polarized light microscopy (PLM) observations (**Figure 2.2e** and **Figure 2.6**, Supporting Information) show optical birefringence of the collagen microparticles suggesting a local ordering of the collagen molecules or fibrils. The resolution of the PLM being in the same order of magnitude than that of the diameter of the microparticles, it is difficult to identify a specific birefringence texture. Nevertheless, after a 45° rotation of the polarizers (**Figure 2.2e'**), extinction of light occurs in areas where the collagen molecules lie parallel to the direction of the polarizers indicating a probable nematic alignment all over the surface of the largest microparticles (see inset). SEM observations at higher magnification provided no evidence of fibrillogenesis in vitro (**Figure 2.7**, Supporting Information). Thus we investigated Transmission Electron Microscopy (TEM) (**Figure 2.2f**) to conclude on the fibrillar nature of the microparticles and on their possible local organization. Local order at such scale is considered as possible since it was previously reported for spray-dried chitin-silica particles where chitin possesses as well liquid crystal properties[22]. In our case, fibrils are not observed (**Figure 2.2f**), even though the high collagen concentration in the microparticles can induce the formation of few collagen fibrils[23]. However, their observation is only possible if the main axis of the fibril is oriented along the section plane. As collagen molecules are evenly distributed all throughout the microparticles (no detection of hollow microparticles), the presence of some small fibrils cannot be totally excluded. Finally, although it remains difficult to assess precisely the local molecular order in the microparticles (diameter of the beads vs. resolution of the optical microscope), it seems that the molecules assembly, preferentially driven by thermodynamics, is limited by the fast drying kinetics. Indeed, in addition to the size of the domains (restricted by the dimensions of droplets), the fast solvent evaporation may prevent the formation of higher ordered mesophases (such as cholesteric phase).

Physico-chemical characterization of the collagen microparticles. To assess the water content of the pure collagen beads, we performed dynamic vapor sorption (DVS) experiments. A typical isothermal curve[24] was obtained with reduced hysteresis (**Figure 2.8**, Supporting Information). At ambient temperature and humidity conditions, 25°C and 40 %RH respectively, the microparticles contain less than 10 wt% water (thus more than 90 wt% type I collagen). Differential scanning calorimetry (DSC) experiments performed on the initial collagen solution and on the dissolved collagen microparticles in acetic acid at 500 mM show the same endothermic peak at 40°C (**Figure 2.9**,

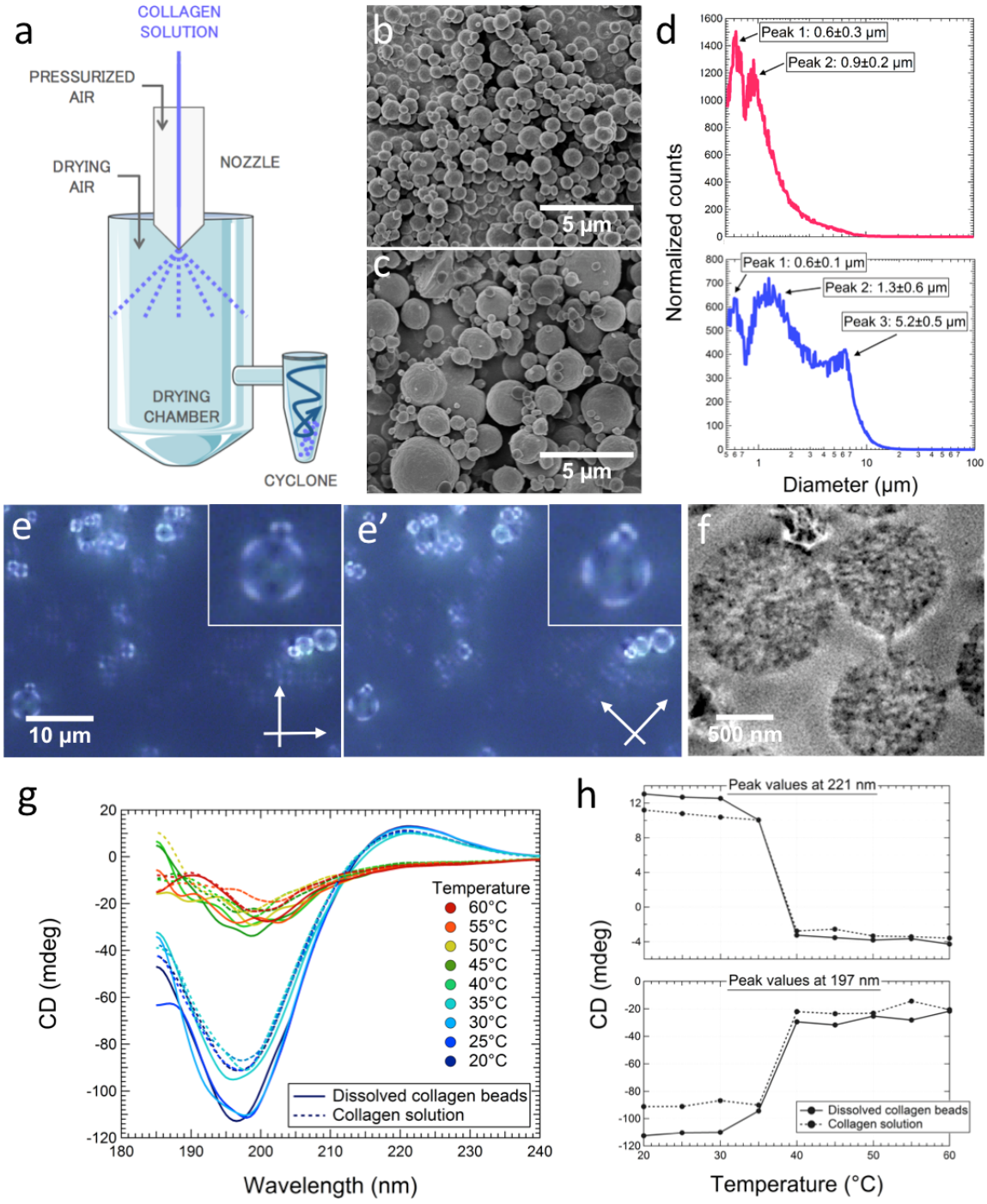

Figure 2.2: a) Schematics of the spray-processing of a collagen solution. b) and c) Scanning Electron Micrographs of pure collagen beads from spray-dried collagen solutions at 0.7 mg/mL and 5.0 mg/mL, respectively. d) Normalized diameter distribution in counts of collagen microparticles from spray-dried collagen solutions at 0.7 mg/mL (upper graph) and 5.0 mg/mL (lower graph). e) Under crossed polarizers, collagen microparticles display birefringence and dark domains (along the direction of the polarizers: 0 and 90°) inside and on their surface e') that turn to bright after a 45° rotation of polarizers. f) Ultrathin stained transmission electron micrograph of pure collagen beads. g) Circular dichroism of a collagen solution (dashed line) and of a solution made of dissolved collagen beads (solid line) at the same concentration and in the same solvent (acetic acid at 0.5 M). h) Average ellipticity at 221 nm (upper graph) and 197 nm (lower graph). The difference between the peak values of the two solutions at low temperature can be attributed to slight differences in pH [20].

Supporting Information). At this temperature, collagen denaturation into gelatin occurs through the irreversible unfolding of the triple helix[25]. In addition, circular dichroism (CD) experiments (**Figure 2.2g-h**) show typical sigmoidal-shaped curves[26] with a large negative peak around 221 nm and a smaller positive peak around 200 nm characteristic of triple-helix conformation[27]. These results confirm that the non-fibrillar collagen microparticles observed by TEM (**Figure 2.2f**) is indeed made of collagen molecules and not gelatin, which is also in agreement with the observation of birefringence by PLM (**Figure 2.2e-e'**). Overall, these results prove that the process is compatible with the use of thermo-sensitive biomolecules. The suitability of dense collagen microparticles for encapsulation was then investigated.

Encapsulation of gMSCs secretion factors in collagen microbeads. In order to minimize the number of synthesis steps, we adapted our preparation strategy to obtain simultaneous aerosolization of collagen solution and Conditioned Medium (CM) composed of the secretion products of gMSCs. A first limitation is related to the risk to induce the thermal denaturation of the CM components during spray-drying. However, given the gMSCs culture conditions (i.e. 37°C) it is reasonable to assume that the secretome will not be denatured since the previously established collagen processing conditions lie below this temperature. In addition to the temperature, a limitation was the difference in pH of the CM (pH∼7) with the collagen solution (pH∼3.5). It is worth mentioning that such a low pH should not interfere with the biomolecules activity since it is described to be involved in the promotion of wound healing[28]. Yet, in order to limit the pH stress for the secretome, we adapted the atomization process by using a three-fluid nozzle (able to mix two solutions at the extreme tip of the nozzle and to atomize it at the same time) to limit the contact time between the two solutions (**Figure 2.3a-a'** and see Experimental Section). The use of a coaxial nozzle to produce particles from two liquids simultaneously allows the control of the average composition of the produced particles. However, we needed to ensure that each particle was composed of both components; the CM could be found only at the surface of the collagen particle (which would limit the intended effect) or not interacting at all with collagen. Microparticles issued from two different collagen:CM volume ratios were produced (1:1 and 1:3) (Table 1). Observations by SEM (**Figure 2.3b-c**) show that the particles display the same morphology as those previously obtained from collagen only. When imaged under the confocal microscope, collagen:CM particles present extensive colocalization of signal intensity of both fluorescence channels, which confirms the effective encapsulation of CM within the collagen particles (**Figure 2.3d-g**). The profile integration (**Figure 2.3e'–g'**) of three individual particles, chosen according to the individual channel intensity confirm the presence of both fluorophores in each of the analysed individual particle. The shape of the profile does not indicate any particular segregation between the two components, suggesting the CM to be evenly distributed within each microparticle. This indicates that (i) there is no macroscopic phase segregation between collagen and the CM and (ii) the encapsulated medium does not destabilize the collagen packing. The coupling of collagen microparticles and gMSCs secretion products, both with central roles in the healing process, was successful. This led us to investigate the possibility to use them as an injectable suspension since administration and dissemination of cell therapy derived products in sites of interest are determinant for efficient therapeutic applications.

Injectable collagen suspension. To assess to which extent these systems could be used to fabricate organized three-dimensional shapes, collagen:CM particles were directly suspended in DMEM to mimic the biological environment of the ECM. The pH of DMEM being close to physiological pH, sus-

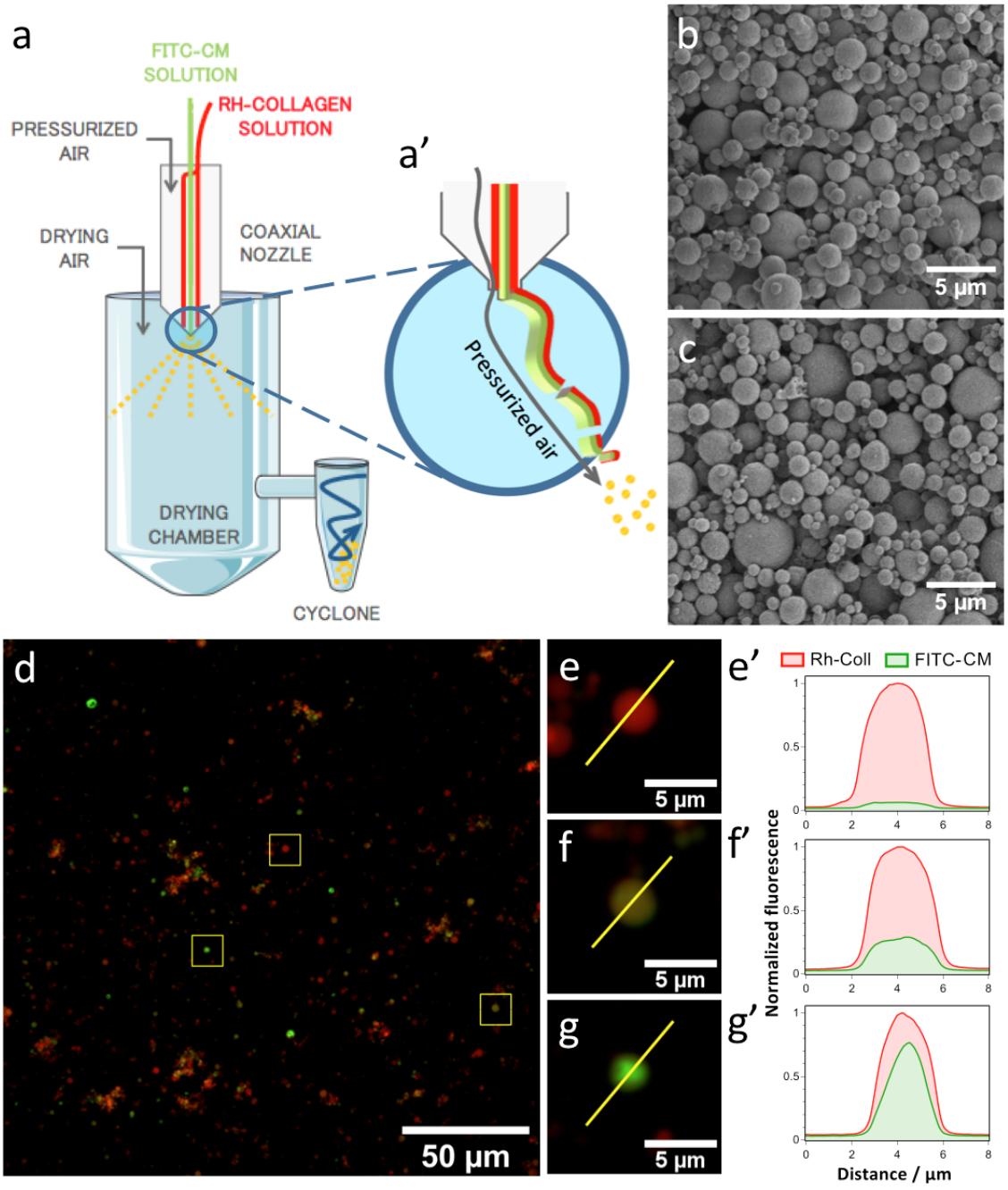

Figure 2.3: a) Coaxial nozzle spray-drying of acid soluble RITC-tagged collagen solution (Rh-Coll) and gMSC derived fluorescein-tagged conditioned medium (FITC-CM). a') Solutions are mixed upon air shearing at the tip of the nozzle. b) and c) SEM images of Coll/CM beads obtained at 1:1 and 3:1 volume ratio, respectively. d) Confocal microscopy images of Rh-Coll/FITC-CM particles with sum z-projection of red and green channels of 52 image planes. e) to g) Detail of selected particles and profile line analyzed. e' to g') Red and green channel plot profiles of particles depicted in e) to g), respectively.

pension of collagen microparticles in such medium will simultaneously solvate the collagen molecules and induce their self-assembly into a fibrillar collagen gel. Indeed, a dense fibrillar matrix is obtained (**Figure 2.10**, Supporting Information), indicating that the fibrillogenesis process of collagen is not destabilized by the encapsulated secretion products. In an attempt to reach higher hierarchical order (i.e. 2D alignment), collagen microbeads were suspended in aqueous solvent and immediately injected in phenol-red free DMEM (**Figure 2.4a**, and Movie in Supporting Information). A final high collagen concentration of 80 mg/mL was successfully injected through a 26G needle, which is comparable to the needles used for fillers. The injection produced strands of fibrillar collagen as characterized by SEM (**Figure 2.4b**). A drop of collagen hydrogel hanging at the needle end after injection is depicted in **Figure 2.11** (Supporting Information). Collagen fibrils appear more organized on the outer part of the strand than in the inner part, which may be a consequence of the extrusion process (i.e. shearing) as showed by PLM (**Figure 2.4c-c"**). Birefringent textures are seen and follow the extrusion direction (orange domains) after inducing a first order retardation with a gamma plate (**Figure 2.4c"'**). Noticeably, our material is processed in aqueous solvents which induces a swelling phenomenon of the collagen strands (from 260 µm diameter at the tip of the needle to about 400 µm after one week in DMEM). As observed by SEM, fibrils diameter appears homogeneous in size. This characteristic together with the fibrils alignment reminds those of biological dermis tissue (**Figure 2.4d**) where the collagen bundles are locally oriented in the same direction under PLM (nematic birefringence texture shown in **Figure 2.4d'**) as observed in our material at higher magnification (**Figure 2.4e**). Such biological features differ from other 2D oriented collagen materials found in the literature, using larger diameter needles for extrusion[29] or electrospinning[30], enlarging the field of applications for injectable anisotropic collagen-based materials.

Conclusion

The advantages of the spray-drying approach for the formation of dense anisotropic collagen microparticles include synthesis in sterile conditions, continuous processing and easy scalability to mass production. The versatility and the robustness of the encapsulation process by aerosol open ways for encapsulating a broad range of bioactive molecules. Injection of the microparticles leads to materials made of 2D oriented collagen fibrils with tunable structure over several length-scales and composition (e.g. hierarchical organic/inorganic scaffold). The fact that the size of the needle can be adapted to the size of the defect and to the type of tissue without altering the patient's comfort opens perspectives in collagen-based biomaterials. One step further, these 2D building blocks may serve in 3D-bioprinting to produce oriented collagen fibrils over several centimeters forming biomimetic collagen scaffolds with desired shape.

Experimental section

Processing of pure collagen microparticles: Collagen solutions were prepared following a procedure described elsewhere[31] and the concentration of the sprayed collagen solutions was adjusted to 0.7, 2.1, 3.6 or 5.0 mg/mL by dilution with 0.5 M acetic acid. The beads were formed by using a Büchi 290 mini spray-dryer. Solution flows between 0.3 $mL.min^{-1}$ and 1.5 $mL.min^{-1}$ were used to reach different final beads sizes. Air flow was set at 414 $L.h^{-1}$ and aspiration rate at 20 $m^3.h^{-1}$. The inlet temperature was set at 30°C, measured inlet temperature at 35±1°C and measured outlet temperature at 21±3°C. The resulting material consists of a white powder which is collected in a flask at the bottom of the cyclone for characterization.

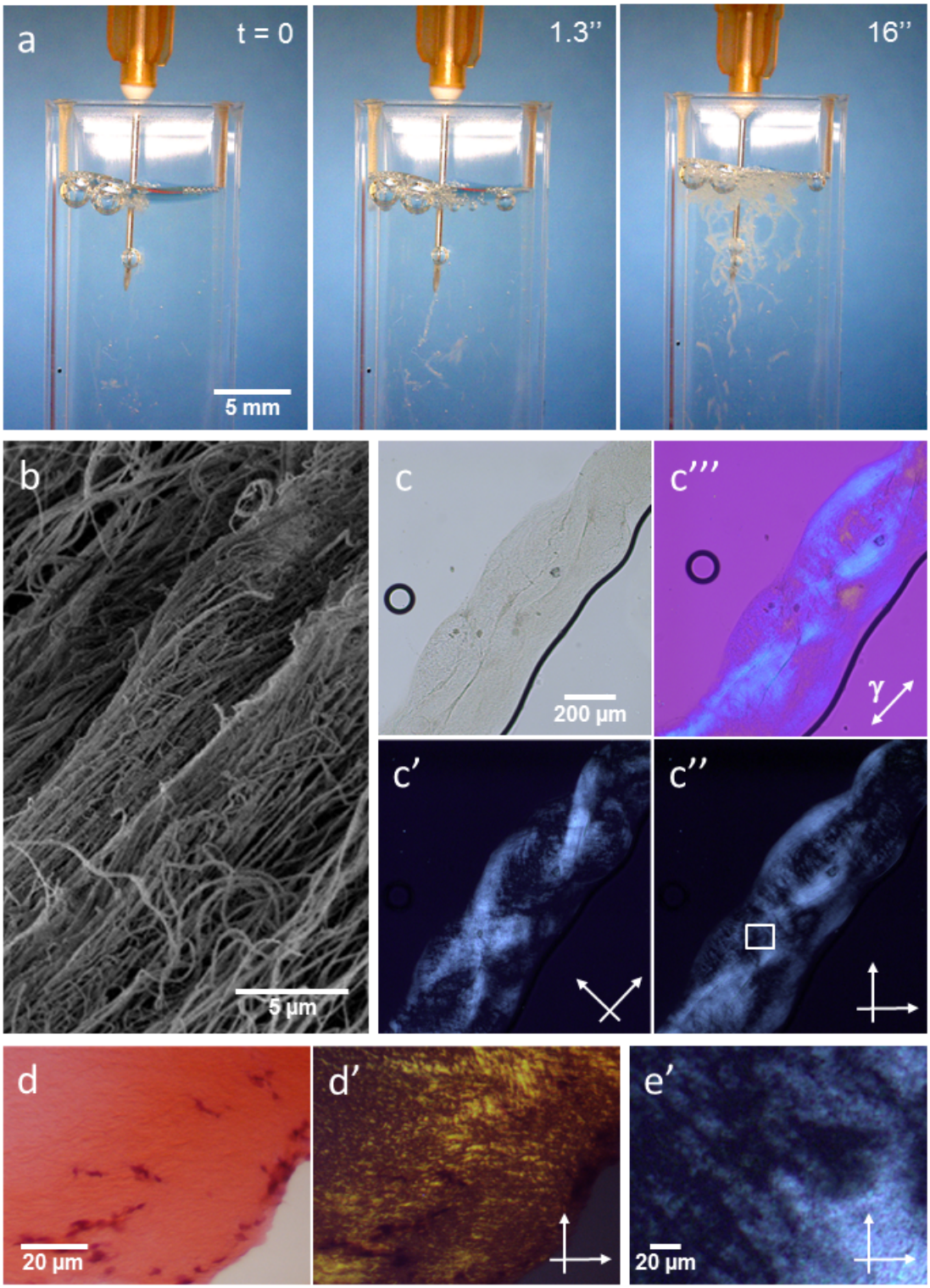

Figure 2.4: a) Sequence of still images taken from the video of collagen beads (80mg/mL) suspended in aqueous solvent being injected in DMEM medium (phenol red free). b) SEM micrograph of the final collagen matrix displaying fibrillar organizations and local alignments. c) to c”) PLM images of injected fibrillar collagen strands in hydrated state containing birefringent patterns on the surface evidenced by rotating the polarizers from 45-135° (c’) to 0-90° (c”), typical of alignment domains. c”’) PLM image after inducing a first order retardation with a gamma plate with polarizers at 0-90°. d) Histology section of rat dermis as observed under the Microscope and d’) displaying nematic birefringent textures when observed under crossed polarizers. e’) High magnification of the inset in c”.

Production of conditioned medium (CM): The conditioned medium (CM) is composed of the secretion products of gingival MSCs (gMSCs). The gMSC were harvested from a voluntary donor at Hospital George Pompidou (Paris). gMSCs were isolated and cultivated as previously described[15]. Briefly, primary explant cultures were amplified in DMEM, Fetal Calf Serum (20%), Penicilin (100 µg/ml), Streptomycin (100 µg/ml), Amphotericin B (2 ng/ml) until they reached confluence. Then, the medium was replaced by secretion medium composed of base medium without growth factors. The CM was recovered 7 days after starving and freezed at -80°C. Gingival MSCs' CM was dialyzed against carbonate buffer (Spectrum© dialysis membrane, 3kDa) and tagged with FITC before being equilibrated in PBS. Collagen was tagged using RITC in slightly basic pH and subsequently dissolved in 0.5 M acetic acid. Two different collagen:CM volume ratios were produced (1:1 and 3:1).

Processing of collagen microparticles containing bioactive molecules: The same spray-drier was used with slight differences as follows. The collagen concentration was kept at 1 wt% and the CM concentration in the final solid particles varied between 0.18 and 0.56 wt% (see Table 1 for details). To limit the pH stress for the secretome we have recurred to a three fluid nozzle (two liquids + air) enabling the contact of the collagen solution and the secretome only at the end of concentric channels at the nozzle tip.

Injection of pure collagen microparticles in cell culture medium: Pure collagen beads made from a collagen solution (3.6 mg/mL) were mixed with an aqueous solvent (200 µL) to reach a final concentration of 80 mg/mL. The mixture was quickly transferred to a 1mL syringe equipped with a 26G1/2" needle. The mixture was injected right after in phenol red-free DMEM in a transparent 5 mL UV cuvette at ambient temperature. After injection the cuvette was hermetically covered with parafilm and kept for a week at 4°C before analysis of the injected material.

Characterization of collagen materials: More information about Differential scanning calorimetry, Laser granulometry, Scanning electron microscopy, Circular dichroism, Dynamic vapour sorption, Confocal microscopy, TEM samples preparation and observations can be found in the Supporting Information.

Supporting Information

Supporting Information is available from the Wiley Online Library or from the author.

Acknowledgments

M. Lama and F.M. Fernandes contributed equally to this work. We thank Bernard Haye and Dr. Carole Aimé for help in TEM preparation and CD experiments, respectively. Dr. Clio Parisi and Camila Bussola Tovani are warmly thanked for fruitful discussions. This work was supported by French state funds managed both by the Agence Nationale de la Recherche (ANR) under reference ANR- 2010-RFCS-0006 and within the Investissements d'Avenir programme under reference ANR-11-IDEX-0004-02, more specifically within the framework of the Cluster of Excellence MATISSE led by Sorbonne Universités. C. Sanchez and N. Nassif acknowledge Fondation Collège de France and Fondation EDF.

2.3 Supporting Informations

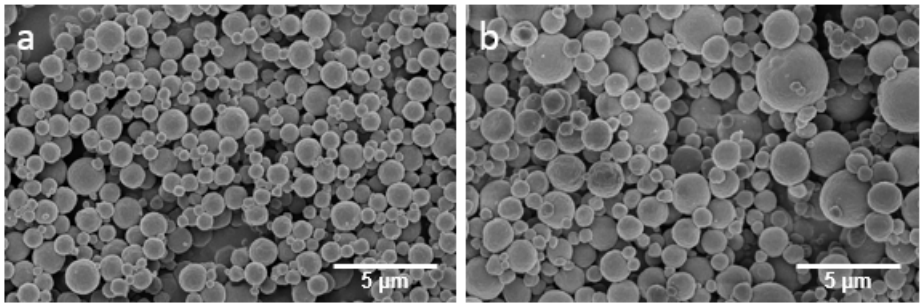

Figure 2.5: a) and b) Scanning electron micrographs of pure collagen beads produced from 2.1 and 3.6 mg.mL^{-1} collagen solutions, respectively. (SI)

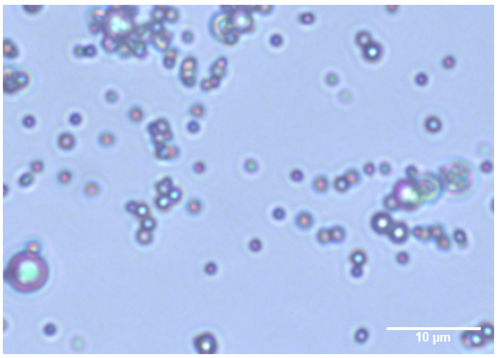

Figure 2.6: Collagen microparticles as observed under the optical microscope. (SI)

Suspension of collagen:CM microparticles in DMEM: Few mg of the collagen:CM powder were put in few mL of DMEM in an Eppendorf. The Eppendorf was kept one week at 4°C before analysis of the suspended material.

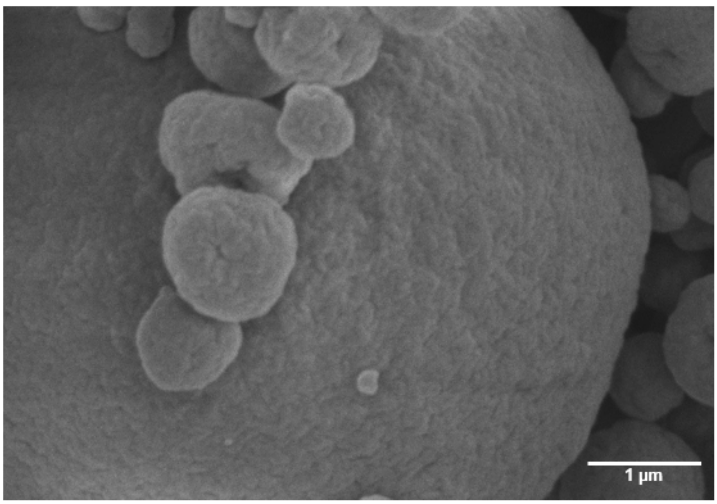

Figure 2.7: High magnification SEM micrograph of pure collagen beads. No fibrillar textures can be evidenced here. (SI)

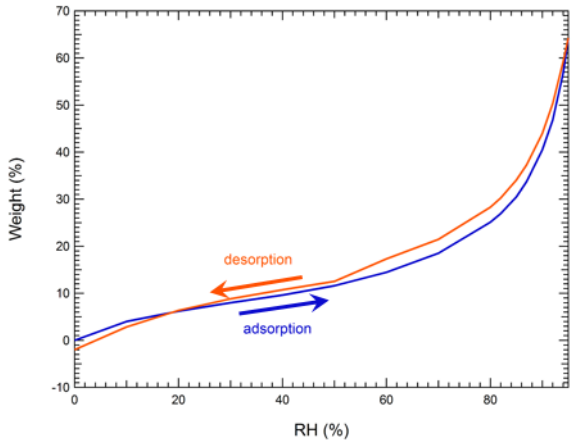

Figure 2.8: Dynamic Vapor Sorption of collagen microparticles at 25°C. A drying step was followed by increasing RH steps from 0% to 95% humidity. Then, decreasing RH steps from 95% to 0% humidity followed. The collagen beads contain approximately 10wt% humidity at ambient temperature and RH conditions. (SI)

Differential scanning calorimetry: Experiments were performed on a TA Q-20 apparatus. Heating rate was set at 5°C/min and temperature range went from 20°C to 80°C. About 20 mg of sample was weighed and put in an aluminium pan, the reference being an empty sealed aluminium pan.

Laser granulometry: For the size of the particles, few mg of collagen beads were dispersed into 20 mL ethanol 96% before going through a PSS-NICOMP particle sizer. For the analysis, the maxima of the following curves: highest investigated concentration in counts and volume, lowest investigated concentration in counts were assumed to follow a Lorentzian distribution. The maxima of the curve of the lowest investigated concentration in volume was assumed to follow a Gaussian distribution. Igor Pro v6.37 software was used for the fit to determine the mean value of each peak and the FWHM or the standard deviation values.

Scanning electron microscopy: Collagen beads were deposited on carbon tape on top of a SEM sample holder, then coated with a 10 nm gold layer. The observations were performed on a Hitachi S-3400N machine with an accelerating voltage of 3.0 kV. Supercritical CO_2 drying was performed on

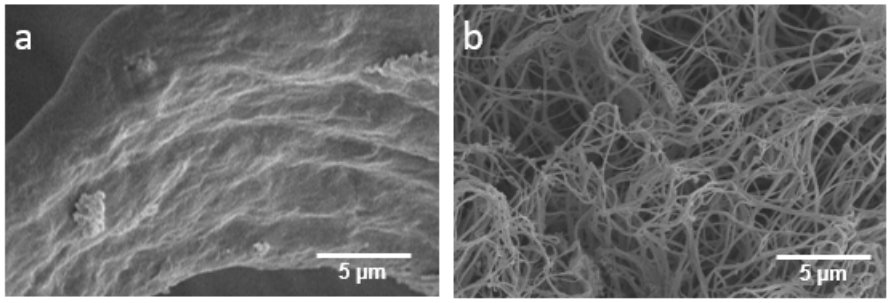

Figure 2.9: a) Scanning Electron Micrograph of Coll/CM microparticles suspended in DMEM. The resulting material displays dense fibrillar textures and some undissolved microparticles remain visible. b) SEM picture of a fibrillar collagen matrix at 40 mg/mL. (SI)

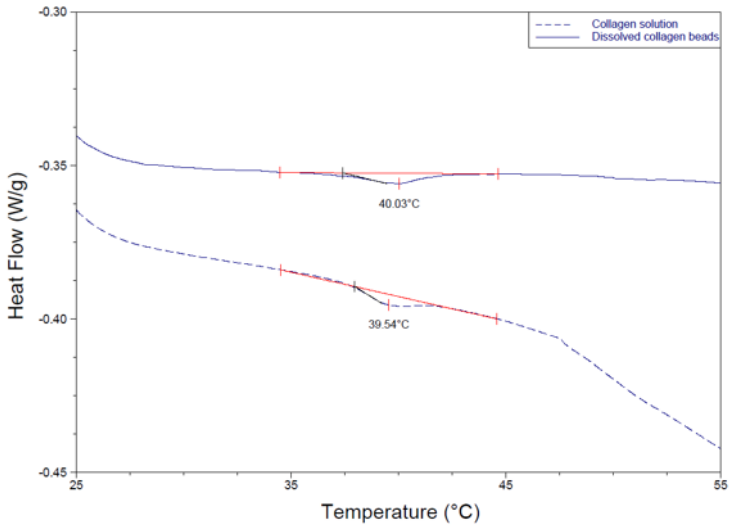

Figure 2.10: Differential Scanning calorimetry of a collagen solution (dashed line) and of a solution made of dissolved collagen beads (solid line). The endothermic peak, typical of collagen triple helix denaturation, occurs at the same temperature for both solutions thus proving that no denaturation occurred during the whole spray-drying process. (SI)

the injected fibrillar collagen strands and on the redissolved collagen beads containing encapsulated CM before deposition on carbon tape and consecutive observation in the same conditions.

Circular dichroism: Experiments were performed on a Jasco-810 apparatus with 1mm width flat cuvettes (about 300 µl volume). A heating ramp of 2°C/min was used. The temperature range was set from 20°C to 60°C with a data pitch of 5°C. The wave length range was set from 190 nm to 240 nm with a data pitch of 0.5 nm. Collagen beads were dissolved in acetic acid at 0.5 M at the same final concentration as the stock collagen solution.

Dynamic vapor sorption: Experiments were performed using a VTI SA+ instrument from TA. Hemispheric quartz sample holders were used. Few mg of collagen powder were first dried to 0%RH before undergoing increasing humidity thresholds (0%RH to 95%RH) with an equilibrium condition set at 0,0010 wt% change or 800 s, then decreasing humidity thresholds with the same RH range and equilibrium conditions.

Confocal microscopy: Observations were performed on a spinning-disk confocal with wide field of view (CSU-W1) and Zeiss Observer Z1 inverted microscope.

TEM samples preparation and observations: Rat dermis was observed thanks to the study carried

Figure 2.11: Detail of hanging drop of gelified collagen obtained at the end of the suspension injection. (SI)

out under authorization no. 006235 of the French ministry of agriculture published in[32]. The sample were fixed in 2.5% glutaraldehyde. After washing in a cacodylate/saccharose buffer solution (0.05 M/0.6 M, pH 7.4), they were post-fixed with 2% osmium tetroxyde in the buffer solution for 1 h at 4°C, washed, dehydrated through successive ethanol baths (50%, 70%, 95%, and 100%). Then, they were embedded in araldite for ultrathin sectioning performed with an Ultracut 7 (Leica). TEM investigations were performed on thin sections (70 nm) deposited on copper grids with a FEI TECNAI G2 Spirit Twin electron microscope operating at 120 kV. The same procedure was followed for collagen microparticles preparation and observations.

2.4 Conclusion

This study enabled us to better understand the properties of the collagen beads and to assess the numerous advantages of spray-drying towards other processing techniques for making highly concentrated 3D collagen materials. Indeed, the technique is easy (once the right conditions are fixed), fast (100 mg of collagen powder can be produced in a few hours), precise (the collagen powder can be weighed to reach a desired collagen concentration in the final gel), reliable (the spray-drying conditions are stable throughout the process and collagen is not denatured under the right conditions) and biomimetic (retains the self-assembly properties of collagen and leads to the precipitation of fibrils that appear homogeneous in diameter).

Other aspects of the study could also be deepened:

- Injection of loaded collagen microparticles in a cell culture medium and comparison of the cell behaviour *in vitro* between a loaded collagen gel and a simple collagen gel. Comparison of both conditions *in vivo*.
- Quantifying the residual amount of acetic acid in the collagen microparticles by using circular dichroism: increasing the pH of the dissolved beads solution step by step should slightly flaten the peak at 221 nm. The quantity of acetic acid brought by the beads could be deduced by comparing the behaviour of the dissolved beads solution to a stock collagen solution dialyzed against different concentrations of acetic acid.
- Delivery of the secretion products (which part of the secretome is actually encapsulated and released), effect of the size of the collagen microparticles on the release.
- Stability of the collagen microparticles: I noticed that after about one month, the collagen microparticles seemed to have lost some of their properties. Usually, mixing collagen microparticles and acetic acid at low concentration (for example) results in the formation of a sticky paste that is quite translucent (physical gel due to collagen molecules self-assembly). However, with older collagen micropaticles, the mix does not form a paste at all: it is still very fluid but turns white. After several weeks in the fridge, the fluid opaque solution turns into an opaque paste that still not has the same consistency as an usual physical collagen gel. Interestingly, the endothermal peak of the opaque solution is close to that of dissolved collagen beads and to a stock collagen solution (**Figure2.12**) which means that the collagen molecules are actually not denatured into gelatin when kept for too long in a dry state. Besides, when observed under Polaized Light Microscopy, the opaque solution at 50 mg/mL does not display any birefringence at all. We can conclude that collagen molecules seem to be destabilized when kept for too long in such conditions (dry and probably acidic) which consequently prevents a normal self-assembly of the molecules when solubilized in an acidic solvent.

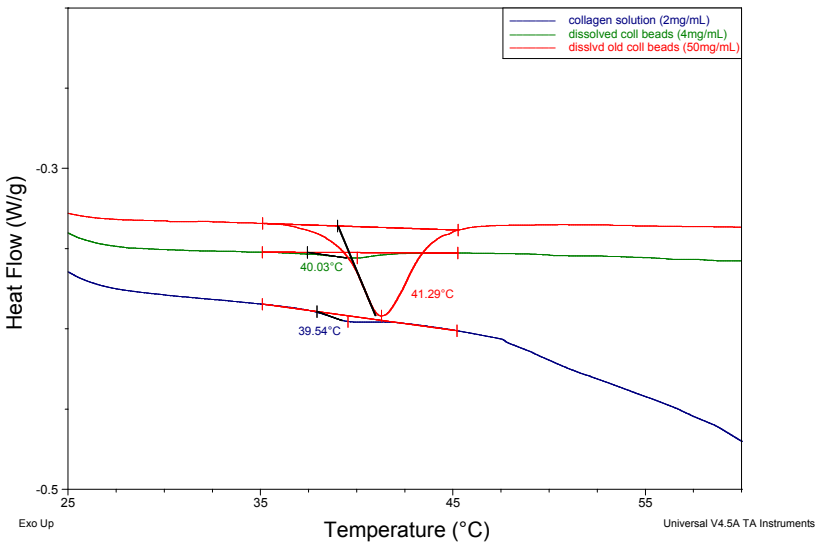

Figure 2.12: Differential Scanning Calorimetry of a collagen solution made of dissolved beads kept longer than one month, compared to two other solutions discussed in the article.

Bibliography

1. Giraud Guille, M. M., Nassif, N. & Fernandes, F. M. Collagen-based Materials for Tissue Repair, from Bio-inspired to Biomimetic. *Materials Design Inspired by Nature: Function Through Inner Architecture,* 107–127 (2013).
2. Friess, W. Collagen - Biomaterial for drug delivery. *European Journal of Pharmaceutics and Biopharmaceutics* **45,** 113–136 (1998).
3. Yin Hsu, F., Chueh, S. C. & Jiin Wang, Y. Microspheres of hydroxyapatite/reconstituted collagen as supports for osteoblast cell growth. *Biomaterials* **20,** 1931–1936 (1999).
4. Miyata. Substrate consisting of regenerated collagen fibrils and method of manufacturing same (1986).
5. Gupta, V., Khan, Y., Berkland, C. J., Laurencin, C. T. & Detamore, M. Microsphere-Based Scaffolds in Regenerative Engineering. *Annual Review of Biomedical Engineering* **19,** 135–161 (2016).
6. Keshaw, H. *et al.* Microporous collagen spheres produced via thermally induced phase separation for tissue regeneration. *Acta Biomaterialia* **6,** 1158–1166 (2010).
7. Shao, W. & Leong, K. W. Microcapsules obtained from complex coacervation of collagen and chondroitin sulfate. *Journal of Biomaterials Science, Polymer Edition* **7,** 389–399 (1995).
8. Tsai, S. W., Chen, C. C., Chen, P. L. & Hsu, F. Y. Influence of topography of nanofibrils of three-dimensional collagen gel beads on the phenotype, proliferation, and maturation of osteoblasts. *Journal of Biomedical Materials Research - Part A* **91,** 985–993 (2009).
9. Yoon, J. *et al.* Fabrication of type i collagen microcarrier using a microfluidic 3D T-junction device and its application for the quantitative analysis of cell-ECM interactions. *Biofabrication* **8,** 1–10 (2016).
10. Gettler, B. C., Zakhari, J. S., Gandhi, P. S. & Williams, S. K. Formation of Adipose Stromal Vascular Fraction Cell-Laden Spheroids Using a Three-Dimensional Bioprinter and Superhydrophobic Surfaces. *Tissue Engineering Part C: Methods* **23,** 516–524 (2017).
11. Huang, P.-J. *et al.* Pneumatically Actuated Soft Micromold Device for Fabricating Collagen and Matrigel Microparticles. *Soft Robotics* **00,** soro.2016.0073 (2017).
12. Giraud-Guille, M. M., Mosser, G. & Belamie, E. Liquid crystallinity in collagen systems in vitro and in vivo. *Current Opinion in Colloid and Interface Science* **13,** 303–313 (2008).
13. Besseau, L. & Giraud-Guille, M. M. Stabilization of fluid cholesteric phases of collagen to ordered gelated matrices. *Journal of Molecular Biology* **251,** 197–202 (1995).
14. DiMarino, A. M., Caplan, A. I. & Bonfield, T. L. *Mesenchymal stem cells in tissue repair* 2013.
15. Fournier, B. P. *et al.* Multipotent Progenitor Cells in Gingival Connective Tissue. *Tissue Engineering Part A* **16,** 2891–2899 (2010).

16. Séguier, S. *et al.* Inhibition of the Differentiation of Monocyte-Derived Dendritic Cells by Human Gingival Fibroblasts. *PLoS ONE* **8,** 2–9 (2013).

17. Boissiere, C., Grosso, D., Chaumonnot, A., Nicole, L. & Sanchez, C. Aerosol route to functional nanostructured inorganic and hybrid porous materials. *Advanced Materials* **23,** 599–623 (2011).

18. Wang, Y. *et al.* The predominant role of collagen in the nucleation, growth, structure and orientation of bone apatite. *Nature materials* **11,** 724–33 (2012).

19. He, P., Davis, S. S. & Illum, L. Chitosan microspheres prepared by spray drying. *International journal of pharmaceutics* **187,** 53–65 (1999).

20. Zhou, Y., Li, S., Wang, D., Zhao, Y. & Lei, X. Estimation of type I collagen structure dissolved in inorganical acids from circular dichroism spectra. *Bioscience Journal* **34,** 778–789 (2018).

21. Giraud-Guille, M. M. & Besseau, L. Banded patterns in liquid crystalline phases of type I collagen: Relationship with crimp morphology in connective tissue architecture. *Connective Tissue Research* **37,** 183–193 (1998).

22. Alonso, B. & Belamie, E. Chitin-silica nanocomposites by self-assembly. *Angewandte Chemie - International Edition* **49,** 8201–8204 (2010).

23. Gobeaux, F. *et al.* Fibrillogenesis in Dense Collagen Solutions: A Physicochemical Study. *Journal of Molecular Biology* **376,** 1509–1522 (2008).

24. Pineri, M. H., Escoubes, M. & Roche, G. Water-collagen interactions: calorimetric and mechanical experiments. *Biopolymers* **17,** 2799–2815 (1978).

25. Miles, C. A., Burjanadze, T. V. & Bailey, A. J. The kinetics of the thermal denaturation of collagen in unrestrained rat tail tendon determined by differential scanning calorimetry. *Journal of molecular biology* **245,** 437–46 (1995).

26. Tiffany, M. L. & Krimm, S. Effect of temperature on the circular dichroism spectra of polypeptides in the extended state. *Biopolymers* **11,** 2309–2316 (1972).

27. Freudenberg, U. *et al.* Electrostatic interactions modulate the conformation of collagen I. *Biophysical Journal* **92,** 2108–2119 (2007).

28. Schneider, L. A., Korber, A., Grabbe, S. & Dissemond, J. *Influence of pH on wound-healing: A new perspective for wound-therapy?* 2007.

29. Kamranpour, N. O., Miri, A. K., James-Bhasin, M. & Nazhat, S. N. A gel aspiration-ejection system for the controlled production and delivery of injectable dense collagen scaffolds. *Biofabrication* **8,** 000000 (2016).

30. Matthews, J. A., Wnek, G. E., Simpson, D. G. & Bowlin, G. L. Electrospinning of collagen nanofibers. *Biomacromolecules* **3,** 232–238 (2002).

31. Gobeaux, F. *et al.* Cooperative ordering of collagen triple helices in the dense state. *Langmuir* **23,** 6411–6417 (2007).

32. Wang, Y. *et al.* Controlled collagen assembly to build dense tissue-like materials for tissue engineering. *Soft Matter* **7,** 9659–9664 (2011).

3

From collagen beads to dense collagen gels: influence of collagen concentration, *in vitro* fibrillogenesis conditions and processing conditions on the ultrastructure

Contents

3.1 Introduction

The objective of this chapter is to make dense and fibrillar collagen gels from the collagen beads of **Chapter 2**. The formation of the gels depends on several parameters such as collagen concentration, fibrillogenesis time, fibrillogenesis medium, etc. Therefore different parameters were varied in order to *(i)* study their influence on the ultrastructure of the gels, to *(ii)* understand the formation processes and to *(iii)* control the synthesis to obtain targeted matrices.

After studying the influence of different parameters on the size of the collagen beads during their sythesis by aerosol, the conditions were optimized and chosen specifically for enabling the injection of the beads. The size of the beads was adjusted to about 1 µm by using initial collagen solutions at 1 mg/mL. From macroscopic observations, this granulometry enabled a better dispersion of the collagen beads in the solvent, which was reduced in the case of larger diameter beads (initial collagen solutions at 2 mg/mL and 5 mg/mL, see **Figure 1.2 b and c, Chapter 2**). It seemed that bigger beads tend to aggregate more which limited their injectability (risk of clogging in the needle). The spray-drying parameters were adjusted to be less energy consuming: temperature, air flow and aspiration rate were reduced. Instead of physiological serum or phosphate buffer, an acidic aqueous solvent was chosen to transport and solubilize the beads during the injection.

The aim was to retain the liquid crystal properties of the collagen molecules (at acidic pH) to form as many anisotropic domains as possible. However, if the dissolution of the beads is too quick, they form a highly concentrated gel that becomes impossible to inject because of its viscosity. Collagen molecules being soluble at acidic pH, a mild acidic solvent was chosen: acetic acid at low concentration. Its pH is closer to the pKa of acetic acid and to the isoelectric point of collagen (pI=7.4) [1] than acetic acid at 500 mM (pH=2.5). Gobeaux *et al.* showed that the pH of the solvent has an influence on the phase diagram of collagen in solution [2] (see **Figure 3.1**). They reported that an increase in acetic acid concentration (from 2 mM to 500 mM initial concentration of the stock collagen solution) delays the appearance of the mesophases. At high acetic acid concentrations, the isotropic/cholesteric threshold can be observed around 70 mg/mL in collagen. Yet, their diagram shows an increase in acetic acid concentration (which evaporates more slowly than water), which leads to an increase of ionic strength as well. Besides, they did not take into account the formation of a nematic phase just above 40 mg/mL in collagen (their diagram only displays the isotropic/cholesteric transition).

Similarly, in our case, there is a high probability that acetic acid remains in the collagen powder (not completely evaporated during the spray-drying process). Indeed, qualitative experiments with a universal colored pH indicator showed that the pH of 2 mL of water decreases by several units when few mg of collagen beads are added. In addition, the spray-drying process may also remove volatile impurities from the collagen solution which can slighlty modify the phase diagram - the importance of their role was highlighted in the case of a commercial aliphatic alcohol possessing lyotropic properties [3].

The objective is to inject the material (collagen beads + acetic acid at low concentration) in a mold mimicking a tissue defect. In biological tissues, the pH is buffered at 7.4 which will induce fibrillogenesis *in situ*. To mimic the enzymatic process of the *in vivo* fibrillogenesis, different options are available *in vitro* such as alkaline NaOH solutions or phosphate buffer saline. By using phosphate buffers at different pH and ionic strength to induce *in vitro* fibrillogenesis, Gobeaux *et al.* showed that a variety of fibril morphologies can be obtained [4]. Ammonia vapors are found to generate

more homogeneous samples due to the slow diffusion process without disturbing the collagen network [5]. Thus, different exposure times to ammonia vapors of the injected collagen solution were studied in order to assess the influence on the ultrastructure, and later on the mechanical properties of the collagen gel (**Chapter 4**).

Then, a comparison with fibrillogenesis in phosphate buffer saline at pH=7.4 was performed since it could represent the closest medium to *in vivo* fibrillogenesis. Indeed, several questions remained open:

- the diffusion rate of the ions transported by ECM fluids inside the injected collagen solution;
- the timelapse needed to form the gel *in situ*;
- the final ultrastructure of the gel.

Finally, optimal fibrillogenesis conditions were fixed.

The injectable dense collagen solutions could be used for filling defects in collagen-rich tissues. Hence it is of importance to determine their ultrastructure with different *in vitro* fibrillogenesis conditions. By building pre-formed matrices instead of injectable ones, other uses are possible in the field of tissue regeneration. In the case of collagen membranes, such materials are often lyophilized to facilitate their storage and avoid any degradation potentially occuring in wet conditions [6]. However, this freeze-drying step may induce changes both in the ultrastructure of the material and on its mechanical properties.

Finally, thanks to a collaboration with LPP (Ecole Polytechnique) and LBIB (Reims University), we tried to promote the formation of chemical crosslinks [7] between collagen molecules by using plasma. We made the hypothesis that the presence of such crosslinks could dramatically enhance the mechanical properties of the gels.

3.2 Influence of the collagen concentration and exposure time to ammonia vapors on the ultrastructure

Collagen gels were synthesized following the protocols described in the **Experimental Chapter**. They were characterized by different microscopy techniques, differential scanning calorimetry and thermogravimetric analysis to gain knowledge about their ultrastructure. From the phase diagram obtained by Gobeaux *et al.* [2], collagen mesophases tend to appear at lower collagen concentrations when the acetic acid concentration is lower (see **Figure 3.1**). In our case, the first mesophase (nematic phase) could appear just above 40 mg/mL due to the low concentration of the low concentrated acetic acid solution. However, the remaining acetic acid in the collagen beads could increase the total acetic acid concentration of several orders of magnitude after collagen beads dissolution. Whenever possible three distinct target concentrations were investigated: 30 mg/mL (isotropic), 50 mg/mL (expected nematic) and 80 mg/mL (expected precholesteric/cholesteric) to scan the phase diagram.

3.2.1 Fibrillogenesis in ammonia vapors for three hours

3.2.1.1 Water and collagen contents, stability in temperature

Given the (low) water content of the collagen beads (measured by DVS in **Chapter 2**, **Figure 1.8**) and possible solution loss during gel synthesis, it appeared necessary to measure the real concen-

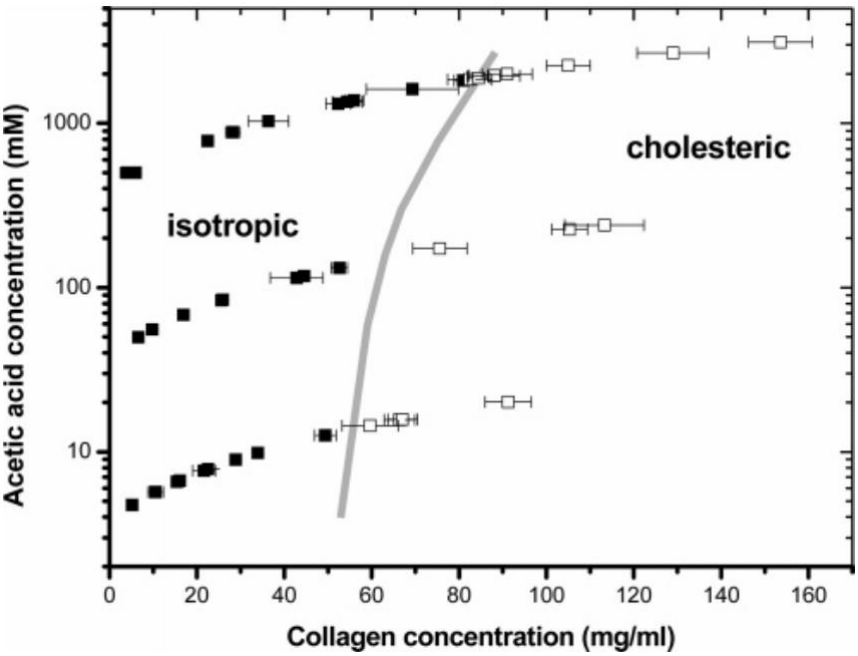

Figure 3.1: Collagen phase diagram made by evaporation of collagen solutions depending on the acetic acid concentration. Reproduced from Gobeaux 2007 [2].

tration of the collagen gels instead of considering only the theoretical concentration.

In the literature, the concentration of collagen is usually titrated by hydroxyproline. Thus we first performed hydroxyproline assays to determine the collagen concentration in the collagen gels and compare it to the targeted concentration. This assay is relevant for dilute collagen solutions or low concentrated collagen gels, but when it comes to dense collagen gels several problems may arise such as:

- the protocol takes into account a volume of collagen solution, and it is difficult to measure the volume of a small piece of gel. Thus we assume that the density of a collagen gel is equal to that of water. Both values are experimentally close for dilute collagen gels or solutions but tend to diverge when collagen concentration increases;
- as noticed by F. Gobeaux [8], the redissolution of collagen gels in acidic conditions is often not complete, especially with high collagen concentrations. Since this is the first step of the titration protocol, some hydroxyproline residues in the collagen molecules may not be accessible to chloramine T for oxidation. Thus the concentration may be underestimated;
- the protocol must be followed with extra precision, especially in terms of timespan, which makes it highly sensitive (experimentally, the titration will fail if one of the bath times is passed by 30 seconds, inducing the formation of a precipitate);
- finally, small pieces of gel are used (not too small but not too large either), about 5 mg which is supposed to correspond to a volume of 50 µL, so the assay is not performed on a representative amount of material.

Here, the tests were performed on three gel pieces from the same material at different locations for reproducibility purposes.

Conversely, TGA requires about 40 mg of material which is more representative of the bulk concentration (about 0.5 wt% for hydroxyproline assay *vs.* about 5 wt% for TGA). Therefore, TGA was also used and both techniques were compared. The TGA measurements were performed on two gels per targeted concentration.

Three thermogravimetric master curves are plotted in **Figure 3.2 (top)**, one for each concentration. The thermal decomposition of the collagen gel with air takes place in two steps [9]: first, the physisorbed water evaporates until 200°C. Then, from 200°C to 600°C, collagen is mainly degraded into water and carbon dioxide. The collagen concentration is thus measured starting at 200°C.

As shown in **Figure 3.2 (middle)**, the endothermal peak evidences the evaporation of free water at 100°C. From the superposition of the differential thermal analysis (DTA) curve (black) and the TGA curve (green), we measure bound water content between the beginning of the endothermal peak plateau after 100°C, and 200°C (evidenced by red dotted lines). The quantity of bound water measured for all samples and the collagen concentration measured by TGA are in **Table 3.1**.

Targeted collagen concentration	30 mg/mL	50 mg/mL	80 mg/mL
Bound water content (%)	0.041±0.005	0.081±0.014	0.146±0.034
Measured collagen concentration (mg/mL)	32±2	44±2	63±8

Table 3.1: Measured collagen concentration and bound water fraction, three hours ammonia condition.

It appears that the bound water content increases with the collagen concentration. This is relevant since the number of collagen molecules (and by extension fibrils) increases the number of water-mediated hydrogen bonds.

The measured collagen concentrations are plotted in **Figure 3.2 (bottom)** against targeted concentrations. The hydroxyproline titration gave highly variable results (varying over a range of concentration of almost 50 mg/mL for two targeted concentrations). Therefore, the hydroxyproline assay was kept only for dilute collagen solutions. The thermogravimetric analysis revealed that the gels at 30 mg/mL actually have the targeted collagen concentration. The gels at 50 mg/mL seem to be slightly less concentrated than expected (around 44 mg/mL) and the more the targeted concentration increases, the more discrepancies are observed (more variability at 80 mg/mL).

From now on, the collagen gels will be named by their theoretical concentrations for consistency purposes even if their measured concentration differs.

As shown in **Figure 3.3**, the denaturation endotherm is composed of one major peak. The stability of the collagen gels after fibrillogenesis in ammonia vapors for three hours does not show a high dependency on concentration, with endotherms centered around 50°C and the most concentrated collagen gel appears slightly more stable.

3.2.1.2 Ultrastructure of the gels

As mentioned in **Chapter 1**, ammonia vapors are classically used to induce fibrillogenesis *in vitro* in collagen solutions. Given the thickness of the samples (2 mm), three hours were sufficient for the gelation to be complete (F. Gobeaux observed that the fibrillogenesis rate of a collagen solution in a

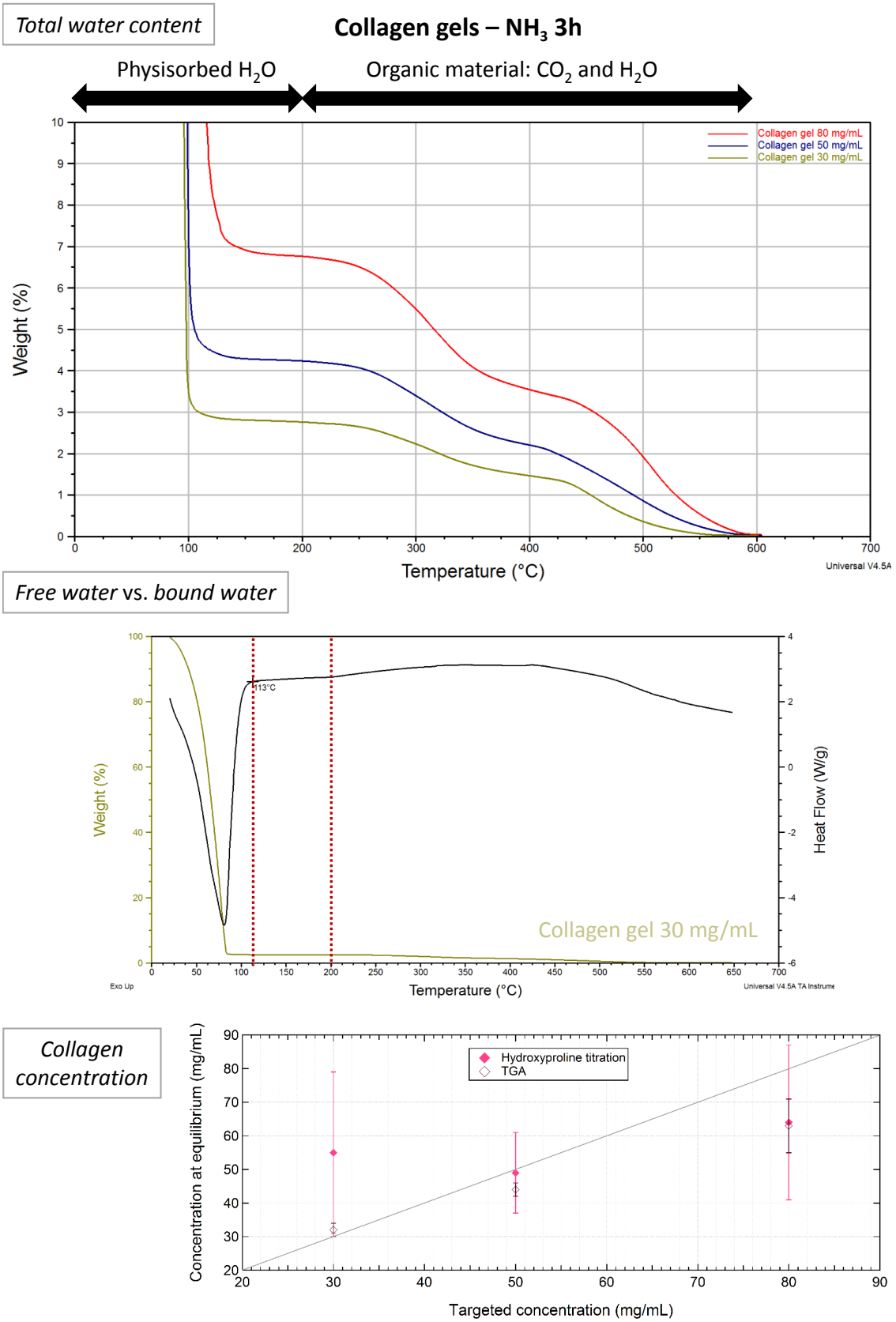

Figure 3.2: Top: thermogravimetric analysis of collagen gels; middle: heat flow plotted for the collagen gel at 30 mg/mL as an example, next to bound water content measured for three selected curves. Bottom: measured concentration *vs.* targeted concentration of collagen gels by Hydroxyproline assay *(two to four samples per targeted collagen concentration)* and TGA *(two samples per targeted collagen concentration)*.

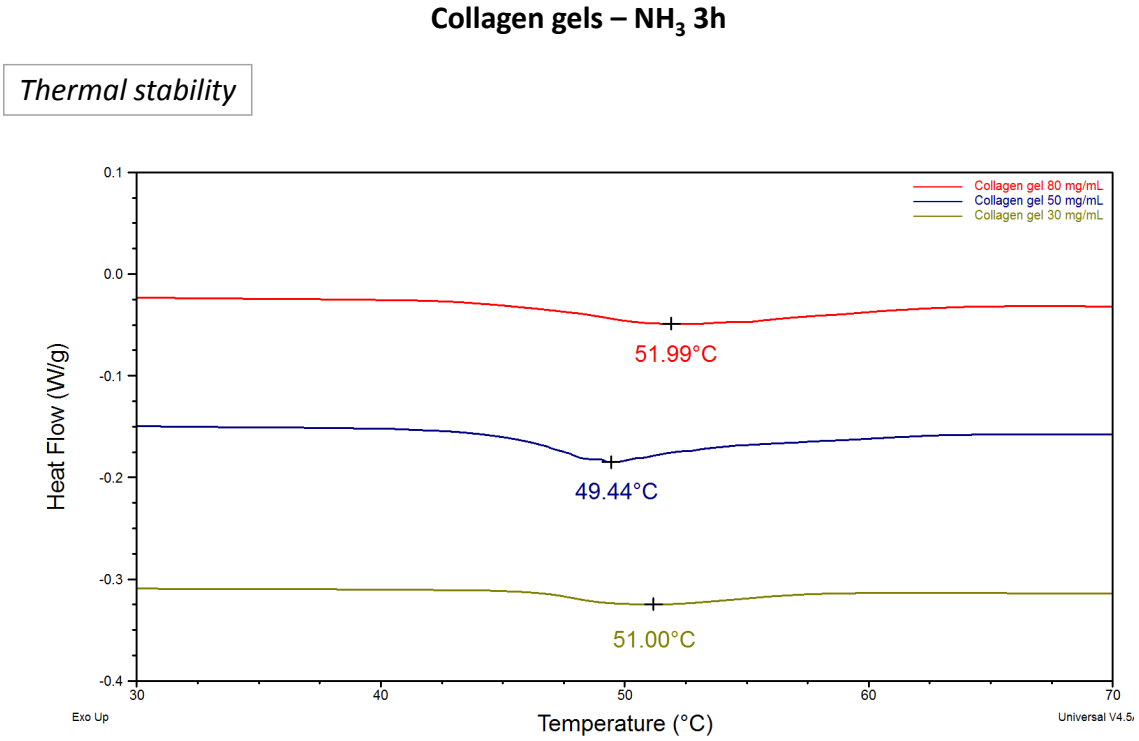

Figure 3.3: Thermal stability of collagen gels assessed by differential scanning calorimetry *(one to two samples per targeted collagen concentration).*

capillary was approximately 1 mm/hour [8], and Y. Wang exposed collagen matrices of 2-3 mm thickness to ammonia vapors for three hours [10]). As shown in **Figure 3.4**, the gels at 30 and 50 mg/mL look transparent while they are opaque when looked on the side. This is due to their thickness. Nevertheless, this transparency indicates that the collagen fibrils could be relatively small. The gel at 80 mg/mL is opalescent and contains opaque zones, which could be more or less concentrated in collagen.

The histology section of the collagen gel at 30 mg/mL in **Figure 3.5** displays weak birefringent zones. Some bright zones (empty arrow) turn dark after rotating the polarizers and vice versa (white arrow). The birefringent texture indicates the presence of nematic organizations locally. Some organized domains may not be observable due to the resolution of the microscope (1 µm). Due to technical problems during histological preparation (fixation, dehydration and/or embedding) the sample at 50 mg/mL could not be observed. At 80 mg/mL (see **Figure 3.6**), the gel displays large bright birefringent textures (white stars) that turn dark after rotating the polarizers (especially at the top of the sample) and more complex birefringent textures in the middle and bottom part of the sample. Alignments are thus present at large scale at this concentration, and possibly with other mesophase geometries locally. At higher magnification, the structure of the gel appears with a granular aspect. The phase diagram seems to be approximately followed (increased anisotropy when the concentration increases), which is consistent with the measured concentrations of the gels. Nevertheless, it is surprising that the gel at 30 mg/mL is somewhat birefringent. The centrifugation step, concentrating collagen beads in some locations, might explain this local anisotropy. Also, uneven section thickness

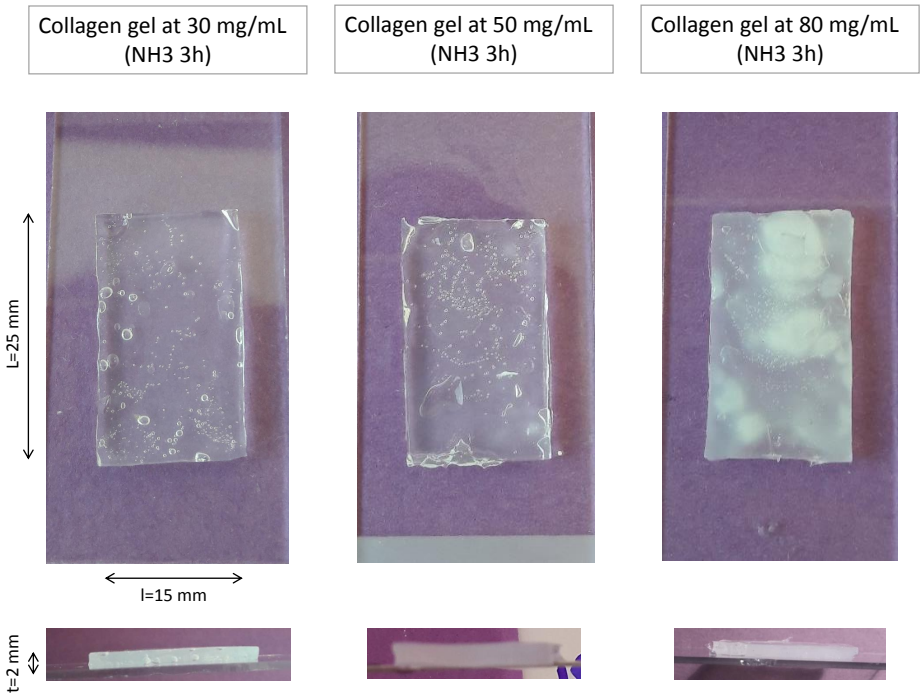

Figure 3.4: Images of collagen hydrogels after *in vitro* fibrillogenesis induced by ammonia vapors for three hours.

can induce birefringence fluctuations. The possible presence of only partially dissolved collagen beads may be the reason for the granular aspect of the collagen gel at 80 mg/mL.

As observed by SEM in **Figure 3.7 (top)**, the gel at 30 mg/mL contains different domains. The fibrils at the right part of each micrograph appear randomly distributed, while the left part of the micrograph at lower magnification shows some fibrillar alignments. The coexistence of both isotropic and anisotropic domains is certainly due to concentration heterogeneities. However, following the phase diagram, no particular organization was expected at this concentration. At 50 mg/mL (see **Figure 3.7, middle**), undissolved collagen beads are present in the gel (left micrograph) together with alignment domains over tens of microns. Collagen fibrils appear to form layers. The micrograph at higher magnification shows that the fibrillar organization is dense, and the size of the fibrils seems quite homogeneous at first sight. A higher amount of undissolved collagen beads remains in some parts of the gel at 80 mg/mL (see **Figure 3.7, bottom**). The beads appear embedded in the collagen matrix. At higher magnification, dense and aligned fibrillar domains are observed. The collagen fibrils seem to be homogeneous in size as well. The presence of undissolved beads in the samples above 50 mg/mL in collagen may locally increase the collagen concentration. Such local heterogeneities could explain the fact that the phase diagram is approximately followed up to 50 mg/mL (isotropic domains at 30 mg/mL, alignment domains at 50 mg/mL - measured concentration 44 mg/mL - typical of a nematic phase). When reaching 80 mg/mL, the restricted dissolution time may prevent the full dissolution of the collagen beads, thus the organization of the collagen molecules in the solution to form a precholesteric or even a cholesteric phase. Nevertheless, even at 30 mg/mL in collagen, the gels appear dense which contrasts with collagen gels found in the literature [11] that display larger interfibrillar spaces and heterogeneous fibril size as shown in **Figure 3.8**.

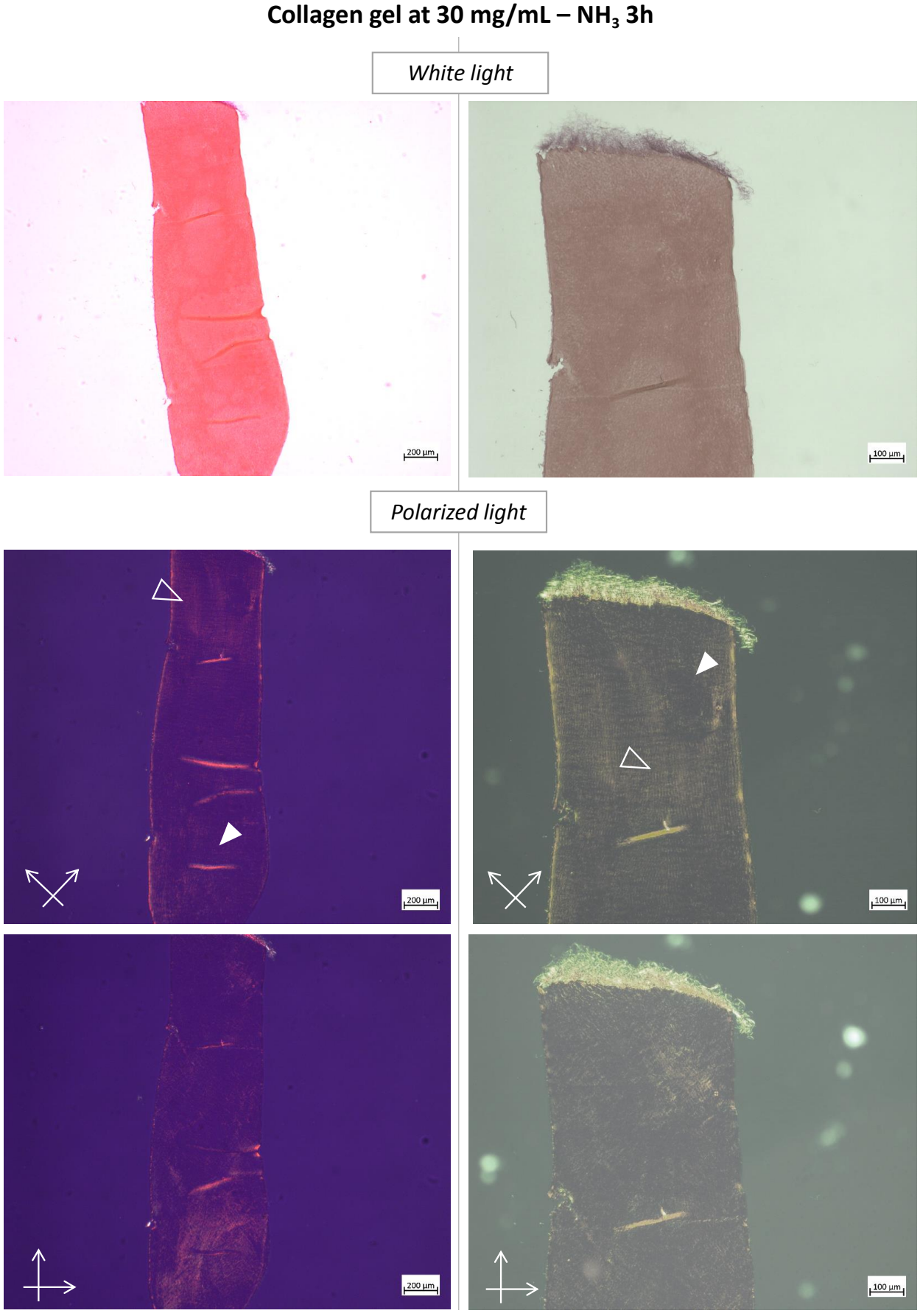

Figure 3.5: Polarized light micrographs of a histological section of a collagen gel at 30 mg/mL after fibrillogenesis in ammonia vapors for three hours.

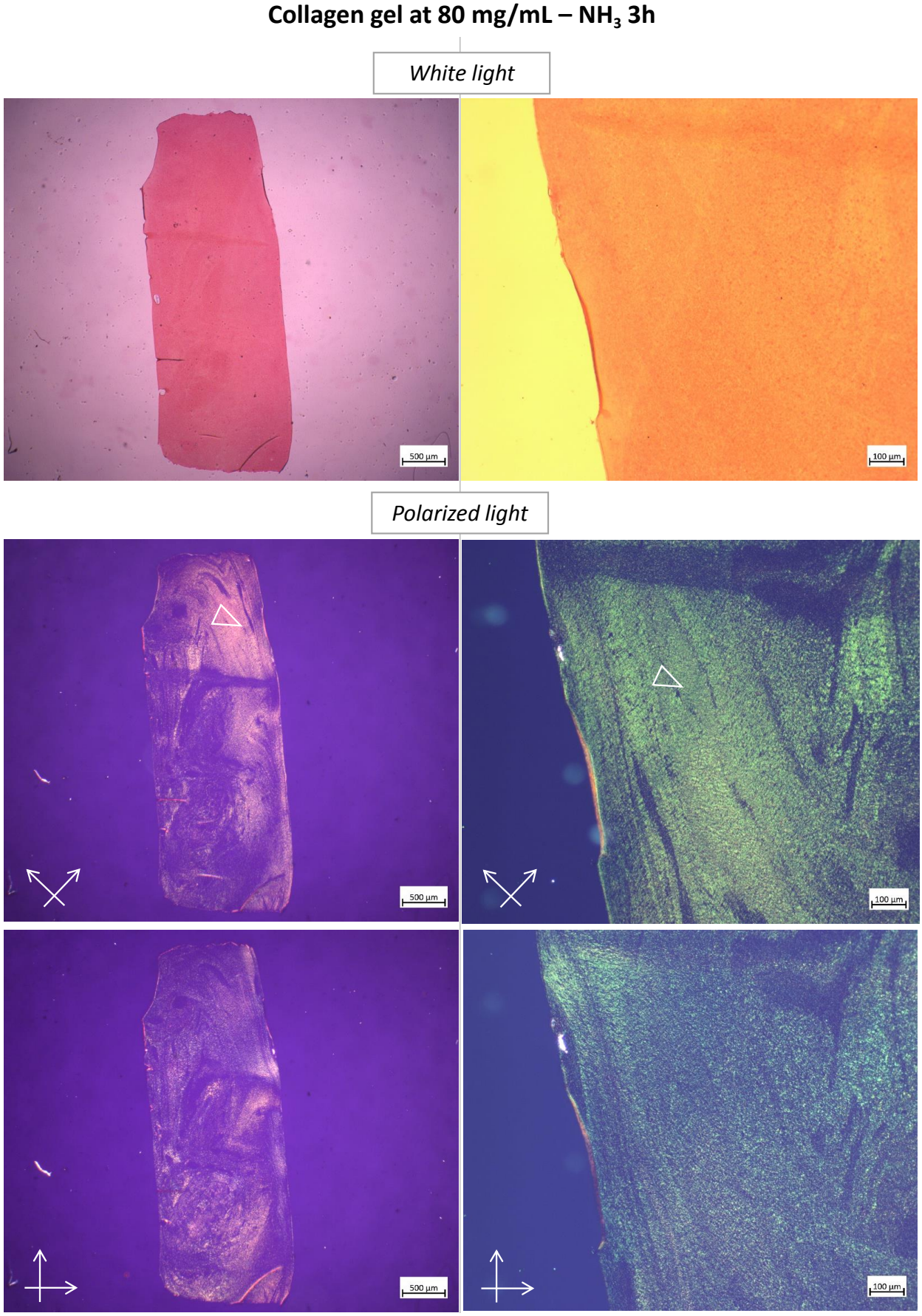

Figure 3.6: Polarized light micrographs of a histological section of a collagen gel at 80 mg/mL after fibrillogenesis in ammonia vapors for three hours.

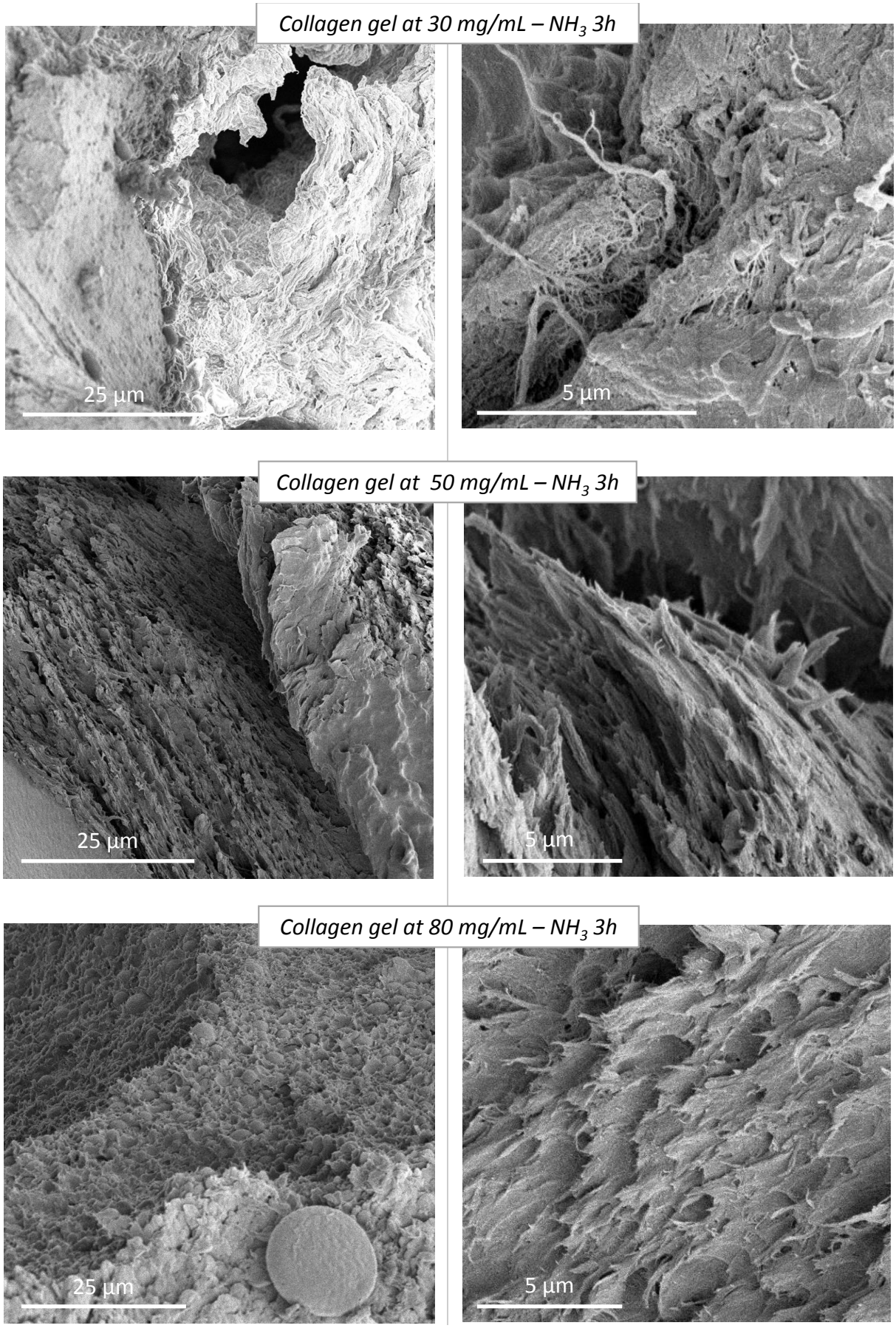

Figure 3.7: Scanning electron micrographs of collagen gels at 30, 50 and 80 mg/mL after fibrillogenesis in ammonia vapors for three hours.

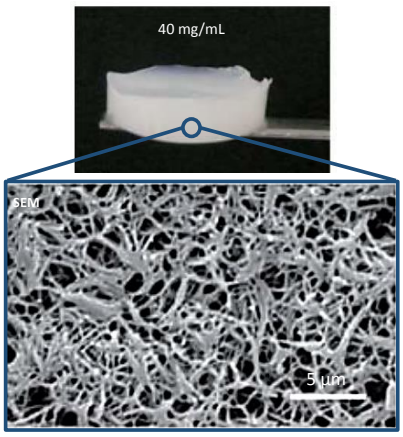

Figure 3.8: Top: macroscopic image of a collagen gel at 40 mg/mL (concentrated by evaporation). Bottom: scanning electron micrograph of the same collagen gel at 40 mg/mL. Reproduced from Giraud-Guille 2010 [11].

The ultrathin section of the collagen gel at 30 mg/mL displays randomly organized collagen fibrils (see **Figure 3.9, top**). At 50 mg/mL (see **Figure 3.9, bottom**), alignment domains are present over several microns and organized in a plywood fashion. Due to heavy technical problems, the sample at 80 mg/mL could not be observed. The TEM observations confirm the SEM ones: in all cases, the fibril size seems homogeneous with a small interfibrillar space compared to other collagen materials from the literature [11] (see **Figure 3.10, top**). At 50 mg/mL a plywood organization is present like in cornea [12] as highlighted in **Figure 3.10 (bottom)**: this organization consists in local successive layers of collagen fibrils perpendicular to one another. Actually, this concentration corresponds to a new mesophase in the collagen phase diagram [13] (see submitted article in *Appendix*). Therefore, it is likely that the TEM micrograph of our 50 mg/mL collagen gel at this precise location corresponds to the concentration of this particular mesophase, due to local fluctuations in concentration. Indeed, the concentration of the gel measured by TGA is actually 44 mg/mL and the so-called blue-phase appears at ≈45 mg/mL. From the SEM observations, the presence of undissolved collagen beads at higher concentrations should induce the formation of dense and aligned domains in between them due to the local increase in collagen concentration. However, it is possible that precholesteric or cholesteric organizations would not be observed due to the amount of undissolved beads, which would be consistent with the PLM observations. To promote the formation of such mesophases, it appears coherent that the dissolution time of the collagen beads should be increased from 30 min to one or a couple of days. More solvated collagen molecules may then be available for the self-assembly process in the solution. It is worth noticing that the increase in collagen concentration (more collagen molecules in solution) goes along with a potential increase in acetic acid, possibly explaining that the cholesteric organization may be reachable at higher concentrations than 80 mg/mL in our system.

3.2.1.3 Conclusion

The precipitation of fibrils *in vitro* by ammonia vapors for three hours led to the formation of dense collagen gels, with fibrils appearing calibrated at first sight. Thorough statistical analysis of fibril diameters should be performed to confirm this hypothesis. Besides, this feature seems independent of the collagen concentration above 40 mg/mL.

From macroscopic observations and TGA experiments, the collagen gels seem slightly heteroge-

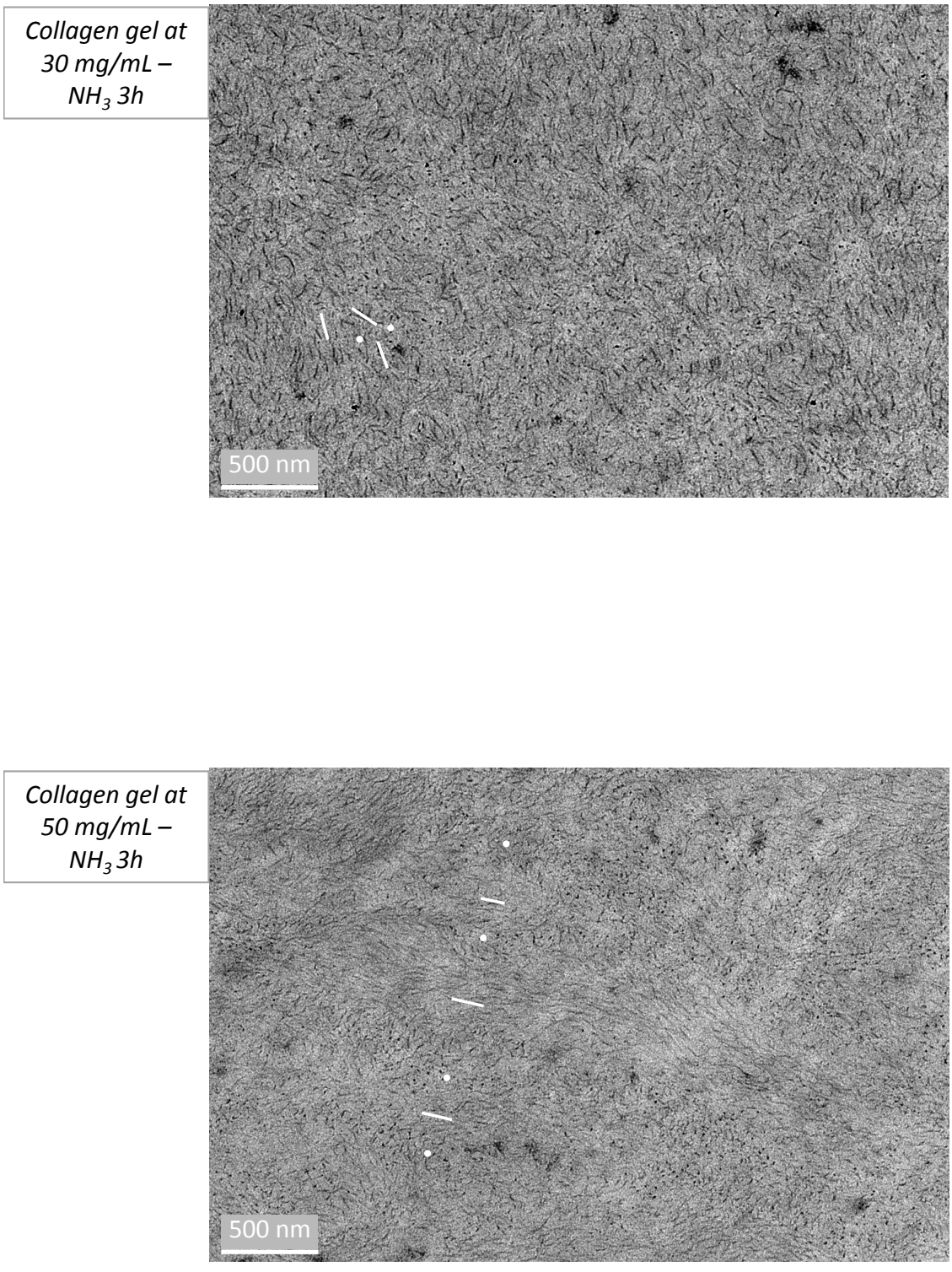

Figure 3.9: Ultrathin stained sections of collagen gels at 30 and 50 mg/mL after fibrillogenesis in ammonia vapors for three hours. White dots indicate fibrils perpendicular to the cross-section, white bars indicate fibrils in the plane of the cross-section as guides to the eye.

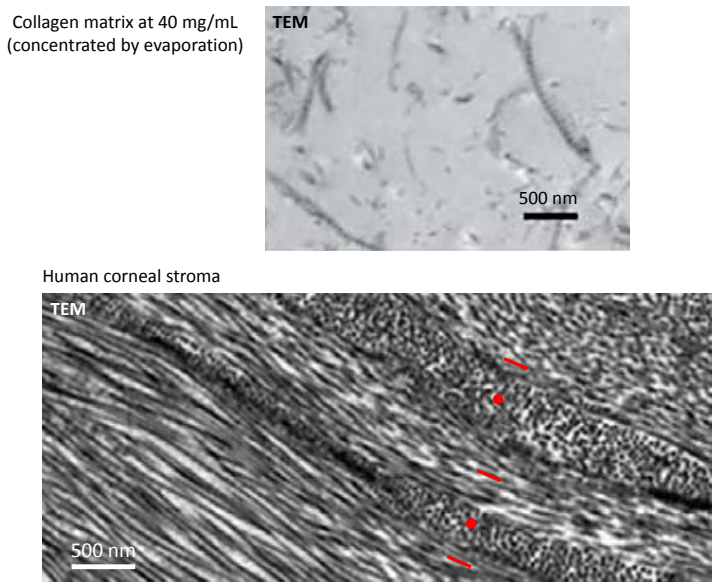

Figure 3.10: Top: transmission electron micrograph of a collagen matrix at 40 mg/mL (reproduced from Giraud-Guille 2010 [11]). Bottom: transmission electron micrograph of human corneal stroma (reproduced from White 2017 [14]); white dots represent collagen fibrils perpendicular to the cross-section and white bars represent collagen fibrils in the plane of the cross-section as guides to the eye.

neous in terms of concentration: the higher the concentration, the higher the heterogeneity. This heterogeneity was confirmed by microscopy observations, with at some locations the presence of large amounts of undissolved collaged beads.

The phase diagram is followed locally, with the presence of isotropic domains at 30 mg/mL. Alignment domains over hundreds of microns appear at 50 mg/mL and are also present at 80 mg/mL, consistent with the measured concentrations. Precholesteric phases could be present in the gels at 80 mg/mL but were not observed yet. To promote the formation of precholesteric or cholesteric phases, the dissolution time of the collagen beads in solution could be increased. Besides, the complete phase diagram of our system could be explored to determine precisely at which concentration the mesophases would be expected.

Finally, even if there is more bound water in the collagen gel at 80 mg/mL, it seems that its effect on the collagen thermal stability is not so strong at first sight. Other DSC experiments should be performed to validate or not this point. Interestingly, Miles *et al.* showed that a reduced amount of intrafibrillar water increases rat tendon thermal stability [15]. Therefore, it would be interesting to determine what proportion of the bound water measured in our gels is intra- or interfibrillar, in order to correlate it with their thermal stability.

It is worth mentioning that different processes used to increase collagen concentration appear to lead to different ultrastructures in terms of density and perhaps fibril size (as seen with evaporation). Thus, different mechanical responses could be obtained.

3.2.2 Fibrillogenesis in ammonia vapors overnight

When ammonia vapors are used in the literature for making collagen gels, exposure times are sometimes not mentioned [16], and can range from several hours [17], overnight [5], a day [18] to several days [19]. The exposure time obviously depends on the collagen concentration, the shape

and the thickness of the sample. But at given concentration and geometry, the exposure time could have an influence on the ultrastructure of the collagen gel. Thus another synthesis of collagen gels was performed in ammonia vapors, this time by leaving the collagen solutions in ammonia vapors overnight.

3.2.2.1 Water and collagen contents, stability in temperature

Thermogravimetric analysis of collagen gels synthesized in ammonia vapors overnight show the same behavior as the gels made in ammonia vapors for three hours with the three characteristic plateaus (see **Figure 3.11, top**). The endotherm corresponding to the loss of free water is located at 100°C as shown in **Figure 3.11 (middle)**. The amount of bound water was measured as previously. Only one sample could be tested for each concentration; other tests are needed to give relevant values of bound water quantities. Informative values are in **Table 3.2**.

Targeted collagen concentration	30 mg/mL	50 mg/mL	80 mg/mL
Bound water content (%)	0.024	0.035	0.123
Measured collagen concentration (mg/mL)	26	45	80

Table 3.2: Measured collagen concentration and bound water fraction, overnight ammonia condition.

As for the gels synthesized in ammonia vapors for three hours, the amount of bound water increases when the collagen concentration increases which is relevant. It seems, at first sight, that the collagen gels synthesized in ammonia vapors overnight may contain slightly less bound water.

The measured concentrations are very close to the targeted concentrations as displayed in the graph in **Figure 3.11 (bottom)**. There are some discrepancies at 30 and 50 mg/mL, confirming that the gels are locally slightly more or less concentrated than the average gel concentration as observed for the three hours ammonia vapors condition.

As displayed in **Figure 3.12**, there was a problem with the sample at 30 mg/mL. Its DSC curve is still plotted to give an idea of the endothermal region. The thermal stability of the collagen gels seems slighlty enhanced when the concentration increases, with endothermal peaks ranging from 48°C to 50 °C. Other tests are needed to confirm the trend.

3.2.2.2 Ultrastructure of the gels

From a macroscopic point of view (see **Figure 3.13**), the gels do not differ from those made in ammonia vapors for three hours neither in opalescence nor in handling. Some opaque spots are still present from 50 mg/mL, indicating possible local increase in concentration.

As observed by PLM in **Figure 3.14**, the collagen gel at 30 mg/mL displays bright birefringent textures (empty arrow) that turn dark after rotating the polarizers. The texture is typical of a nematic organization, which is unexpected at this concentration. Unfortunately, due to technical problems during histological preparation (sample size too small, thus unsuccessfull embedding in paraffin), no PLM observations could be performed yet for the samples at 50 mg/mL and 80 mg/mL. We tried to perform PLM observations on semi-thin sections (from TEM preparation), without success due to the insufficient thickness of the sections.

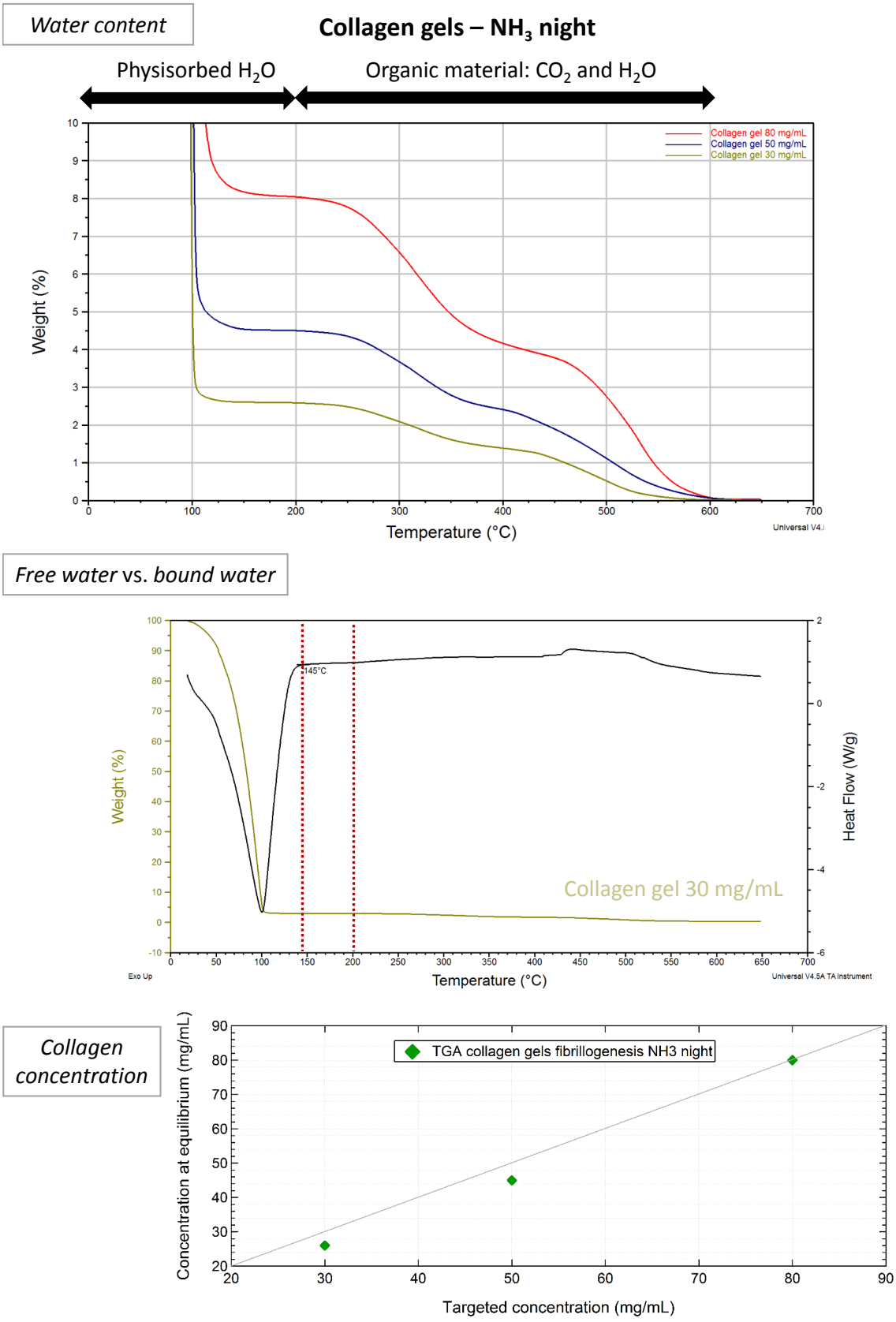

Figure 3.11: Top: thermogravimetric analysis of collagen gels; middle: quantity of bound water in the gels; bottom: measured concentration *vs* targeted concentration of collagen gels by TGA *(one sample per targeted collagen concentration)*.

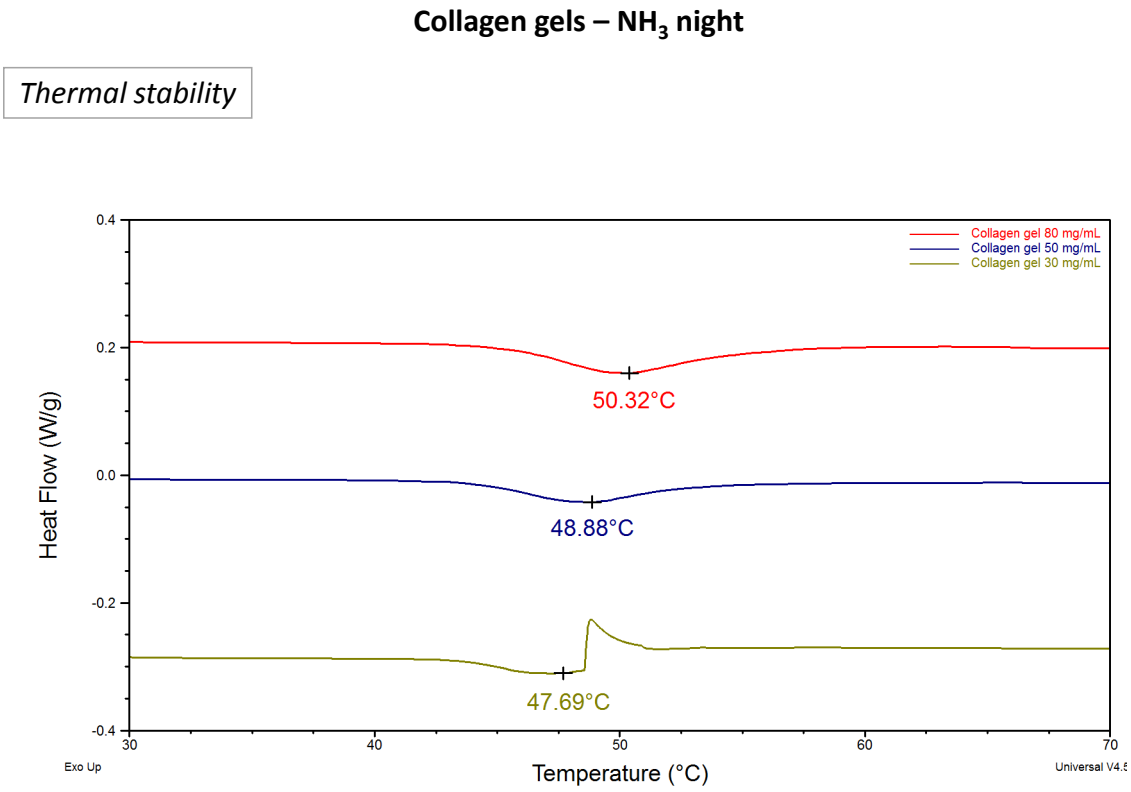

Figure 3.12: Differential scanning calorimetry analysis of collagen gels *(one sample per targeted collagen concentration)*.

Scanning electron micrographs of a collagen gel at 30 mg/mL in **Figure 3.15 (top)** displays fibrillar organizations but it is difficult to conclude on the presence of large scale alignments at low magnification. Local alignment domains are observed at higher magnification, as well as layer-like structures. At 50 mg/mL (see **Figure 3.15, middle**), the collagen fibrils display local alignment domains. Some undissolved beads are visible at high magnification (white arrow). When the concentration increases at 80 mg/mL (see **Figure 3.15, bottom**), collagen fibrils are organized in superimposed layers and present alignments domains over tens of microns. Again, the micrograph at higher magnification displays a dense organization.

Due to technical problems, no fibrillar organizations were observed by TEM for the collagen gel at 30 mg/mL (see **Figure 3.16, top**). Even if the cutting zone was carefully selected on the semi-thin section, it seems that only the resin is present (or the grid was not enough stained). The same problem arose for the collagen gel at 50 mg/mL (see **Figure 3.16, middle**) even if undissolved collagen beads seem to be present (white arrow). At 80 mg/mL (see **Figure 3.16, bottom**) partially dissolved collagen beads are present (white arrow) with alignment domains in between beads, either in the plane of the section (white bars) or perpendicular to the cutting plane (white dots). The density of aligned fibrils delimits the contour of the partially dissolved collagen beads. The collagen fibrils seem to have an homogeneous size, even though the sample was not stained enough to make it clearly visible. Statistical analysis of fibril diameters should be performed to confirm it.

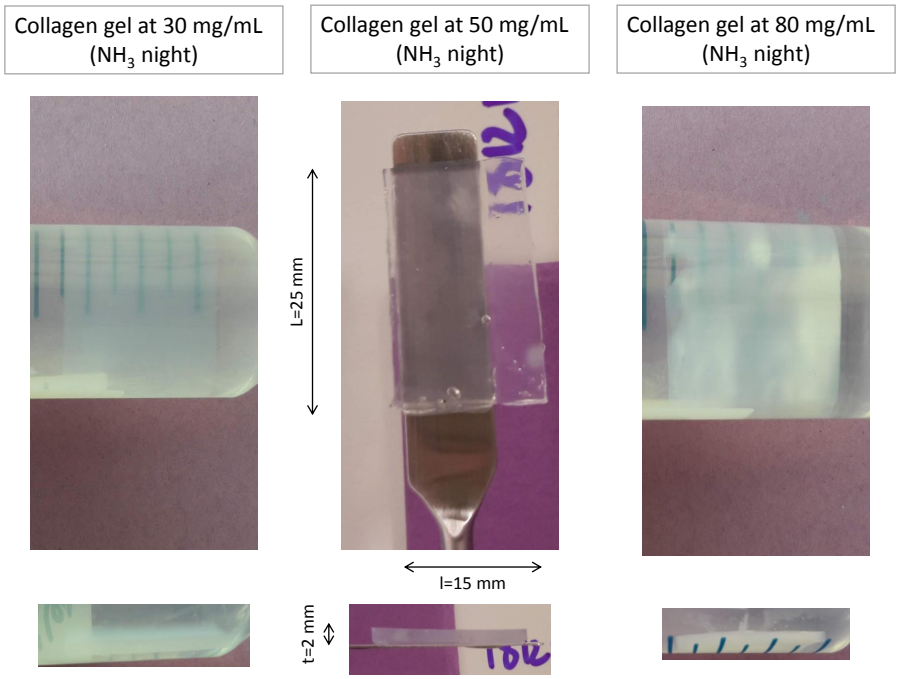

Figure 3.13: Images of collagen hydrogels after *in vitro* fibrillogenesis induced by ammonia vapors overnight.

3.2.2.3 Conclusion

Collagen solutions left overnight in ammonia vapors formed collagen gels highly resembling to collagen gels from the three hours condition, in terms of macroscopic aspect and ultrastructure. More thermogravimetric tests should be performed, but it seems that the gels contain less bound water than with the three hours condition. Also, their thermal stability seems reduced. If these observations are confirmed, it would mean that structural changes occur when the gel is left longer than three hours under ammonia vapors. We hypothesize that the bound water measured by TGA is related to a "specific surface area" of the fibrils, which would increase when fibril size reduces.

At fixed solvent quantity per targeted concentration, two consequences are possible: *(i)* the amount of bound water may decrease following a decrease in the number of fibrils thus an increase in fibril size (at fixed concentration) or *(ii)* the number of fibrils would increase (at fixed concentration) thus their size would be reduced (more free water due to the increased interfibrillar space). This hypothesis could be confirmed or not by performing a statistical analysis of fibrils diameters and comparing the results to those obtained for collagen gels synthesized in ammonia vapors for three hours, and by performing Small Angle X-ray Scattering experiments to probe intermolecular and interfibrillar distances [20].

3.2.3 Discussion

The formation of collagen gels with fibril sizes that seem homogeneous originates from the use of ammonia vapors, and may also come from the use of spray-dried collagen beads. Collagen matrices concentrated by reverse dialysis exhibit polydisperse fibril sizes [21, 22]. Due to the use of a large initial volume of dilute collagen solution, the dialysis membrane shrinks when collagen concentration increases. At high concentrations, the collagen solution sticks to the membrane. To remove it, shear forces are induced which disturb the initial collagen assembly. Therefore, fibrils of different sizes are

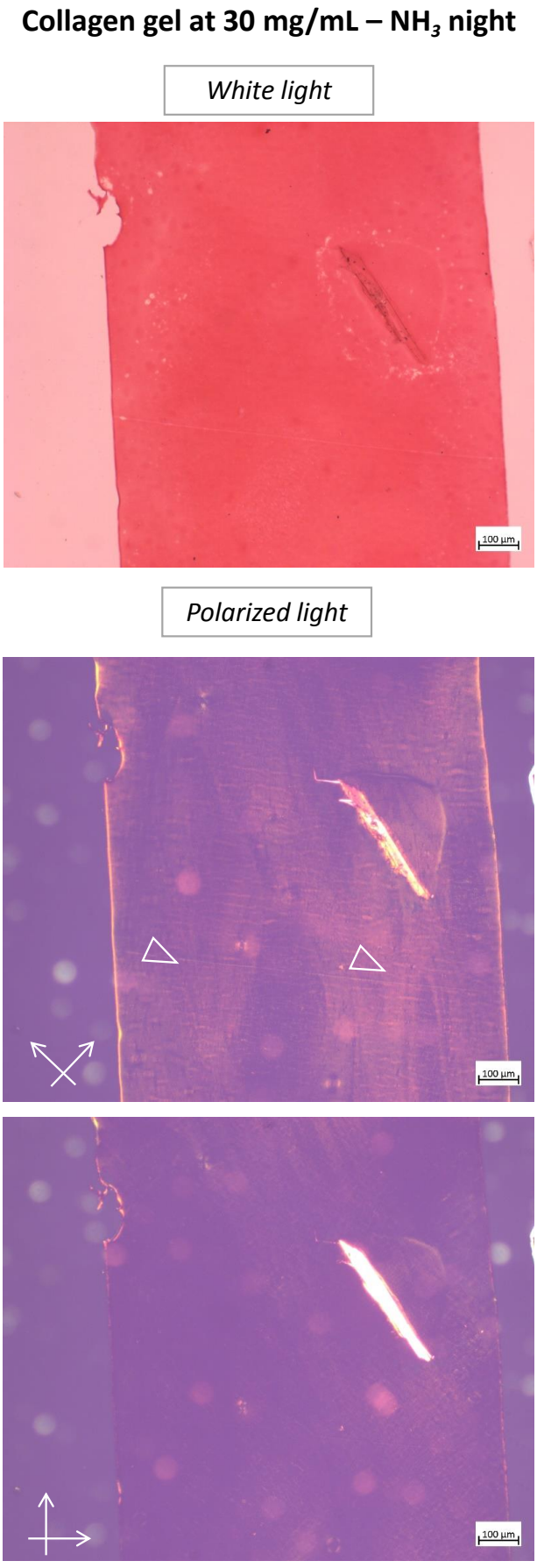

Figure 3.14: Histological section of a collagen gel synthesized under ammonia vapors overnight at 30 mg/mL as observed by polarized light microscopy.

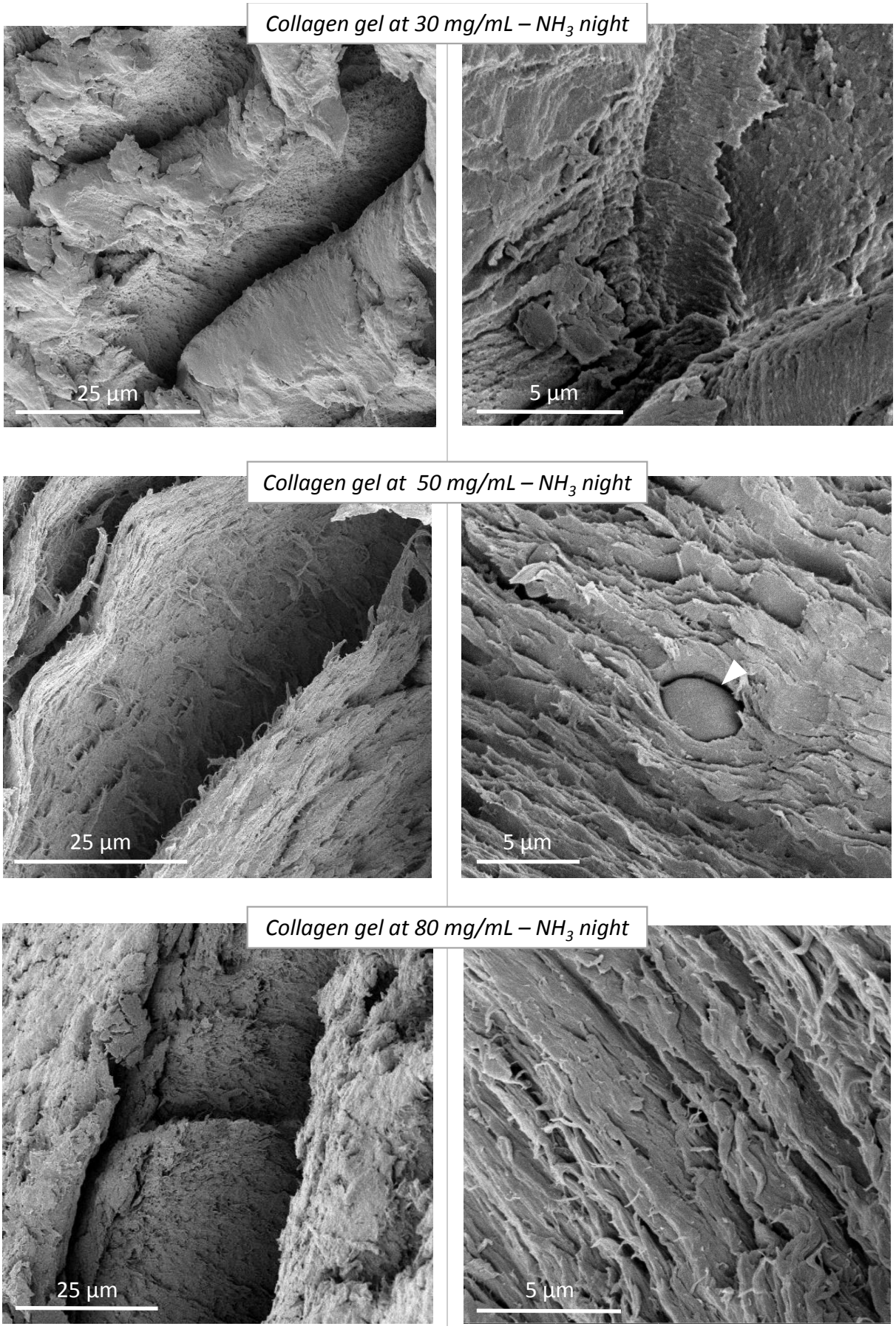

Figure 3.15: Scanning electron micrographs of collagen gels at 30, 50 and 80 mg/mL after fibrillogenesis in ammonia vapors overnight.

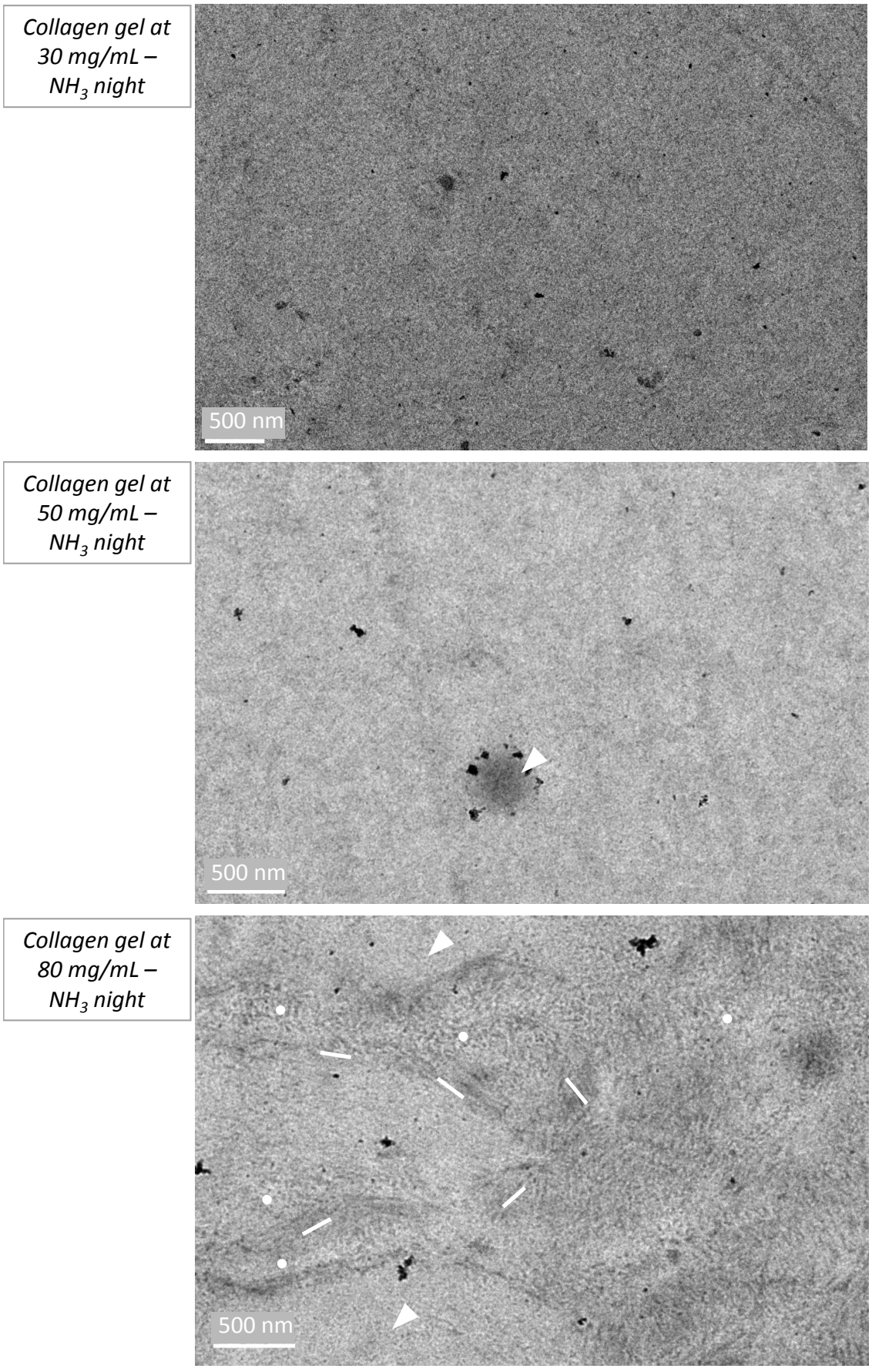

Figure 3.16: Transmission micrographs of collagen gels at 30, 50 and 80 mg/mL after fibrillogenesis in ammonia vapors overnight.

precipitated by ammonia vapors. In the case of evaporation [11], shear forces are also applied during mixing in order to homogeneise the collagen solution (the top tends to evaporate faster than the bottom). Thus, heterogeneous fibrils are also formed after using ammonia vapors.

Up to now, one of the most successful process to control the fibril size and the collagen concentration in 3D is injection coupled with reverse dialysis [19]. This process enables a slow concentration of the collagen solution in the mold, thus leaving enough time for the collagen molecules to self-assemble. Using dry, concentrated collagen beads in a slightly acidic solvent is similar: the beads dissolve progressively, enriching their surroundings with collagen molecules which increases continuously the collagen concentration in solution, and in 3D. No mixing is required to homogeneize the concentration since ideally, the collagen beads are evenly dispersed (in practice a centrifugation step is performed to remove air bubbles which creates zones that are more or less concentrated). So the process seems to have an impact on the formation of fibrils with quite homogeneous sizes in the volume of the gel.

Ideally, the spray-drying process would also enable a long range ordering of the collagen molecules in 3D at each targeted concentration, thus potentially creating mesophases in bulk. In practice, the long range ordering of collagen molecules is prevented by the centrifugation step: undissolved or partially dissolved collagen beads tend to aggregate at the bottom of the eppendorf due to their increased weight compared to the rest of the solution. This phenomenon is macroscopically visible when highly concentrated collagen gels are removed from the mold after *in vitro* fibrillogenesis: they contain opaque zones (more concentrated) next to translucent zones (less concentrated). Therefore, depending on the average concentration of the sample, it would be possible to obtain locally the formation of any mesophase of the collagen phase diagram. Thus, the collagen gels may contain anisotropic domains at the scale of collagen beads aggregates.

As mentioned in **Chapter 1**, the fibril morphologies obtained *in vitro* are highly dependent on the pH, collagen concentration, ionic strength and incubation temperature. The process used to make concentrated collagen gels seems to influence the polydispersity of fibril sizes, while the exposure time to alkaline pH during *in vitro* fibrillogenesis could influence the size of the fibrils. Yet, there is no clear consensus on the subject. For example, when Gobeaux *et al.* performed their study on the fibrillogenesis of dense collagen solutions with phosphate buffers [4], they did not observe any change in fibril diameter from pH 6 to 12. It is worth noticing that F. Gobeaux mentions that they did not control the ionic strenght for the pH study [8]. Another study on the fibrillogenesis of dilute collagen solutions (2 mg/mL) [23], still using phosphate buffer saline to precipitate fibrils *in vitro* but at 30°C, actually found different results. The diameter of the collagen fibrils increased when the pH of the phosphate buffer used to induce fibrillogenesis increased. They also demonstrated that the more time the collagen solution was left at a given fibrillogenesis pH, the more the diameter of the collagen fibrils increased. However, this study questions the influence of the temperature on the resulting size as well.

By using ammonia vapors at room temperature, the major expected effect on collagen is the pH effect. Collagen molecules are only assembled with physical interactions in our case (no chemical crosslinker). ^{13}C solid-state NMR studies performed on different collagen-rich tissues [24, 25] showed that even though collagen fibrils are quite stiff, their dynamics is provided by the mobility of the molecules (and the amino acids side groups) which have fast motion (on the order of magnitude of tenth of milliseconds or less). Therefore, it is possible that after three hours under ammonia vapors, the collagen molecules within fibrils continue interacting with each other by physical interactions which may form bigger fibrils. In addition, more time is left for ammonia molecules to deprotonate water molecules which also modifies the dynamics of the system. We may thus hypothesize that the

collagen fibrils produced in the gels exposed to ammonia vapors overnight are bigger (either in length or diameter or both) than those produced during the three hours condition. Systematic comparison of fibrils diameters in TEM micrographs would be necessary to validate this assumption.

It is worth mentioning that after fibrillogenesis, the gels are rinsed with sterile milliQ H_2O until the water reaches neutral pH. The gels are then put in sterile tubes containing sterile water until further use. Therefore, the influence of the preservation medium on the ultrastructure of the gel could also be explored (buffered or not, pH, ionic strength, type of ions).

3.3 Influence of processing conditions on the ultrastructure: fibrillogenesis medium, freeze-drying and freeze-thawing, chemical crosslinking by plasma

3.3.1 Fibrillogenesis in phosphate buffer saline

Phosphate buffer saline (PBS x1) was chosen as the fibrillogenesis medium due to the closeness of its pH (7.4) and ionic strength (164 mM) with human plasma. Collagen gels at concentrations of 30 mg/mL, 50 mg/mL and 80 mg/mL were synthesized following the protocol described in the **Experimental Chapter**.

3.3.1.1 Water and collagen contents, stability in temperature

As seen in **Figure 3.17 (top graph)**, the thermal decomposition of collagen with air takes place in three steps [9]: first, the water adsorbed on collagen evaporates until 200°C. Then, from 200°C to 600°C, combustion occurs and collagen is mainly degraded into water and carbon dioxide. Inorganic matter from the PBS salts is degraded from 600°C. The collagen concentration is measured at 200°C while taking into account the salt weight. **Figure 3.17 (middle)** displays the endothermal peak of free water evaporation at 100°C for a collagen gel at 30 mg/mL as an example.

After free water loss, bound water is measured as previously (see **Figure 3.17, middle**). The measured bound water quantities and collagen concentrations are summarized in **Table 3.3**.

Targeted collagen concentration	30 mg/mL	50 mg/mL	80 mg/mL
Bound water content (%)	0.036±0.0011	0.055	0.070±0.042
Measured collagen concentration (mg/mL)	35±1	45	57±8

Table 3.3: Measured collagen concentration and bound water fraction, PBS condition.

As measured for the gels synthesized in ammonia vapors, the amount of bound water increases when the collagen concentration increases. The values are lower than for the gels synthesized in ammonia vapors for three hours, especially for the gel at 80 mg/mL. The thermal stability of the collagen gels synthesized in PBS is thus expected to be lower.

The measured collagen concentrations are plotted in **Figure 3.17 (bottom)** against theoretical concentrations. Surprisingly, the collagen gels at 30 mg/mL actually have a slightly higher concentration than expected (35±1 mg/mL). The measured concentration of the gels at 50 mg/mL is fairly close to the targeted concentration (45 mg/mL) while the gels supposedly at 80 mg/mL actually appear less concentrated (57±8 mg/mL). This demonstrate local fluctuations in collagen concentration for

each gel.

The collagen gels have a similar thermal behavior no matter their concentration, as shown in **Figure 3.18**: their denaturation process seems to happen in two steps. The first one starting just before 40°C, with an extremum around 43°C. The major part of the denaturation happens between 50°C and 53°C. However, the gel at 80 mg/mL appears less stable (second endothermal peak is lower). As mentioned in **Chapter 1**, both water content and self-assembly have an influence on the thermal stability of collagen. Therefore, the first denaturation endotherm could be linked to the presence of smaller fibrils that are more hydrated: their peak denaturation temperature is closer to that of collagen molecules in solution (37°C). It could also be linked to the presence of collagen molecules that were not precipitated during the fibrillogenesis process. The second peak could correspond to bigger fibrils, which increases their thermal stability. Indeed, the second endothermal peak is closer to the denaturation peak of collagen-rich tissues (around 60°C for acellular dermis [26]). Further structural characterizations are needed to validate or not these hypotheses.

3.3.1.2 Ultrastructure of the gels

After demolding, the macroscopic aspect of the gels was highly different from that of the ammonia condition. Unlike the collagen gels synthesized in ammonia vapors, the collagen gels made in PBS were opaque (white) whatever the concentration as shown in **Figure 3.19**. Given the thickness of the samples (about 2 mm), the colour of the gels indicate that they are probably composed of large fibrils or fibril aggregates that scatter light, unlike the collagen gels synthesized in ammonia vapors.

When observed by polarized light microscopy after histological preparation (see **Figure 3.20**), the collagen gel at 30 mg/mL displays few bright birefringent domains (empty arrow), and a majority of dark domains. The bright domains turn dark after rotating the polarizers. At higher magnification, birefringent textures can be observed with a weak intensity. Even though no birefringence at all is expected at this concentration (isotropic phase), the sample appears to have local alignment domains (nematic phase). Thus the concentration over the sample is not homogeneous. For 50 mg/mL (see **Figure 3.21**), the sample displays bright birefringent domains (empty arrow) over a larger scale, that turn dark after rotating the polarizers. They indicate the presence of alignments which are expected at this concentration (above the nematic phase threshold). At higher magnification, a pore is observed in the matrix, filled with collagen fibrils. Very small birefringent domains are observed (few microns large). They may be due to the presence of only partially dissolved collagen beads. When the concentration is increased at 80 mg/mL (see **Figure 3.22**), the birefringent domains are larger and the intensity of the brightness increases. The increase in intensity indicates that more fibrils are aligned in the same direction. At higher magnification, nematic textures are observed (empty arrow). Different textures seem present locally but it is difficult to conclude on the type of the mesophase.

Scanning electron micrograph of the gel at 30 mg/mL (see **Figure 3.23, top left and right**) shows randomly organized domains with larger fibril size together with denser domains made of fibrils that appear smaller. At 50 mg/mL (see **Figure 3.23, middle left and right**), the collagen fibrils appear not particularly organized. The micrograph at higher magnification displays some undissolved beads embedded in a dense collagen matrix (white arrow), next to fibrillar domains (empty arrow). Finally, at 80 mg/mL (see **Figure 3.23, bottom left and right**) the gel contains alignment domains.

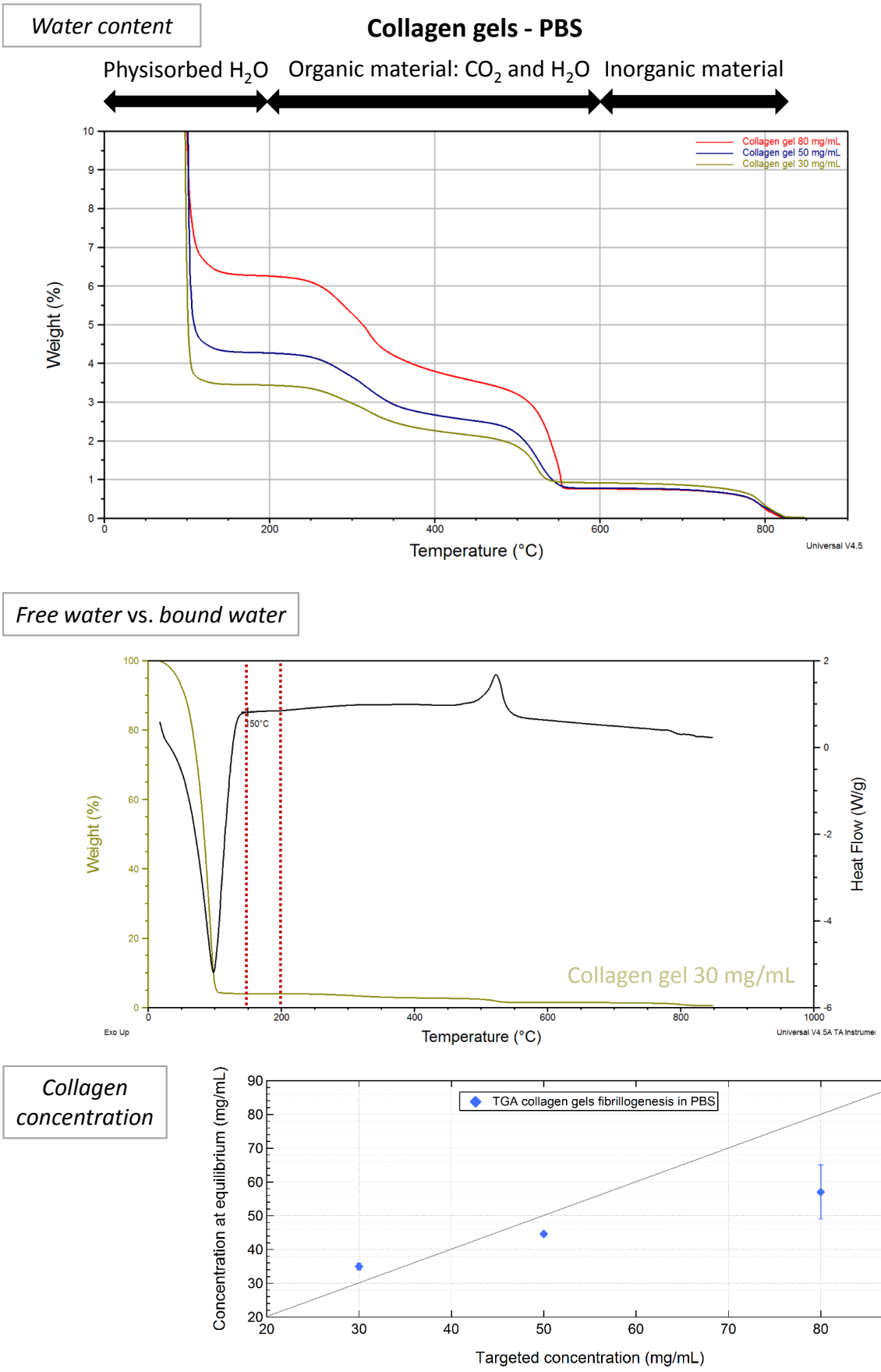

Figure 3.17: Top: thermogravimetric analysis of collagen gels; middle: quantity of bound water; bottom: measured concentration *vs* targeted concentration of collagen gels *(one to two samples per targeted collagen concentration)*.

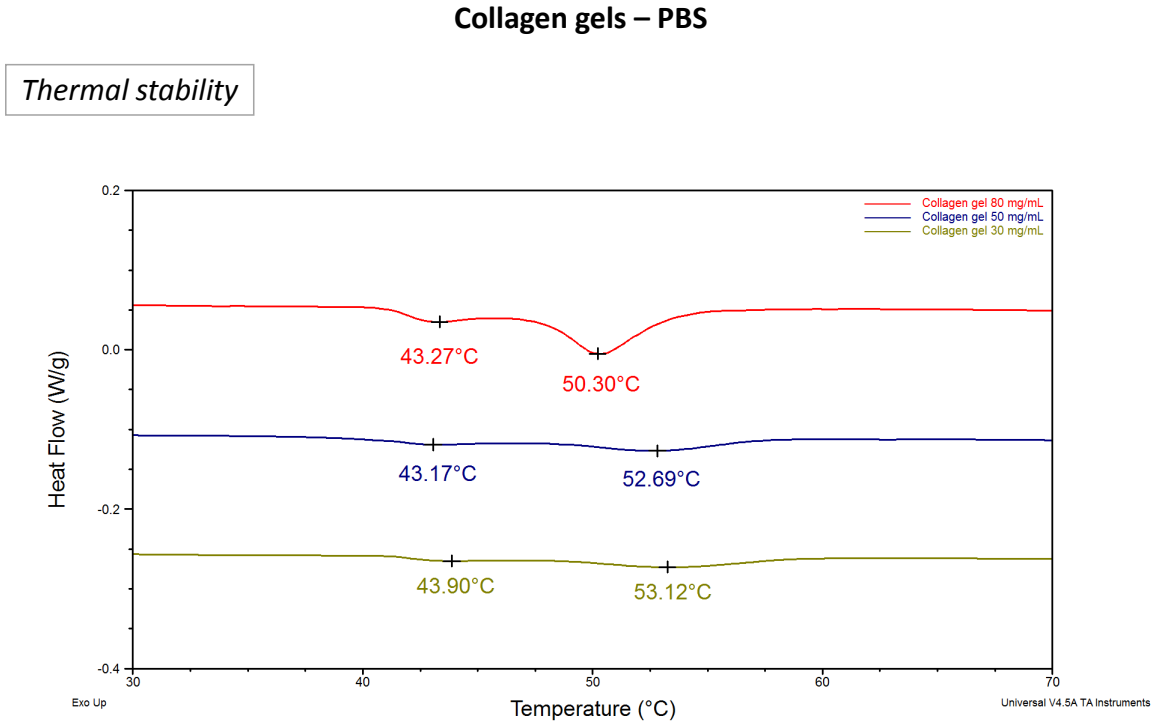

Figure 3.18: Thermal stability of collagen gels synthesized in PBS assessed by DSC *(one sample per targeted collagen concentration).*

The micrograph at higher magnification displays aligment domains that seem to be organized in layers. These micrographs show that all samples have different ultrastructures. The fibril size appears to vary, larger fibrils forming loose aggregates and smaller fibrils forming denser domains. Statistical analysis of fibril sizes should be performed to confirm this trend. In the case of the sample at 50 mg/mL, this effect may be related to the presence of partially dissolved collagen beads that increase locally the collagen concentration and may lead to the formation of smaller fibrils in their vicinity.

As observed by transmission electron microscopy, the collagen gel at 30 mg/mL contains randomly organized cross-striated fibrils (see **Figure 3.24, top**), thus confirming SEM observations. The gel at 50 mg/mL (see **Figure 3.24, middle**) also displays cross-striated fibrils. Undissolved collagen beads are present (white arrow) and collagen fibrils aggregate in between beads where the collagen concentration is locally increased (empty arrow). At 80 mg/mL (see **Figure 3.24, bottom**), tissue-like fibrils are present with clearly visible cross-striations, unlike the ones observed in the gels made in ammonia vapors. The fibrils align over tens of microns and form larger aggregates. Partially dissolved collagen beads seem also present (in darker grey, shown by white arrow).

3.3.1.3 Conclusion

As observed by electron microscopies, the gels formed in PBS seem to have two different populations: one made of partially dissolved collagen beads, the other made of cross-striated fibrils. The presence of these two populations could explain the thermal behavior of the gels (two endothermal

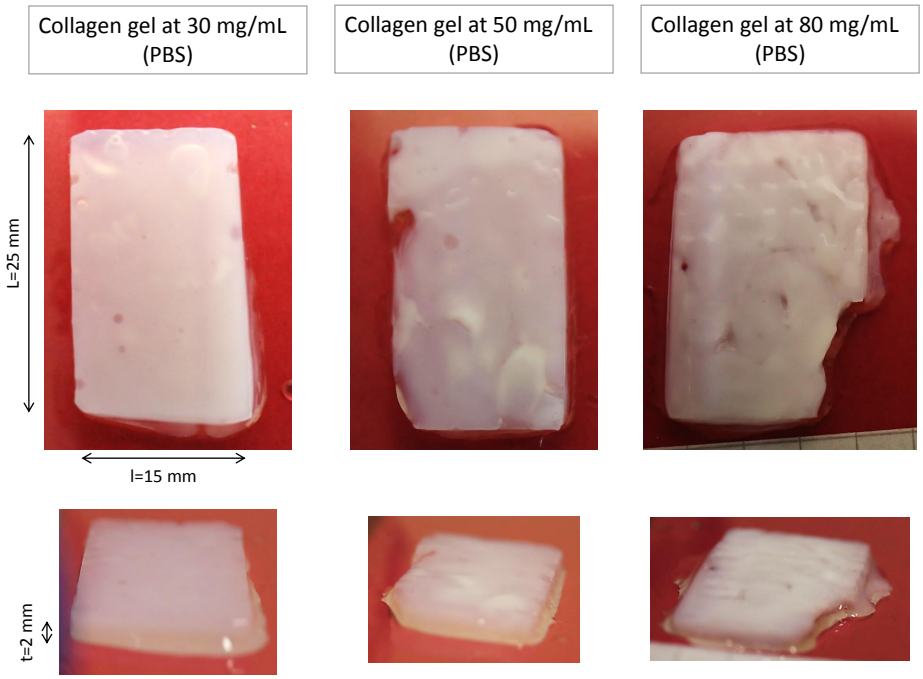

Figure 3.19: Images of collagen hydrogels after *in vitro* fibrillogenesis in PBSx1.

peaks). The presence of alignment domains at 80 mg/mL is consistent with the measured concentration of the gel. Moreover, this gel has more tissue-like fibrils than its equivalent made in ammonia vapors.

It was noticed in the literature that phosphate ions seem to play a particular role during collagen fibrillogenesis [27, 28]. Phosphate ions have the ability to interact with some amino acids side groups, therefore creating a screening between collagen molecules and interfering in the electrostatic interactions of these molecules. Thus, using a phosphate buffer to induce fibrillogenesis *in vitro* can induce side effects that may explain *(i)* the different fibril morphologies (when compared to the ammonia condition), *(ii)* a reduced capacity to bind water molecules, and *(iii)* a slightly higher thermal stability in temperature (second peak) when compared to collagen gels made in ammonia vapors, where only a pH trigger is used without imposing an ionic strength.

3.3.2 Discussion

The difference in fibril morphology between collagen gels made in phosphate buffer and ammonia vapors can be explained by different parameters.

Gobeaux *et al.* demonstrated that pH and ionic strength have an influence on fibril morphology [4]. When the pH is increased over 13, the collagen fibrils do not assemble with the typical D-spacing of 67 nm but rather form shorter and thinner fibrils (see **Figure 3.25**). When ionic strength increases, collagen fibrils tend to be larger but also tend to form two distinct populations of small and large fibrils.

The pH of PBS is 7.4. Measurements performed on collagen gels during fibrillogenesis in ammonia vapors with a liquid universal pH indicator revealed that the pH of the gels is 10-11 (the gels initially red turned purple). So the precipitation of cross-striated fibrils is expected in both cases, leading to the presence of a typical banding pattern. Such fibrils were observed by TEM for the collagen

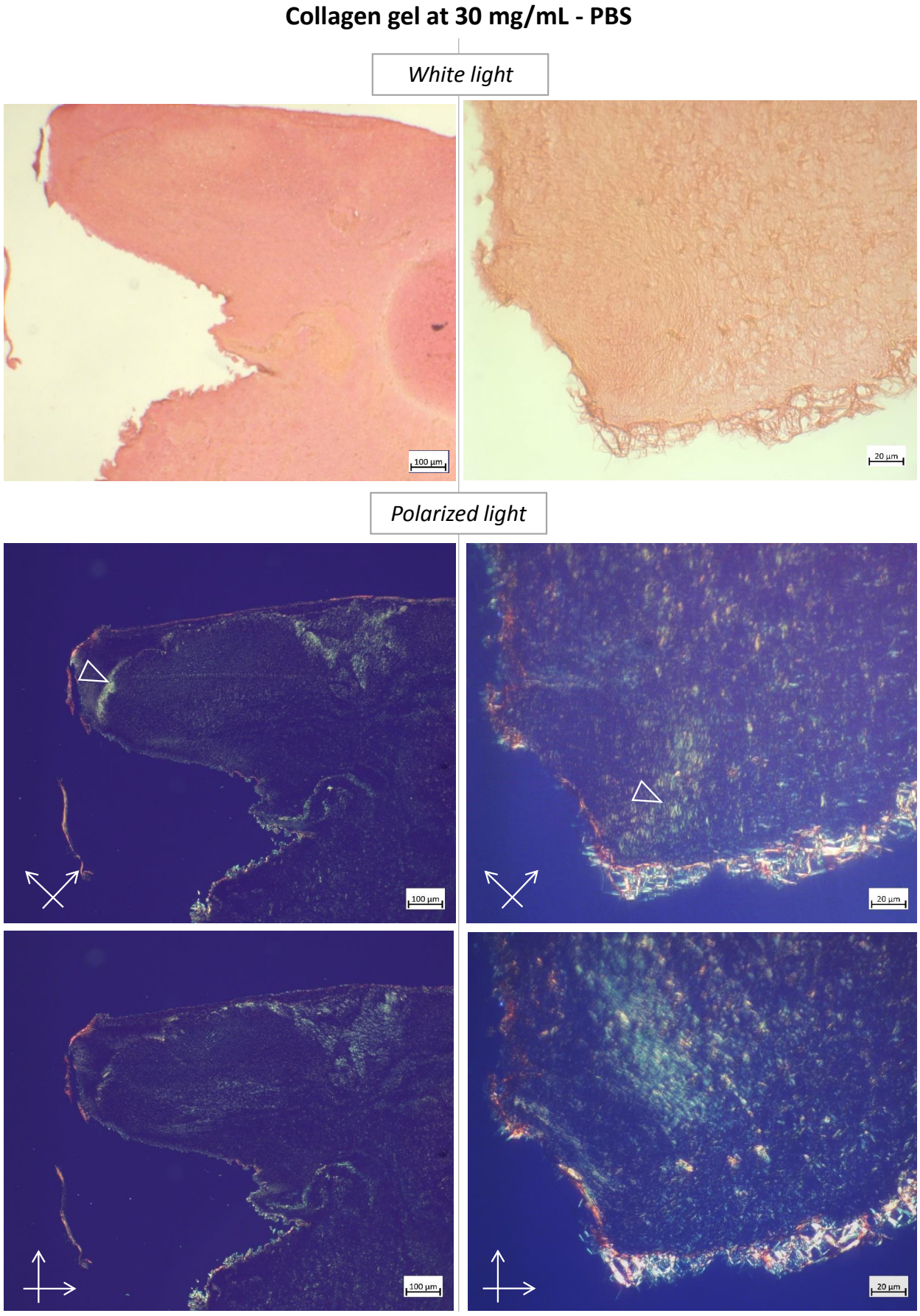

Figure 3.20: Polarized light micrographs of a histological section of a collagen gel at 30 mg/mL.

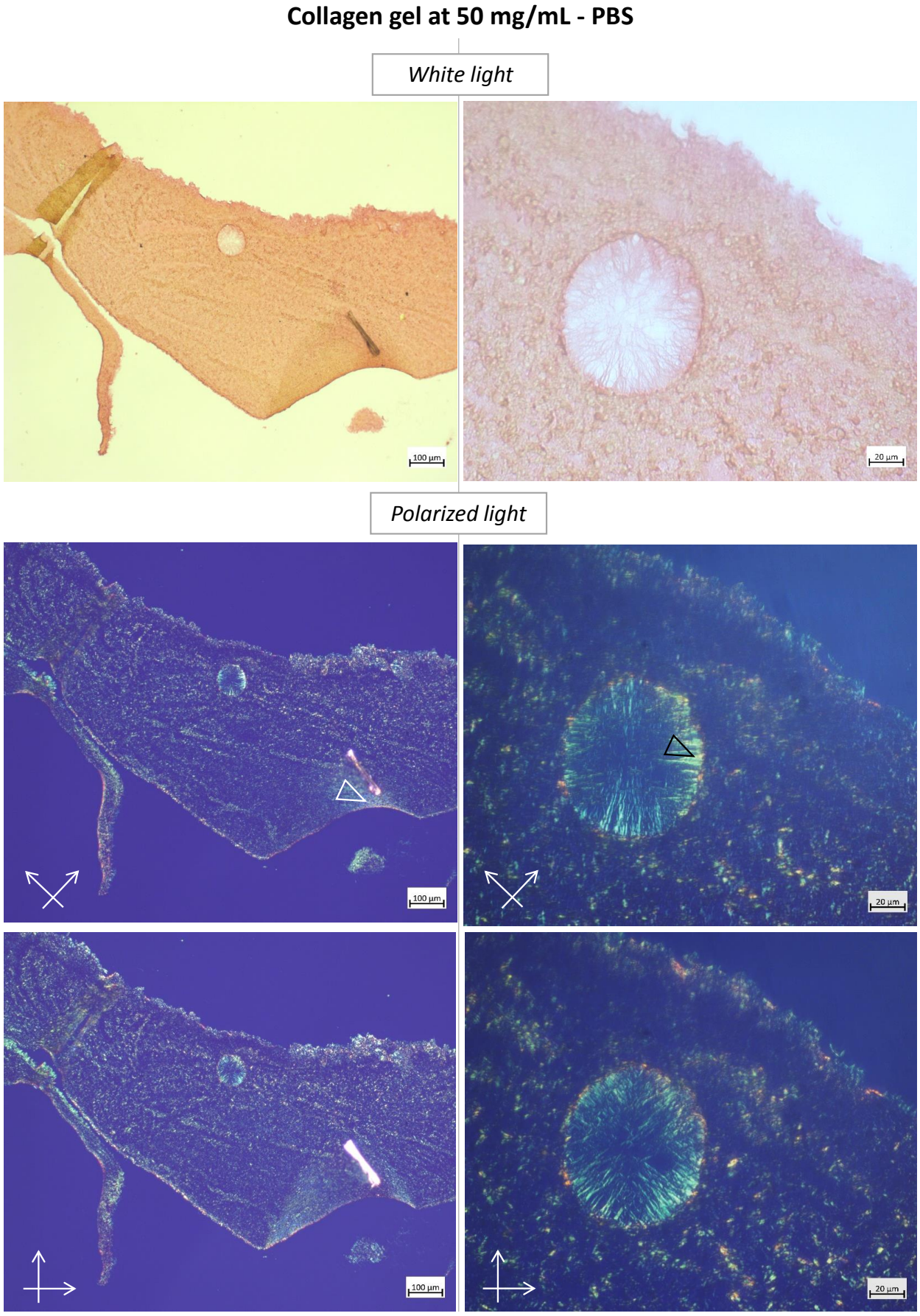

Figure 3.21: Polarized light micrographs of a histological section of a collagen gel at 50 mg/mL.

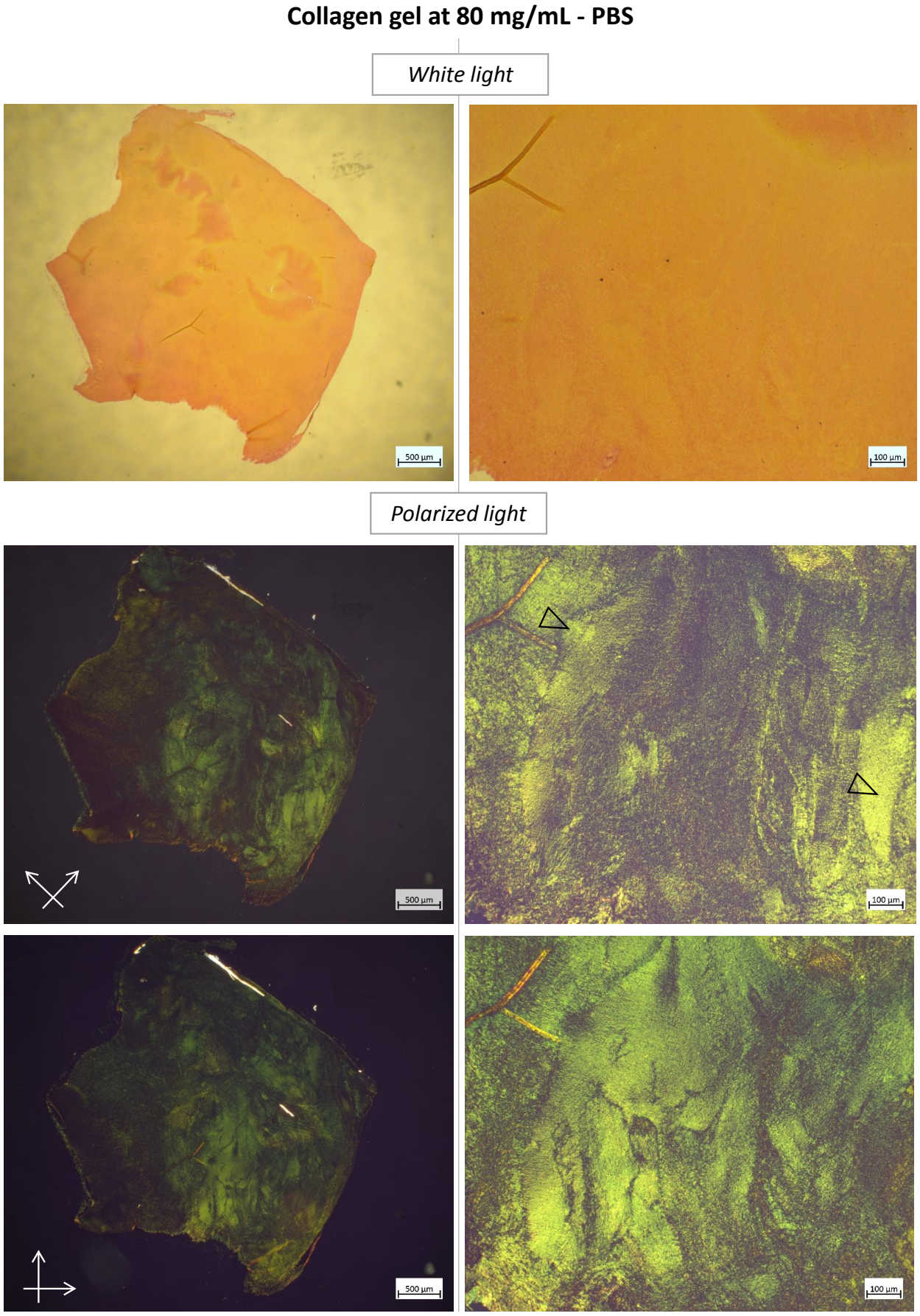

Figure 3.22: Polarized light micrographs of a histological section of a collagen gel at 80 mg/mL.

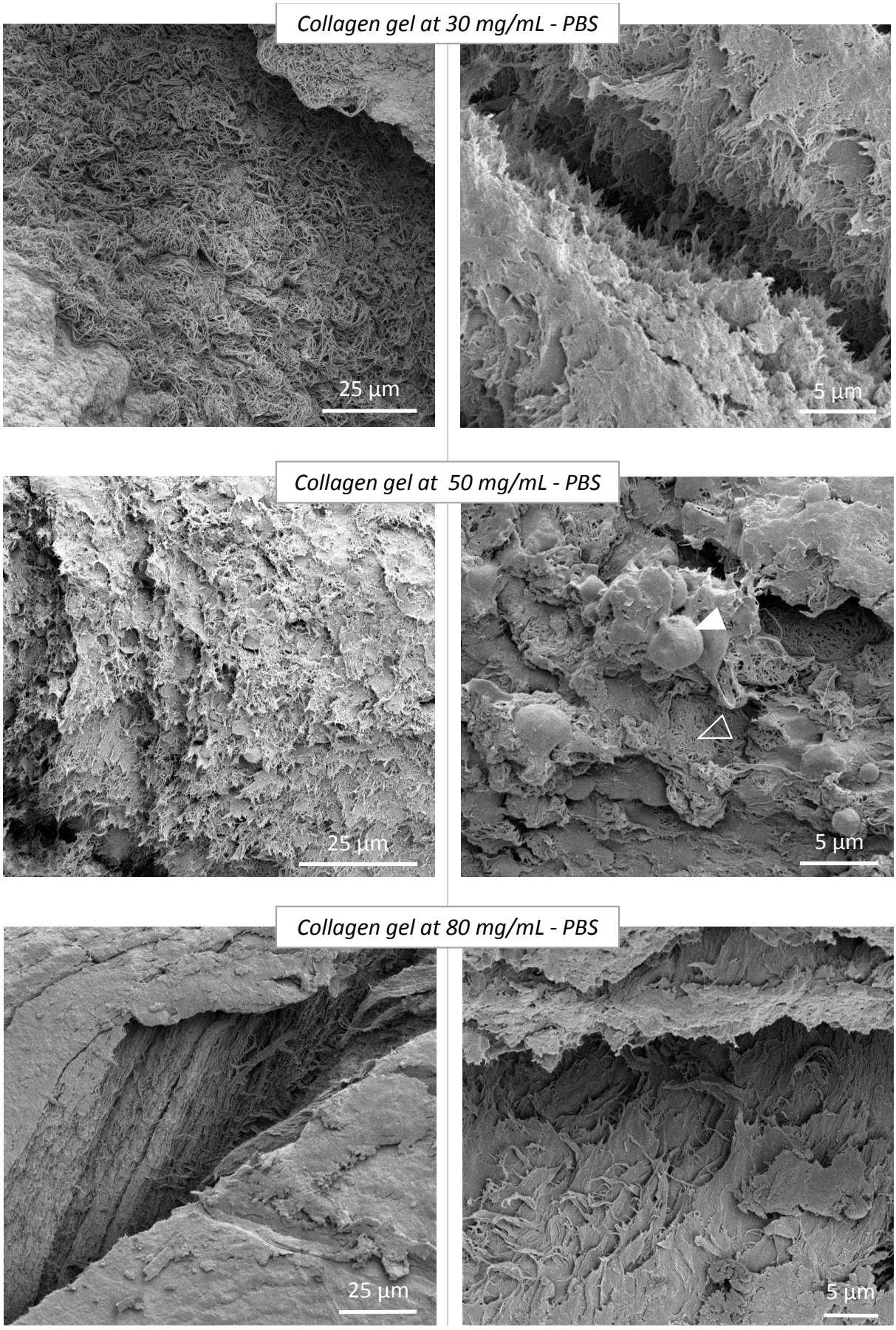

Figure 3.23: Scanning electron micrographs of collagen gels at 30, 50 and 80 mg/mL.

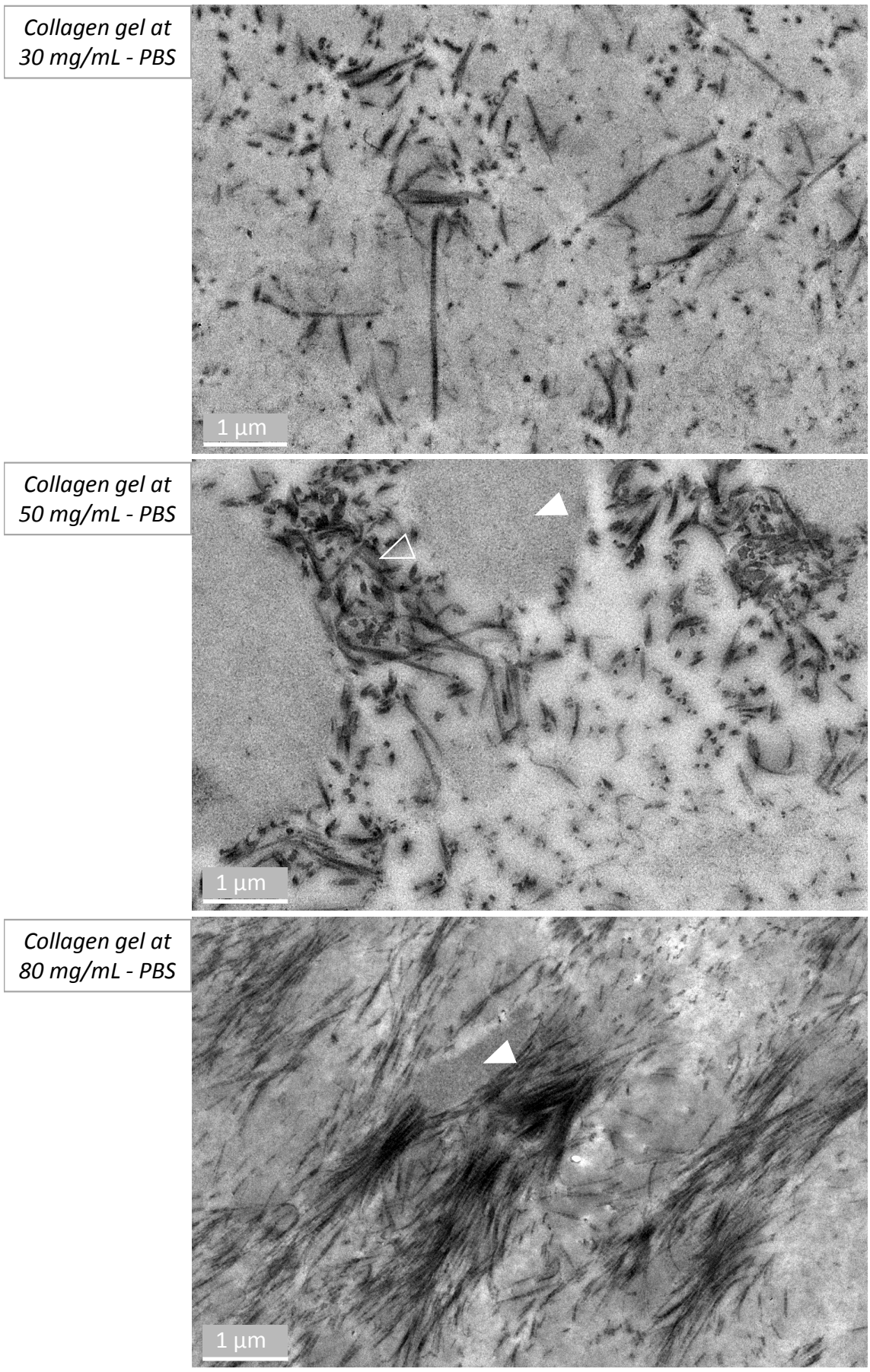

Figure 3.24: Ultrathin stained sections of collagen gels at 30, 50 and 80 mg/mL.

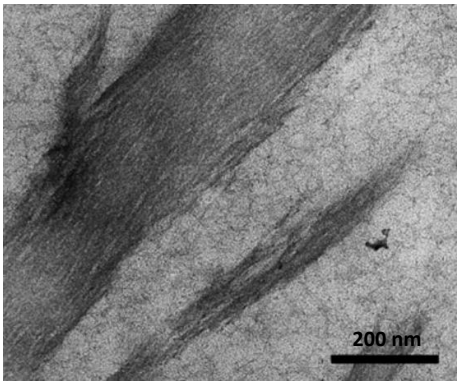

Figure 3.25: Fibril morphology at pH over 13: the self-assembly of collagen molecules seems destabilized, no banding patterns are observed. Reproduced from Gobeaux 2008 [4].

gels precipitated in PBS and for collagen gels precipitated in ammonia vapors at low concentrations (less than 150 µL in volume, fibrillogenesis during 24h, concentrations at 10 mg/mL and 20 mg/mL: see **Figure 3.26**). The ionic strength of PBS is equal to 164 mM, therefore the formation of two populations of objects in the gel could be promoted. Indeed, Gobeaux *et al.* [4] describe the appearance of two populations between 124 mM and 261 mM.

It is more complex to define ionic strength when ammonia vapors are used. Ammonia diffuses inside the gel and acquires hydrogen ions (from H_2O, acetic acid and potentially accessible chemical functions of amino acids) which leads to an increase of pH. Using ammonia therefore simplifies the gelation process, because it enables to put the ionic strength aside.

The gelation time is also to be taken into account, with approximately four days for collagen gels made in PBS and much less for collagen gels made in ammonia vapors (three hours). Experimentally, we noticed that the gelation of collagen solutions in PBS was not complete at the center of the sample under four days. Using ammonia vapors may reduce the lifetime of a pH gradient in the sample from the outside to the inside, unlike PBS. Morphology heterogeneities could thus be expected in the case of collagen gels made in PBS between the outside of the sample (in contact with the PBS solution through the dialysis membrane) and the inside of the sample (still at acidic pH while the ions from the phosphate buffer diffuse slowly inside the sample). Similar observations were performed by using either sodium hydroxide or ammonia vapors as *in vitro* fibrillogenesis medium [29].

The homogeneity in fibril size may also play a role in the stability of the collagen gels. Upon handling, collagen gels made in ammonia vapors seemed stiffer than collagen gels made in PBS. Both bound water content and thermal stability of collagen gels synthesized in PBS are affected. Therefore, their mechanical stability may depend on the interactions between collagen molecules and water molecules which can be modified by phosphate ions as mentioned above.

3.3.3 Freeze-dried and freeze-thawed collagen gels

Freeze-drying is a widely used technique to make collagen materials: in the form of non-fibrillar collagen sponges (collagen solutions are lyophilized) [30], porous collagen scaffolds with controlled porosity [31], or for collagen materials characterisation (*e.g.* prior to microscopy) [32]. However,

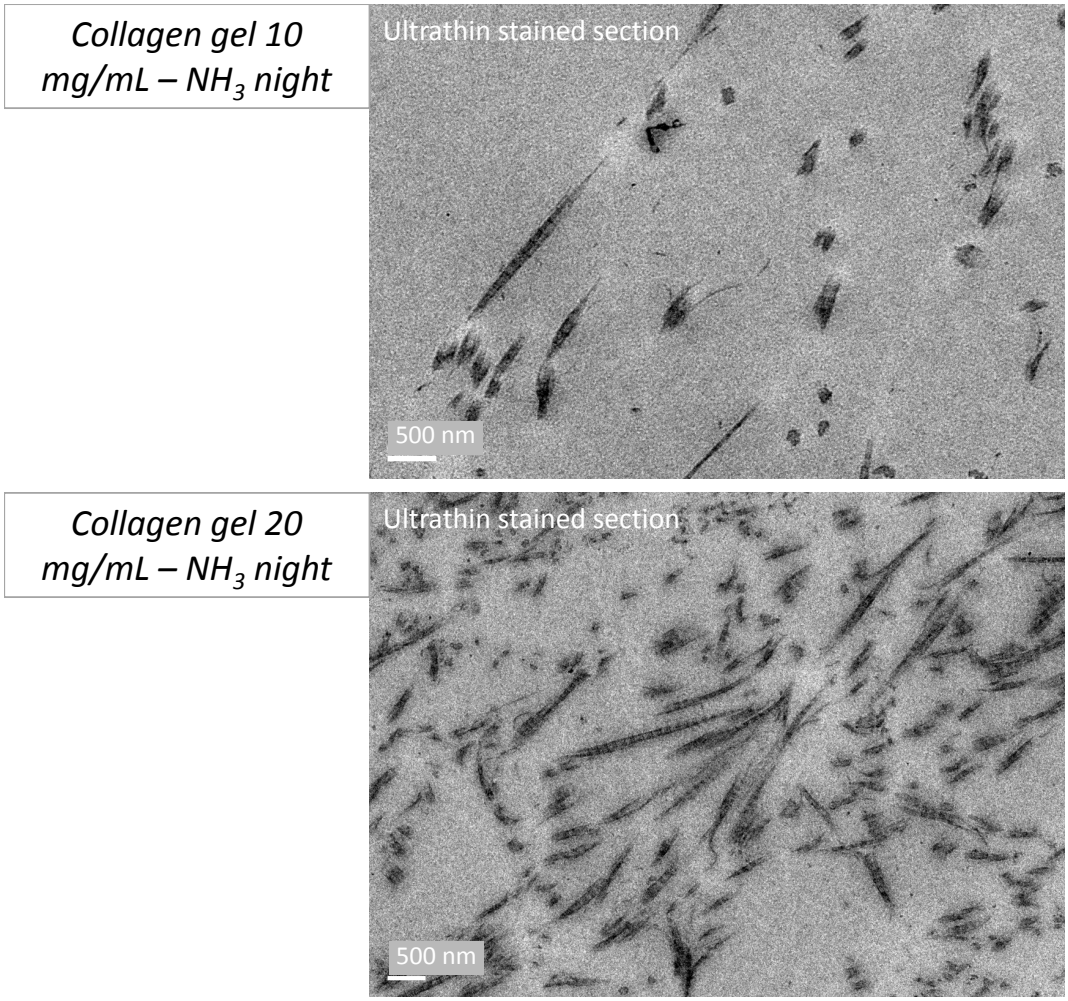

Figure 3.26: TEM micrographs of collagen gels synthesized in ammonia vapors for 24h with cross-striated fibrils.

freeze-drying may induce changes at the fibril scale: the collagen molecules could get closer by removal of intermolecular water [33], which could promote the formation of more electrostatic or hydrophobic bonds for instance. Thus, the underlying idea was to try and promote the formation of such physical crosslinks that would replace some hydrogen bonds, in order to reinforce the mechanical properties of the gel.

For this part of the study, the fibrillogenesis conditions were kept constant: three hours in ammonia vapors. Only one concentration was investigated: 50 mg/mL in collagen, which is theoretically above the threshold of the nematic phase. The gel was lyophilized after fibrillogenesis then rehydrated. To dissociate the effects of freezing from that of freeze-drying, a frozen then thawed collagen gel was also made as a control (same conditions, except the lyophilization step).

3.3.3.1 Water and collagen contents, stability in temperature

Thermogravimetric analysis of freeze-dried collagen gels is displayed in **Figure 3.27 (top)**. The collagen concentration was measured at 200°C. As for the reference gels, free water evaporates at 100°C as shown in **Figure 3.27 (bottom)**. The amount of bound water, measured as previously, is compared to that of the reference gel at 50 mg/mL (three hours ammonia condition) in **Table 3.4**.

The concentration of the freeze-dried collagen gels is close to the targeted concentration. Unfor-

Targeted collagen concentration	50 mg/mL - freeze-dried	50 mg/mL
Bound water content (%)	0.14±0.066	0.081±0.014
Measured collagen concentration (mg/mL)	46±4	44±2

Table 3.4: Measured collagen concentration and bound water fraction, freeze-dried condition compared to ammonia three hours condition.

tunately, the freeze-thawed collagen gel could not be characterized.

It appears that freeze-dried collagen gels contain more bound water than the reference collagen gel at 50 mg/mL. This is surprising, since the lyophilization step is supposed to remove some of the bound water, and this bound water may not be replaced upon rehydration of the sample. However, it is worth mentioning that the measure of bound water between 120°C and 200°C does not start at the same point of the endothermal curve, as for the previous conditions.

The thermal behavior of the freeze-dried collagen gels seems different from that of the reference gel (three hours ammonia condition) at 50 mg/mL (see **Figure 3.28**). Once again, the freeze-thawed gel could not be tested. The denaturation process appears to occur in two steps, as for the collagen gels synthesized in PBS. The first endothermal peak is shifted towards lower temperatures, while the second endorthermal peak corresponds to the denaturation temperature of the reference gel at 50 mg/mL. Therefore, we can expect two populations of objects in the gel. This hypothesis requires electron microscopy observations to be confirmed.

3.3.3.2 Ultrastructure of the gels

The macroscopic aspect of the freeze-dried collagen gel in **Figure 3.29** is different from the reference gel at 50 mg/mL (three hours ammonia condition). It does not appear homogeneously transparent, meaning that the inital organization may have been disturbed by the freezing process (the ice growth is not controlled). It could also contain bigger fibrils. It is worth mentioning that the macroscopic aspect of freeze-thawed collagen gels is the same.

Here again, unfortunately, histology samples were not observed by polarized light microscopy.

Scanning electron micrographs in **Figure 3.30 (top)** confirmed that the freeze-dried gel contain fibrils of different sizes and morphologies, unlike observations for the other conditions. Fibers are evidenced by white empty arrows, fibrils by black empty arrows. The interfibrillar space between collagen fibers appears larger than that between collagen fibrils. The fibers seem to be randomly located in the sample. At higher magnification, cross-striations are clearly visible on collagen fibers (white empty arrow). Partially dissolved collagen beads (white arrow) are embedded in a fibrillar matrix.

Such architecture is confirmed by TEM observations in **Figure 3.30 (bottom)**. Partially dissolved or undissolved beads remain in the gel (white arrow). In between beads, aggregated fibrils are present (black empty arrow) or collagen fibers (white empty arrow). Such fibers exhibit typical banded patterns, proving that no denaturation of collagen occured during the whole process.

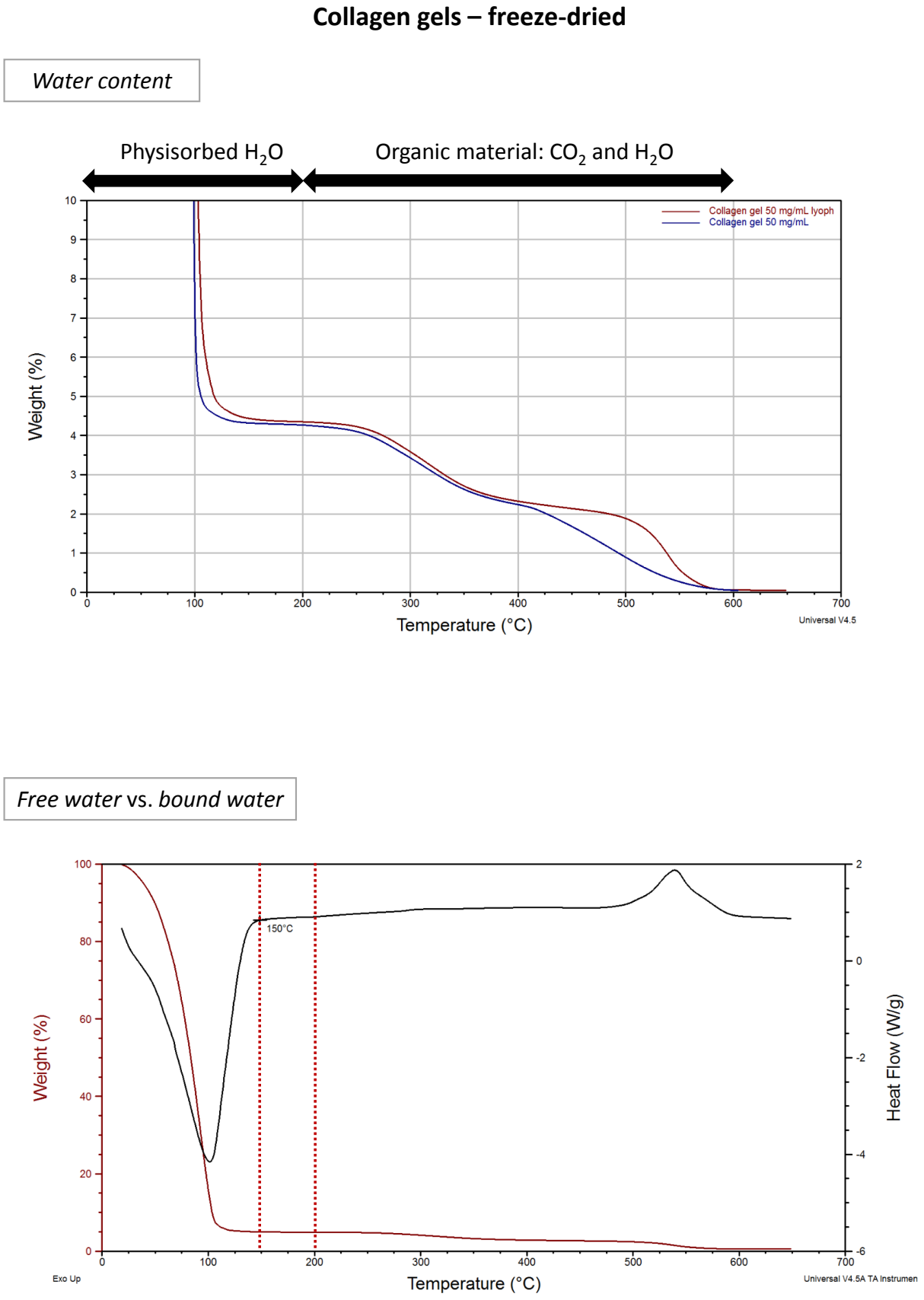

Figure 3.27: Top: thermogravimetric analysis of a freeze-dried collagen gel compared to a collagen gel at 50 mg/mL; bottom: bound water content *(two samples)*.

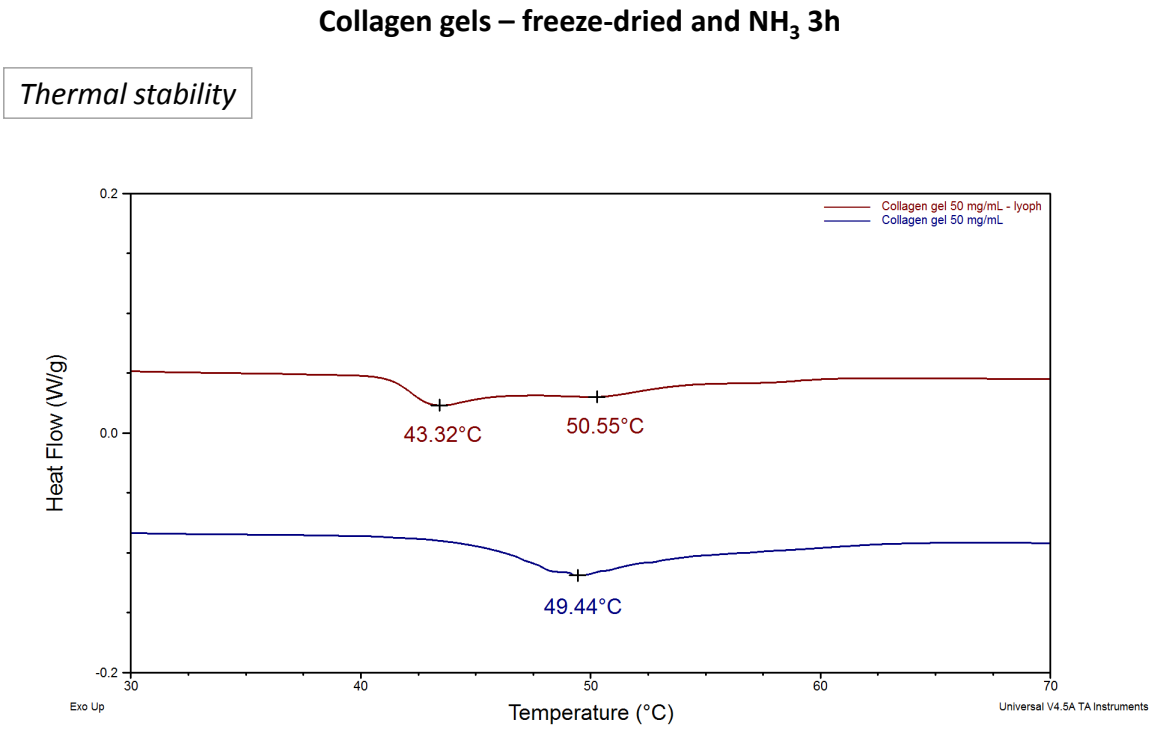

Figure 3.28: Thermal stability of freeze-dried collagen gels *(two samples)* compared to a collagen gel at 50 mg/mL.

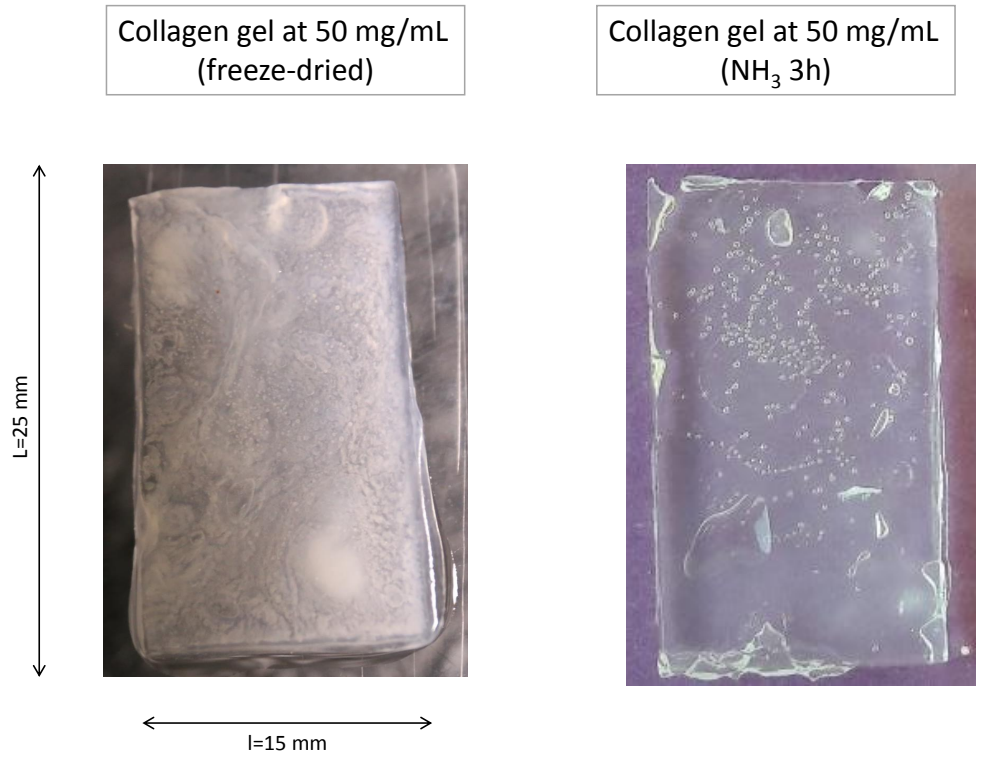

Figure 3.29: Macroscopic image of a lyophilized then rehydrated collagen gel at 50 mg/mL.

Freeze-dried collagen appear to be formed by different fibril sizes: fibers (diameter $\approx$ 100 nm), small fibrils (diameter $\approx$ 50 nm) and collagen molecules (in the form of partially dissolved collagen beads). It is possible that the ice crystal growth induced the formation of pores in the collagen gel structure. After freeze-drying and subsequent rehydration, the collagen fibrils or molecules present in the pores may have been recruited to form collagen fibers by aggregation.

3.3.3.3 Conclusion

The initial ultrastructure of the freeze-dried collagen gels appeared disturbed by the ice growth. Interestingly, collagen fibers are formed upon rehydration of the material, possibly where the ice crystals were located. The formation of bigger supramolecular aggregates (reduced "specific surface area") is not consistent with an increased amount of bound water. However, the gels are less stable in temperature, perhaps because of the larger interfibrillar space between collagen fibers that leaves space for free water to penetrate the material. Besides, water/collagen interactions may be modified during freeze-drying and/or rehydration in PBS. Performing zeta-potential measurements could help confirming this hypothesis.

From our observations, it is difficult to conclude on the presence or not of more electrostatic and/or hydrophobic interactions. Mechanical tests will provide more informations on the molecular/fibrillar interactions after freeze-drying.

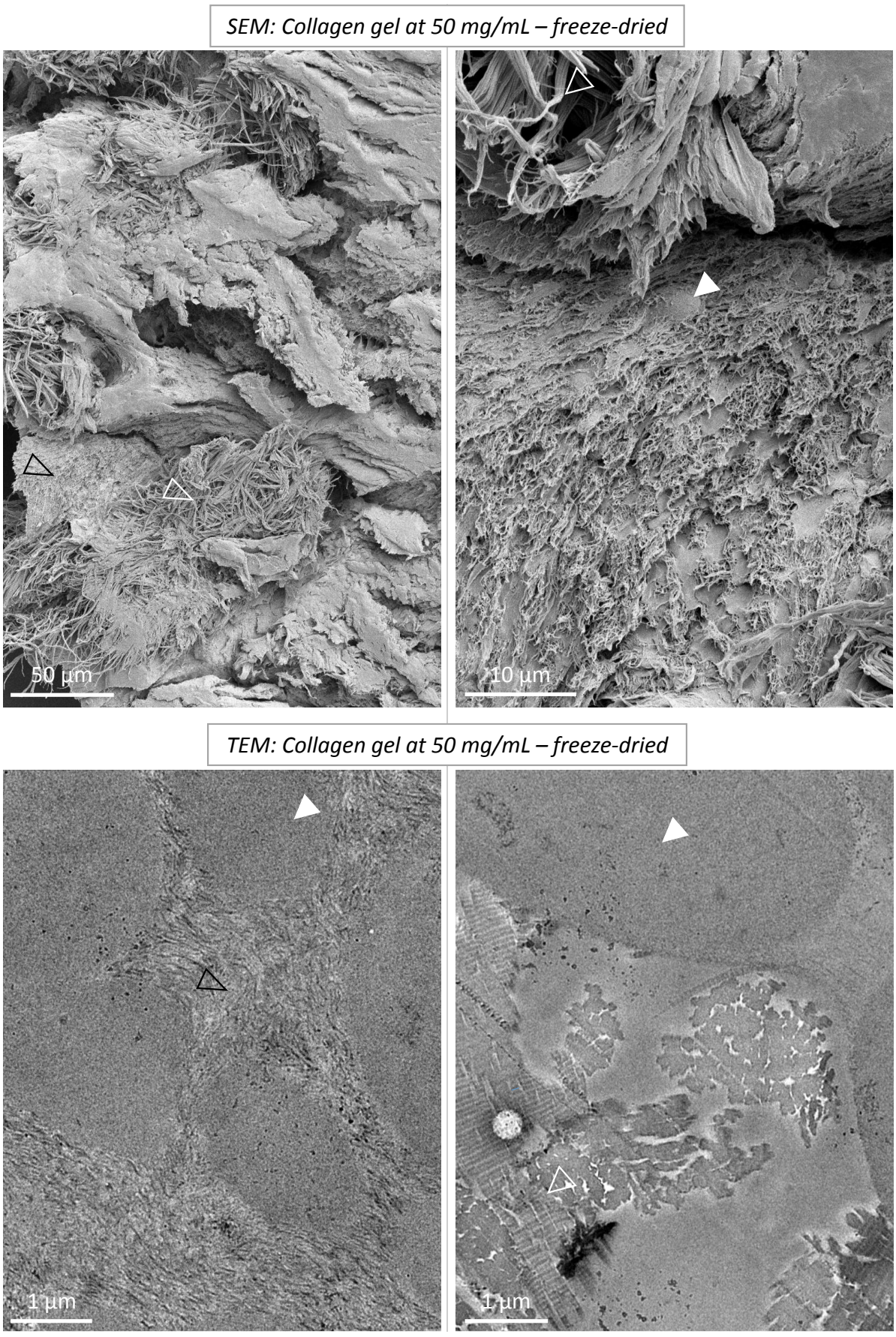

Figure 3.30: Scanning electron micrographs (upper) and transmission electron micrographs (lower) of lyophilized collagen gels at 50 mg/mL.

3.3.4 Discussion

It is difficult to separate the impact of the freezing process from the impact of lyophilization on the gels. ^{1}H NMR could be performed on our gels before freezing, after freezing (and thawing), after lyophilization and after rehydration to follow the evolution of the quantity of bound water [34]. Such informations could be used to predict the mechanical behavior of the freeze-dried collagen gels [35, 36]. Nevertheless, ^{1}H NMR was mainly performed on biological tissues in the literature, which contain less water than our collagen gels. It is likely that such a high free water content screens the signal of bound water.

3.3.5 Chemical crosslinking by plasma

As a side-project, we also worked in collaboration with physicists (Pr. Svetlana Starikovskaia and Inna Orel) from the Plasma Physics Laboratory at Polytechnique and with a biologist (Dr. Halima Kerdjoudj) from the Biomaterials and Bone Inflammations Laboratory at Reims University, to try another process to induce the formation of crosslinks in collagen solutions. It consists in using plasma irradiation on low concentrated collagen solutions in order to observe if the diffusion of charges would promote the formation of chemical bonds [7]. Different trials were performed by the physicists with different collagen concentrations and plasma time exposure (see **Experimental chapter**). Due to the low amount of collagen, it was difficult to conclude on the efficiency of the process.

3.4 Conclusion

As a conclusion, we were able to produce three dimensional collagen gels with spray-dried collagen. By using different fibrillogenesis media, we could tune the morphology of the fibrils. The more calibrated ones seemed to be obtained by using ammonia vapors as previously described in the literature.

The ultrastructure of the collagen gel at 50 mg/mL synthesized in ammonia vapors for three hours has similarities with that of gels synthesized by other processes that reproduced the ultrastructure of cornea (see **Appendix**). The gel at 80 mg/mL synthesized in PBS has cross-striated fibrils close to that of biological tissues. We were not able to conclude on the formation of stronger physical crosslinks by means of freeze-drying. Mechanical tests will help bringing informations on this aspect.

Different parameters can be used to control the ultrastructure of collagen gels and adapt it to mimick that of tissues *e.g.* collagen concentration, ionic strength, pH, fibrillogenesis time, incubation heat. We choose as a reference system collagen gels synthesized in ammonia vapors for three hours because it is the most simple one. Several parameters have not been explored in this study: the influence of the storage conditions (water or phosphate buffer ? - keeping in mind the interactions of phosphate with collagen), swelling (which may modify the ultrastructure [37]).

All these phenomenon may have an influence on the mechanical properties of the collagen gels.

Bibliography

1. Highberger, J. H. The Isoelectric Point of Collagen. *Journal of the American Chemical Society* **61,** 2302–2303 (1939).
2. Gobeaux, F. *et al.* Cooperative ordering of collagen triple helices in the dense state. *Langmuir* **23,** 6411–6417 (2007).
3. Dong, Y. D. *et al.* Impurities in commercial phytantriol significantly alter its lyotropic liquid-crystalline phase behavior. *Langmuir* **24,** 6998–7003 (2008).
4. Gobeaux, F. *et al.* Fibrillogenesis in Dense Collagen Solutions: A Physicochemical Study. *Journal of Molecular Biology* **376,** 1509–1522 (2008).
5. Besseau, L. & Giraud-Guille, M. M. Stabilization of fluid cholesteric phases of collagen to ordered gelated matrices. *Journal of Molecular Biology* **251,** 197–202 (1995).
6. Schlegel, A. K., Möhler, H., Busch, F. & Mehl, A. Preclinical and clinical studies of a collagen membrane (Bio-Gide®). *Biomaterials* **18,** 535–538 (1997).
7. Friedrich, J. Mechanisms of plasma polymerization - Reviewed from a chemical point of view. *Plasma Processes and Polymers* **8,** 783–802 (2011).
8. Gobeaux, F. *Phases denses de collagène de type I : transition isotrope/cholestérique, fibrillogénèse et minéralisation* PhD thesis (2008).
9. Mkukuma, L. D. *et al.* Effect of the proportion of organic material in bone on thermal decomposition of bone mineral: An investigation of a variety of bones from different species using thermogravimetric analysis coupled to mass spectrometry, high-temperature X-ray diffraction. *Calcified Tissue International* **75,** 321–328 (2004).
10. Wang, Y. *Elaboration de modèles collagène/apatite pour l'étude de la biominéralisation du tissu osseux* PhD thesis (2012).
11. Giraud Guille, M. M., Helary, C., Vigier, S. & Nassif, N. Dense fibrillar collagen matrices for tissue repair. *Soft Matter* **6,** 4963–4967 (2010).
12. Allouch-Nahmias, C. *et al.* Anatomie de la cornée. *EMC - Ophtalmologie* **8,** 1–16 (2011).
13. Salameh, C. *et al.* Structure-properties correlation of stable transparent domain in fibrillar collagen gradient. *Submitted.*
14. White, T. L. *et al.* Elastic microfibril distribution in the cornea: Differences between normal and keratoconic stroma. *Experimental Eye Research* **159,** 40–48 (2017).
15. Miles, C. A., Avery, N. C., Rodin, V. V. & Bailey, A. J. The increase in denaturation temperature following cross-linking of collagen is caused by dehydration of the fibres. *Journal of Molecular Biology* **346,** 551–556 (2005).
16. Mosser, G., Anglo, A., Helary, C., Bouligand, Y. & Giraud-Guille, M. M. Dense tissue-like collagen matrices formed in cell-free conditions. *Matrix Biology* **25,** 3–13 (2006).

17. Wang, Y. *et al.* The predominant role of collagen in the nucleation, growth, structure and orientation of bone apatite. *Nature materials* **11,** 724–33 (2012).

18. Helary, C. *et al.* Evaluation of dense collagen matrices as medicated wound dressing for the treatment of cutaneous chronic wounds. *Biomater. Sci.* **3,** 373–382 (2015).

19. Wang, Y. *et al.* Controlled collagen assembly to build dense tissue-like materials for tissue engineering. *Soft Matter* **7,** 9659–9664 (2011).

20. Fratzl, P. & Daxer, A. Structural transformation of collagen fibrils in corneal stroma during drying. An x-ray scattering study. *Biophysical Journal* **64,** 1210–1214 (1993).

21. Nassif, N. *et al.* Self-assembled collagen-apatite matrix with bone-like hierarchy. *Chemistry of Materials* **22,** 3307–3309 (2010).

22. Knight, D. P., Nash, L., Hu, X. W., Haffegee, J. & Ho, M. W. In vitro formation by reverse dialysis of collagen gels containing highly oriented arrays of fibrils. *Journal of Biomedical Materials Research* **41,** 185–191 (1998).

23. Li, Y., Asadi, A., Monroe, M. R. & Douglas, E. P. pH effects on collagen fibrillogenesis in vitro: Electrostatic interactions and phosphate binding. *Materials Science and Engineering C* **29,** 1643–1649 (2009).

24. Sarkar, S. K., Sullivan, C. E. & Torchia, D. A. Solid state 13C NMR study of collagen molecular dynamics in hard and soft tissues. *Journal of Biological Chemistry* **258,** 9762–9767 (1983).

25. Huster, D., Schiller, J. & Arnold, K. Comparison of collagen dynamics in articular cartilage and isolated fibrils by solid-state NMR spectroscopy. *Magnetic Resonance in Medicine* **48,** 624–632 (2002).

26. Sun, W. Q. & Leung, P. Calorimetric study of extracellular tissue matrix degradation and instability after gamma irradiation. *Acta Biomaterialia* **4,** 817–826 (2008).

27. Hayashi, T. & Nagai, Y. Factors affecting the interactions of collagen molecules as observed by in Vitro fibril formation: III. non-helical regions of the collagen molecules. *Journal of Biochemistry* **76,** 177–186 (1974).

28. *1994.Pogany.The in vitro interaction of proteoglycans with type I collagen is modulated by phosphate.pdf*

29. Besseau, L., Coulomb, B., Lebreton-Decoster, C. & Giraud-Guille, M. M. Production of ordered collagen matrices for three-dimensional cell culture. *Biomaterials* **23,** 27–36 (2002).

30. Ueda, H. *et al.* Use of collagen sponge incorporating transforming growth factor-β1 to promote bone repair in skull defects in rabbits. *Biomaterials* **23,** 1003–1010 (2002).

31. Kane, R. J. & Roeder, R. K. Effects of hydroxyapatite reinforcement on the architecture and mechanical properties of freeze-dried collagen scaffolds. *Journal of the Mechanical Behavior of Biomedical Materials* **7,** 41–49 (2012).

32. Olszta, M. J., Douglas, E. P. & Gower, L. B. Scanning electron microscopic analysis of the mineralization of type I collagen via a polymer-induced liquid-precursor (PILP) process. *Calcified Tissue International* **72,** 583–591 (2003).

33. Bella, J. Collagen structure: new tricks from a very old dog. *Biochemical Journal* **473,** 1001–1025 (2016).

34. Migchelsen, C. & Berendsen, H. J. Proton exchange and molecular orientation of water in hydrated collagen fibers. An NMR study of H2O and D2O. *The Journal of Chemical Physics* **59,** 296–305 (1973).

35. Nyman, J. S., Ni, Q., Nicolella, D. P. & Wang, X. Measurements of mobile and bound water by nuclear magnetic resonance correlate with mechanical properties of bone. *Bone* **42,** 193–199 (2008).

36. Fernández-Seara, M. A., Wehrli, S. L., Takahashi, M. & Wehrli, F. W. Water Content Measured by Proton-Deuteron Exchange NMR Predicts Bone Mineral Density and Mechanical Properties. *Journal of Bone and Mineral Research* **19,** 289–296 (2004).

37. Chimich, D., Shrive, N., Frank, C., Marchuk, L. & Bray, R. Water content alters viscoelastic behaviour of the normal adolescent rabbit medial collateral ligament. *Journal of Biomechanics* **25** (1992).

4

Correlating ultrastructure and mechanical behavior: influence of concentration and processing conditions on the mechanical response of dense collagen gels

Contents

4.1 Introduction

The ultrastructure of the collagen gels was assessed depending on their collagen concentration, fibrillogenesis and processing conditions. Besides composition and organization at fibril scale, another important feature in mimicking collagen-rich tissues consists in interrogating the material from a mechanical point of view. It is generally accepted that cellular processes are regulated by the stiffness of their environment [1]. However, the role of other mechanical parameters such as the mechanical response at large strain (non-linearity) and the viscoelastic components have been significantly less investigated.

Here, we adopt a materials science approach to analyze the mechanical response with the following parameters:

- the general shape of the large strain tensile behavior of the gels until rupture;
- the viscoelastic behavior of the gels *via* stress-relaxation experiments;
- the durability of the gels through fatigue and fracture experiments, such mechanical loadings being similar to *in vivo* repetitive loadings undergone by tendons or ligaments.

The analysis of the mechanical behavior will *(i)* enable us to assess the degree of biomimetism of our collagen materials, *(ii)* provide informations about their ultrastructure and *(iii)* determine if our gels can actually be used as model materials for a deeper understanding of the mechanical response of biological tissues.

4.2 Influence of the concentration on the mechanical behavior of model collagen gels

In this chapter, the nominal stress is equal to the engineering stress. We use nominal strain defined as the strain measured by the extensometer before using the new designed clamps (see **Experimental Chapter**), and strain when the new clamps are used (negligible sliding). The toe modulus is measured by a linear fit of the first 10% of the tensile curve, the linear modulus is measured by a linear fit of the linear part of the curve before fracture.

4.2.1 Non-linear mechanical response at large strains: tensile behavior

The tensile behavior of the collagen gels was first explored from 20 mg/mL to 80 mg/mL to follow its evolution over the whole phase diagram. The particular experimental conditions associated to these first tests are described in the **Experimental chapter**.

As depicted in **Figure 4.1 (top)**, all the collagen gels exhibit a typical J-shaped behavior as observed in biological tissues. The mechanical behavior becomes stiffer and seems more non-linear when the concentration increases. The strain at break reduces while the ultimate tensile stress increases with the concentration. All samples systematically broke in the clamps where tightening locally induces stress concentration. It is worth mentioning that at 70 mg/mL and 80 mg/mL (stars), a fracture spontaneously occured in the middle of the samples during the stretching experiments, leading to their macroscopic rupture after crack propagation over the entire section of the specimen (see images in the inset on the left).

Toe and linear moduli were plotted against the concentration in **Figure 4.1 (middle)**. As expected, the rigidity of the gels increases with the collagen concentration. Under 40 mg/mL strain hardening seems to be less noticeable. This could be related to the isotropic/anisotropic phase transition of the collagen self-assembly in the gels. Besides, the variability of the mechanical behavior increases when the concentration increases, especially for the linear modulus; the toe modulus thus appears more relevant for comparing the stiffness of the gels.

In order to estimate the dependency of the stiffness of the gels on the collagen concentration, toe and linear moduli were plotted against the collagen volume fraction in **Figure 4.1 (bottom)**. Due to the increasing variability between 70 and 80 mg/mL, the data for linear modulus were fitted only until 70 mg/mL. The increase of stiffness appears to scale non-linearly with the collagen volume fraction. Both fits are plotted in linear scale in the inset at the bottom right of the graph to show the trend.

To further characterize the non-linear response of the gels, we decided to focus on three concentrations in order to scan the whole phase diagram of collagen: 30 mg/mL (isotropic), 50 mg/mL (nematic) and 80 mg/mL (precholesteric/cholesteric). The dissolution time of the beads was fixed at 30 min. The ammonia vapors exposure time was first fixed to three hours (see **Experimental chapter**). Only one gel could be synthesized for each concentration; these experiments should be repeated to confirm the trends. Nevertheless, thanks to the use of the new clamps (see **Experimental Chapter**), the curves tend to be much less variable for this condition.

Figure 4.2 (top) displays the three curves. Interestingly, the ultimate tensile strain does not seem to depend highly on the concentration. As mentioned in **Chapter 1**, different equations can be used to fit the behavior of collagen gels. Such equations can be useful to compare fitting coefficients with the ones obtained from the literature, calculate tangent moduli instead of secant or partial fitting; but more importantly, to define variables to characterize our system. Here, we chose to fit our curves with an exponential equation [2] (more details in **Chapter 1**):

$$\sigma(\epsilon) = A \times (\exp(B \times \epsilon) - 1) \tag{4.1}$$

which enable us to start at zero stress when strain is equal to zero. A (in kPa) and B are positive fitting constants. The equation was implemented with the IgorPro software and the fitting constants were adjusted after few iterations (following initial guesses).

The obtained fitting curves are displayed in grey together with their associated tensile curve in **Figure 4.2 (middle)** and the values of A and B. The fit of the gel at 30 mg/mL is almost perfectly superimposed, but the fit of the gel at 50 mg/mL slightly underestimates the slope between 0% and 25% strain, as for the gel at 80 mg/mL between 0% and 20% strain.

The non-linear behavior of collagen gels is expressed by the J-shape of their tensile curve. Therefore, in an attempt to characterize it, we propose to define the following ratio:

$$J_{ratio} = \frac{E_{linear} - E_{toe}}{E_{toe}} \tag{4.2}$$

This ratio is related to the more or less pronounced non-linearity of the tensile curve: it is closer to zero when the tensile curve approximates a straight line. Tangent E_{Ttoe} and $E_{Tlinear}$ moduli were calculated thanks to the fitting equation at 0% and ultimate tensile strain respectively, and their values compared to the measured moduli in order to assess the accuracy of the fitting parameters. The values are displayed in **Table 4.1**.

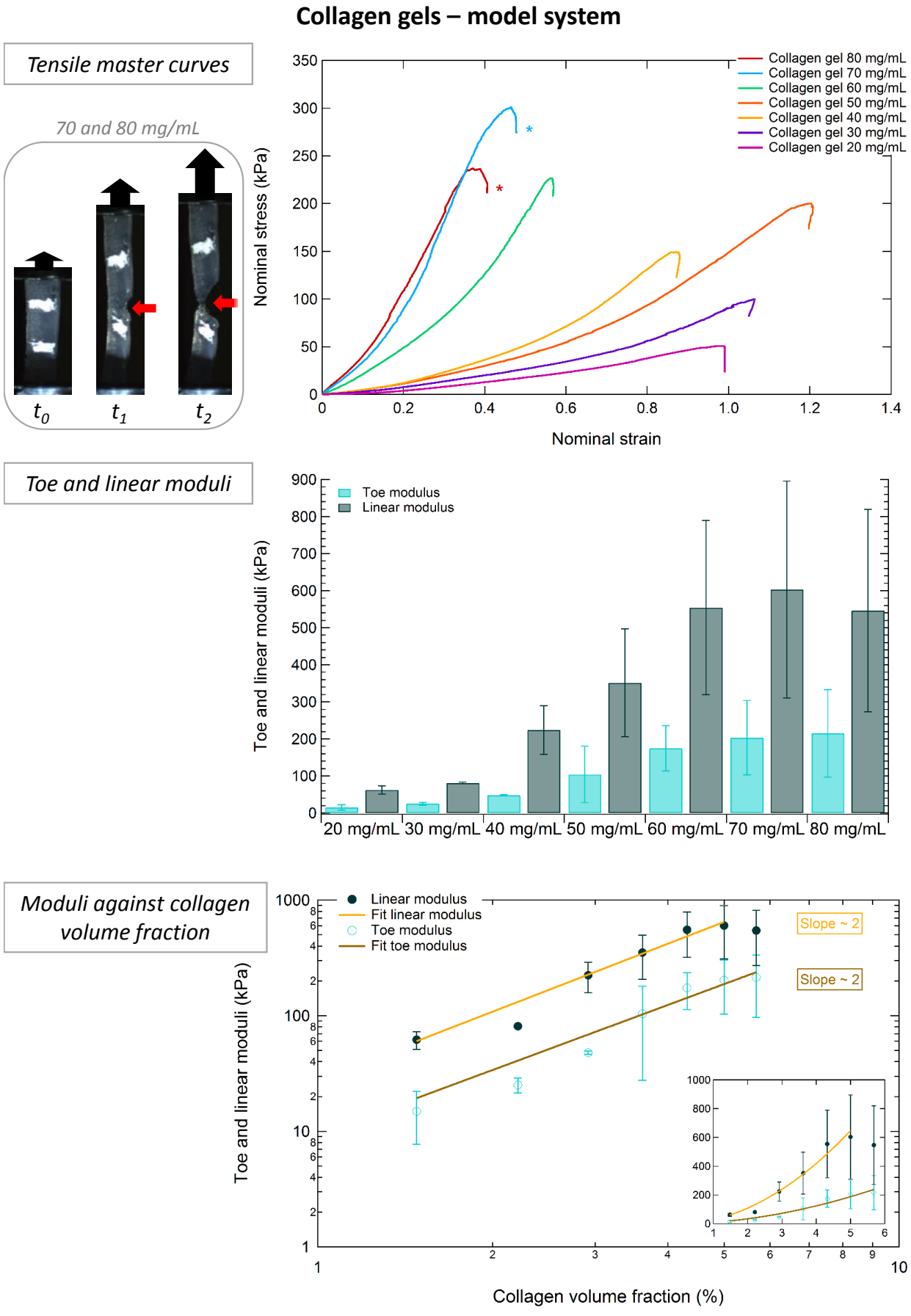

Figure 4.1: Tensile behavior of collagen gels synthesized in ammonia vapors from 20 mg/mL to 80 mg/mL (*three samples per collagen concentration*).

Concentration of the gel	30 mg/mL	50 mg/mL	80 mg/mL
Fitting parameters	A=19.3±0.1 kPa B=2.6	A=17.2±0.1 kPa B=4.4	A=167.1±0.9 kPa B=1.2
E_{Ttoe} **;** $E_{Tlinear}$ **(kPa)**	50 ; 184	76 ; 780	201 ; 464
E_{toe} **;** E_{linear} **(kPa)**	69 ; 147	136 ; 617	224 ; 366
J_{ratio}	1.14	3.53	0.63

Table 4.1: Measured and calculated moduli, J_{ratio} for the three hours condition.

The values of calculated E_{Ttoe} and $E_{Tlinear}$ are on the same order of magnitude than the values of the measured toe and linear moduli, respectively, thus indicating a good approximation of the fit to the tensile curve. However, the calculated value of linear modulus overestimates the measured linear modulus: the measured values appear more reliable than the calculated values at high strain. The J_{ratio} reaches a maximum at 50 mg/mL, meaning that the J shape of the curve is more pronounced. Even if a J-shape tensile curve is obtained with our collagen gels, their stiffness is still orders of magnitude below that of biological tissues mentioned in **Chapter 1** (about three orders of magnitude below for the toe modulus).

Finally, we compared the measured toe modulus of the gels at two different strain rates (see **Figure 4.2, bottom**) to explore their viscoelastic response: 0.06 s^{-1} (strain rate of the tensile tests) and 0.6 s^{-1} (strain rate of the loading curve of the stress-relaxation experiments, from 0% to 20% strain). It appears that the strain rate does not have a significant influence on the toe modulus. This feature may seem counter-intuitive because viscoelastic processes should depend on the strain rate at which a material is stretched, as for synthetic physical hydrogels [3]; *i.e.* the reorganizations at the microscale are different if the material is stretched slowly or fast because of the different involved timescales. However, this independency of toe modulus on strain rate was also observed in rat tendon for example [4].

4.2.2 Viscoelastic response: stress-relaxation behavior

Keeping in mind that the strain rate does not have a high influence on the toe modulus of the collagen gels, stress-relaxation tests were performed to explore further the viscoelastic response of the gels. The level of applied strain chosen (20%) was a compromise to be sufficiently far from toe region and from damage mechanisms (before failure).

The stress-relaxation behavior of the gels is displayed in **Figure 4.3 (top)**. The curves are characterized by a peak stress, arising tens of seconds after the beginning of the experiment (the sample is stretched to 20% strain at a strain rate of 0.6 s^{-1}), then a decrease of the stress down to approximately half of the peak stress after 400s. Drying of the sample was estimated to be negligible in this time interval (about 3%). The curves are displayed in inset in a log-log scale plot: the stress appears to have a similar decay for all concentrations. The peak stress appears to increase linearly with the concentration: we may hypothesize that the behavior of the collagen gels is linear viscoelastic.

Interestingly, the stress-relaxation behavior of the collagen gels is highly reproducible and does not seem to depend on their concentration thus on their ultrastructure, as shown in the normalized stress plot (see **Figure 4.3, middle**). The three master curves superimpose when plotted in logarithmic scale. The stress-relaxation amplitude measured at 400s is equal to $\sigma_{viscous}$= 0.57±0.04, meaning that almost 60% of the peak stress is relaxed.

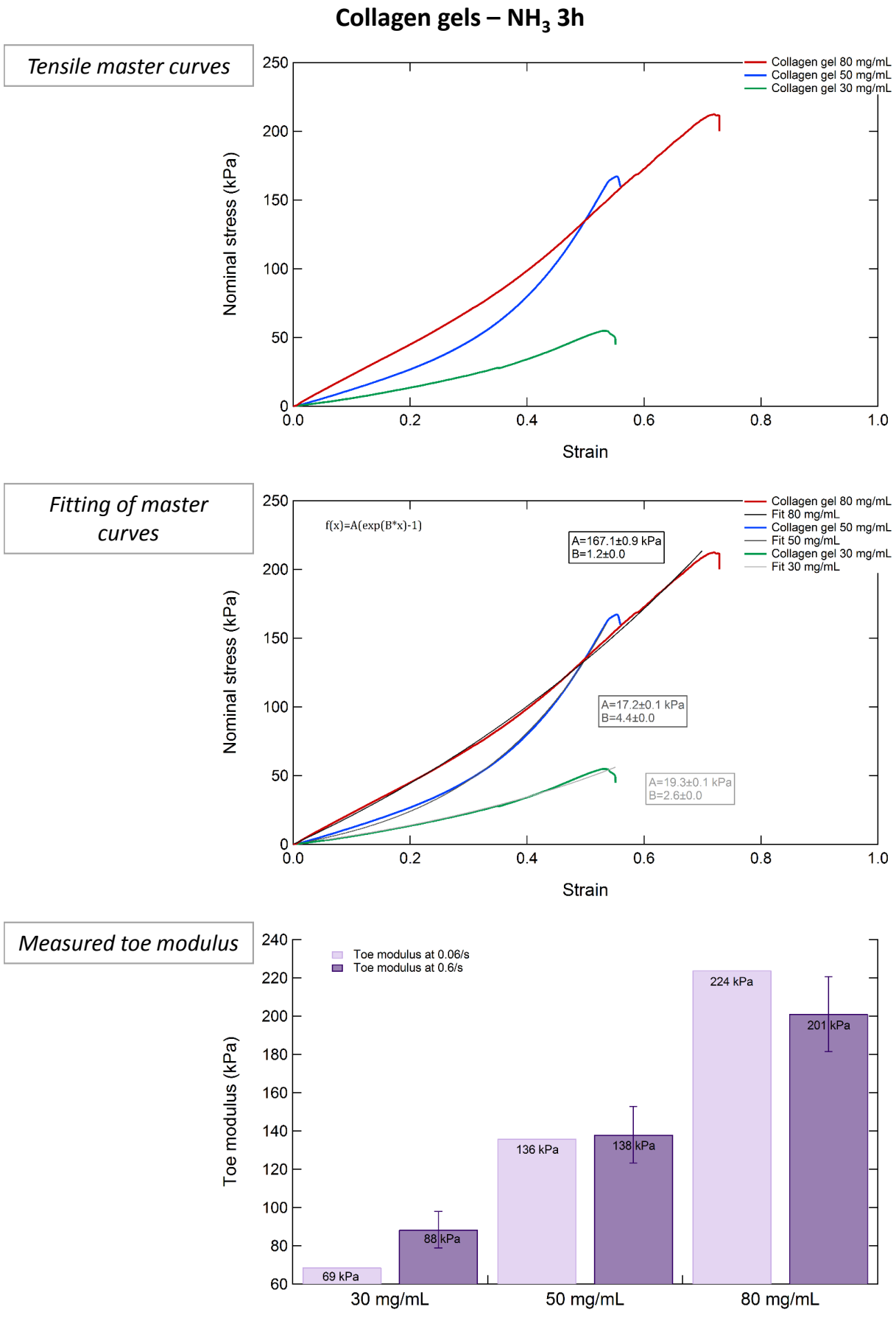

Figure 4.2: Tensile behavior of collagen gels synthesized in ammonia vapors for three hours (*one sample per collagen concentration*).

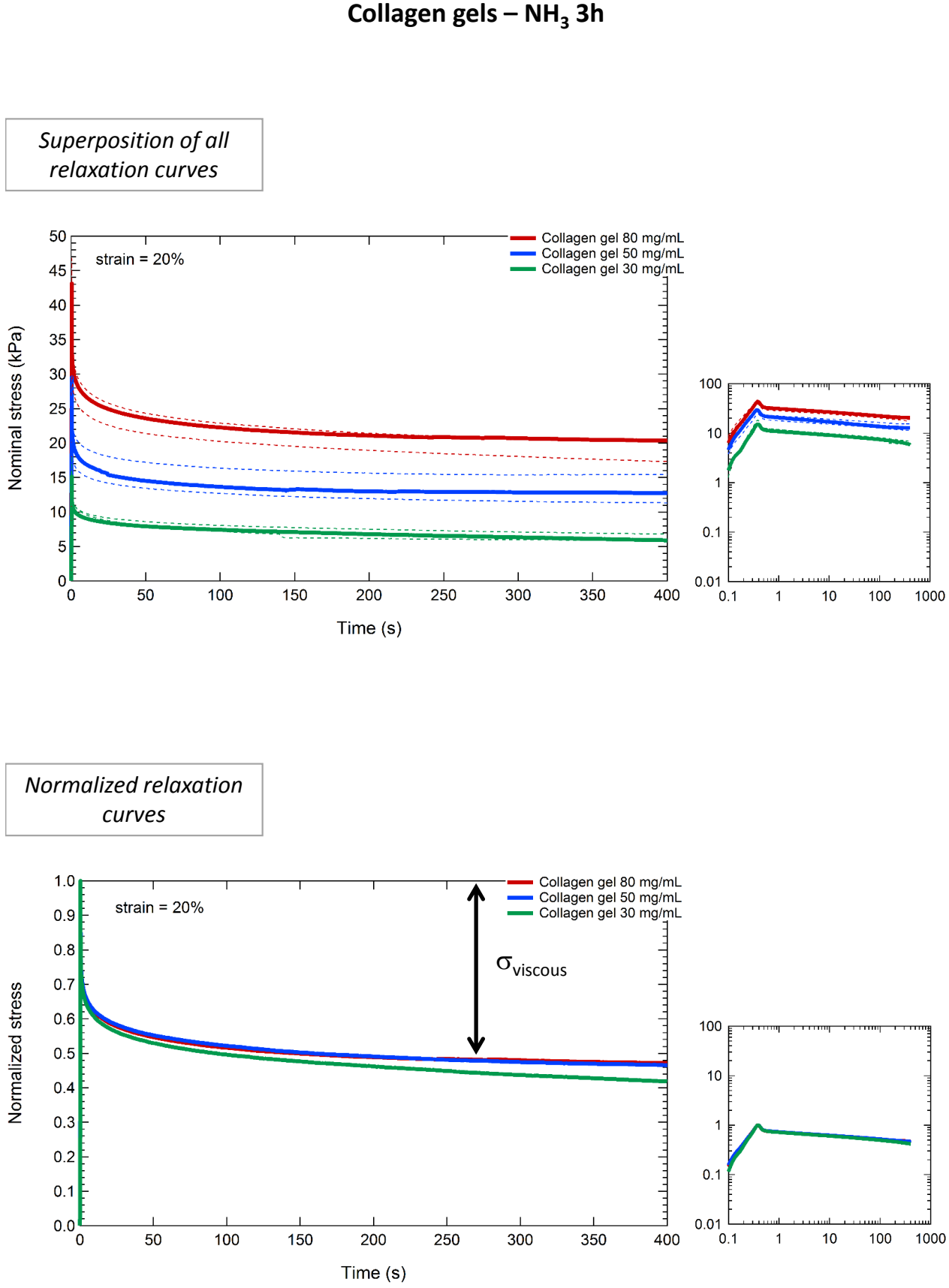

Figure 4.3: Stress-relaxation behavior of collagen gels synthesized in ammonia vapors for three hours. The dotted lines represent the behavior of other samples at each collagen concentration (*three samples per collagen concentration*).

From the log-log scale and linear plots, it seems that the stress-relaxation follows an exponential decrease; the major decay being within the first 100 seconds. This decrease can be associated with a characteristic time, τ, related to viscous dissipations within the sample, through the following equation:

$$\sigma(t) = \sigma_0 \times \exp(\frac{-t}{\tau}) + \sigma_{t=100s} \tag{4.3}$$

σ_0 (in kPa) represents the vertical shift of the curve. By plotting $\sigma(t) - \sigma_{t=100s}$ versus time in log-log scale as depicted in **Figure 4.4 (left)**, a characteristic time $\tau = 32.7 \pm 0.9\ s$ was calculated for all collagen concentrations by fitting the curves. This characteristic time appears independent of the concentration and may be related to local rearrangements at the microscale within the sample. We may hypothesize that such reorganizations tend to occur at fibrillar or molecular scales, since the ultrastructure does not have an influence on the characteristic time.

The stress-relaxation behavior can also be characterized by a relaxation rate if the relaxation function is assumed to follow a non-linear superposition [5, 6]:

$$\sigma(\epsilon, t) = \sigma_0 \times t^{n(\epsilon)} \tag{4.4}$$

with σ_0 as the vertical shift of the curve. Here, we performed stress-relaxation experiments at 20% strain. Therefore the n exponent was calculated at $\epsilon = 20\%$. By fitting the curves for all concentrations in **Figure 4.4 (right)**, the exponent was found to be $n = -0.0805 \pm 0.006$. Once again, this value is independent of the concentration. The order of magnitude is the same as for the relaxation rate of the rabbit ligament [5], with values ranging from -0.2619 (lower applied strain) to -0.0582 (higher applied strain). Thus it would be interesting to apply different strain levels to our collagen gels and see if the exponent reduces when the strain is increased.

4.2.3 Energy dissipation and durability: fatigue and fracture behaviors

Fatigue tests are typically performed on tendon because they represent the mechanical loading they undergo during walking, running or jumping. Cyclic tests were performed on two or three samples per collagen concentration to assess their durability. Experiments were carried out in PBS immersion, enabled by an environmental chamber designed in SIMM laboratory. Here, the samples were stretched up to 20% strain to remain in the toe/heel region of the tensile curves. Three representative samples are displayed in **Figure 4.5**. In all cases, the first cycle presents an accute hysteresis which is also present when tendon are subjected to fatigue testing [7]. The hysteresis reduces when the number of cycles increases. The presence of stress-relaxation (peak stress decreases when cycle number increases) and creep - especially residual strain at zero stress - (the stress-strain curve is shifted to the right) is also a typical feature of collagen-rich tissues [7] and concentrated collagen gels [8]. To qualitatively assess the behavior of the gels when the number of cycles increases, selected loops were plotted and shifted to zero strain for each concentration in **Figure 4.5**. The general trend consists in a slight increase of stiffness up to the 100th cycle followed by a decrease in stiffness (more visible at strains between 15% and 20%).

The area of each cycle appears to decrease when the cycle number increases. The area of each selected cycle was calculated, giving dissipated energies in kJ/m^3 (see **Figure 4.6, left**). The gel at 80 mg/mL seems to dissipate more energy than the gel at 50 mg/mL. The difference in dissipated energy is slightly reduced between 30 mg/mL and 50 mg/mL. Following the microscopy observations

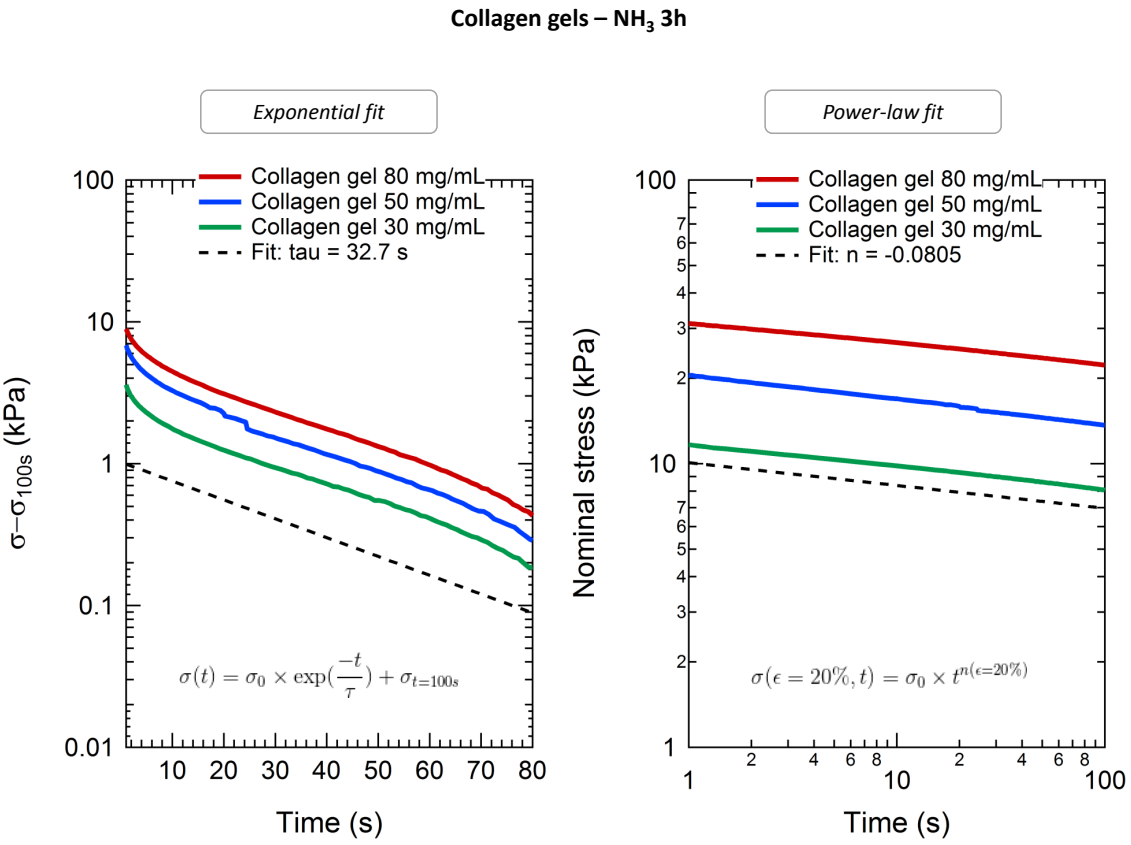

Figure 4.4: Exponential fit and power-law fit of the stress-relaxation of the collagen gels within the first 100 seconds.

in **Chapter 3**, the collagen gel at 80 mg/mL is more dense which could provide more fatigue resistance. The dissipated energy was normalized by the total area under the loading curve of each cycle to take into account changes in stiffness within the sample throughout the test. Results are displayed in **Figure 4.6 (right)**. After the 100th cycle, the normalized dissipated energy appears stable over time. Despite the different ultrastructures of the gels, the normalized dissipated energy is not significantly different after the 10th cycle whatever the concentration; confirming the linear viscoelastic feature already observed in the stress-relaxation behavior. Thus we may hypothesize that the mechanical loading induces rearrangements mostly at the fibril scale after the 100th cycle.

To better assess the evolution of the stiffness of the gel, which is a parameter related to the degree of damage inside the material, the secant modulus of each loop was calculated at 10% to minimize errors (compared to a secant modulus calculated at 20% where the curve is more convex). The secant modulus at 10% strain, called E, was then normalized by the secant modulus of the first cycle to allow comparisons between the different gel concentrations. The results are plotted in **Figure 4.7** with a linear scale and log strain scale to enhance the variations. First, it appears that the mechanical behavior of the gels has a variable reproducibility. This may be due to the global isotropy of the gels: local organized domains were found (see **Chapter 3**) but these anisotropic domains are randomly distributed all over the sample. Second, the fatigue process seems to happen in three steps: *(i)* the gel's stiffness increases and *(ii)* reaches a maximum between the 50^{th} and 100^{th} cycle before *(iii)* decreasing until the 1000^{th} cycle. The first and second steps may be associated to a reinforcement

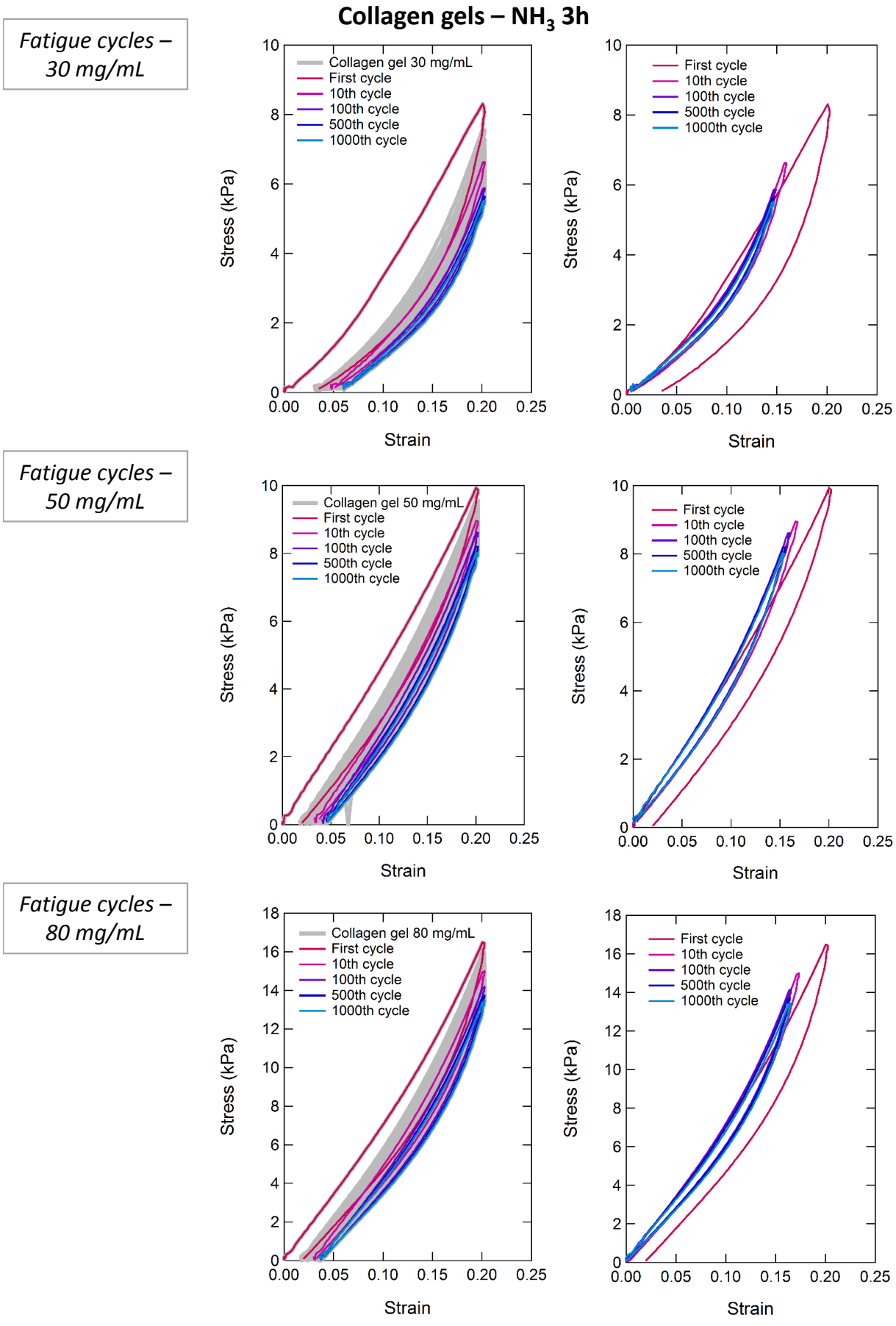

Figure 4.5: Left: fatigue behavior of collagen gels synthesized in ammonia vapors for three hours (selected master curves - *two to three samples per collagen concentration*). Right: selected curves shifted to zero strain for stiffness comparison purposes.

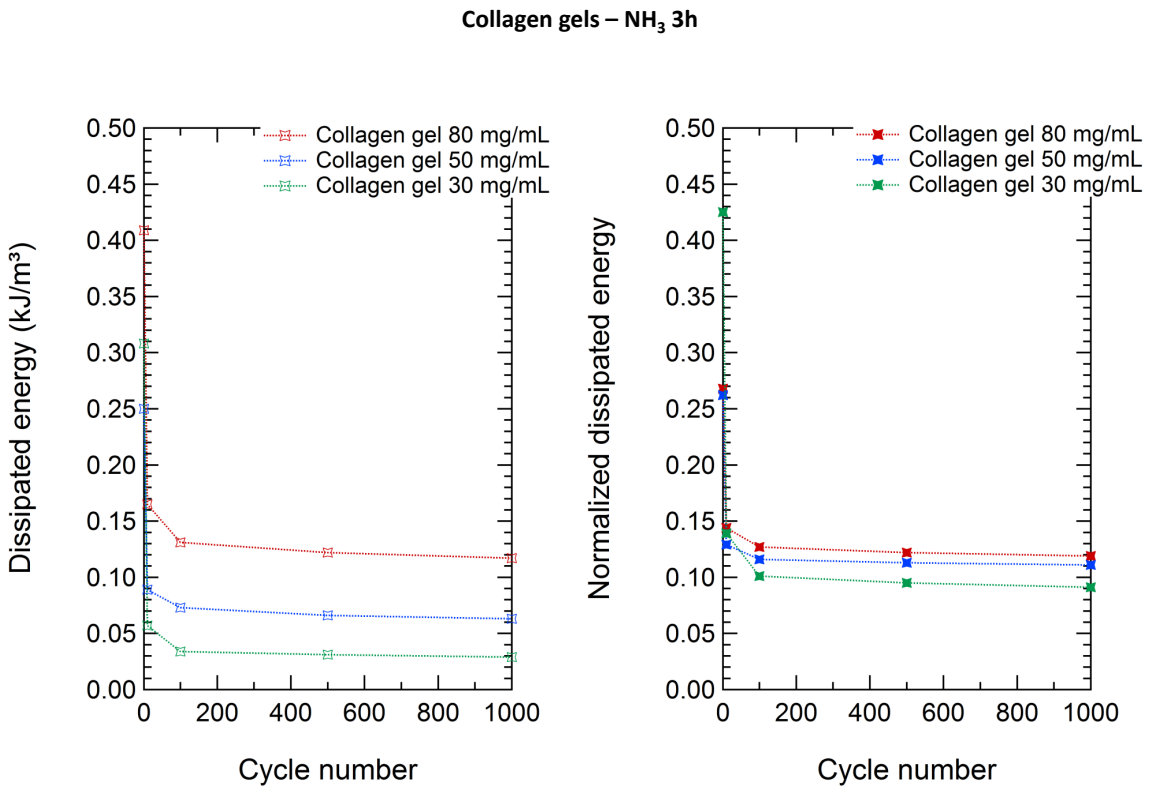

Figure 4.6: Normalized cycle areas for each collagen concentration against cycle number. Dotted lines link points as a guide to the eye.

of the material due to the cyclic loading, followed by a collapse or damage of the structure after the stiffness peak. Finally, it seems that during fatigue testing most of the suprafibrillar rearrangements take place during the first hundred cycles (see **Figure 4.7, right**). Then, as the dissipated energy reaches a threashold, the material appears to undergo most of the damage during the last 100th cycles.

The ability of the gels to dissipate energy under stress is often related to their resistance to crack propagation [9]. Collagen-rich tissues such as tendon demonstrate an incredible resistance to crack propagation [10]. A preliminary study was performed on our collagen gels to assess their fracture resistance and to look at the fracture profile (which is wide open in the case of tendon). The fracture energy density plotted *vs.* the concentration of the gel is displayed in **Figure 4.8 (top)**. It appears that the concentration does not have a dramatic effect on the fracture energy of the gels. However this hypothesis should be confirmed by performing more fracture tests. For the gels at 80 mg/mL, the crack propagation occured in three steps depicted in **Figure 4.8 (middle)**: first, the crack starts to open. Then, crack blunting is observed but the crack does not propagate. Finally, the crack reaches a critical opening displacement, leading to fast crack propagation followed by catastrophic failure of the sample. This behavior resembles to some extent that of crack propagation in tendon specimens (see **Figure 4.8, bottom**). This crack opening before propagation could perhaps be enhanced by letting the collagen beads dissolve completely prior to fibrillogenesis in order to form liquid crystalline domains over larger scales.

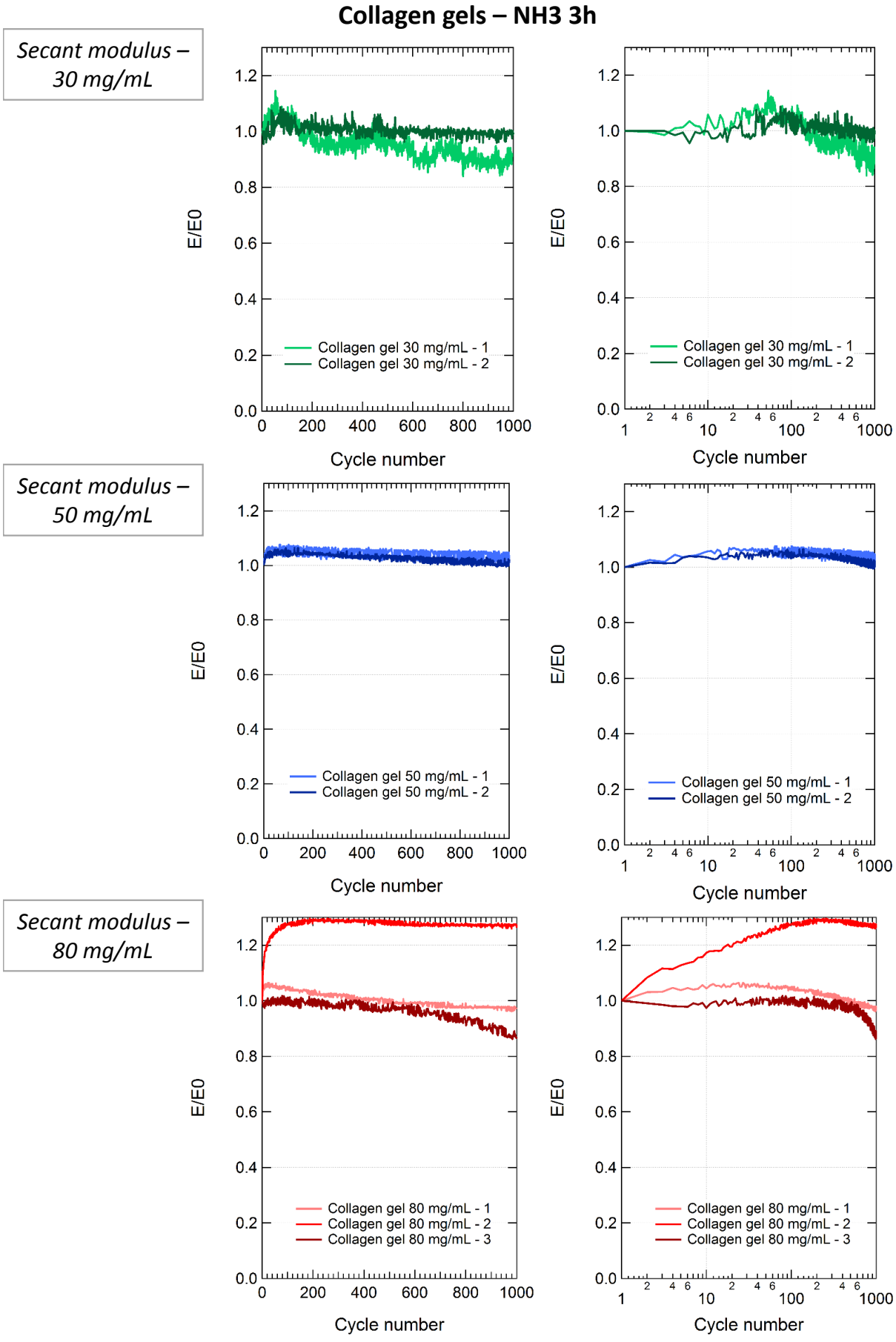

Figure 4.7: Evolution of the secant modulus at 10% strain during cyclic testing of collagen gels synthesized in ammonia vapors for three hours.

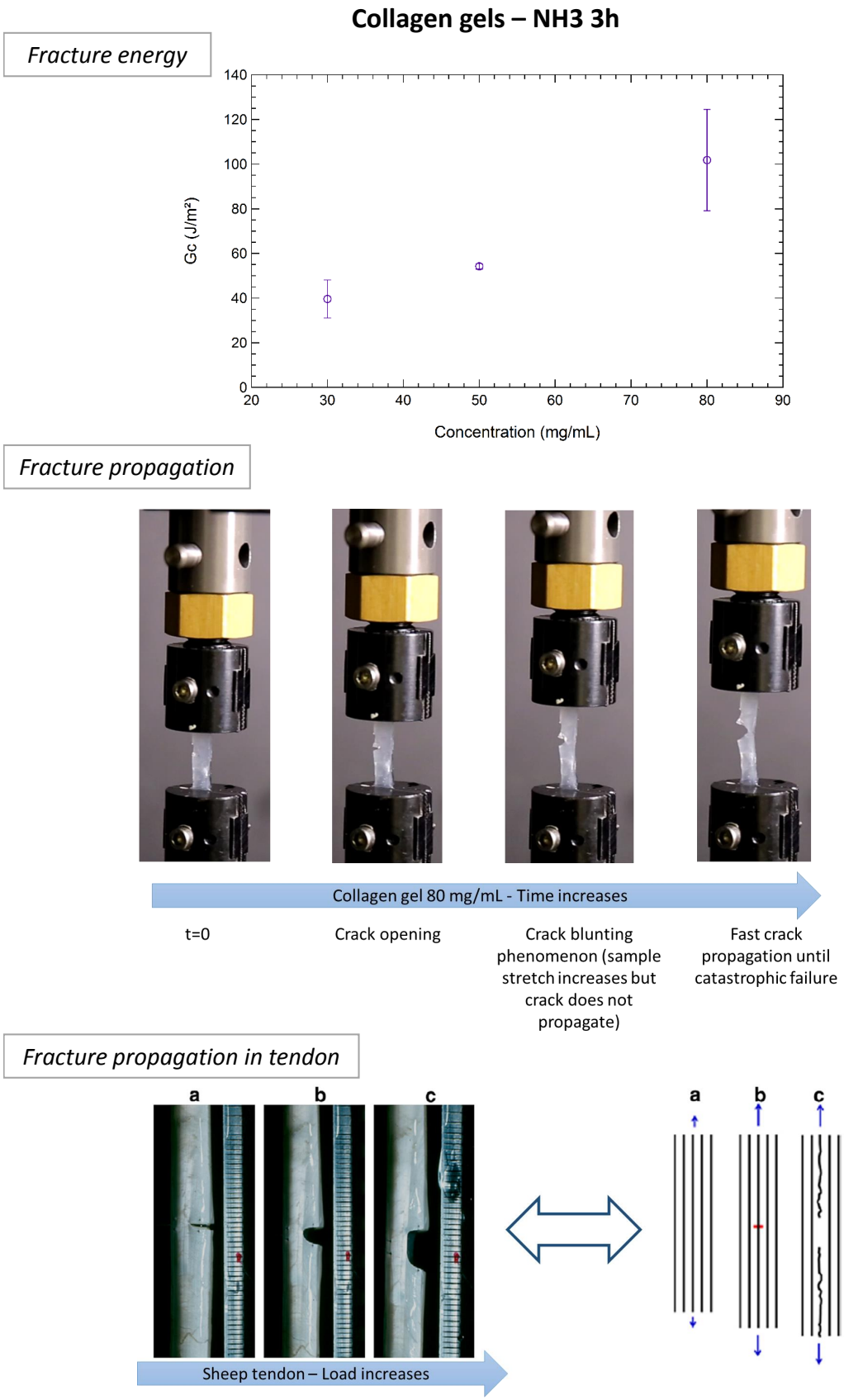

Figure 4.8: Top: Fracture energy of collagen gels synthesized in ammonia for three hours against gel concentration (*two samples per collagen concentration*); middle: sequence of images taken from the movie of fracture test of a collagen gel at 80 mg/mL synthesized in ammonia vapors for three hours; bottom: fracture propagation in tendon and possible mechanism, reproduced and modified from Ker 2007 [10].

4.2.4 Discussion

In all cases our collagen gels exhibit the behavior of collagen-rich tissues and show a global trend where the stiffness of the material increases with the concentration - even if they are only physically crosslinked, unlike biological tissues. The typical J-shape of the tensile behavior of collagen gels is related to a non-linear behavior, and demonstrates the biomimetic feature of the mechanical response. The elasticity is provided by the folded ends of the collagen molecules present in the gap regions and is thus entropy-driven [11]. The physical crosslinks, which may break and form again during stretching of the material, enable gliding at molecular and fibril scales at larger strains [12] hence inducing strain-hardening. To better understand the origin of this behavior, an exponential dependence of stress on strain was proposed by Fung [13]. It provided a good approximation for fitting the tensile behavior of collagen-rich tissues. It seems that even if collagen-rich tissues exhibit a J-shape stress-strain response, this equation is able to fit their behavior with more or less accuracy depending on the tissue type. For example, Lewis and Shaw [14] found that it was more appropriate to model the behavior of a human patellar tendon than that of a white rabbit ligament. Even in the case of the patellar tendon, the equation tends to slightly overestimate the toe region of the curve, as noticed for some of our collagen gels. Introducing the J_{ratio} appears to be a more relevant way to better compare and estimate the non-linear behavior of the gels because it can be calculated independently of the fitting equation.

Performing stress-relaxation tests enable to have access to dissipative mechanisms and characteristic times within a viscoelastic material. Thanks to the linear increase in peak stress with the concentration, we hypothesized a linear viscoelastic behavior. Indeed, the increase of stress with applied strain level was observed in tendon [6], together with a faster relaxation rate when the the strain level increases. Duenwald *et al.* [6] applied strain levels within the physiological range which is located in the toe region of the tensile curve. Our stress-relaxation tests can also be considered as within the physiological range because 20% strain is more or less the end of the toe region of the tensile curve. This toe regime is assumed to be mostly driven by elastic processes as described above. Thus it would be interesting to perform stress-relaxation tests at strains within the linear part of the curve to compare the behavior of the gel when time-dependent processes are more present, and to explore the influence on the characteristic relaxation times.

Further, it appeared that our collagen gels have the typical fatigue behavior of collagen-rich tissues. Their fatigue behavior is similar to that of tendon [15–17], and proceeds by an increase of stiffness followed by structural damage. Different mechanisms could explain this behavior. A lateral fusion of fibril units was observed in dense collagen gels made by plastic compression [18], potentially leading to increased fibril stiffness that could be the source of the macroscopic increase in tangent modulus [19]. Therefore, it could be possible that fibril lateral and/or longitudinal fusion occurs in our gels and would explain the macroscopic increase in stiffness between the 50^{th} and 100^{th} cycles. Further, this increase seems more important for the gel at 30 mg/mL than for the gels at 50 mg/mL and 80 mg/mL (except for one of them): re-alignment of collagen fibrils could also occur thanks to sliding mechanisms enabled by the presence of water. Histological or SEM observations right after the 100th cycle could confirm or not this hypothesis.

If the interfibrillar space in the less concentrated gel is larger due to the presence of less collagen fibrils, it would be easier for fibrils to realign, before undergoing damage mechanisms. SAXS experiments could help concluding on this point by probing the interfibrillar distance and potential load-induced alignments. Nevertheless, it is notable that the abovementioned hypotheses obtained from the fatigue of collagen gels were actually deduced from non-self-organized collagen gels even if

their concentration is high (290 mg/mL for Susilo *et al.* [8] and Chen *et al.* [19]), meaning that the interfibrillar space in those gels is much higher than in our collagen gels or in collagen-rich tissues.

To investigate the recovery properties of our gels, the samples were allowed resting for two hours before being submitted to 1000 cycles at 0.06 Hz. However, the results were highly variable with unexpected behaviors thus difficult to explain. Therefore they will not be discussed.

Finally, by investigating the fracture properties of the gels, it appeared that their fracture energy density is three orders of magnitude lower than that of biological tissues (200 kJ/m²). After little crack blunting, the crack propagated quickly until catastrophic failure of the sample. Therefore, it is unlikely that the mechanism proposed by Ker [10] applies in our collagen gels. Indeed, tendons are organized over larger scales, and contain other components of the ECM, which could explain their higher resistance.

As a conclusion, the stiffness of the gels depends on the collagen concentration as expected. However, all the gels present the same stress-relaxation mechanisms within the toe region (same n exponent, same stress-relaxation amplitude), and close dissipated energies during fatigue. Such mechanisms involve physical crosslinks at fibrillar scale, such as hydrogen bonds. Therefore, modifying the bound water content by increasing the exposure time to ammonia vapors could indirectly have an influence on the dynamics of the gel at fibrillar scale.

4.3 Increasing the exposure time to ammonia vapors

In this section, the collagen solutions were left overnight in ammonia vapors. Three gel concentrations were investigated: 30, 50 and 80 mg/mL.

4.3.1 Non-linear mechanical response at large strains: tensile behavior

Figure 4.9 (top) displays stress-strain curves of the collagen gels. Their behavior is non-linear, but less than that of the three hours condition, despite slightly higher extensibility (higher strain at break). The three master curves were fitted following equation 4.1 as plotted in **Figure 4.9 (middle)**, with a good accuracy. Finally, the measured toe and linear moduli are displayed in **Figure 4.9 (bottom)** and compared to that of the three hours condition. It appears that toe moduli are not significatively different between the two conditions, unlike the linear moduli. The fitting parameters A and B and the values of E_{Ttoe}, $E_{Tlinear}$, E_{toe}, E_{linear} and J_{ratio} are in **Table 4.2**.

Concentration of the gel	30 mg/mL	50 mg/mL	80 mg/mL
Fitting parameters	A=19.0±0.1 kPa B=2.2	A=55.3±0.4 kPa B=2.0	163.3±1.2 kPa B=1.2
E_{Ttoe} **;** $E_{Tlinear}$ **(kPa)**	42 ; 227	111 ; 353	196 ; 317
E_{toe} **;** E_{linear} **(kPa)**	47±7 ; 110±68	131±19 ; 235±97	202±39 ; 256±54
J_{ratio}	1.35	0.79	0.27

Table 4.2: Measured and calculated moduli, J_{ratio} for the ammonia overnight condition.

Calculated toe and linear moduli with the fitting parameters correlate well with the measured values of E_{toe} and E_{linear}. Contrary to the three hours ammonia condition, the J_{ratio} decreases when the concentration incrases, meaning that the behavior of the gels becomes less non-linear. Since the non-linearity at high strains arises from breaking and reforming interfibrillar physical crosslinks as

mentioned before, the tensile response evidences that there was a change in the microstructure of the gels when the ammonia vapors exposure time was increased from three hours to one night. Their linear modulus being lower, we may hypothesize that less mobile interfibrillar physical crosslinks are available at each concentration. Such crosslinks involve water molecules, so less interfibrillar water could be present. This is consistent with the measured bound water content in **Chapter 3**, that was found reduced when the exposure time to ammonia vapors was increased. Thus, the size of the fibrils may have increased from three hours to one night exposure times, which correlates with the hypothesis of **Chapter 3**.

4.3.2 Viscoelastic response: stress-relaxation behavior

Due to apparent changes at the microscale, we may expect a different stress-relaxation behavior between three hours and overnight conditions. The stress-relaxation behavior of the gels is displayed in **Figure 4.10 (top)**. Compared to the three hours condition, the gels seem to relax slightly more rapidly, especially within the first tens of seconds. The deviation is more visible in the log-log scale plot in inset. Note that the sample at 50 mg/mL was among the rare ones to be colonized by fungi, possibly explaining a lower peak stress than expected. As for the collagen gels synthesized in ammonia vapors for three hours, the normalized stress-relaxation curves in **Figure 4.10 (bottom)** are almost superimposed showing once again that the relaxation processes seem independent of the microstructure of the gel at fixed processing conditions. However, the gels seem to relax less stress than the gels synthesized in ammonia vapors for three hours. Indeed, the viscous fraction at 400s is equal to $\sigma_{viscous}$= 0.44±0.02, meaning that less than half of the preak stress is relaxed, unlike the three hours condition where more than half was relaxed. The log-log scale plot in inset is consistent with a slightly different relaxation time between the two conditions.

Seeking to quantify the relaxation time of the gels, the stress-time curves were fitted within the first 100s by equations 4.3 (see **Figure 4.11, left**) and 4.4 (see **Figure 4.11, right**). The characteristic stress-relaxation time was found to be $\tau = 30.7 \pm 1.1\, s$ and the power at 20% $n(\epsilon = 20\%) = -0.0444 \pm 0.003$. Both values are lower than that found for the three hours condition, even if the stress-relaxation experiments should be repeated to confirm the characteristic time. This indicates that the collagen gels synthesized in ammonia overnight relax faster.

4.3.3 Discussion

Here, we conclude that increasing the exposure time to ammonia vapors appears to reduce the non-linearity of the tensile response and reduces the stress-relaxation time together with stress-relaxation amplitude of the collagen gels. As mentioned in **Chapter 1**, studies on the fibril size tend to show that a longer exposition time to alkaline pH is more likely to increase fibril size, either in length or diameter. Increased fibril size would promote the formation of intrafibrillar crosslinks thus enhancing elastic deformations. The reduced amount of bound water measured in **Chapter 3** could explain the less non-linear behavior of the tensile response.

Screen *et al.* proposed on purely uniaxial systems (tendon) that the phenomenon responsible for stress-relaxation in collagen-rich tissues is linked to the swelling of collagen fibrils [20]. Interfibrillar water, confined in a proteoglycan matrix, is released and transforms into intrafibrillar water during stress-relaxation. In the case of the night condition, less bound water would be available for this phenomenon to occur thus explaining that the relaxed stress is lower than for the three hours condition.

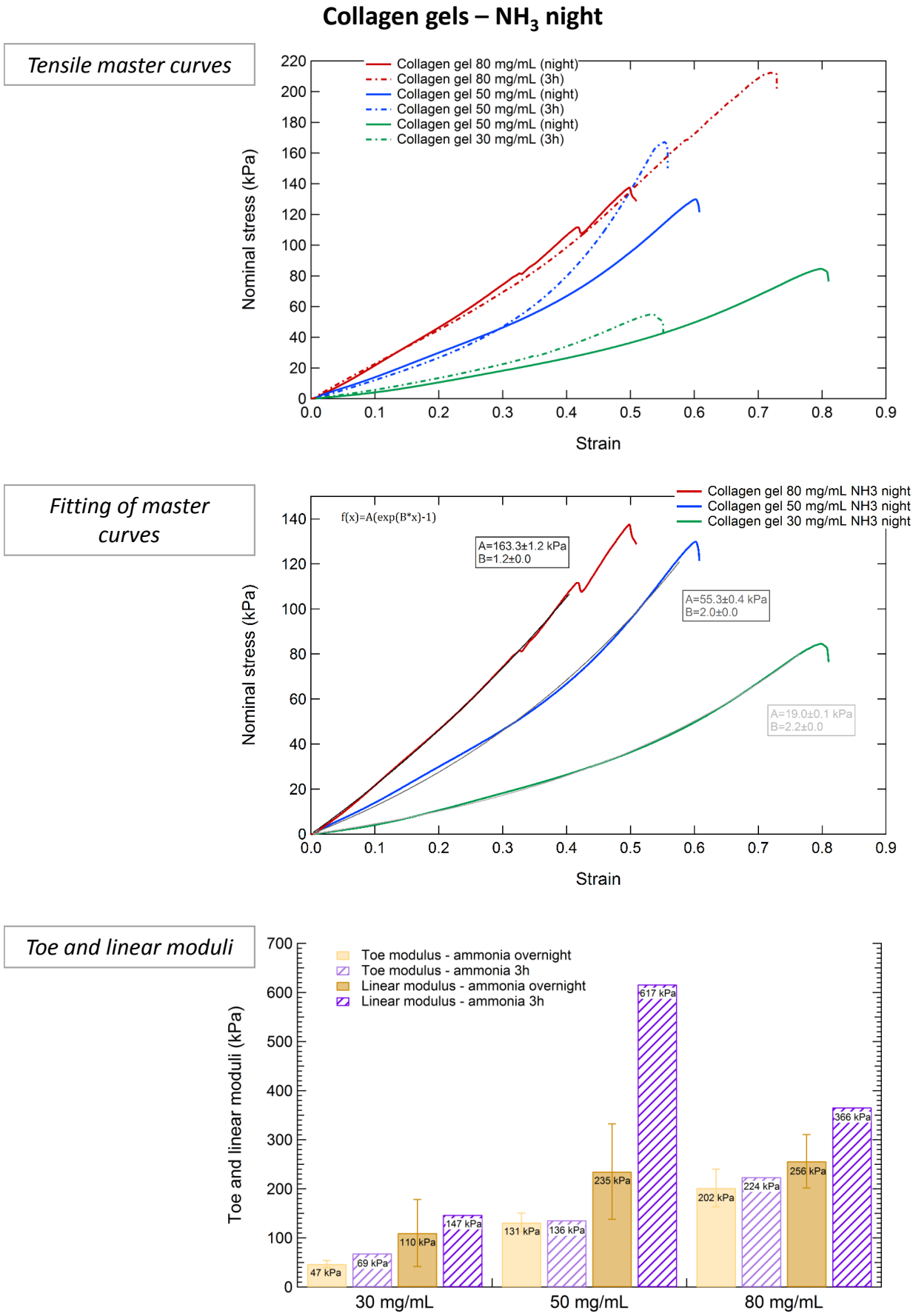

Figure 4.9: Tensile behavior of collagen gels synthesized in ammonia vapors overnight (*two samples per collagen concentration*) compared to that of three hours and associated toe and linear moduli.

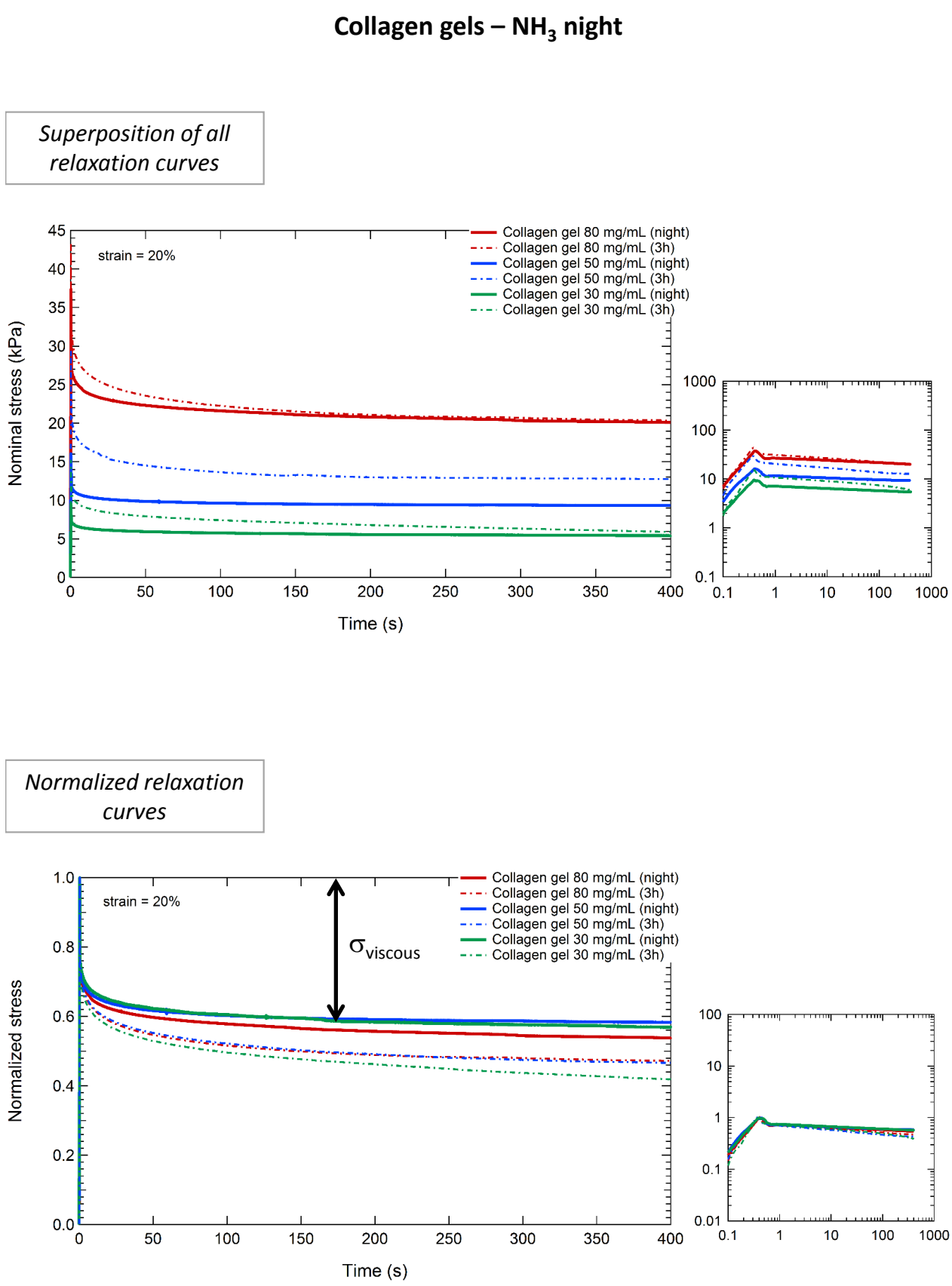

Figure 4.10: Stress-relaxation behavior of collagen gels synthesized in ammonia vapors overnight (*one sample per collagen concentration*).

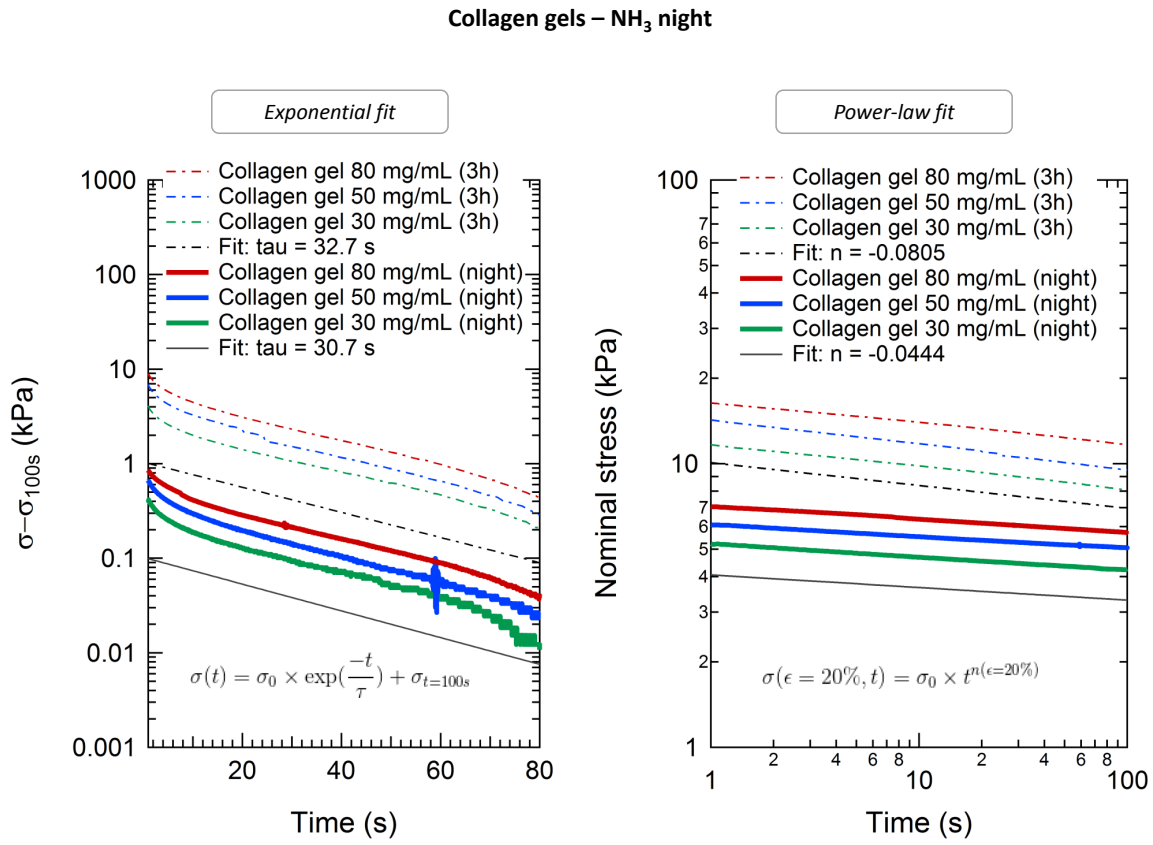

Figure 4.11: Exponential fit and power-law fit of the stress-relaxation of the collagen gels within the first 100 seconds compared to the three hours condition.

As mentioned earlier, SAXS experiments during stress-relaxation would also be needed here to follow the intermolecular distance in the two conditions and confirm or not this phenomenon. Interestingly, if this phenomenon truly occurs in our gels, it would mean that the role of the proteoglycans is only minor because our gels are only composed of collagen and water.

4.4 Influence of different processing parameters on the mechanical behavior of collagen gels

4.4.1 Using PBS as the *in vitro* fibrillogenesis medium

4.4.1.1 Non-linear response at large strains: tensile behavior

Using a buffered fibrillogenesis medium with an ionic strength closer to that of the ECM may have an influence on the final mechanical behavior of the collagen gels. In **Chapter 3**, their structure was already found different from that of collagens gels synthesized in ammonia vapors.

Figure 4.12 (top) displays the large deformation tensile behavior of collagen gels at 30, 50 and 80 mg/mL from two different synthesis (from two different collagen stock solutions). The first batch is plotted in dotted lines, the second one in plain lines. First, a high variability in the same sample is noticed. There is also a variability between batches, in terms of ultimate tensile stresses and extensibility. For both batches, the curves have the typical J-shape associated to collagen-rich materials. The mechanical properties tend to be dissimilar: there is a cross-over at the end of the toe region of a

sample at 50 mg/mL (higher linear modulus) and a sample at 80 mg/mL (lower linear modulus), as displayed in **Figure 4.12 (middle)** for three selected curves. However, ultimate tensile stresses were not quantified since the samples always broke in the clamps, suggesting premature rupture due to damage in the clamps. When compared to the stress-strain curve of the three hours ammonia vapors condition (**Figure 4.12, middle**), it appears that the mechanical response is quite close at 30 mg/mL and 50 mg/mL but more different at 80 mg/mL. The three master curves were fitted with equation 4.1. When compared to the three hours ammonia vapors condition, the collagen gels synthesized in PBS are less stiff in average both in terms of toe and linear moduli (see **Figure 4.12, bottom**).

The fitting parameters A and B and the values of calculated E_{Ttoe}, calculated $E_{Tlinear}$, measured E_{toe}, measured E_{linear} and J_{ratio} are in **Table 4.3**. First, it appears that the fit is not as good as

Concentration of the gel	30 mg/mL	50 mg/mL	80 mg/mL
Fitting parameters	A=14.0±0.2 kPa B=3.2	A=18.1±0.2 kPa B=4.4	34.6±0.2 kPa B=2.3
E_{Ttoe} **;** $E_{Tlinear}$ **(kPa)**	45 ; 229	80 ; 443	80 ; 251
E_{toe} **;** E_{linear} **(kPa)**	29±3 ; 89±62	40±25 ; 136±127	72±16 ; 149±42
J_{ratio}	2.10	2.40	1.06

Table 4.3: Measured and calculated moduli, J_{ratio} for the PBS condition.

for the gels made in ammonia vapors because calculated moduli overestimate the measured values. Second, the J_{ratio} is variable but closer to that of the gels synthesized in ammonia vapors for three hours than the night condition, even if the mechanical behavior is highly variable, especially in terms of stiffness.

Due to the high variability in the tensile behavior (among samples and collagen stock solutions), no further study was performed on the mechanical behavior of the collagen gels synthesized in PBS.

4.4.1.2 Conclusion

Even if the collagen gels synthesized in PBS seem more sensitive to collagen batch variations, it would be interesting to explore their stress-relaxation behavior to determine the effect of a potential screening of the physical interactions by the ions brought in the gel by the solvent. Nevertheless, the non-linear tensile response of the collagen gels synthesized in PBS and those of the three hours condition are quite close, meaning that this mechanical behavior could be expected after injection of the collagen solution in a defect *in vivo*.

4.4.2 Freeze-dried and freeze-thawed collagen gels

4.4.2.1 Non-linear response at large strains: tensile behavior

To discriminate between the effect of the freezing step (where the ice growth is not controlled) and that of the drying step, one collagen gel was frozen after fibrillogenesis *in vitro* then put in sterile milliQ water to thaw the ice. The tensile behavior of the freeze-dried (then rehydrated) and frozen (then thawed) gels are displayed in **Figure 4.13 (top)** together with the stress-strain curve of a gel synthesized in ammonia vapors for three hours at the same concentration. Freezing the gel seems to increase the extensibility of the gel (up to 100% strain instead of 55% for the three hours condition).

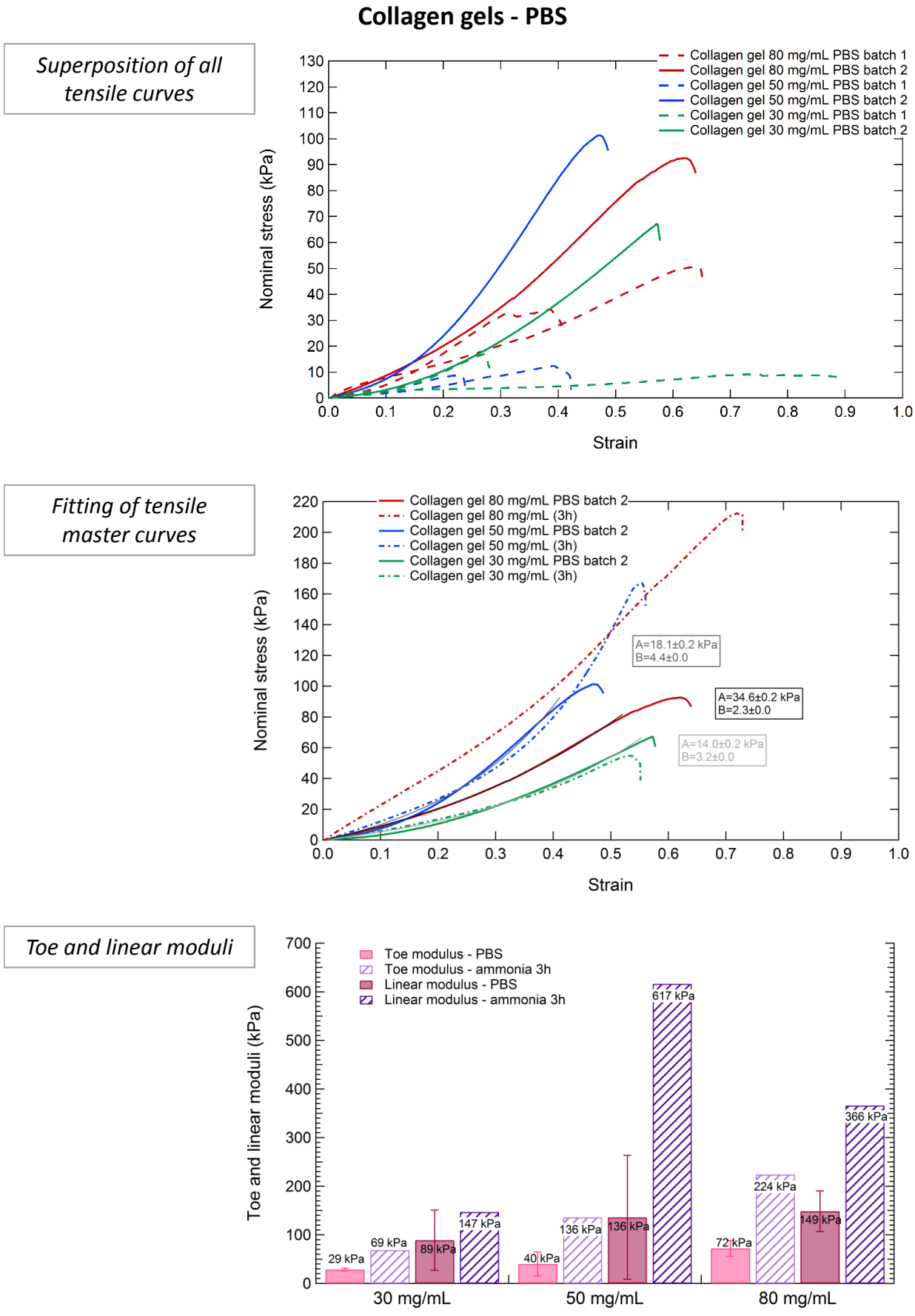

Figure 4.12: Tensile behavior of collagen gels synthesized in PBS and associated toe and linear moduli.

Complete rupture occured in the clamps for all samples. Freeze-drying produces gels with reduced extensibility and almost no increase in stress at higher strains thus without reduced J-shape. In **Figure 4.13 (middle)**, one master curve for each condition was chosen for fitting with equation 4.1. **Figure 4.13 (bottom)** displays the measured toe and linear moduli of freeze-dried gels and frozen gels compared to that of the three hours condition. Freeze-drying seems to reduce dramatically the stiffness of the gel. Freezing as well but to a less extent (experiments should be repeted to confirm the trend).

The fitting parameters A and B and the values of calculated E_{Ttoe}, calculated $E_{Tlinear}$, measured E_{toe}, measured E_{linear} and J_{ratio} are in **Table 4.4**. Calculated and measured toe and linear moduli

Concentration of the gel	50 mg/mL freeze-dried	50 mg/mL freeze-thawed	50 mg/mL 3h
Fitting parameters	A=17.1±0.1 kPa ; B=1.8	A=37.1±0.3 kPa ; B=1.6	17.2±0.1 kPa; B=4.4
E_{Ttoe} **;** $E_{Tlinear}$ **(kPa))**	31 ; 73	59 ; 319	76 ; 780
E_{toe} **;** E_{linear} **(kPa)**	45±11 ; 65±19	62 ; 218	136 ; 617
J_{ratio}	0.46	2.54	3.53

Table 4.4: Measured and calculated moduli, J_{ratio} for the freeze-dried (*three samples*), freeze-thawed (*one sample*) and three hours ammonia conditions.

are of the same order of magnitude, indicating that the fit worked well. Freezing the gel did not significantly reduced the non-linearity of the mechanical response while freeze-drying dramatically reduced their J_{ratio} leading to an almost linear response. Therefore, a change in the physical crosslinks may have occured. This change can impact the viscoelastic response of the freeze-dried gels.

4.4.2.2 Viscoelastic response: stress-relaxation behavior

As seen in **Figure 4.14 (top)**, the stress-relaxation behavior of freeze-dried collagen gels is similar to that of the model gel. However, the relaxation rate seems a bit different as observed on the log-log scale plot in inset. The peak stress of the freeze-dried gel appears highly reduced compared to the reference gel. The normalized relaxation curves in **Figure 4.14 (bottom)** show that the freeze-dried collagen gels appear to relax a little less stress than the reference at 400s: $\sigma_{viscous}$= 0.52. However, the experiment should be repeted to confirm the trend. The slight difference in relaxation time appears more clearly in the log-log plot in inset.

The time-dependency of the freeze-dried collagen gels was quantified by using equations 4.3 and 4.4. There seemed to be no significant difference between the characteristic relaxation time of the freeze-dried gels and that of the reference as displayed in **Figure 4.15 (left)**. The power-law fit enhanced the time-dependency, with an exponent that appeared slightly reduced (see **figure 4.15, right**). Thus, a faster stress-relaxation could imply changes in the ultrastructure. Note that the experiment should be repeted to confirm the trend.

4.4.2.3 Conclusion

As measured in **Chapter 3**, the bound water content in the freeze-dried gels is higher than in the reference gels (three hours ammonia). Ultrastructural changes were confirmed by *(i)* reduced non-linearity in the tensile behavior (J_{ratio} closer to zero) and *(ii)* increase of the stress-relaxation n exponent.

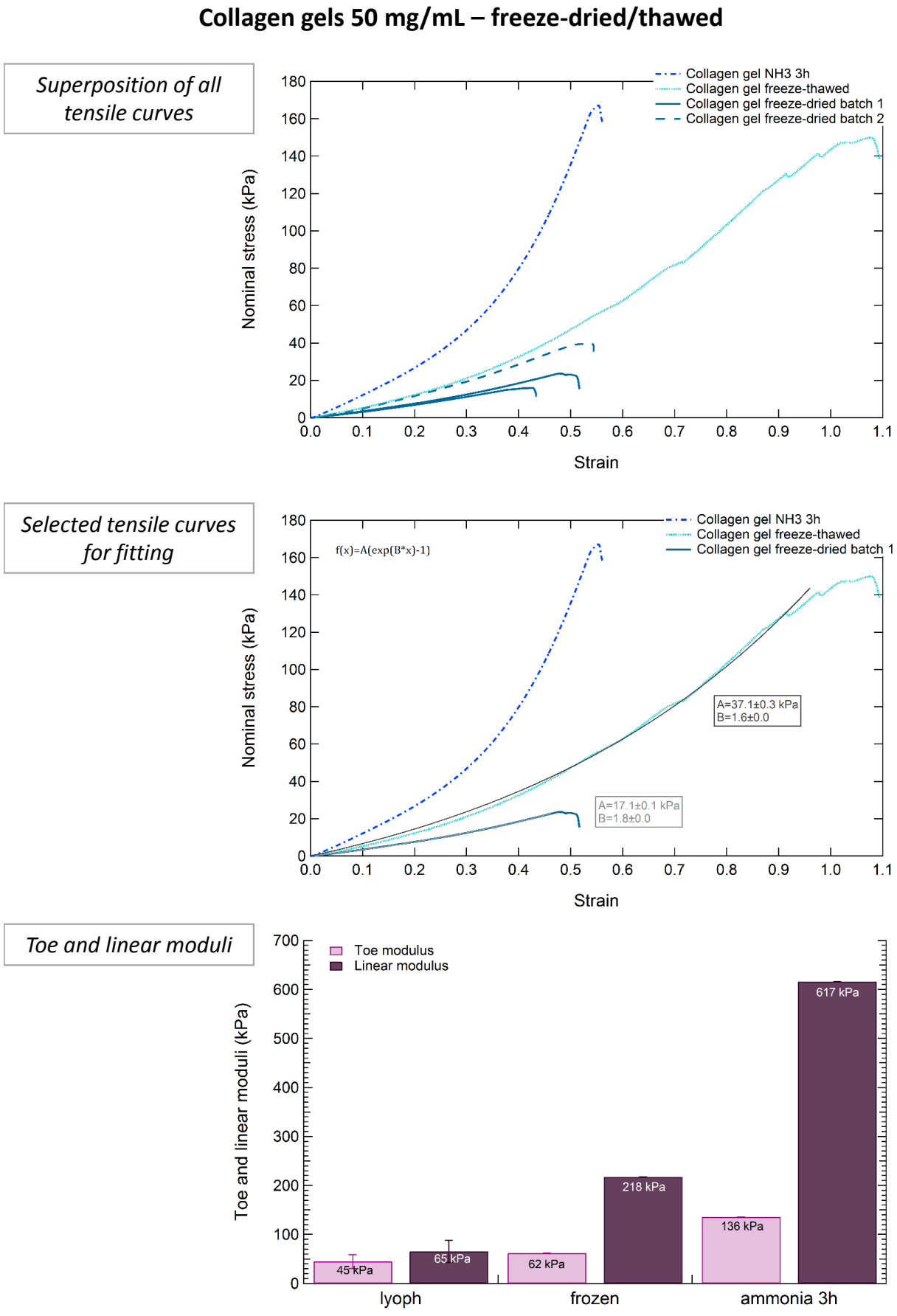

Figure 4.13: Tensile behavior of collagen gels lyophilized or frozen and associated toe and linear moduli.

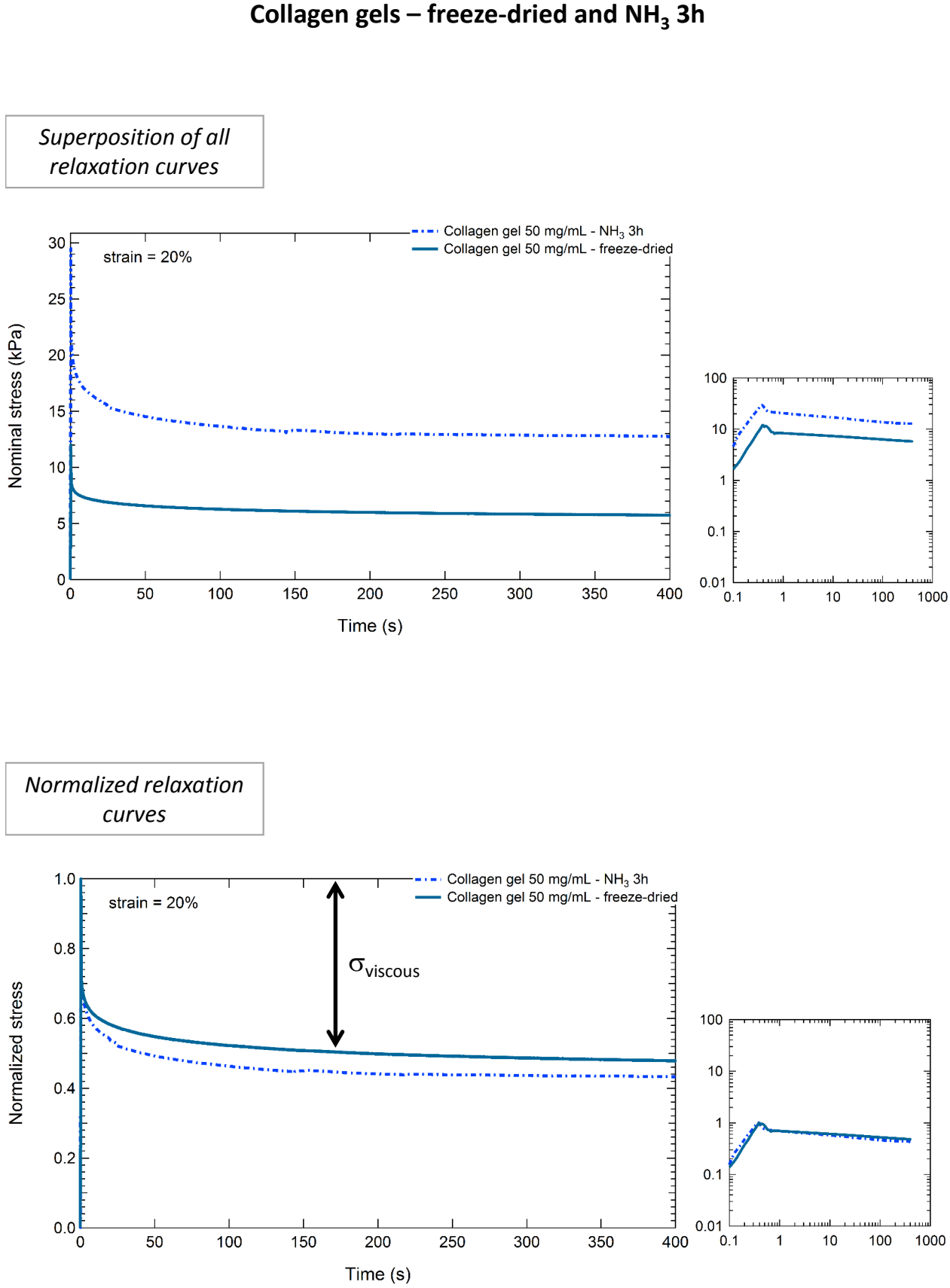

Figure 4.14: Stress-relaxation behavior of freeze-dried collagen gel (*one sample*) compared to collagen gel synthesized in ammonia vapors for three hours.

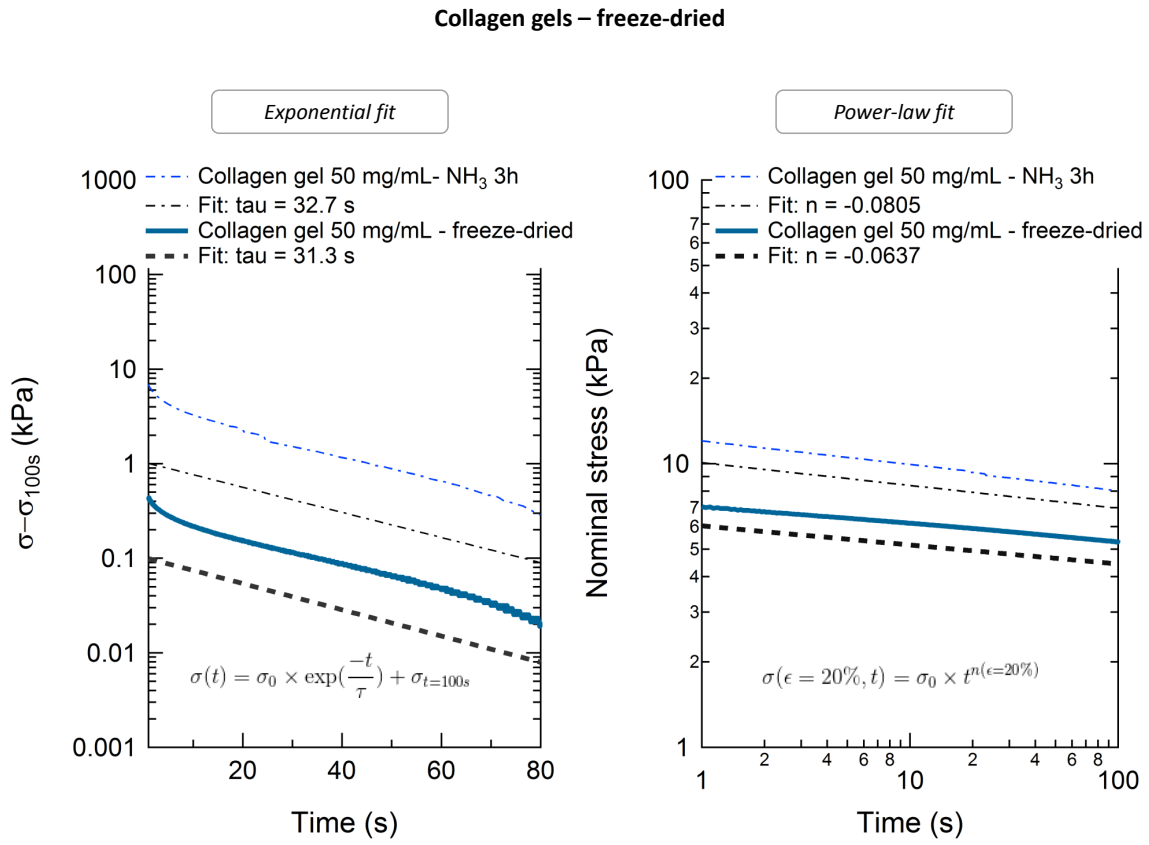

Figure 4.15: Exponential fit and power-law fit of the stress-relaxation of freeze-dried collagen gel within the first 100 seconds compared to the three hours condition.

When collagen gels are frozen, free water anarchically forms ice crystals that are expected to disturb the initial fibrillar organization (changed macroscopic aspect, observed in **Chapter 3**). Some of the bound water may participate to the freezing process. Upon ice thawing, it appears that changes occur in the mechanical behavior of the material. These modifications may be attributed to the changes in fibrillar organization or to the quantity of free or bound water that could also have changed. After freeze-drying, the mechanical behavior of collagen gels is greatly modified: it seems that their stress-strain curve is almost linear, with undifferentiated toe and linear regions. When dry collagen samples are stretched their mechanical behavior relies on the fibrils thus on molecular stretching [21]; there is no more water dedicated to lubrication that would enable sliding thus viscous dissipation effects. A similar phenomenon could occur in the freeze-dried gels: their tensile behavior seems more elastic, and the remaining viscous fraction appears not sufficient to provide high tensile stress. However, it would be inconsistent with their increased amount of bound water.

Both fibril length and diameter may shrink during freeze-drying. Masic *et al.* proposed a model of collagen fibril morphology change upon drying [22]: the mechanism would involve an homogeneous shrinkage of the fibril with removal of intermolecular water together with reduction of the gap length (gap and overlap regions having the same shrinkage coefficient) and/or an heterogeneous shrinkage with reduction of the gap length and increase of the overlap length. Given the increase in the amount of bound water, the second mechanism appear to be more likely to occur in the freeze-dried gels, therefore reducing their stiffness at large strains. Nevertheless, this model is based on tendon, which has a different hierarchical organization from our 3D collagen gels.

4.4.3 Chemical crosslinking by plasma

As menioned in **Chapter 3**, the collagen volumes provided to Pr. Starikovskaia and I. Orel from "Laboratoire de Physique des Plasmas" at Ecole Polytechnique were too small to perform any mechanical characterization.

4.5 Conclusion

The results showed that our collagen gels appear to have a biomimetic mechanical behavior. The tensile behavior of our collagen gels was successfully fitted with an exponential equation that has been used to characterize the non-linear mechanical response of collagen-rich tissues, demonstrating the relevance of the mechanical response of our gels to other biological tissues, tendons or ligaments for instance. **Table 4.5** sums up the major characteristics of the collagen gels. It appears that their stiffness not only depends on the collagen concentration, but also on the processing conditions. Moreover, it is lower than thatof tendon but on the same order of magnitude than that of skin. The J_{ratio} provides consistent informations about the non-linearity of the tensile response of the gels, that can be compared between different processing conditions. An attempt to calculate it from data obtained in the literature (different authors, values in **Chapter 1**) gives an idea of this ratio for tendon and skin for comparison purposes. It appears that the non-linearity of our gels is closer to that of tendon. The best quantification of their time-dependency behavior was obtained with the n parameter, suggesting a power-law relaxation process. The obtained values lie within the range of that calculated for collagen-rich tissues, meaning that our collagen gels mimick the time-dependency properties and the dynamics of their collagen network. Altogether, these parameters can give indications about the ultrastructure of the gels compared to the reference which is the synthesis under ammonia vapors for three hours.

Processing conditions	Collagen concentration (mg/mL)	E_{toe} (kPa)	Fit parameters A (kPa); B	J_{ratio}	$\sigma_{viscous}$ (%)	n power
Ammonia 3h	30	69	19.3 ; 2.6	1.14	57±4	-0.0805
	50	136	17.2 ; 4.4	3.53		
	80	224	167.1 ; 1.2	0.63		
Ammonia night	30	47	19.0 ; 2.2	1.35	44±2	-0.0444
	50	131	55.3 ; 2.0	0.79		
	80	202	163.3 ; 1.2	0.27		
PBS	30	29	14.0 ; 3.2	2.10		
	50	40	18.1 ; 4.4	2.40		
	80	72	34.6 ; 2.3	1.06		
Freeze-dried	50	45	17.1 ; 1.8	0.46	52	-0.0637
Freeze-thawed	50	62	37.1 ; 1.6	2.54		
Tendon		20.10^4	88.10^4 ; 0.005	4		-0.078
Skin		10		2.10^3		

Table 4.5: Summary of the major characteristics of the mechanical response of the collagen gels, together with values from the literature (detailed in **Chapter 1**) for tendon and skin.

Puxkandl *et al.* proposed a model for the viscoelastic properties of collagen: intermolecular chemical and physical crosslinks, and entanglements of the proteoglycan-rich matrix with collagen molecules

(outer part of the fibrils) provide elastic properties; while intermolecular friction at fibrillar scale (interactions *via* electrostatic and hydrogen bonds) and hydrogen bonding in the proteoglycan-rich matrix provide viscous energy dissipation[23]. Our collagen gels are not chemically crosslinked and contain a negligible amount of proteoglycans after purification, meaning that their viscoelastic response should mainly rely on physical crosslinks. Therefore, the process-dependent change in mechanical response of the collagen gels may indicate that the physical crosslinks (related to the amount of bound water and to the fibril size), linked to the ability to dissipate viscous energy, appear to be a determinant parameter. Indeed, the non-linearity of the tensile response is represented by a dramatic increase of stress for small strain changes in the linear part of the stress-strain curve; meaning that the J_{ratio} may be related to the ability to form and break physical crosslinks under loading. By analogy with the thixotropic effect in rheology, Silver *et al.* hypothesized that this increase could be attributed to the interfibrillar water: acting as a lubricant, water could become more fluid at higher strains thus enabling more sliding between fibrils [24]. Collagen fibrils would then tend to align more easily along the tensile direction. This realignment phenomenon was observed by Tower *et al.* in soft tissues by plotting birefringence maps [25]. This hypothesis could be consistent with the tensile response of the gels for the ammonia overnight condition (reduced amount of bound water and J_{ratio}); PLM observations before and after testing could confirm it. However, it does not seem consistent with the tensile response of the freeze-dried gels.

Indeed, results of freeze-drying experiments appear contradictory: they contain a higher amount of bound water than the reference gel, but the dramatic increase of stress in the linear region of their tensile curve is almost inexistant. Silver *et al.* proposed a mechanism for elastic energy storage in collagen fibrils [26]: some parts of the collagen molecules can be considered as springs that release elastic energy when the molecule is stretched because of the breaking of electrostatic bonds. These electrostatic bonds can be located within the same molecule or between two adjacent molecules (or a molecule and its bound water). It seems that after freeze-drying, only the elastic energy within the molecules remains accessible, which decreases the relaxed stress compared to the three hours fibrillogenesis condition. Nevertheless, freeze-drying may not promote intermolecular electrostatic interactions; otherwise the elastic mechanisms would have reinforced the gel.

From bound water content and mechanical tests, we hypothesized that fibril size increases when the exposure time to ammonia vapors is increased from couple of hours to one night. The fibril size may have an influence on the tensile behavior of our gels, possibly exacerbating either elastic or viscous fractions. Therefore the fibril size could also have an influence on the fatigue behavior of the collagen gels, and also on their fracture toughness. More experiments would be needed to conclude on these points. Indeed, from simulations of the relative behavior of two collagen fibrils, M. J. Buehler showed that the fibril size is actually a trade-off between elastic and viscous properties and also depends on the mechanical loading that the tissue should withstand [27].

Nevertheless, if the exponential model is convenient in its simplicity for giving qualitative and quantitative informations, it appears that this equation is unable to accurately fit the behavior of some collagen-rich tissues such as pig cornea in the toe region as displayed in **Figure 4.16**. The tensile behavior was compared to the different gels at 50 mg/mL, according to the new phase in the collagen phase diagram [28]. This phenomenon was also noticed in the case of our gels but less pronounced. This may be related to the presence of viscous dissipation mechanisms operating during

loading in the case of the pig cornea. Indeed, from the values in **Table 4.6** (assuming that the fitting

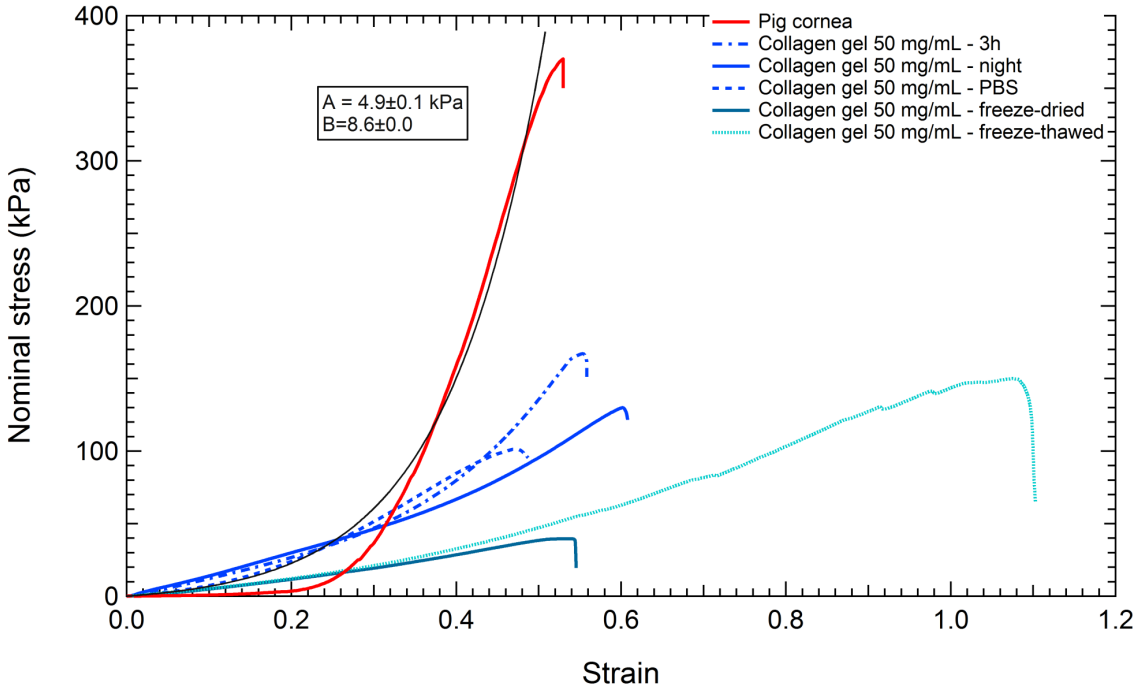

Figure 4.16: Tensile behavior of pig cornea fitted with the exponential equation and compared to our collagen gels at 50 mg/mL.

errors are minimal at zero strain and maximum strain), it appears that the J_{ratio} of pig cornea is much higher than that of our collagen gels. This value is consistent with the mechanical responses of the collagen gels when compared to that of the pig cornea.

Sample	Pig cornea
Fitting parameters	A=4.9 kPa ; B=8.6
E_{Ttoe} **;** $E_{Tlinear}$ **(kPa)**	42.1 ; 2847.1
E_{toe} **;** E_{linear} **(kPa)**	16.3 ; 1749.5
J_{ratio}	106.3

Table 4.6: Measured and calculated moduli and J_{ratio} of the pig cornea tensile behavior.

Finally, it is worth noticing that a tissue is more complex than our model collagen gels. The fibril size may not be homogeneous for example [29] which adds complexity to the understanding of their mechanical behavior. By producing collagen gels in PBS, we actually had an insight on the possible more realistic mechanical behavior of collagen-rich tissues brought by different fibril morphologies in the gel. Indeed, samples taken from the same tissue can have different tensile behavior depending on the location and on the orientation of the punch relatively to the whole sample [30, 31]. Besides, the composition of a tissue is highly complex: for example, it contains proteoglycans that provide tensile stiffness thanks to their interaction with collagen fibrils [32]. Our model collagen gels provide a basis for understanding the molecular, fibrillar and water interactions. It would be interesting to perform

cyclic tests on the other conditions to assess the influence of the fibril size and of freeze-drying on the fatigue behavior of the gels. For example, one could expect almost no hysteresis from freeze-dried samples (due to their more elastic-like tensile behavior) and a early collapse due to friction (less water molecules lubricate the collagen molecules). To better mimick the mechanical behavior of collagen-rich tissue, the composition of the collagen gels could be adjusted by adding other components of the extracellular matrix. Such gels could be used to explore the influence of the ability to dissipate more or less viscous energy on cell differentiation.

Bibliography

1. Engler, A. J., Sen, S., Sweeney, H. L. & Discher, D. E. Matrix Elasticity Directs Stem Cell Lineage Specification. *Cell* **126,** 677–689 (2006).
2. Fung, Y. C. in *Biomechanics* 196–260 (Springer Science+Business Media, New York, 1981).
3. Sun, T. L. *et al.* Physical hydrogels composed of polyampholytes demonstrate high toughness and viscoelasticity. *Nature materials* **12,** 932–7 (2013).
4. Lynch, H. A. Effect of Fiber Orientation and Strain Rate on the Nonlinear Uniaxial Tensile Material Properties of Tendon. *Journal of Biomechanical Engineering* **125,** 726 (2003).
5. Hingorani, R. V., Provenzano, P. P., Lakes, R. S., Escarcega, A. & Vanderby, R. Nonlinear viscoelasticity in rabbit medial collateral ligament. *Annals of Biomedical Engineering* **32,** 306–312 (2004).
6. Duenwald, S. E., Vanderby, R. & Lakes, R. S. Viscoelastic relaxation and recovery of tendon. *Annals of Biomedical Engineering* **37,** 1131–1140 (2009).
7. Herod, T. W. & Veres, S. P. Development of overuse tendinopathy: A new descriptive model for the initiation of tendon damage during cyclic loading. *Journal of Orthopaedic Research* **36,** 467–476 (2018).
8. Susilo, M. E., Paten, J. A., Sander, E. A., Nguyen, T. D. & Ruberti, J. W. Collagen network strengthening following cyclic tensile loading. *Interface Focus* **6** (2016).
9. Rose, S., Dizeux, A., Narita, T., Hourdet, D. & Marcellan, A. Time dependence of dissipative and recovery processes in nanohybrid hydrogels. *Macromolecules* **46,** 4095–4104 (2013).
10. Ker, R. F. Mechanics of tendon, from an engineering perspective. *International Journal of Fatigue* **29,** 1001–1009 (2007).
11. Misof, K., Rapp, G. & Fratzl, P. A new molecular model for collagen elasticity based on synchrotron x- ray scattering evidence. *Biophysical Journal* **72,** 1376–1381 (1997).
12. Fratzl, P. *et al.* Fibrillar structure and mechanical properties of collagen. *Journal of Structural Biology* **122,** 119–122 (1997).
13. Fung, Y. Elasticity of soft tissues in simple elongation. *American Journal of Physiology-Legacy Content* **213,** 1532–1544 (1967).
14. Lewis, G. & Shaw, K. M. Modeling the tensile behavior of human Achilles tendon. *Bio-Medical Materials and Engineering* **7,** 231–244 (1997).
15. Fung, D. T. *et al.* Early response to tendon fatigue damage accumulation in a novel in vivo model. *Journal of Biomechanics* **43,** 274–279. arXiv: NIHMS150003 (2010).
16. Szczesny, S. E., Aeppli, C., David, A. & Mauck, R. L. Fatigue loading of tendon results in collagen kinking and denaturation but does not change local tissue mechanics. *Journal of Biomechanics* **71,** 251–256 (2018).

17. Wren, T. A., Lindsey, D. P., Beaupré, G. S. & Carter, D. R. Effects of creep and cyclic loading on the mechanical properties and failure of human Achilles tendons. *Annals of Biomedical Engineering* **31,** 710–717 (2003).

18. Cheema, U., Chuo, C. B., Sarathchandra, P., Nazhat, S. N. & Brown, R. A. Engineering functional collagen scaffolds: Cyclical loading increases material strength and fibril aggregation. *Advanced Functional Materials* **17,** 2426–2431 (2007).

19. Chen, M. L., Ruberti, J. W. & Nguyen, T. D. Increased stiffness of collagen fibrils following cyclic tensile loading. *Journal of the Mechanical Behavior of Biomedical Materials* **82,** 345–354 (2018).

20. Screen, H. R., Seto, J., Krauss, S., Boesecke, P. & Gupta, H. S. Extrafibrillar diffusion and intrafibrillar swelling at the nanoscale are associated with stress relaxation in the soft collagenous matrix tissue of tendons. *Soft Matter* **7,** 11243–11251 (2011).

21. Gautieri, A., Pate, M. I., Vesentini, S., Redaelli, A. & Buehler, M. J. Hydration and distance dependence of intermolecular shearing between collagen molecules in a model microfibril. *Journal of Biomechanics* **45,** 2079–2083 (2012).

22. Masic, A. *et al.* Osmotic pressure induced tensile forces in tendon collagen. *Nature Communications* **6,** 1–8 (2015).

23. Puxkandl, R. *et al.* Viscoelastic properties of collagen: Synchrotron radiation investigations and structural model. *Philosophical Transactions of the Royal Society B: Biological Sciences* **357,** 191–197 (2002).

24. Silver, F. H., Seehra, G. P., Freeman, J. W. & DeVore, D. Viscoelastic properties of young and old human dermis: A proposed molecular mechanism for elastic energy storage in collagen and elastin. *Journal of Applied Polymer Science* **86,** 1978–1985 (2002).

25. Tower, T. T., Neidert, M. R. & Tranquillo, R. T. Fiber alignment imaging during mechanical testing of soft tissues. *Annals of Biomedical Engineering* **30,** 1221–1233 (2002).

26. Silver, F. H., Christiansen, D. L., Snowhill, P. B. & Chen, Y. Transition from viscous to elastic-based dependency of mechanical properties of self-assembled type I collagen fibers. *Journal of Applied Polymer Science* **79,** 134–142 (2001).

27. Buehler, M. J. Nature designs tough collagen: explaining the nanostructure of collagen fibrils. *Proceedings of the National Academy of Sciences of the United States of America* **103,** 12285–12290 (2006).

28. Salameh, C. *et al.* Structure-properties correlation of stable transparent domain in fibrillar collagen gradient. *Submitted.*

29. Ottani, V., Raspanti, M. & Ruggeri, a. Collagen structure and functional implications. *Micron (Oxford, England : 1993)* **32,** 251–260 (2001).

30. Annaidh, A. N. *et al.* Characterization of the anisotropic mechanical properties of excised human skin To cite this version : HAL Id : hal-00974586 Characterization of the anisotropic mechanical properties of excised human skin (2017).

31. Yang, W. *et al.* On the tear resistance of skin. *Nature Communications* **6,** 1–10 (2015).

32. Akizuki, S. *et al.* Tensile properties of human knee joint cartilage: I. Influence of ionic conditions, weight bearing, and fibrillation on the tensile modulus. *Journal of Orthopaedic Research* **4,** 379–392 (1986).

5

CONFIDENTIAL CHAPTER

6 Experimental conditions

Contents

6.1 Raw material

6.1.1 Collagen extraction and purification for making stock collagen solution

This is a usual protocol at LCMCP [1]. It is recommended to extract collagen from about 40 rat tails at a time. Tails were obtained from Wild Type Wistar rats below 1 year old, to extract a maximum of uncrosslinked collagen in the tendons (collagen tends to crosslink with age in tissues). This yields approximately 1L of final collagen solution concentrated between 2 and 4mg/mL.

Preparation of the solutions

- Acetic acid (AA) at 0.5 M: 29 mL of glacial acetic acid (CH_3COOH) + 971 mL H_20 milliQ (E-POD)
- NaCl 4 M: 233. 8g of NaCl in 1 L H_20 milliQ (E-POD)
- NaCl 4 M in AA 0.5 M: 233.8 g of NaCl in 1 L of acetic acid at 0.5 M
- PBSx10: 80 g NaCl + 2 g KCl + 28.9 g$Na_2HPO_4,12H_2O$ + 2.027 g $NaH_2PO_4,1H_2O$ + 1 L H_20 milliQ (E-POD)
- PBSx1: dilution of PBSx10 ($1/10^{th}$)

Equipment

- Air conditioned laboratory (19-20°C)
- PSM hood (cell culture hood for sterile environment)
- Centrifuge for biological samples only
- Scale with 0.1mg precision
- Filtration units to sterilize solutions and a vacuum pump
- Autoclave
- **Sterile** scissors, pliers, nail clipper pliers, several beakers (1 L), several bottles (1 L), several magnetic stirrers (biggest and longest ones), PPCO (50 mL) centrifuge tubes, Falcon (50 mL) centrifuge tubes, 4 or 5 plastic burettes (2 L), sterile pipettes (25 mL and 10 mL), glass funnel

All equipment has to be clean and sterile.

Extraction of the tendons

A nail clipper plier is used to slightly pinch the tail at 1cm from the smallest extremity. This 1 cm end is hold in the plier while slightly twisting the wrist to break the vertebra. The tendon (long white and shiny strands) is then delicately pulled from the rest of the tail. It is cut with sharp scissors and kept in 500 mL sterile PBS, in a sterile 1L beaker. The same tail is then pinched with the nail clipper plier from 1 cm of the smallest extremity (that was just removed) and the same protocol is applied until reaching the last 3 cm of the tail (from the extremity that was attached to the rat). Attention is payed not to put blood vessels in the PBS beaker with the tendons. See **Figure 6.1**.

Tendons cleaning

To remove cells and traces of blood, the tendons are centrifuged with PBS in 50mL Falcon tubes

Figure 6.1: Extraction of rat tail tendons by two operators (Nadine on the left, myself on the right). Credits: Cédric Boissière

(slowest rotor of the centrifuge) at 4°C for 5min at 5500rpm until the supernatent is transparent and colourless (approximately 4 or 5 centrifugations). PBS is changed between each centrifugation. The tubes are carefully weighed and equilibrated 2 by 2 before centrifugation to avoid damaging the centrifuge. The tendons were then soaked in at least 500 mL of 4 M NaCl solution for 30min to lyse the remaining cells and precipitate some of the high molecular weight proteins. Then, the tendons are centrifuged with PBS in 50mL Falcon tubes (slowest rotor of the centrifuge) at 4°C for 5 min at 5500 rpm (approximately 4 or 5 centrifugations).

Solubilization of the tendons and collagen purification

The clean tendons are immersed in sterile 1L acetic acid solution at 0.5 M in a 1 L closed bottle with a magnetic stirrer. The solution is stirred for 24h at 20°C. Some stirring plates may heat when used for too long; the solution should be put in the fridge overnight, and agitated during the day while checking regularly that the stirring plate remains cool. To remove the biggest undissolved aggregates, the solution is centrifuged in 50mL sterile PPCO tubes at 4°C at 21000 rpm (fastest rotor of the centrifuge) for 2h. The PPCO tubes are carefully weighed and equilibrated 2 by 2 before centrifugation to avoid damaging the centrifuge. The supernatant (biggest volume) is slowly poured in a bottle. The bottom is poured in a bottle with acetic acid at 0.5 M to try and dissolve them.

NaCl 4 M at AA 0.5 M solution is added to the supernatant solution in order to obtain a final NaCl concentration at 300 mM. The NaCl 4 M at AA 0.5M solution is poured very slowly with a sterile pipette (3mL by 3mL) under high agitation. Agitation of the solution is kept for 3h. This step enables the precipitation of undesirable components (such as plasma proteins) but not collagen. The precipitated solution is then centrifuged in 50mL PPCO tubes at 4°C at 21000 rpm (fastest rotor of the centrifuge) for 3h. The PPCO tubes are carefully weighed and equilibrated 2 by 2 before centrifugation to avoid damaging the centrifuge.

The supernatant (smallest volume) is slowly poured in a sterile 1 L bottle. The bottom of the tubes is discarded. NaCl 4 M at AA 0.5 M is added to the supernatant solution in order to reach a final NaCl concentration of 700mM. The NaCl 4 M at AA 0.5 M solution is poured very slowly with a

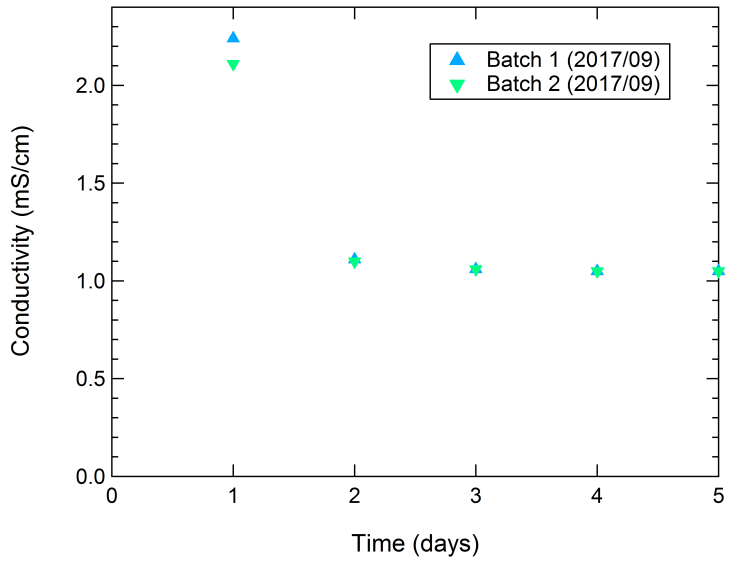

Figure 6.2: Averaged conductivity (over 6L) of AA 0.5M as a dialysis solvent during five days for two collagen batches in 2017.

sterile pipette (3mL by 3mL) under high agitation. Agitation of the solution is kept for 24h. This step enables the selective precipitation of collagen. The precipitated solution is then centrifuged in 50 mL Falcon tubes at 10°C at 4400 rpm (slowest rotor of the centrifuge) for 45 min. The Falcon tubes are carefully weighed and equilibrated 2 by 2 before centrifugation to avoid damaging the centrifuge. The supernatant (biggest volume) is discarded and the bottoms are solubilized in acetic acid at 0.5 M under agitation for 12h.

To remove excess of NaCl, collagen is dialyzed against acetic acid at 0.5 M. The ratio is 10 volumes of acetic acid for 1 volume of collagen. 14 kDa dialysis membranes are used. About 200 mL collagen solution is poured in previously boiled for 10min then cooled down dialysis membrane, in a 2L plastic burette. The membrane is closed and 2L sterile acetic acid at 0.5 M are added slowly. The protocol is applied until all the collagen solution is in dialysis membranes. The solvent (sterile AA 0.5 M) is changed twice a day for five days, until the conductivity of the solution has reached a plateau (see Figure 6.2).

The dialyzed collagen solution is poured in a sterile bottle and centrifuged for 4h at 4°C in 50mL PPCO tubes (fastest rotor of the centrifuge) at 21000rpm. The supernatant (biggest volume) is poured in a sterile bottle, the bottoms are discarded.

The final collagen solution is called "stock collagen solution". The concentration of this solution is to be determined by hydroxyproline titration.

During this thesis, 6 batches of collagen were produced (1 in March 2017, 2 in November 2017 "16Q" and "Flo", 2 in April 2018 "4/18" and "5/18", 1 in February 2019 "2/19").

6.1.2 Collagen titration by hydroxyproline

Table of the solutions.

Name of the solution	Composition	Quantities	Remarks
Titration buffer	Citric acid monohydrate (0.25M) Sodium acetate trihydrate (1M) Sodium hydroxyde (0.85M) Acetic acid glacial H_2O milliQ	6.25g 17.5g 4.25g (tablets) 1.5mL 125mL	Adjust the pH to 6 by adding acetic acid glacial. Store in the fridge at 4°C.
Perchloric acid (3.15M)	Perchloric acid 65% H_2O milliQ	30mL 70mL	Store in the fridge at 4°C.
Hydroxyproline (20µg/mL)	Hydroxy-L-proline H_2O milliQ	2mg 100mL	Dissolve 20mg of HP in 100mL H_2O milliQ then add 1mL of the obtained solution to 19mL H_2O milliQ.
Chloramine T solution	Chloramine T H_2O milliQ 2-Methoxyethanol (methyl cellosolve) Titration buffer	400mg 5mL 7.5mL 12.5mL	To be prepared under hood.
DMBA solution	Dimethylamino-4-benzaldehyde 2-Methoxyethanol	2g 10mL	Heat for 30min at 60°C

Collagen hydrolysis

Mix 50µL of the collagen solution (or 50mg of collagen matrix) with 50µL HCl 33% in a 1.5mL Eppendorf. Vortex the Eppendorf then put it for 24h in an oven at 108°C. This step breaks the bonds between the amino-acids in the collagen molecules thus releasing hydroxyproline residues. Open the tube and let it in the oven for 1h to dry the solution. Then, add 1mL of H_2O milliQ in the Eppendorf and vortex it. Prepare 3 aliquots of this solution in three 1.5mL Eppendorfs: 20µL, 40µL and 40µL.

Hydroxyproline range (titration reference)

This range is made from the stock solution at 20µg/mL following the table below (5 Eppendorfs, 1 concentration per Eppendorf from 0-0.8-1.6-2-2.8µg/mL).

Hydroxyproline titration

	Hydroxyproline range					**Collagen sample**		
Hydroxyproline or sample (µL)	0	40	80	100	140	20	40	40
H_2O milliQ (µL)	400	360	320	300	260	380	360	360
Dilution						1/20	1/10	1/10
Chloramine T	200µL, vortex, at room temperature during 20min							
Perchloric acid 3.15M	200µL, vortex, at room temperature during 5min							
DMBA	200µL, vortex, at 60°C during 20min (thermo-regulated bath)							

The different solutions are added to the hydroxyproline range Eppendorfs and to the sample Eppendorf following the table. First, Chloramine T oxidizes hydroxyproline residues. This reaction is stopped by adding perchloric acid. DMBA induces the formation of a coloured complex (purple).

Determination of the hydroxyproline concentration

This step requires a UV-visible spectrophotometer. The optical density is determined at a fixed wavelength of 557nm. The solution of the "0" Eppendorf of hydroxyproline range is poured in a thin spectrophotometer cuvette. The cuvette is placed in the spectrophotometer, then hit "Autozero" to set the baseline of the measurements. Then, each solution of the hydroxyproline range Eppendorfs is poured in a cuvette (with increasing concentration) and optical density is measured 3 times in a row for each cuvette by putting the cuvette in, then removing it (to get an average value). The same procedure is repeated for the sample Eppendorf.

Determination of the collagen concentration

The optical density values are put in an excel spreadsheet (see **Figure 6.3**). The calculation is performed by using the following formula:

$$[collagen] = Q_{hydroxyproline} \times (100/10.9)/V_{collagen} \tag{6.1}$$

with:

- $[collagen]$: collagen concentration (mg/mL)
- $Q_{hydroxyproline}$: hydroxyproline amount per collagen molecule
- 100/10.9: 10.9 is the percentage of hydroxyproline amount in a single collagen molecule
- $V_{collagen}$: collagen volume

6.1.3 Collagen solutions for spray-drying

The stock collagen solution was diluted under PSM hood to the chosen concentration with sterile acetic acid at 0.5M.

6.1.4 Collagen solutions concentration (reverse dialysis)

To reach a final concentration of 5mg/mL the following formula was used [2]:

$$C_F = C_{PEG}/1.5 \tag{6.2}$$

with:

- C_F final collagen concentration
- C_{PEG} PEG concentration in the dialysis solution

PEG was dissolved in acetic acid 0.5M. 250mL of stock collagen solution was put in a dialysis membrane (cut-off 14kDa) then sunk in a beaker containing PEG in AA0.5M. The solution was agitated for a week. Then the collagen solution was poured in a bottle with an hermetic cap.

6.1.5 Collagen solutions storage and use conditions

All collagen solutions were kept at 4°C (in the fridge) to avoid any denaturation into gelatin because of the heat. They were kept in closed and sterile containers to avoid contaminations.
The stock collagen solutions and diluted collagen solutions for spray-drying are all sterile.

As an example:

- for a 40 µl sample, the optical density gives a hydroxyproline content of 0.8 µg (read on the graph)
- total hydroxyproline content in the aliquot = 0.8/40 = 0.02 µg/µL
- in 1 mL milliQ water, there is: 0.02*1000 = 20 µg hydroxyproline
- in the initial 50 µL aliquot from the stock collagen solution there is: 20/50 * 100/10.9 = 3.04 mg/mL collagen.

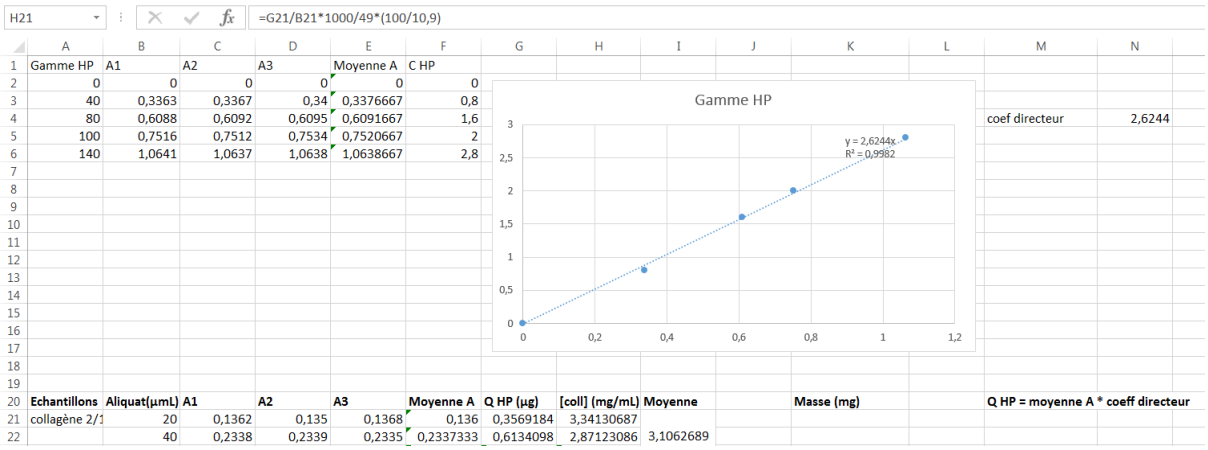

	A	B	C	D	E	F	G	H	I	J	K	L	M	N
1	Gamme HP	A1	A2	A3	Moyenne A	C HP								
2	0	0	0	0	0	0								
3	40	0,3363	0,3367	0,34	0,3376667	0,8								
4	80	0,6088	0,6092	0,6095	0,6091667	1,6							coef directeur	2,6244
5	100	0,7516	0,7512	0,7534	0,7520667	2								
6	140	1,0641	1,0637	1,0638	1,0638667	2,8								
7														
8														
9														
10														
11														
12														
13														
14														
15														
16														
17														
18														
19														
20	**Echantillons**	**Aliquat(µmL)**	**A1**	**A2**	**A3**	**Moyenne A**	**Q HP (µg)**	**[coll] (mg/mL)**	**Moyenne**		**Masse (mg)**		**Q HP = moyenne A * coeff directeur**	
21	collagène 2/1	20	0,1362	0,135	0,1368	0,136	0,3569184	3,34130687						
22		40	0,2338	0,2339	0,2335	0,2337333	0,6134098	2,87123086	3,1062689					

Figure 6.3: Excel spreadsheet for collagen concentration

6.2 Synthesis of collagen materials

6.2.1 Collagen microparticles

The machine is a Büchi B290 mini spray-drier. It is located under a floor-to-ceiling hood.

6.2.1.1 Spray-drying conditions

The following processing conditions were determined to spray-dry collagen solutions at different concentrations. For example:

Concentration	**Solution flow**	**Air flow**	**Aspiration rate**	**Inlet (set)**	**Inlet (measured)**	**Outlet (measured)**
1 mg/mL (0.1 wt%)	1% (0.3 mL/min)	35 (414 L/h)	50% (20 m^3/h)	30°C	34-35°C	19-25°C

A white powder is obtained at the end. Pressurized air from SU campus was used at all times except when specified. The first value in each row of: solution flow, air flow, aspiration rate is the one to be set on the machine following the scheme above. Any heat loss is to be avoided during the process, to prevent the formation and accumulation of liquid doplets that would wet the powder in the cyclone and further in the collecting flask.

6.2.1.2 Collagen microparticles storage

After closing the glass flask with a cap right after spray-drying, the flask was put in a drawer in the laboratory thus kept a 20°C before use.

6.2.1.3 Stability of the microparticles

The collagen microparticles should be used in the month following their production to avoid any destabilization. Cf. **Chapter 2**.

6.2.2 Collagen hydrogels

6.2.2.1 Preparation of injectable collagen solutions

The desired amount of collagen beads was weighed in a small mortar on a precision scale. Acetic acid at low concentration was pipetted and put in the small mortar on the collagen beads. Both were mixed with a small pestle.

For injected collagen gels

The mixture was transferred with a small spatula into a 3mL luer lock syringe (without its plunger). The plunger was then inserted in the syringe. A $26G^{1/2''}$ needle was connected at the end of the syringe for further injection. This method led to the formation of high amounts of air bubbles inside the gel. Therefore another protocol was preferably used (see below).

For spread collagen gels

The mixture was transferred in a 2mL Eppendorf. Another 2mL Eppendorf was filled with water to obtain the same weight in order to balance the centrifuge. The Eppendrof tubes are carefully weighed and equilibrated 2 by 2 (adjust the weight of the one containing water) before centrifugation to avoid damaging the centrifuge. The Eppendorfs were centrifuged in the ALLEGRA64R centrifuge at 4°C for 2min at 26000g. The collagen solution was then spread in the mold with a spatula and evened to obtain an homogeneous sample thickness. The mold was then covered and secured on the sides.

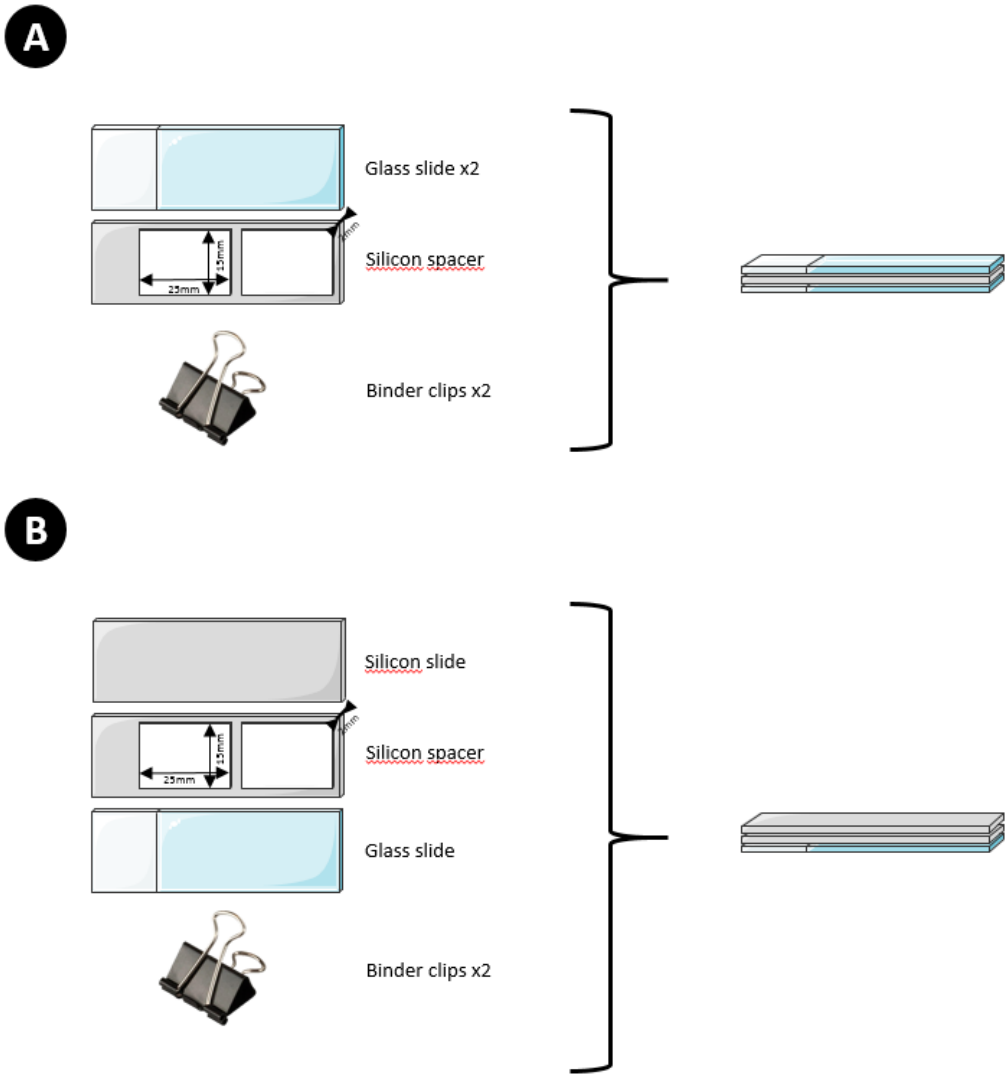

Figure 6.4: Home-made molds for fibrillogenesis of collagen matrices under ammonia vapors. A: molds used before December 2017. B: molds used after Januray 2018.

6.2.2.2 Fibrillogenesis *in vitro* by ammonia vapours: Chapters 3 and 4

The following molds were used (Figure 6.4). The molds were designed to keep a constant sample thickness while providing three samples from each hydrogel for mechanical characterizations (dimensions of a typical sample: $25 \times 5 \times 2mm^3$). The mold A was used during the beginning of the thesis (until December 2018) because of its convenience for injection: the collagen solution can be seen through both glass slides and spread inside the holes with reduced friction compared to other materials. Then, to obtain samples with less air bubbles, the mold B was used. It also enabled to get rid of potential flow effects (due to the ammonia vapours) and to minimize the fibrillogenesis time which could be adjusted more precisely.
After having injected the collagen solution through the silicon spacer (another needle was inserted at the other end of the mold to avoid leaks by inducing higher pressures) - **mold A** - or spreading the centrifuged solution in the hole then covering it with the silicon slide - **mold B** - the mold was secured with binder clips at each end. The mold was put in a 1L beaker together with ammonia solution (33%). The 1L beaker was then hermetically covered with parafilm sheets. The fibrillogenesis time

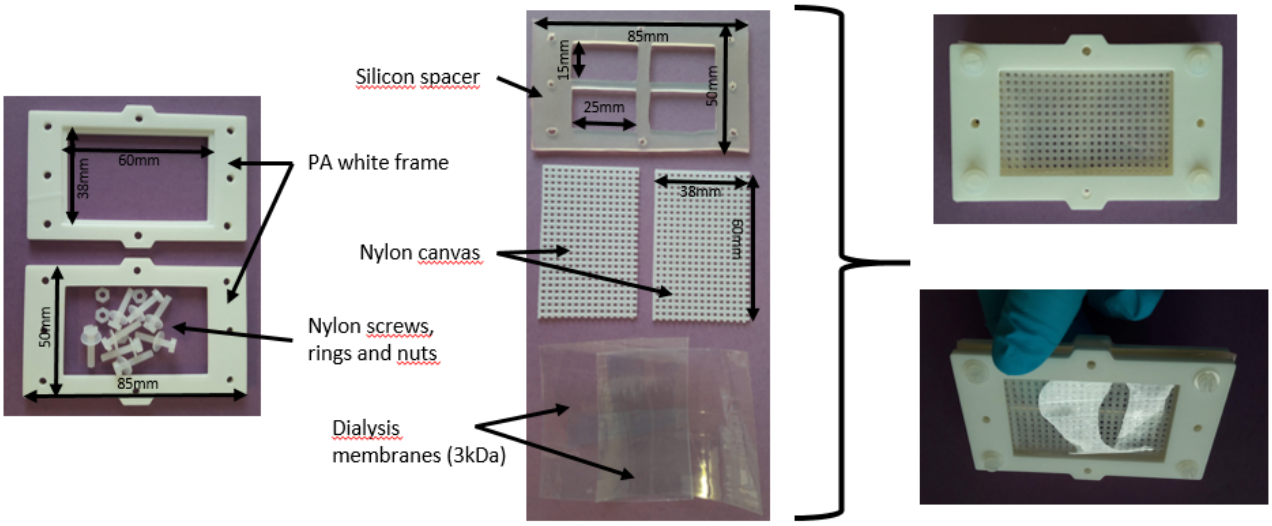

Figure 6.5: Home-made molds for fibrillogenesis of collagen matrices in PBSx10.

was set to 3 hours (cf. Gobeaux's thesis: fibrillogenesis speed is about 1mm per hour) or overnight or longer depending on the samples. When not precised in the sample names, fibrillogenesis was 3 hours. After fibrillogenesis, the sample was carefully removed from the mold. It was weighed, then put in a small sterile crystallizer under the PSM containing either sterile PBSx1 or sterile H_2O milliQ to rinse the ammonia left in the sample and reach a pH around 7. The first bath was set to 10min, the second and third ones to 20min. The solvent was changed in between baths. After the third bath, the pH of the bath was checked with a pH paper strip. If it is above 7, a fourth bath (20min) can be made. If it is at 7, the sample is removed from the bath and put in a 50mL Falcon tube filled with 40mL of sterile solvent (either PBS or sterile H_2O milliQ). A thin parafilm strip is wrapped around the cap of the tube to ensure that it remains hermetic.

6.2.2.3 Fibrillogenesis *in vitro* by ammonia vapours, first explored conditions: Chapter 4

The gels were synthesized from 10 mg/mL to 80 mg/mL as described above, except:

- the collagen solution was put in a syringe connected to a 26G needle;
- the solution was injected in the mold (air bubbles);
- fibrillogenesis was made under ammonia vapors for one night;
- the gels were removed from the mold and directly put in 10 mL PBSx1 in a sterile Falcon without rinsing.

Therefore, these gels remained several weeks at very alkaline pH (10-11), potentially modifying their ultrastructure over time.

6.2.2.4 Fibrillogenesis *in vitro* in phosphate buffer: Chapters 3 and 4

The following mold was used (Figure 6.5).

- White frame: the frame was designed in 3D specifically for this experiment then 3D-printed by RadioSpare in PA 2200 (polyamide white). The material was chosen for its chemical stability.
- White grid: purchased in Cultura Shop, originally for canvas work
- Dialysis membrane: with a 3kDa cut-off
- Silicon spacer: home-made in the same material than that for ammonia vapours mold
- Small screws, rings, nuts in PA: purchased from RS
- Small screwdriver: purchased from RS

The molds were designed to keep a constant sample thickness while providing three samples from each hydrogel for mechanical characterization. The dimensions of the holes are the same than that of the ammonia vapours molds. The immersion molds were only used with the spreading technique, not for injection due to the increase of technical constraints. All the synthesis steps (except weighing of the collagen powder) were performed under the PSM in sterile conditions. The dialysis membrane was cut at the dimensions of the grid, boiled for 10min in H_2O milliQ and put in sterile PBSx1 under the PSM afterwards. After assembling the first half of the mold (grid in wet dialysis membrane + white frame + silicon spacer) the collagen solution was spread in the mold. Attention was payed to keep the dialysis membrane wet, by immersing the bottom of the mold in sterile PBSx10 in a shallow crystallizer before spreading and after spreading. Then, the other half of the mold (white frame + grid in wet dialysis membrane) was put above the mold and was assembled by 8 mini-screws. 400mL of sterile PBSx1 was poured in a 1L beaker and the mold was sunk in it. The beaker was hermetically covered with parafilm and put in the fridge for at least 4 days for the fibrillogenesis to be complete. Then, the beaker is put under the PSM. The hydrogel is removed, weighed, and placed in a sterile 50mL Falcon tube containing about 40mL sterile PBSx1. A thin parafilm strip is wrapped around the cap of the tube to ensure that it remains hermetic.

6.2.2.5 Freeze-drying: Chapters 3 and 4

Collagen solutions

After making an air bubble-free collagen solution, the solution was spread in half of the mold for ammonia vapours (glass slide + silicon spacer). The half-mold was put in a small cardboard box, frozen for one night at -80°C then lyophilized for 24 hours at 0.016mbar and 65°C. The sample was detached from the glass slide then rehydrated in 40mL sterile PBSx1 in a 50mL Falcon tube.

Collagen hydrogels

Collagen hydrogels were produced following the spreading method and under ammonia vapours in mold B. Then, the hydrogel is rinsed with PBSx1 as described above to set its pH around 7. The gel is placed on a silicon sheet in a small cardboard box. It is frozen for one night at -80°C then lyophilized for 24 hours at 0.016mbar and 65°C. The sample is removed from the silicon sheet then rehydrated in 40mL sterile PBSx1 in a 50mL Falcon tube.

6.2.2.6 Freeze-thawing: Chapters 3 and 4

Collagen hydrogels

Collagen hydrogels were produced following the spreading method and under ammonia vapours in

mold B. Then, the hydrogel is rinsed with sterile milliQ water as described above to set its pH around 7. The gel is placed on a silicon sheet in a small cardboard box. It is frozen for one night at -80°C then put in 50 mL sterile milliQ water for ice thawing.

6.2.2.7 Collagen hydrogels nomenclature

The name of the hydrogels always start with the date they were put in the Falcon tube, followed by the letter G with the concentration (in mg/mL). If nothing more is written, the hydrogel was made following the spreading method in mold B under ammonia vapours for 3 hours *e.g.* 180226_G30 is a 30mg/mL gel made on 26th February 2018.
The name of gels starting by the letter "S" mean that the collagen solution was lyophilized.

6.2.3 Other collagen materials

6.2.3.1 Collagen injection in DMEM : Chapter 2

Pure collagen beads made from a collagen solution (3.6 mg/mL) were mixed with an aqueous solvent (200μL) to reach a final concentration of 80 mg/mL. The mixture was quickly transferred to a 1mL syringe equipped with a 26G1/2" needle. The mixture was injected right after in phenol red-free DMEM in a transparent 5mL UV cuvette at ambient temperature. After injection the cuvette was hermetically covered with parafilm and kept for a week at 4°C before analysis of the injected material.

6.2.3.2 Crosslinking by plasma: Chapter 3

About 1 mg/mL collagen solutions were used. Collagen solution volumes and plasma exposure time are summed up in **Figure 6.6**. Two collagen volumes were used: 20 µL and 50 µL. Exposure times ranged from 3s to 100s.

6.2.4 Collagen materials storage and use conditions

All collagen materials were stored in (as) sterile (as possible) conditions at 4°C. When precised in the protocol, the material was made under the PSM. When not precised, the material was not made in sterile conditions. The materials are not characterized in sterile conditions but in (as) clean (as possible) conditions.

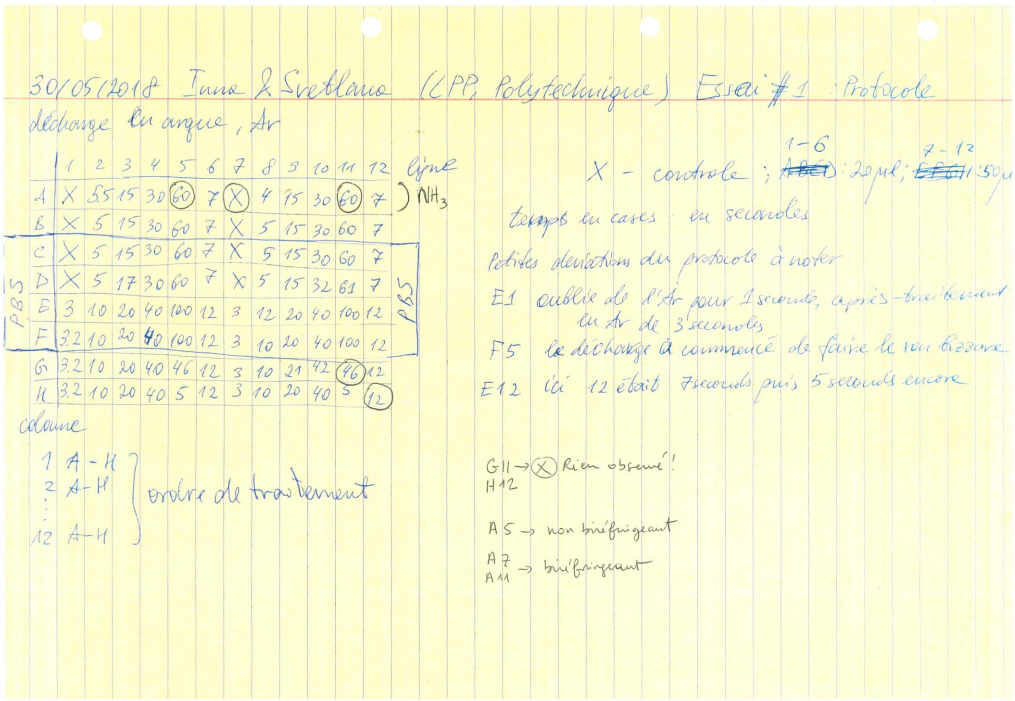

Figure 6.6: Plasma crosslinking experimental conditions. Values in the table represent exposure time in seconds.

6.3 Characterizations

6.3.1 Microstructure: samples preparation and observation: Chapter 3

6.3.1.1 Transmission Electron Microscopy

Samples preparation

Two protocols were followed. The first one from the beginning of the thesis until December 2018, the second one from January 2019.

The samples should have a volume of about $1mm^3$.

First protocol

- Glutaraldehyde crosslinking (fix the structure)

Preparation of the glutaraldehyde solution			**Glutaraldehyde solution bath: 1 hour at 4°C**
Glutaraldehyde	8%	10mL	
Cacodylate buffer	0.05M	22mL	
Preparation of the washing solution			**Washing solution bath: 3 times 10min**
Cacodylate buffer	0.1M	1 volume	
Saccharose solution	0.6M	1 volume	

- Osmium crosslinking (fix the structure and dye the sample)

Preparation of the osmium solution			**Osmium solution bath: 1 hour at 4°C**
Osmium tetraoxide	4%	2 volumes	
Saccharose solution	0.6M	1 volume	
Cacodylate buffer	0.4M	1 volume	
Washing solution bath: 3 times 10min			

- Dehydration (solubilize the resin and maximize impregnation)

EtOH baths	EtOH 50%	overnight
	EtOH 70%	5min
	EtOH 95%	5min
	EtOH 100%	2x10min
Propylene oxide baths	EtOH 100% 1 volume + propylene oxide 1 volume	10min
	Propylene oxide	10min

- Resin impregnation

Resin preparation (Araldite)	E812	20mL
	DDSA	16mL
	BDMA	1.2mL
	NMA	8mL
Propylene oxide + resin baths	Propylene oxide 2/3 volume + resin 1/3 volume	Let evaporate under hood until concentrated at 100% resin

- Resin polymerization: 3 days at 60°C.

Second protocol (Djediat 1990)
Preparation of the solutions.

Phosphate buffer 0.1M	Na_2HPO_4	40.5mL
	$NaHPO_4$	9.5mL
Glutaraldehyde solution 2%	Glutaraldehyde	2g
	Sorensen phosphate buffer	100mL

- Glutaraldehyde 2% crosslinking for 30min at room temperature.
- Add osmium tetraoxide with a final concentration of 1% in the Eppendorf for 30min at room temperature (sample should become dark).
- Wash 3 times 10min with phosphate buffer 0.1M (under agitation).
- Wash once with H_2O milliQ (under agitation for 10min).
- Dehydration: 30min in each EtOH bath - 30%, 50%, 70%, 90%, 100% - at room temperature under agitation.
- Resin impregnation: 1 bath half 100% EtOH-half resin for 90min at room temperature, 2 baths full resin for 1h at room temperature
- Resin polymerization: put the samples in molds, add resin and polymerize in the oven for 2-3 days at 70°C.

After the polymerization samples were cut on a microtome. Semi-thin cross-sections were deposited on a glass slide then stained with toluidin blue for 1min at 60°C to select the desired zone to be observed under an optical microscope. Ultrathin sections were deposited on carbon-copper grids then stained with uranyle acetate 2% for 15min.
Samples observation
Observations were performed on a FEI TECMAI G^2 Spirit Twin transmission electron microscope. A diaphragm was used to avoid melting the resin.

6.3.1.2 Scanning Electron Microscopy

The observations are made under vacuum. A prior drying of the samples that preserve their structure is therefore required to avoid any collapse of the samples when entering the SEM chamber.

Samples preparation

Two protocols were followed. The first one from the beginning of the thesis until December 2018, the second one from January 2019.

First protocol

Same as first TEM protocol with minor changes: glutaraldehyde crosslinking, no osmium, dehydration in EtOH baths only. Then a manual LEICA CO_2 critical point dryer CPD30 was used.

Second protocol

Same as first TEM protocol with minor changes: glutaraldehyde crosslinking, no osmium, dehydration in EtOH 30%-50%-70%-80%-90%-95%-2×100% (5 to 10min in each bath). Then an automated LEICA CO_2 critical point dryer CPD300 was used with the following parameters: cooling temperature 14°C, heating temperature 35°C, 32 cycles, stirring for 4min.

Samples observation

The samples were cut into pieces then deposited on carbon tape on top of a sample holder then coated with 15nm gold layer. Two different scanning electron microscopes were used: Hitachi S-3400N (3kV, 25pA) and FEG Magellan 400 FEI Thermofisher microscope (3kV, 25pA).

6.3.1.3 Histology

This preparation is required for optimized polarized light microscopy observations.

Sample size should be about 5mm×5mm×1 or 2mm. Protocol is as follows: chemical crosslinking, paraffin inclusion, cutting sections, dyeing sections.

Chemical crosslinking

Preparation of the solution: 4g paraformaldehyde (PFA) in 100mL PBSx1 (4%wt/v) under hood. Stir at 60°C for several hours (until dissolved) then filtrate. Make 5 or 10mL aliquot in separated tubes then freeze the tubes (if the solution is to be used for longer than 6 months). The solution can be kept 6 months in the fridge.

PFA creates bridges between NH_2 groups which induces physical and thermal rigidity. If sample concentration is 40-50mg/mL: let sample overnight in PFA solution. If sample concentration is 200mg/mL: let 48 hours. Adjust the crosslinking time depending on the concentration of the sample.

Dehydration: EtOH 70% for 24h, EtOH 95% for 3h, EtOH 100% for 3h. Then butan-1-ol baths for 3 days, change bath each day. Samples have to be fully dehydrated. To be done under hood. Easier if done in 2mL Eppendorfs.

Paraffin inclusion

One day prior inclusion: melt 56-58°C paraffin in the oven at 60°C. When samples are fully dehydrated, put them in small beakers filled with liquid paraffin in the oven for 4-5h (suited for concentrations below 80mg/mL; otherwise increase the time). One sample per small beaker. Assemble 2 metallic frames to form a square on a glass panel. Fill the squares with liquid paraffin, then put the sample on a side (but should not touch bottom or frame) and put the sample label on the other side of the cube to know where the sample is. Add liquid paraffin in the center after 5min then after 10min to avoid the formation of a hole (due to paraffin cooling) in the center that would make the paraffin cube too fragile to be cut. Note: I noticed a shrinkage of the samples; perhaps dehydration steps are too

fast/not gradual enough?

Cutting sections

Sculpt a square or trapeze in the paraffin cube to frame the sample. Place the cool paraffin cube in the histology microtome. Cut ribbons of 7µm thickness. Put 5-6 pieces on a H_2O milliQ drop (should cover the glass slide) on a glass slide. Put the glass slide on a heating plate at 60°C to remove the wrinkles in the paraffin. Let the water fully evaporate. The heat also sticks the section to the glass slide. (For cellularized materials: a cell is passed every 10 sections)

Dyeing sections

Put glass slides in glass basket. Take the basket with a metallic strand. Do the following baths to remove paraffin:

- Toluene 10min ×2
- EtOH 100% 100min
- EtOH 95% 5min
- EtOH 70% 5min
- H_2O milliQ 5min (it is possible to leave the slides a longer time in this bath)

Do the following baths to dye the sections:

- Picrosirius red 15min
- EtOH 100% 3min
- Toluene 3min×2 (it is possible to leave the slides a longer time in the second toluene bath)

For fixing the sections on the glass slides: wipe 25mm×50mm cover slips with kimtech. Take a glass slide with a coloured sample on it from the toluene bath, spread resin without touching the sections (eukit hardening mounting medium). Do not let toluene evaporate. Place the coverslip on the glass slide, center it. Slightly press the coverslip to remove excess resin and wipe it on kimtech. Let it dry on sample holder for 1 or 2 hours.

6.3.1.4 Polarized Light Microscopy

Observations were performed either on stained semi-thin sections (from TEM protocol) or histology sections. A Zeiss optical microscope was used with a polarizer, an analyzer and a first order retardation plate (gamma plate). Observations were performed in the following order:

- White light observation
- Polarized light: analyzer at 135°-polarizer at 45°
- Polarized light: analyzer at 90°-polarizer at 0°
- Add gamma plate, rotate the sample holder to see colour change

Pictures were acquired through ZenCore software.

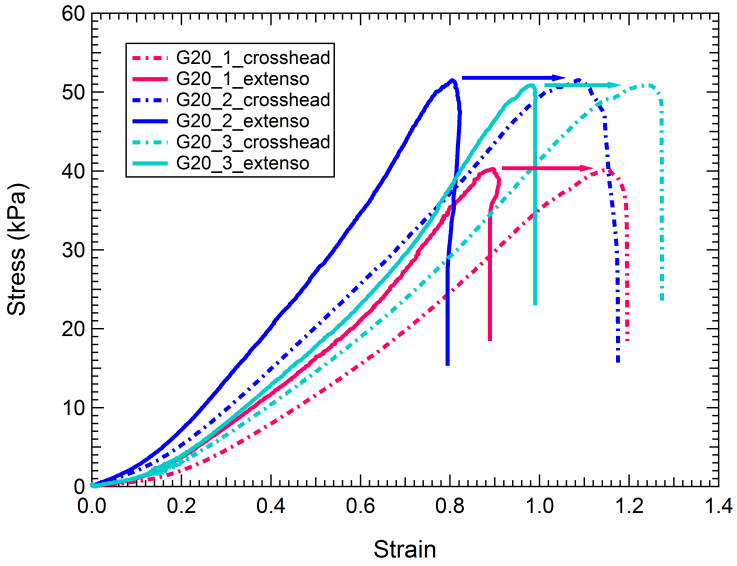

Figure 6.7: Tensile curves of three collagen samples at 20mg/mL (from the same hydrogel) with displacement recorded both by crosshead and extensometer. Arrows show the slippage.

6.3.2 Mechanical behaviour: Chapter 4

Mechanical tests were performed on an Instron tensile testing machine (models 5565 and 5965) equipped with a 10N load cell (with relative uncertainty of 0.16% in the range from 0 to 0.1N), a video extensometer (whenever precised) which follows the displacement up to 120mm (with a relative uncertainty of 0.11% at full scale) and a BlueHill software. Strain can be measured using both the video extensometer and the displacement of the crosshead. The video extensometer measures the initial length between white dots made on the sample and follows it throughout the test. Force and displacement are recorded. Nominal strain was obtained either from optical extensometer or crosshead and defined as the ratio $\frac{l-l_0}{l_0}$ where l and l_0 are respectively the length during stretching and the initial length. Nominal stress, defined as engineering stress, was calculated from the tensile force and the initial cross-section area.

The sample geometry is rectangular. The hydrogels were punched and had typical dimensions of 25mm×5mm×2mm.

All tests were performed at a nominal strain rate of 0.06/s.

The reference position of the upper clamp is defined by placing a soft object with a known height (for example a piece of eraser) on the lower clamp. The upper clamp is carefully put into contact with the object until reaching a force of about -0.1N. Then, the displacement is set to zero. The reference position is now equal to the height of the object.

6.3.2.1 Optimization of the clamps

From the beginning of the thesis until December 2017 clamps with white grips were used. However, the samples would slip between them due to their high rigidity (Figure 6.7). This slippage was noticed thanks to the use of the extensometer during tensile testing. This slippage can also be the source of less repoducibility in the mechanical behaviour of the gels. Besides, it is not possible to use the extensometer in the case of mechanical tests in immersion. So we needed to build new grips that would be more efficient both in the case if simple tensile tests or immersion tests that last longer. We

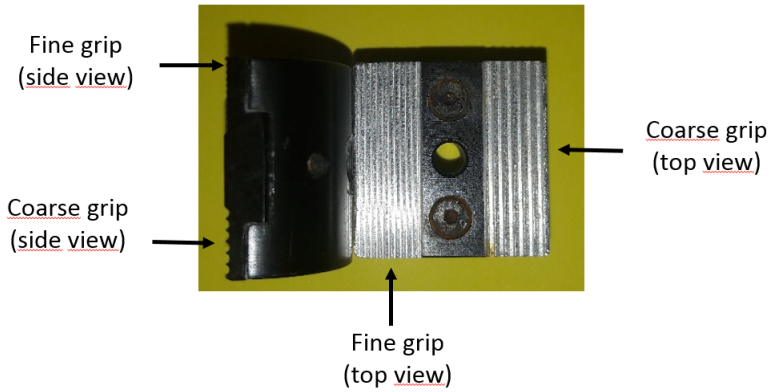

Figure 6.8: New clamp surface: fine grip and coarse grip.

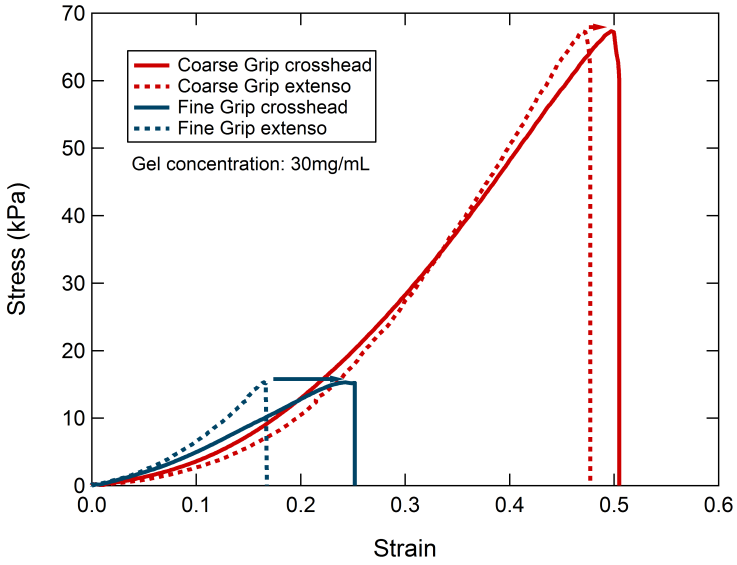

Figure 6.9: Tensile curves of two collagen samples at 20mg/mL (from different hydrogels) with displacement recorded both by crosshead and extensometer. Arrows show the slippage.

designed two kind of metallic grips with fine or coarse striations (Figure 6.8). Tightening tests were also performed with a torque wrench to determine the optimal torque at which the samples would be clamped: tight enough to avoid slippage, but not too tight to avoid damaging the sample in the clamps. After comparing the different conditions on different samples (example in Figure 6.9) we chose the **coarse striated clamps** with a **tightening torque of 7cN/m**.

6.3.2.2 Tensile test

After placing the sample in the clamps (the length of the sample between clamps should be about 10mm long) the tensile speed was calculated by using the following formula: $(reference\ length + position\ of\ the\ upper\ clamp) \times strain\ rate \times 60$ to obtain a tensile speed in mm/min. The sample is stretched at the determined velocity until it breaks.

6.3.2.3 Fracture test

Fracture tests were performed using the classical single edge notch geometry, which is known as Single Edge Notch Tensile (SENT). For that purpose, a ĩmm cut was made in the center of the side of a rectangular sample using a blade. The notched sample was placed next to a ruler and the notch was measured by optical microscopy or by taking a picture with a camera in order to determine c, the exact length of the initial notch. The sample was then placed in the clamps (notch should be placed at the same distance of each clamp) and the test was performed like a classic tensile test as described above.

6.3.2.4 Stress-relaxation test

Samples at different concentrations were submitted to drying experiments at room temperature to determine the duration of the test. Samples should loose as few water as possible throughout the relaxation test. It was determined that the water loss was minimal up to 400s (3%). The test was then defined as follows:

- ramp at a strain rate 0.6/s to go as quickly as possible to the step value
- hold step value for 400s

The step value was defined as 20% strain to make sure that the samples would not break and that the test is performed within the linear elastic part of the stress-strain curve. The tensile setup was reversed: the load cell was placed upside-down and a home-made load-cell like clamp was inserted in the crosshead. This was done to reduce noise at the beginning of the curve. At the end of the relaxation time, a tensile test was performed either at 0.6/ or 0.06/s strain rate following the protocol for tensile tests.

6.3.2.5 Cyclic test (fatigue)

Samples were first equilibrated in PBSx1 for at least a week. Cyclic tests were performed using an immersion cell filled with PBSx1 (Figure 6.10). The reference distance was set following the classic procedure for tensile tests. Then, the sample was placed in the clamps. The cell was filled with PBSx10 and progressively risen until the bottom of the cell was in contact with the upper part of the clamp to make sure the sample would stay immersed during the test. The test was performed in the following conditions:

- Strain rate 0.06/s
- 1000 cycles
- 20% deformation (to be consistent with relaxation tests)
- maximum condition: displacement calculated for 20% deformation of the sample
- minimum condition: F=0N

After 1000 cycles, the sample was removed from the clamps. The immersion cell and the upper clamp were positioned as for the beginning of the fatigue test. 10 "blank" cycles were made in the same conditions, except for the minimum condition which was set at the minimum displacement (sample length). This was done to measure Archimede's force in order to substract it from the data obtained during the fatigue test.

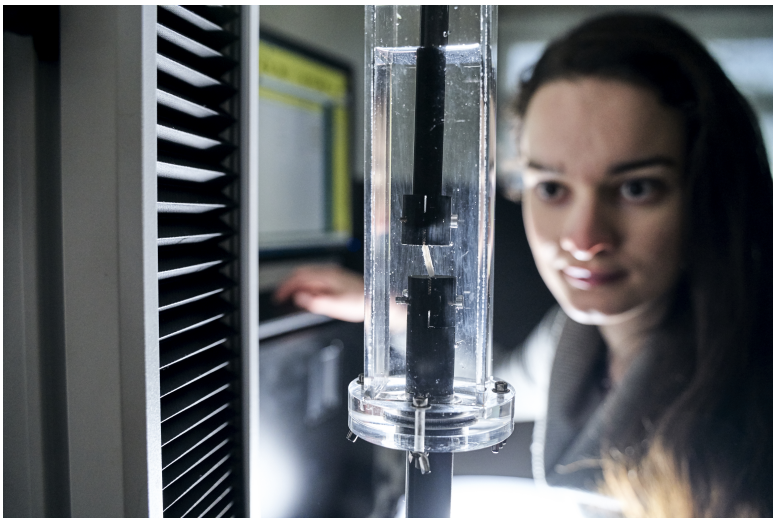

Figure 6.10: Collagen sample placed in the clamps, immersed in PBSx10 just before fatigue testing. Credits: ESPCI.

6.3.3 Physico-chemical characterizations

6.3.3.1 Laser Granulometry

For the size of the particles, few mg of collagen beads were dispersed into 20 mL ethanol 96% before going through a PSS-NICOMP particle sizer. For the analysis, the maxima of the following curves: highest investigated concentration in counts and volume, lowest investigated concentration in counts and volume were assumed to follow a Lorentzian distribution. The maxima of the curve of the lowest investigated concentration in volume was assumed to follow a Gaussian distribution. Igor Pro v6.37 software was used for the fit to determine the mean value of each peak and the FWHM or the standard deviation values.

6.3.3.2 Dynamic Vapour Sorption

Experiments were performed using a VTI SA+ instrument from TA. Hemispheric quartz sample holders were used. Few mg of collagen powder were first dried to 0%RH before undergoing increasing humidity thresholds (0%RH to 95%RH) with an equilibrium condition set at 0,0010wt% change or 800s, then decreasing humidity thresholds with the same RH range and equilibrium conditions. Other runs were performed in the same conditions but from 0%RH to 50%RH, three times to make cycles.

6.3.3.3 Differential Scanning Calorimetry

Experiments were performed on a TA Q-20 apparatus. Heating rate was set at 5°C/min and temperature range went from 20°C to 80°C, three times. About 20mg of sample was weighed and put in an aluminium pan, the reference being an empty sealed aluminium pan.

6.3.3.4 Circular Dichroism

Experiments were performed on a Jasco-810 apparatus with 1mm width flat cuvettes (about 300µl volume). A heating ramp of 2°C/min was used. The temperature range was set from 20°C to 60°C with a data pitch of 5°C. The wave length range was set from 190nm to 240nm with a data pitch of

0.5nm. Collagen beads were dissolved in acetic acid at 0.5M at the same final concentration as the stock collagen solution. A 10-fold dilution was performed to avoid saturation of the detector.

6.3.3.5 Thermo-Gravimetry Analysis

TGA experiments were performed on a SDTQ600 apparatus to determine the water content and the collagen content of collagen materials. After setting the balance to zero, about 40mg of the sample was cut, excess water was removed by blotting with kimtech. The sample was deposited in a platinum pan. A heating ramp of 5°C/min was used. The sample was heated under air from room temperature to 850°C for complete degradation of collagen and solvent residues.

Bibliography

1. Gobeaux, F. *et al.* Cooperative ordering of collagen triple helices in the dense state. *Langmuir* **23,** 6411–6417 (2007).
2. Gobeaux, F. *et al.* Fibrillogenesis in Dense Collagen Solutions: A Physicochemical Study. *Journal of Molecular Biology* **376,** 1509–1522 (2008).

General conclusion and outlook

The main drawbacks of the different processes used in the literature for making dense collagen scaffolds are:

- no spontaneous collagen self-assembly (aspiration-ejection [1], plastic compression [2]), leading to highly porous ultrastructures without control of fibril morphology;
- no 3D building (injection-evaporation [3]), thus not taking into account one of the parameters that make biological tissues so complex;
- no control of the 3D organization (evaporation [4], reverse dialysis [5]), forming non-biomimetic ultrastructures.

Up to now, the only process combining these three features was injection coupled with reverse dialysis. However, this process takes about two weeks to produce a single collagen matrix, and this matrix is not injectable which limits its potential use for tissue regeneration.

Thanks to spray-drying, we were able to produce dense and self-assembled collagen beads. By controlling the parameters during the process, we prevented the denaturation of collagen into gelatin and we were able to control the size of the beads. Hundreds of mg of collagen powder could be produced within few hours. We chose the most restrictive conditions at our disposal to demonstrate the injectability of the beads by mixing with an aqueous solvent, and injecting the suspension (80 mg/mL) through a 26G needle (used for fillers). Upon rehydration, collagen molecules further precipitated *in vitro* in a cell culture medium to form tissue-like collagen fibrils. The ultrastructure of the obtained gel displayed birefringent textures mainly associated to alignment domains. The influence of the size of the beads was not explored during this study. It may play a role on the dissolution time of the beads, thus on their injectability. Nevertheless, it could be more advantageous to use smaller beads in order to faster homogeneize the collagen concentration locally upon dissolution.

To further study the self-assembly properties of our system, we designed 3D molds to produce dense collagen gels. By mixing the beads with a midly acidic solvent, we were able to induce the self-assembly of collagen molecules in 3D. The organization was fixed by inducing *in vitro* fibrillogenesis by ammonia vapours during three hours, to obtain a model system. Tissue-like properties were observed, such as the formation of a cornea-like plywood at the microscale in the gel at 50 mg/mL. Then, we tuned the processing conditions to explore their influence on the ultrastructure of the gels. Even if no ultrastructural proof was directly evidenced, we hypothesized that increasing the exposure time to ammonia vapours increased the size of the collagen fibrils. Inducing *in vitro* fibrillogenesis with PBS led to the formation of two populations of objects: collagen molecules (with possible presence of microfibrils) and cross-striated fibrils that tend to form larger aggregates at 80 mg/mL. Finally, freeze-drying and freeze-thawing collagen gels also formed these two populations. However, we found no evidence on the potential formation of stronger physical crosslinks (electrostatic and hydrophobic interactions). The first plasma tests to promote chemical crosslinks in dilute collagen solutions were not conclusive.

The mechanical response of our model collagen gel displayed qualitatively biomimetic features: non-linear tensile behaviour, time-dependency close to that of biological tissues, biomimetic fatigue behaviour. Their fracture propagation process even shows some similarities with fracture tests performed in tendons. Still, the stiffness and fracture toughness of our gels is well below that of biological tissues (several orders of magnitude); but our gels are only made of collagen and water, hence lacking the other components present in the ECM that could reinforce them. Thanks to the different

mechanical response exhibited by the collagen gels left under ammonia vapours onvernight (reduced non-linearity in the tensile response and stress-relaxation time), our hypothesis on a larger fibril size was found relevant. The mechanical behaviour of the gels made in PBS was found too variable to further characterize them. Finally, freeze-drying did not reinforce the mechanical properties of the gels and even dramatically reduced their non-linear response. Thus, the formation of electrostatic or hydrophobic bonds may not have been promoted, and water molecules involved in hydrogen bonding seemed irreversibly lost. However, the gels were tested after 2-3 weeks rehydration; the influence of rehydration time could be explored. Since the gels were rehydrated in PBS, it is possible that the ions (especially phosphate ions) also played a role. Tests with freeze-dried gels rehydrated in milliQ water are in progress.

The formation of a model system, the collagen gel synthesized with ammonia vapours for three hours, helped us get deeper into the understanding of the ultrastructure-mechanical properties relationship. However, this model gel may not be relevant for all biological tissues. Therefore, processing parameters and composition could be adjusted to match more closely the features of the biological tissue of interest. We compared the mechanical properties of our gels to that of biological tissues with data available in the literature. Yet, a great amount of studies were performed with tendons, especially about the microscale deformation processes. The organization of tendon is closer to a 2D organization (long range unidirectional hierarchy), which limits the pertinence of the comparison with the deformation processes in 3D collagen gels. Our collagen gels exhibit anisotropic features as evidenced by different microscopy techniques, but it seems that the organized domains are not present at the scale of the whole gel. Promoting long-range ordering (over the bulk) of the collagen molecules before fibrillogenesis could reinforce the mechanical properties of the gels. Finally, it was difficult to observe cross-striations in the fibrils of the collagen gels synthesized by ammonia vapours, unlike that in gels made in PBS. Thus, exploring fibrillogenesis conditions more thoroughly (exposure time to ammonia vapours, temperature, use of other media *e.g.* physiological serum) in order to produce more biomimetic fibril morphologies could be of interest.

One of the observations that stood out of this study is the importance of water. More specifically, the state of water (free, bound) appeared to influence ultrastructure, thermal stability and mechanical properties of the collagen gels. When collagen gels were left longer in ammonia vapors, less bound water was measured which seemed contradictory with our hypothesis of fibril growth. However, it would be consistent with the hypothesis that fibril specific surface area is related to the amount of bound water. The decrease in bound water could consequently decrease the interfibrillar water-mediated hydrogen bonds, which may be the cause for *(i)* reduced non-linear tensile response (such bonds may enable slippage of neighbouring collagen fibrils and potential re-alignments to occur along the tensile direction) and *(ii)* reduced viscous dissipation (provided by interfibrillar friction) during stress-relaxation process. Further, when collagen gels were freeze-dried, their tensile behaviour changed dramatically. It was almost linear, possibly indicating that interfibrillar water interacts differently with collagen molecules: its lubricating effect at higher strains could be greatly reduced, possibly preventing reorganizations to occur before failure. In order to confirm our hypotheses, SAXS experiments could be performed to obtain an estimation of the interfibrillar space (more important if there is more interfibrillar water). Also, performing tensile tests between crossed polarizers could give informations about structural changes during the test such as re-alignments.

The state of water itself together with its role in the mechanics of biological tissues is not straightforward. Four states of water were proposed in collagen-rich tissues (summarized in Zhang *et al.*) [6]: free water, water in transition, bound water and tightly bound water. These states were determined by physico-chemical parameters (*e.g.* adsorption/desorption heat, location, binding strength). To determine if this classification applies in our collagen gels, dynamic vapor sorption experiments could be performed and compared to results obtained by TGA. Then, the mechanical response of our gels could be characterized at different drying stages by using the immersion chamber as a humidity-controlled chamber. The above mentioned hypotheses on the role of water during mechanical loading were based on biological tissue mechanical response. By modeling the mechanical response model collagen-like peptides with the presence of tightly bound water or not, Zhang *et al.* proposed that water could also act as a sliding-resisting medium, thus promoting strain-hardening [6]. Using model systems can thus provide other hypotheses on mechanisms. Nevertheless, the ECM being highly complex, it is possible that the mechanisms would slightly differ between a model collagen gel and a biological tissue. Adding molecules of interest in our collagen gels, *e.g.* proteoglycans, could help provide insight on the role played by more complex interactions during mechanical loading.

By adding components to form hybrid gels (either organic/organic or organic/inorganic), we showed the high versatility of our collagen gels. From an industrial point of view, *in vivo* assays are required to validate their efficiency for tissue regeneration (colonization, vascularization, resorption). Given the positive results previously obtained with collagen matrices made by injection-reverse dialysis (implanted in rat and sheep models), we have good hope that our collagen gels will be well integrated within the host tissue.

Altogether, the spray-drying process associated to the established synthesis and characterizations conditions provide an incredible tool for thorough studies on our system. We could perform a study on mineralized collagen gels as bone model system, in order to explore the role of hydroxyapatite in the mechanical response of the gels. Spontaneous fibrillogenesis at acidic conditions could be studied by making more concentrated collagen gels (*e.g.* 1000 mg/mL). The interactions between collagen molecules could be tuned by modifying the pH of the initial stock collagen solution before spray-drying, possibly giving informations on the role of the pH before *in vitro* fibrillogenesis, in the ultrastructure and the mechanical behavior of the gels. This multidisciplinary work could go one step further: our collagen gels could be used to explore cell differentiation on substrates possessing different mechanical properties, ultrastructures, water content (swelling), compositions.

Bibliography

1. Kamranpour, N. O., Miri, A. K., James-Bhasin, M. & Nazhat, S. N. A gel aspiration-ejection system for the controlled production and delivery of injectable dense collagen scaffolds. *Biofabrication* **8,** 000000 (2016).
2. Brown, R. A., Wiseman, M., Chuo, C. B., Cheema, U. & Nazhat, S. N. Ultrarapid engineering of biomimetic materials and tissues: Fabrication of nano- and microstructures by plastic compression. *Advanced Functional Materials* **15,** 1762–1770 (2005).
3. Mosser, G., Anglo, A., Helary, C., Bouligand, Y. & Giraud-Guille, M. M. Dense tissue-like collagen matrices formed in cell-free conditions. *Matrix Biology* **25,** 3–13 (2006).
4. Besseau, L., Coulomb, B., Lebreton-Decoster, C. & Giraud-Guille, M. M. Production of ordered collagen matrices for three-dimensional cell culture. *Biomaterials* **23,** 27–36 (2002).
5. Knight, D. P., Nash, L., Hu, X. W., Haffegee, J. & Ho, M. W. In vitro formation by reverse dialysis of collagen gels containing highly oriented arrays of fibrils. *Journal of Biomedical Materials Research* **41,** 185–191 (1998).
6. Zhang, D., Chippada, U. & Jordan, K. Effect of the structural water on the mechanical properties of collagen-like microfibrils: A molecular dynamics study. *Annals of Biomedical Engineering* **35,** 1216–1230 (2007).

List of Figures

List of Tables

Résumé du manuscrit

6.4 Introduction

Les tissus biologiques possèdent une grande diversité de propriétés mécaniques, intimement reliées à leur fonction. Leur rigidité varie de quelques kPa à quelques milliers de kPa pour les tissus mous, jusqu'à quelques GPa pour les tissus biominéralisés. Pourquoi ne pas s'inspirer de la Nature pour créer des (bio)matériaux améliorés, en particulier pour la régénération tissulaire ?

Différentes stratégies peuvent être utilisées pour faire des biomatériaux [1] :

- biocompatibles mais non biodégradables (par exemple : des métaux utilisés dans le domaine orthopédique, la plupart des polymères synthétiques pour prothèses, des céramiques pour implants dentaires);
- biocompatibles et biodégradables (par exemple : des hydrogels synthétiques comme vecteurs de médicaments, la plupart des biopolymères pour l'ingénierie tissulaire).

Par définition, un biomatériau est un matériau non-viable utilisé dans un appareil médical, dont la finalité est d'interagir avec des systèmes biologiques [2]. A part les dispositifs médicaux externes, l'un des objectifs dans l'utilisation de biomatériaux est de complètement remplacer l'organe ou de fournir une structure pour la croissance d'un nouveau tissu. idéalement, le biomatériau est une structure en 3D qui est biocompatible et induit après implantation *(i)* la colonisation par les cellules-hôtes, *(ii)* la vascularisation et *(iii)* la résorption complète afin de permettre la reconstruction du tissu-hôte sans induire de réponse inflammatoire.

Cependant, aucune des stratégies sus-mentionnées n'a été trouvée suffisamment satisfaisante pour remplacer l'étalon-or : l'autogreffe. Il y a deux raisons principales à cela. Premièrement, il est extrêmement difficile de traverser la "vallée de la mort" séparant les résultats obtenus en laboratoire de recherche et la commercialisation sur le marché. Par exemple, les difficultés peuvent apparaître du côté des régulations (mise à jour fréquente, deviennent de plus en plus strictes), d'idées de projets de recherche non-réalistes (usage de composés exotiques, industrialisation compliquée, faible rapport qualité/prix) ou encore du manque de ressources financières des laboratoires de recherche publique, conduisant à une validation incomplète des pré-requis (les implantations dans des animaux-modèles coûtent cher mais sont nécessaires). Deuxièmement, aucun des biomatériaux biodégradables n'est aussi efficace qu'une greffe autologue en termes d'intégration : une réponse inflammatoire peut provenir d'une composition non-biomimétique, une résorption trop rapide d'un manque de densité (architecture et concentration non-biomimétiques). Néanmoins, l'utilisation d'une greffe autologue reste un enjeu car la quantité de tissu disponible est limitée, de potentielles infections peuvent surgir suite à cette deuxième opération chirurgicale, impliquant possiblement une aggravation de l'état du patient.

Le collagène est le composant majoritaire de la matrice extracellulaire (environ 30% de toutes les protéines). Il existe 28 types de collagène, et parmi eux le collagène de type I est le plus abondant. C'est une protéine de structure, ce qui signifie qu'elle fournit le support majoritaire des cellules et des organes par extension. Par conséquent, afin de construire un matériau structuré en 3D aussi efficace qu'un tissu autologue, nous formons les hypothèses suivantes:

- à part l'eau, le constituant principal de ce matériau doit être le collagène de type I (composition biomimétique);
- le matériau doit contenir une grande concentration en collagène (densité biomimétique);

- l'architecture 3D du collagène dans le matériau est aussi importante que les deux points précédemment cités;

(ces trois pré-requis ont été partiellement validés par des matrices denses de collagène pré-formées [3])

- le comportement mécanique du matériau doit être proche de celui des tissus biologiques;
- le matériau doit être injectable afin de limiter l'usage de procédures chirurgicales invasives.

Afin de contourner la forte augmentation de viscosité du collagène lorsque sa concentration augmente, notre stratégie est d'utiliser le séchage par atomisation afin de former des billes denses de collagène [4]. Les billes peuvent être mises en suspension dans un fluide injectable afin de former une suspension de collagène très concentrée. Après injection dans un moule servant de modèle de défaut tissulaire, les billes de collagène se dissolvent et forment un gel de collagène *in situ*. Pour établir sa pertinence pour l'ingénierie tissulaire, trois problématiques apparaissent : *(i)* l'architecture du gel est-elle vraiment biomimétique ? *(ii)* son comportement mécanique reproduit-il celui des tissus visés ? *(iii)* comment le gel interagit-il avec son environnement (par exemple : gonflement, adhésion, colonisation par les cellules-hôtes, vascularisation, durée de résorption) ?

L'étude de lma relation architecture-propriétés mécaniques de gels dense de collagène constitue la problématique principale de ce manuscrit. Par conséquent, cette thèse est à l'interface entre différents domaines :

- physico-chimie et procédés du collagène, savoir-faire spécifique du LCMCP;
- le design de systèmes-modèles (en particulier d'hydrogels) et la caractérisation de leur comportement mécanique, savoir-faire spécifique du laboratoire SIMM.

La meilleure référence d'une telle relation dans notre cas est le tissu biologique. Cependant, selon son origine (animal, type de tissu), la façon dont il a été traité (congelé, séché, lyophilisé, hydraté, type de solvant), ses caractérisations (préparation pour microscopie, type de microscope, type de tests mécanique), les résultats peuvent changer de manière drastique. Ainsi, cette relation dans les tissus biologiques n'est pas évidente. En fabriquant des matériaux en collagène pur, notre objectif est également de fournir des systèmes modèles afin d'étudier plus en profondeur et de manière plus précise les propriétés de tels matériaux, et plus particulièrement le lien entre les changements architecturaux à l'échelle microscopique et le comportement mécanique global.

Ce travail multidisciplinaire requiert de définir quelques termes utilisés tout au long de ce résumé : la concentration sera donnée en mg/mL (1 mg/mL = 0.1 wt%); l'ultrastructure est définie comme l'architecture du matériau à l'échelle d'un microscope électronique (de 10 µm à 100 µm); la microstructure est l'architecture du matériau à l'échelle de la cellule (de 1 µm à 10 µm); matériau en collagène, gel/hydrogel de collagène et matrice de collagène seront utilisés de manière équivalente.

Ce résumé est organisé de la manière suivante :

- la première section donne un aperçu synthétique de la littérature sur le collagène injectable (résumé du **Chapitre 1**);
- la deuxième section est une étude sur les billes denses de collagène (résumé du **Chapitre 2**);

- la troisième section explore l'ultrastructure des gels de collagène produits à partir des billes denses de collagène (résumé du **Chapitre 3**);
- la quatrième section relie les propriétés mécaniques des gels de collagène à leur ultrastructure (résumé du chapitre **Chapitre 4**);
- la cinquième section est confidentielle.

Les conditions expérimentales sont à retrouver dans la **Partie Expérimentale**.

6.5 Etat de l'art

Les inconvénients majeurs des différents procédés utilisés dans la littérature pour produire des gels denses de collagène sont :

- pas d'auto-assemblage spontané du collagène (aspiration-éjection [5], compression plastique [6]) menant à des ultrastructures très poreuses sans contrôle sur la morphologie des fibrilles;
- pas de matériau 3D (injection-évaporation [7]), qui ne prend donc pas en compte l'un des paramètres qui rend les tissus biologiques si complexes;
- pas de contrôle de l'organisation 3D (évaporation [8], dialyse inverse [9]), formant ainsi des ultrastructures non biomimétiques.

Jusqu'à présent, le seul procédé combinant ces trois aspects était l'injection couplée à la dialyse inverse. Cependant, ce procédé prend environ deux semaines pour produire une seule matrice de collagène, et cette matrice n'est pas injectable ce qui limite son usage potentiel pour la régénération tissulaire.

6.6 Des microparticules de collagène auto-assemblées par aérosol, une plateforme versatile pour matériaux anisotropes et injectables

Les matrices extracellulaires (MEC) riches en collagène de type I exhibent des ultrastructures typiquement anisotropes. Néanmoins, travailler *in vitro* avec cette biomacromolécule est encore à présent un enjeu de taille. Par l'usage de procédés, la dénaturation de molécules de collagène est facilement induite *in vitro*, empêchant l'auto-assemblage attendu en fibrilles et la formation d'organisations hiérarchiques d'ordre supérieur. Ici, une approche innovante permet la production de microparticules de collagène très concentrées et injectables, basée sur l'auto-assemblage du collagène grâce à l'utilisation du séchage par atomisation. La versatilité du système est montrée en encapsulant des produits de sécrétions de cellules souches mésenchymateuses gingivales (gSCMs), qui furent choisies en tant que vecteur thérapeutic bio-actif pour leur efficacité potentielle dans la stimulation de la régénération d'une MEC endommagée. L'injection de microparticules de collagène dans un milieu de culture cellulaire résulte en la formation d'une matrice fibrillaire organisée localement. L'efficacité de cette approche pour produire des microparticules de collagène facilement manipulables pour l'encapsulation et l'injection ouvre des perspectives dans le domaine de la régénération tissulaire active et des biomatériaux par impression 3D.

Cette étude nous a permis de mieux comprendre les propriétés des billes de collagène et d'établir les nombreux avantages du séchage par atomisation par rapport à d'autres techniques pour former des matériaux 3D en collagène très concentré. En effet, la technique est facile d'utilisation (une fois les bonnes conditions fixées), rapide (100 mg de poudre de collagène peut être produite en quelques heures), précise (la poudre de collagène peut être pesée pour atteindre la concentration finale désirée dans le gel de collagène), fiable (les conditions de séchage par atomisation sont stables tout au long du process, et le collagène n'est pas dénaturé avec les bonnes conditions), et biomimétique (permet de conserver les propriétés d'auto-assemblage du collagène et mène à la précipitation de fibrilles qui dont le diamètre a l'air homogène).

6.7 Des billes de collagène aux gels denses de collagène : influence de la concentration en collagène, des conditions de fibrillogénèse *in vitro* et des conditions de procédé sur l'ultrastructure

L'objectif de cette section est de former des gels de collagène denses et fibrillaires, à partir des billes de collagène de la section précédente. La formation des gels dépend de plusieurs paramètres comme la concentration en collagène, le temps de fibrillogénèse, le milieu de fibrillogénèse, etc. Par conséquent, différents paramètres furent variés afin *(i)* d'étudier leur influence sur l'ultrastructure des gels, *(ii)* de comprendre les processus de formation et *(iii)* de contrôler la synthèse pour obtenir les matrices d'intérêt.

Après avoir étudié l'influence de différents paramètres sur la taille des billes de collagène lors de leur synthèse par aérosol, les conditions furent optimisées et choisies spécifiquement pour permettre l'injection des billes. La taille des billes fut ajustée à environ 1 µm en utilisant une solution initiale de collagène concentrée à 1 mg/mL. D'après les observations à l'oeil nu, cette granulométrie permit une meilleure dispersion des billes de collagène dans le solvant, qui était réduite dans le cas de billes de plus grand diamètre (solutions de collagène initialement concentrées à 2 et 5 mg/mL). Il apparaissait que des billes plus grosses avaient tendance à plus s'agréger ce qui limitait leur injectabilité (risque de boucher l'aiguille). Les paramètres du sécheur par atomisation furent ajustés afin de consommer moins d'énergie : la température, le flux d'air et l'aspiration furent diminués. Au lieu d'utiliser une solution aqueuse à pH neutre, un solvant aqueux acide fut choisi pour transporter et solubiliser les billes lors de leur injection.

L'objectif était de conserver les propriétés de cristal liquide des molécules de collagène (à pH acide) afin de former autant de domaines anisotropes que possible. Cependant, si la dissolution des billes est trop rapide, elles forment un gel très concentré qui devient impossible à injecter à cause de sa viscosité. Les molécules de collagène étant soluble à pH acide, un solvant légèrement acide fut choisi : de l'acide acétique peu concentré. Son pH est plus proche du pKa de l'acide acétique et du point isoélectrique du collagène (pI=7.4) [10] que l'acide acétique à 500 mM (pH=2.5). Gobeaux *et al.* ont montré que le pH du solvant a une influence sur le diagramme de phase du collagène en solution [11]. Ils ont observé qu'une augmentation de la concentration en acide acétique (de 2 mM à 500 mM en concentration initiale de la solution-mère de collagène) retarde l'apparition des mésophases. A haute concentration en acide acétique, le seuil de transition isotrope/cholestérique peut être observé autour de 70 mg/mL en collagène. Cependant, leur diagramme de phase montre une augmentation de la concentration en acide acétique (qui s'évapore moins rapidement que l'eau), conduisant également à

une augmentation de la force ionique. Par ailleurs, ils n'ont pas pris en compte la formation d'une phase nématique juste au-dessus de 40 mg/mL en collagène (leur diagramme montre seulement la transition isotrope/cholestérique).

De la même manière dans notre cas, il y a une probabilité non nulle que de l'acide acétique reste dans la poudre de collagène (pas complètement vaporisé lors du séchage par atomisation). En effet, une expérience qualitative avec un indicateur de pH coloré universel a montré que le pH de 2 mL d'eau diminuait de plusieurs unités lors de l'ajout de quelques mg de billes de collagène. De plus, le séchage par atomisation pourrait aussi enlever les impuretés les plus volatiles de la solution de collagène ce qui peut modifier légèrement le diagramme de phase - l'importance de leur rôle a été soulignée dans le cas d'un alcool aliphatique commercial possédant des propriétés lyotropes [12].

L'objectif est d'injecter le matériau (billes de collagène + acide acétique peu concentré) dans un moule servant de modèle à un défaut tissulaire. Dans les tissus biologiques, le pH est tamponné à 7.4 ce qui induira la fibrillogénèse *in situ*. Afin d'imiter le processus enzymatique de la fibrillogénèse *in vivo*, différentes options sont à notre disposition *in vitro* comme des solutions basiques de NaOH, ou du tampon phosphate salin. En utilisant des tampons phosphate à différents pH et force ionique pour induire la fibrillogénèse *in vitro*, Gobeaux *et al.* on montré qu'une grande variété de morphologies de fibrilles peut être obtenue [11]. Il a été montré que les vapeurs d'ammoniaque forment des échantillons plus homogènes grâce à la diffusion lente sans perturber le réseau de collagène [13]. Ainsi, des temps d'expositions différents aux vapeurs d'ammoniaque sur les solutions de collagène injectées ont été étudiés, dans le but de déterminer l'influence sur la microstructure, et plus tard sur les propriétés mécaniques des gels de collagène (**Chapitre 4**).

Puis, une comparaison avec fibrillogénèse dans un tampon phosphate salin à pH=7.4 a été réalisée, car ce milieu pourrait représenter ce qui se rapproche le plus d'une fibrillogénèse *in vivo*. En effet, plusieurs questions restent ouvertes:

- la vitesse de diffusion des ions transportés par les fluides de la MEC à l'intérieur des solutions de collagène injectées;
- le laps de temps requis pour former le gel *in situ*;
- l'ultrastructure finale du gel.

Enfin, des conditions optimales de fibrillogénèse furent fixées.

Les solutions de collagène dense et injectable pourraient être utilisées pour combler des défauts dans des tissus riches en collagène. Par conséquent, il est important de déterminer leur ultrastructure avec différentes conditions de fibrillogénèse *in vitro*. En fabriquant des matrices pre-formées au lieu de matrices injectables, d'autres applications sont possibles dans le domaine de la régénération tissulaire. Dans le cas de membranes de collagène, ces matériaux sont souvent lyophilisés pour faciliter leur stockage et éviter toute dégradation éventuelle qui aurait plus de chances de se produire en conditions humides [14]. Cependant, cette étape de séchage par atomisation peut induire des changements à la fois dans l'ultrastructure du matériau et dans ses propriétés mécaniques.

Enfin, grâce à une collaboration avec le LPP (Ecole Polytechnique) et le LBIB (Université de Reims), nous avons essayé de favoriser la formation de points de réticulation chimiques [15] entre les molécules de collagène en utilisant du plasma. Nous avons formulé l'hypothèse que la présence de tels points de réticulation pourraient augmenter de manière significative les propriétés mécaniques des gels.

En conclusion, nous avons été capables de produire des gels de collagène en trois dimensions avec du collagène séché par atomisation. En utilisant différents milieux de fibrillogénèse, nous avons pu modifier la morphologie des fibrilles. Les fibrilles les plus calibrées semblent être celles obtenues par vapeurs d'ammoniaque, comme décrit précédemment dans la littérature.

La microstructure du gel à 50 mg/mL synthétisé par vapeurs d'ammoniaque pendant trois heures a des similarités avec des gels synthétisés par d'autres procédés et qui ont reproduit l'ultrastructure de la cornée (voir **Annexe**). Le gel à 80 mg/mL synthétisé dans le tampon phosphate salin a des fibrilles striées proches de celles des tissus biologiques. Nous n'avons pas été capables de conclure sur la formation de points de réticulations physiques plus forts avec la lyophilisation. La caractérisation mécanique aidera à donner plus d'informations sur cet aspect.

Différents paramètres peuvent être utilisés pour contrôler l'ultrastructure des gels de collagène et l'adapter afin d'imiter celle des tissus, par exemple la concentration en collagène, la force ionique, le pH, le temps de fibrillogénèse, la température d'incubation. Nous choisissons comme système de référence les gels de collagène synthétisés par vapeurs d'ammoniaque pendant trois heures car c'est le système le plus simple. D'autres paramètres n'ont pas été explorés lors de cette étude : l'influence des conditions de stockage des échantillons (eau ou tampon phosphate ? - gardant en tête les interactions entre le phosphate et le collagène), le gonflement (qui peut modifier la microstructure [16]).

Tous ces phénomènes peuvent avoir une influence sur les propriétés mécaniques des gels de collagène.

6.8 Lien entre l'ultrastructure et le comportement mécanique : influence de la concentration et des conditions de traitement sur la réponse mécanique des gels denses de collagène

L'ultrastructure des gels de collagène a été étudiée en fonction de leur concentration en collagène, des conditions de fibrillogénèse et des conditions de traitement. A côté de la composition et de l'organisation à l'échelle de la fibrille, un autre aspect important dans le fait d'imiter le tissus riches en collagène consiste à interroger le matériau du point de vue mécanique. Il est accepté de manière générale que les processus cellulaires sont régulés par la rigidité de leur environnement [17]. Cependant, le rôle d'autres paramètres comme la réponse mécanique à grande déformation (non-linéarité) et la composante visco-élastique ont été bien moins explorés.

Ici, nous adoptons une approche de science des matériaux afin d'analyser la réponse mécanique avec les paramètres suivants:

- la forme générale du comportement des gels à grande déformation jusqu'à rupture;
- le comportement visco-élastique des gels à travers des expériences de relaxation de contrainte;
- la durabilité des gels à travers des expériences de fatigue et fracture, de tels chargements mécaniques étant similaires *in vivo* à ceux subis par des tendons ou des ligaments.

L'analyse du comportement mécanique *(i)* nous permettra d'établir le degré de biomimétisme de nos matériaux en collagène, *(ii)* nous donnera des informations sur leur ultrastructure et *(iii)* nous permettra de déterminer si nos gels peuvent réellement être utilisés comme matériaux-modèles pour une compréhension plus poussée de la réponse mécanique des tissus biologiques.

Les résultats ont montré que nos gels de collagène ont l'air d'avoir un comportement mécanique biomimétique. Le comportement en tension de nos gels de collagène a été fitté avec succès avec une équation exponentielle qui a été utilisées dans la littérature pour caractériser la réponse mécanique non-linéaire des tissus riches en collagène, démontrant ainsi la pertinence de la réponse mécanique de nos gels par rapport à celle d'autres tissus biologiques comme les tendons ou les ligaments par exemple. Le tableau 6.1 résume les principales caractéristiques des gels de collagène.

Processing conditions	Collagen concentration (mg/mL)	E_{toe} (kPa)	Fit parameters A (kPa); B	J_{ratio}	$\sigma_{viscous}$ (%)	n power
Ammonia 3h	30	69	19.3 ; 2.6	1.14	57±4	-0.0805
	50	136	17.2 ; 4.4	3.53		
	80	224	167.1 ; 1.2	0.63		
Ammonia night	30	47	19.0 ; 2.2	1.35	44±2	-0.0444
	50	131	55.3 ; 2.0	0.79		
	80	202	163.3 ; 1.2	0.27		
PBS	30	29	14.0 ; 3.2	2.10		
	50	40	18.1 ; 4.4	2.40		
	80	72	34.6 ; 2.3	1.06		
Freeze-dried	50	45	17.1 ; 1.8	0.46	52	-0.0637
Freeze-thawed	50	62	37.1 ; 1.6	2.54		
Tendon		20.10^4	88.10^4 ; 0.005	4		-0.078
Skin		10		2.10^3		

Table 6.1: Summary of the major characteristics of the mechanical response of the collagen gels, together with values from the literature (detailed in **Chapter 1**) for tendon and skin.

Il apparaît que leur raideur ne dépend pas seulement de la concentration, mais aussi des conditions de traitement. De plus, elle est plus faible que celle du tendon mais du même ordre de magnitude que celle de la peau. Le J_{ratio} fournit des informations cohérentes sur la non-linéarité de la réponse des gels en tension, qui peut être comparée entre les différentes conditions de procédé. En essayant de le calculer à partir de données présentes dans la littérature (différents auteurs, valeurs dans le **Chapitre 1**) donne une idée de ce ratio pour le tendon et le skin à des fins de comparaison. Il apparaît que la non-linéarité de nos gels est plus proche que celle des tendons. La meilleure quantification de leur comportement dépendant du temps a été obtenue avec le paramètre n, suggérant un processus de relaxation en loi de puissance. Les valeurs obtenues sont du même ordre de grandeur que celles calculées pour des tissus riches en collagène, signifiant que nos gels de collagène imitent les propriétés de dépendance au temps et la dynamique de leur réseau de collagène. Dans l'ensemble, ces paramètres peuvent donner des indications sur l'ultrastructure des gels comparée à la référence qui est la synthèse sous vapeurs d'ammoniaque pendant trois heures.

Puxkandl *et al.* ont proposé un modèle pour les propriétés viscoélastiques du collagène : les points de réticulation intermoléculaires chimique et physique, et les enchevêtrements de la matrice riche en protéoglycans avec les molécules de collagène (à l'extérieur des fibrilles) fournissent les propriétés élastiques; tandis que la friction intermoléculaire à l'échelle fibrillaire (interactions par liaisons électrostatique et hydrogène) et les liaisons hydrogène dans la matrice riche en protéoglycans fournissent de la dissipation d'énergie visqueuse [18]. Nos gels de collagène ne sont pas réticulés chimiquement et contiennent une quantité négligeable de proteoglycans après purification, ce qui signifie que leur réponse visco-élastique devrait reposer en majeure partie sur les points de réticulations physique. Par conséquent, le changement de réponse mécanique procédé-dépendant des gels de collagène pourrait

indiquer que les points de réticulation physique (dépendant de la quantité d'eau liée et de la taille des fibrilles), liés à la capacité de dissiper de l'énergie visqueuse, apparaissent comme un paramètre déterminant. En effet, la non-linéarité de la réponse en tension est représentée par une augmentation drastique de la contrainte lors de petits changements de déformation dans la partie linéaire de la courbe contrainte-déformation; ce qui signifie que le J_{ratio} pourrait être relié à la capacité de former et casser des points de réticulation physique lors du chargement. Par analogie avec l'effet thixotrope en rhéologie, Silver *et al.* ont émis l'hypothèse que cette augmentation pourrait être due à l'eau interfibrillaire: en agissant comme un lubrifiant, l'eau pourrait devenir plus fluide à plus grande déformation permettant ainsi plus de glissement entre les fibrilles [19]. Les fibrilles de collagène tendraient alors à s'aligner plus facilement le long de la direction de chargement. Ce phénomène de ré-alignement a été observé par Tower *et al.* dans des tissus mous en traçant des cartes de biréfringence [20]. Cette hypothèse pourrait être cohérente avec la réponse en tension des gels pour la condition sous ammoniaque pendant une nuit (moins d'eau liée et J_{ratio} plus faible); des observations par PLM avant et après test pourraient le confirmer. Cependant, cette hypothèse n'apparaît pas cohérente avec la réponse en tension des gels lyophilisés.

En effet, les résultats des expériences de lyophilisation apparaissent contradictoires: elles montrent une plus grande quantité d'eau liée que le gel de référence, mais l'augmentation drastique de contrainte dans la région linéaire de leur courbe de traction est quasiment inexistante. Silver *et al.* ont proposé un mécanisme de sotckage d'énergie élastique dans les fibrilles de collagène [21]: certaines parties des molécules de collagène peuvent être considérées comme des ressorts qui relâchent de l'énergie élastique quand la molécule est étirée à cause de la rupture de liaisons électrostatiques. ces liaisons électrostatiques peuvent être situées au sein de la même molécule ou entre deux molécules adjacentes (ou une molécule et son eau liée). Il semble qu'après lyophilisation, seule l'énergie élastique au sein des molécules reste accessible, ce qui diminue la relaxation de contrainte comparée à la conditions de fibrillogénèse pendant trois heures. Néanmoins, la lyophilisation n'a pas l'air de promouvoir les interactions électrostatiques entre les molécules; sinon les mécanismes élastiques auraient renforcé le gel.

D'après la quantité d'eau liée et les tests mécaniques, nous avons émis l'hypothèse que la tailles des fibrilles augmente lorsque le temps d'exposition aux vapeurs d'ammoniaque est augmenté de quelques heures à une nuit. La taille des fibrilles peut avoir une influence sur le comportement en tension de nos gels, possiblement en exacerbant les fractions visqueuse ou élastique. Par conséquent, la taille des fibrilles pourrait aussi avoir une influence sur le comportement en fatigue des gels de collagène, et sur leur ténacité. D'autres expériences sont nécessaires pour pouvoir conclure sur ces points. En effet, d'après des simulations sur le comportement relatif de deux fibrilles de collagène, M.J. Buehler a montré que la taille de fibrille est en fait un compromis entre propriétés élastiques et visqueuses, et dépend aussi du chargement mécanique auquel le tissu doit résister [22].

Néanmoins, si le modèle exponentiel est pratique de par sa simplicité pour donner des informations qualitatives et quantitatives, il apparaît que cette équation n'est pas approprié pour fitter le comportement de certains tissus riches en collagène comme la cornée de porc dans la région du pied de courbe comme montré sur la **Figure 4.16**. Le comportement en tension a été comparé à différents gels à 50 mg/mL, selon le nouveau diagramme de phase du collagène [23]. Ce phénomène a aussi été remarqué dans le cas de nos gels, mais de manière moins prononcée. Ce peut être relié à la présence de mécanismes de dissipation visqueuse mis en place pendant le chargement dans le cas de la cornée de porc. En effet, d'après les valeurs du **Tableau 6.2** (en supposant que les valeurs de fit sont minimales

à contrainte nulle et déformation maximale), il apparaît que le J_{ratio} de la cornée de porc est bien plus grand que celui de nos gels de collagène. Cette valeur est cohérente avec la réponse mécanique des gels de collagène en comparaison avec celle de la cornée de porc.

Sample	Pig cornea
Fitting parameters	A=4.9 kPa ; B=8.6
E_{Ttoe} **;** $E_{Tlinear}$ **(kPa)**	42.1 ; 2847.1
E_{toe} **;** E_{linear} **(kPa)**	16.3 ; 1749.5
J_{ratio}	106.3

Table 6.2: Measured and calculated moduli and J_{ratio} of the pig cornea tensile behavior.

Enfin, il est intéressant de remarquer qu'un tissu est bien plus complexe que nos gels de collagène modèles. La taille des fibrilles peut ne pas être homogène par exemple [24], ce qui apporte de la complexité dans la compréhension de leur comportement mécanique. En fabriquant des gels de collagène dans du PBS, nous avons réussi à avoir une idée potentiellement plus réaliste du comportement mécanique des tissus riches en collagène, amené par des fibrilles de différentes morphologies dans le gel. En effet, des échantillons pris du même tissu peuvent avoir différents comportements en traction selon leur localisation et l'orientation de l'emporte-pièce par rapport à l'échantillon complet [25, 26]. Par ailleurs, la composition d'un issu est extrêmement complexe: par exemple, il contient des proteoglycans qui fournissent de la raideur en traction grâce à leur interaction avec les fibrilles de collagène [27]. Nos gels de collagène modèles fournissent une base pour comprendre les interactions moléculaires, fibrillaires et liées à l'eau. Il serait intéressant de faire des tests de cyclage sur les autres conditions pour établir l'influence des tailles de fibrilles et de la lyophilisation sur le comportement en fatigue des gels. Par exemple, nous pourrions nous attendre à une hystérèse faible dans le cas des échantillons lyophilisés (à cause de leur comportement en traction plus élastique) et un effondrement plus rapide de leur structure à cause de la friction (moins de molécules d'eau présentes pour lubrifier les molécules de collagène). Afin de mieux imiter le comportement mécanique des tissus riches en collagène, la composition des gels de collagène pourrait être ajustée en ajoutant d'autres composants de la matrice extracellulaire. De tels gels pourraient être utilisés pour explorer l'influence de la capacité à dissiper plus ou moins d'énergie visqueuse sur la différenciation cellulaire.

6.9 SECTION CONFIDENTIELLE

6.10 Conclusion

Grâce au séchage par atomisation, nous avons pu produire des billes de collagène denses et autoassemblées. En contrôlant les paramètres lors du procédé, nous avons empêché la dénaturation du collagène en gélatine et nous avons pu contrôler la taille des billes. Une centaine de mg de poudre de collagène a pu être produite en quelques heures. Nous avons choisi les conditions les plus restrictives à notre disposition pour démontrer l'injectabilité des billes en les mélangeant avec un solvant aqueux, et en injectant la suspension (80 mg/mL) à travers une aiguille de taille 26G (utilisée pour les produits de comblement). En se réhydratant, les molécules de collagène ont par la suite précipité *in vitro* dans un milieu de culture cellulaire pour former des fibrilles ressemblant à celles des tissus biologiques. L'ultrastructure du gel obtenu a montré des textures biréfringentes associées en majorité à des domaines d'alignement. L'influence de la taille des billes n'a pas été explorée lors de cette étude. Elle

pourrait jouer un rôle sur le temps de dissolution des billes, donc sur leur injectabilité. Néanmoins, il pourrait être avantageux d'utiliser des billes plus petites dans le but d'homogénéiser plus rapidement la concentration locale en collagène lors de la dissolution.

Pour étudier plus en profondeur les propriétés d'auto-assemblage de notre système, nous avons designé des moules en 3D pour produire des gels denses de collagène. En mélangeant les billes avec un solvant peu acide, nous avons pu induire l'auto-assemblage des molécules de collagène en 3D. L'organisation a été fixée en induisant la fibrillogénèse *in vitro* par vapeurs d'ammoniaque pendant trois heures, afin d'obtenir un système modèle. Des propriétés semblables à celles des tissus ont été observées, comme la formation d'un contre-plaqué ressemblant à celui de la cornée à l'échelle microscopique dans le gel à 50 mg/mL. Puis, nous avons modifié les conditions de procédé pour explorer leur influence sur l'ultrastructure des gels. Même si aucune preuve ultrastructurale n'a été mise en évidence directement, nous avons émis l'hypothèse qu'augmenter le temps d'exposition aux vapeurs d'ammoniaque augmente la taille des fibrilles de collagène. La fibrillogénèse *in vitro* induite par PBS a conduit à la formation de deux populations d'objets : des molécules de collagène (avec la présence possible de microfibrilles) et des fibrilles striées qui ont tendance à former de plus gros agrégats à 80 mg/mL. Finalement, lyophiliser et congeler-fondre les gels de collagène ont aussi formé ces deux populations. Cependant, nous n'avons trouvé aucune preuve de formation potentielle de points de réticulation physique renforcés (interactions électrostatique et hydrophobe). Les premiers tests avec du plasma pour essayer de promouvoir la formation de points de récitulation chimique dans des solutions diluées de collagène n'ont pas été concluants.

La réponse mécanique de notre gel de collagène modèle a montré des aspects biomimétiques qualitatifs : comportement en traction non-linéaire, dépendance au temps proche de celle des tissus biologiques, comportement en fatigue biomimétique. Leur processus de propagation de fracture montre même quelques similarités avec des tests de fracture faits sur des tendons. Cependant, la raideur et la ténacité de nos gels est bien en-dessous celle des tissus biologiques (de plusieurs ordres de grandeur); mais nos gels sont seulement faits d'eau et de collagène, d'où le manque d'autres composants présent dans la MEC qui pourraient les renforcer. Grâce à la réponse mécanique différente produite par les gels de collagène laissés sous vapeurs d'ammoniaque toute une nuit (moins de non-linéarité dans la réponse en tension et temps de relaxation de contrainte plus faible), notre hypothèse sur une taille de fibrille plus grande apparaît pertinente. Le comportement mécanique des gels faits dans du PBS était trop variable pour pouvoir les caractériser de manière plus complète. Finalement, la lyophilisation n'a pas renforcé les propriétés mécaniques des gels et a même drastiquement réduit leur réponse non-linéaire. Ainsi, la formation de liaisons électrostatique ou hydrophobe pourrait ne pas avoir été favorisée, et les molécules d'eau impliquées dans les liaisons hydrogène apparurent perdues de manière irréversible. Cependant, les gels furent testé après 2 à 3 semaines de réhydratation; l'influence du temps de réhydratation pourrait être exploré. Puisque les gels ont été réhydratés dans du PBS, il est possible que les ions (surtout les ions phosphate) ont aussi joué un rôle. Des essais avec des gels lyophilisés et réhydratés dans de l'eau sont en cours.

Enfin, nous avons exploré des compositions plus complexes pour essayer d'imiter des tissus biologiques spécifiques, grâce à deux collaborations.

La formation d'un système modèle, le gel de collagène synthétisé par vapeurs d'ammoniaque pendant trois heures, nous a aidé à approfondir notre compréhension de la relation ultrastructure-propriétés mécaniques. Cependant, ce modèle peut ne pas être pertinent pour tous les tissus biologiques. Par conséquent, les paramètres de procédé et la composition pourraient être ajustés pour

garantir une meilleure ressemblance avec les tissus biologiques d'intérêt. Nous avons comparé les propriétés mécaniques de nos gels avec celles de tissus biologiques, avec les données disponibles dans la littérature. Cependant, beaucoup d'études ont été faites sur le tendon, surtout concernant les procédés de déformation à l'échelle microscopique. L'organisation du tendon est plus proche d'une organisation 2D (hiérarchie unidirectionnelle à grande échelle), ce qui limite la pertinence de la comparaison avec les processus de déformation dans les gels de collagène en 3D. Nos gels de collagène possèdent des aspects anisotropes comme montré par différentes techniques de microscopie, mais il semble que les domaines organisés ne sont pas présents à l'échelle du gel entier. Favoriser une organisation à plus grande échelle (dans le bulk) des molécules de collagène avant fibrillogénèse pourrait renforcer les propriétés mécaniques du gel. Enfin, il a été difficile d'observer des striations sur les fibrilles des gels de collagène synthétisés par vapeurs d'ammoniaque, au contraire des gels faits dans du PBS. Ainsi, explorer des conditions de fibrillogénèse de manière plus poussée (temps d'exposition aux vapeurs d'ammoniaque, température, autres milieux comme le sérum physiologique) pourrait être intéressant afin de produire des morphologies de fibrilles encore plus biomimétiques.

Bibliography

1. Ratner, B. D., Hoffman, A. S., Schoen, F. J. & Lemons, J. E. *Biomaterials science: an introduction to materials in medicine* (Elsevier, 2004).
2. Williams, D. F. *Definitions in biomaterials: proceedings of a consensus conference of the European Society for Biomaterials* Volume 4 (Elsevier Ltd, Chester, England, 1987).
3. Giraud-Guille, M.-M., Nassif, N., Wang, Y., Helary, C. & Pellé, A. *Dense fibrillar collagen matrices for tissue repair and the preparation method thereof, Patent US9867902B2* 2010.
4. Nassif, N., Fernandes, F. M., BOISSIERE, C., Sanchez, C. & Giraud-Guille, M.-M. *Injectable collagen suspensions, the preparation method thereof, and the uses thereof, particularly for forming dense collagen matrices, Patent WO2016146954A1* 2015.
5. Kamranpour, N. O., Miri, A. K., James-Bhasin, M. & Nazhat, S. N. A gel aspiration-ejection system for the controlled production and delivery of injectable dense collagen scaffolds. *Biofabrication* **8,** 000000 (2016).
6. Brown, R. A., Wiseman, M., Chuo, C. B., Cheema, U. & Nazhat, S. N. Ultrarapid engineering of biomimetic materials and tissues: Fabrication of nano- and microstructures by plastic compression. *Advanced Functional Materials* **15,** 1762–1770 (2005).
7. Mosser, G., Anglo, A., Helary, C., Bouligand, Y. & Giraud-Guille, M. M. Dense tissue-like collagen matrices formed in cell-free conditions. *Matrix Biology* **25,** 3–13 (2006).
8. Besseau, L., Coulomb, B., Lebreton-Decoster, C. & Giraud-Guille, M. M. Production of ordered collagen matrices for three-dimensional cell culture. *Biomaterials* **23,** 27–36 (2002).
9. Knight, D. P., Nash, L., Hu, X. W., Haffegee, J. & Ho, M. W. In vitro formation by reverse dialysis of collagen gels containing highly oriented arrays of fibrils. *Journal of Biomedical Materials Research* **41,** 185–191 (1998).
10. Highberger, J. H. The Isoelectric Point of Collagen. *Journal of the American Chemical Society* **61,** 2302–2303 (1939).
11. Gobeaux, F. *et al.* Fibrillogenesis in Dense Collagen Solutions: A Physicochemical Study. *Journal of Molecular Biology* **376,** 1509–1522 (2008).
12. Dong, Y. D. *et al.* Impurities in commercial phytantriol significantly alter its lyotropic liquid-crystalline phase behavior. *Langmuir* **24,** 6998–7003 (2008).
13. Besseau, L. & Giraud-Guille, M. M. Stabilization of fluid cholesteric phases of collagen to ordered gelated matrices. *Journal of Molecular Biology* **251,** 197–202 (1995).
14. Schlegel, A. K., Möhler, H., Busch, F. & Mehl, A. Preclinical and clinical studies of a collagen membrane (Bio-Gide®). *Biomaterials* **18,** 535–538 (1997).
15. Friedrich, J. Mechanisms of plasma polymerization - Reviewed from a chemical point of view. *Plasma Processes and Polymers* **8,** 783–802 (2011).

16. Chimich, D., Shrive, N., Frank, C., Marchuk, L. & Bray, R. Water content alters viscoelastic behaviour of the normal adolescent rabbit medial collateral ligament. *Journal of Biomechanics* **25** (1992).

17. Engler, A. J., Sen, S., Sweeney, H. L. & Discher, D. E. Matrix Elasticity Directs Stem Cell Lineage Specification. *Cell* **126,** 677–689 (2006).

18. Puxkandl, R. *et al.* Viscoelastic properties of collagen: Synchrotron radiation investigations and structural model. *Philosophical Transactions of the Royal Society B: Biological Sciences* **357,** 191–197 (2002).

19. Silver, F. H., Seehra, G. P., Freeman, J. W. & DeVore, D. Viscoelastic properties of young and old human dermis: A proposed molecular mechanism for elastic energy storage in collagen and elastin. *Journal of Applied Polymer Science* **86,** 1978–1985 (2002).

20. Tower, T. T., Neidert, M. R. & Tranquillo, R. T. Fiber alignment imaging during mechanical testing of soft tissues. *Annals of Biomedical Engineering* **30,** 1221–1233 (2002).

21. Silver, F. H., Christiansen, D. L., Snowhill, P. B. & Chen, Y. Transition from viscous to elastic-based dependency of mechanical properties of self-assembled type I collagen fibers. *Journal of Applied Polymer Science* **79,** 134–142 (2001).

22. Buehler, M. J. Nature designs tough collagen: explaining the nanostructure of collagen fibrils. *Proceedings of the National Academy of Sciences of the United States of America* **103,** 12285–12290 (2006).

23. Salameh, C. *et al.* Structure-properties correlation of stable transparent domain in fibrillar collagen gradient. *Submitted.*

24. Ottani, V., Raspanti, M. & Ruggeri, a. Collagen structure and functional implications. *Micron (Oxford, England : 1993)* **32,** 251–260 (2001).

25. Annaidh, A. N. *et al.* Characterization of the anisotropic mechanical properties of excised human skin To cite this version : HAL Id : hal-00974586 Characterization of the anisotropic mechanical properties of excised human skin (2017).

26. Yang, W. *et al.* On the tear resistance of skin. *Nature Communications* **6,** 1–10 (2015).

27. Akizuki, S. *et al.* Tensile properties of human knee joint cartilage: I. Influence of ionic conditions, weight bearing, and fibrillation on the tensile modulus. *Journal of Orthopaedic Research* **4,** 379–392 (1986).

Appendix

Structure-property correlations of stable transparent domain in fibrillar collagen gradient

Chrystelle Salameh[1†], Flore Salviat[1,2†], Elora Bessot[1], Miléna Lama,[1,3] Jean-Marie Chassot[4], Elodie Moulongui[1], Yan Wang[1], Marc Robin[1], Alba Marcellan[3], Clément Sanchez[1,5], Marie-Madeleine Giraud-Guille[1], Marco Faustini[1], Rémi Carminati[4] and Nadine Nassif*[1,4]

[1]*Sorbonne Université, Laboratoire Chimie de la Matière Condensée de Paris, UMR 7574 CNRS, Collège de France, 4 place Jussieu, 75231 Paris Cedex 05, France*

[2]*Cornea, External Disorders and Refractive Surgery, Fondation Ophtalmologique Rothschild, 29 rue Manin, 75019 Paris, France*

[3]*Sciences et Ingénierie de la Matière Molle, ESPCI Paris, PSL University, CNRS, Sorbonne Université, 10 rue Vauquelin, 75005 Paris, France*

[4]*Institut Langevin, ESPCI Paris, CNRS, PSL University, 1 rue Jussieu, 75005 Paris, France*

[5]*Collège de France, PSL University, 11 place Marcelin Berthelot, 75231 Paris Cedex 05, France*

*E-mail: nadine.nassif@sorbonne-universite.fr

† These authors contributed equally to this work.

Transparent biological tissues are found in living organisms such as vertebrate cornea or invertebrate teguments but the physical means by which they are rendered transparent is still poorly understood. Here, a gap of transparency has been found in the fibrillar collagen phase diagram within a very narrow range of concentration. We show that transparency is related to a "blue-like" liquid-crystal phase, which occurs at the boundary of the nematic and precholesteric phases. A fundamental approach is proposed to investigate the relation between the three-dimensional fibrillar network, and the optical and mechanical properties of the macroscopic collagen matrices. Interestingly, transparency results from structural correlations inhibiting light scattering, while preserving mechanical stability, stiffness and nonlinearity. Beyond the understanding of transparency in natural tissues, this opens perspectives in the design and production of biocompatible materials with controlled photonic and mechanical properties.

Aside structural colours and pigmentation, optically transparent or translucent organisms are found in nature. They are quite abundant in aquatic environments (*e.g* medusa, planktonic organisms) but rare on land *(e.g*. butterfly *Greta oto*). The biological role of transparency appears to be related to protection from predators[1,2,3]. The physical basis of biological transparency is not straightforward. Living tissues are composed of various components and hence of different refractive indices. Light scattering should result from such ultrastructural inhomogeneity at the submicron scale. Therefore deciphering the relation between transparency and structure in living organisms is of great interest.

Aside invertebrates, cornea is a transparent connective tissue that forms the front part of the eye. It works as a refracting lens possessing dioptric properties. Light transmission occurs through the tissue containing collagen, proteoglycans and cells, and scattering is suppressed

by interferences induced by partial order in the structure. Interestingly, disorders, opacifying the cornea, are a major cause of refractive errors but also blindness[4]. Hence, particular attention was paid to the distribution of type I collagen, the principal constituent of the corneal stroma, exploring the link between fibrillar network and optical transparency through mathematical/physical models[5,6,7,8].

Collagen type I, a major structural protein in the body, displays a strong assembled fibrillar organization in numerous connective tissues such as bone, dermis and cornea. Depending on the tissue, collagen organizes differently which leads to different mechanical properties (from hard to soft) and optical properties (from opaque to transparent)[9]. For instance, a cholesteric structure is observed in the compact bone that contributes to its mechanical properties[10], while the tendon is composed of unidirectional collagen fibrils[11]. For cornea, collagen fibrils organize in a general lamellar orientation with some local plywood forms[4]. Hence, an interesting correlation exists between the collagen phase diagram and the tissue ultrastructure although the occurrence of collagen liquid-crystal (LC) phases was never demonstrated *in vivo*[12].

Transparent collagen matrices were recently reported in natural tissues, *i.e*. elephant ivory[13] and teeth of the deep-sea dragonfish[14], and in synthetic collagen scaffolds[15]. However, transparency remains an intriguing property as it can be present in different degrees, measured by the optical thickness L/ℓ, where L is the sample thickness and ℓ the scattering mean free path. The thickness of transparent collagen matrices reported so far was quite low (below 1 mm)[15], therefore transparency ($L/\ell << 1$) is more likely to be related to the thickness of the matrix rather than to the organization of collagen fibrils. To be able to accurately discuss transparency and correlate it to structure, it is indeed important to shape the collagen matrices into a correct physical design, thick enough, to confirm the strong relation between the intrinsic ultrastructure of collagen fibrils and their macroscopic optical properties.

Here, we report on the existence of a gap of transparency in the fibrillar collagen phase diagram. The domain is stable with time and related to a narrow range of collagen concentration. This feature made it possible to produce fully 3D transparent collagen materials up to 1 cm in thickness, following different processes ensuring both that the transparency is linked to the intrinsic matrix structure *versus* its thickness and that it is only related to the collagen concentration. An experimental investigation of the structure-property correlations was carefully conducted, showing in particular that the optical transparency is related to the local structure at a specific collagen concentration. Interestingly, the material exhibits locally the corneal collagen structure and close optical and mechanical features. Before the fibrils precipitation (fibrillogenesis *in vitro*), a metastable LC phase with facets ordered into a 3D network forms between the nematic and the precholesteric phases in the lyotropic collagen diagram. Such properties remind the blue phase extensively reported in thermotropic LC and only once in lyotropic LC for very long DNA polymer[16] but never for free molecules suspension. This observation strengthens the hypothesis on the existence of biological LC analogues[17]. Collagen being well-known for its low immunogenicity, biocompatibility and biodegradability[18,19], the resulting 3D fibrillar transparent matrix may be of interest for biomedical applications in particular in ophthalmology for developing keratoprosthesis models but also for studying the relationship between the materials structure and the occurring transparency, which remains difficult to assess in cornea, for example[20,21,22]. Finally, our understanding of transparency may provide a new approach to the design of biocompatible materials with prescribed optical properties, and manufacturable using self-assembly processes.

Collagen concentration gradient: gap in transparency

Two matrices were prepared, characterized by gradient in collagen concentration ranging from ~20 to ~100 mg/mL by using either the continuous injection/reverse dialysis protocol previously published for preparing pure or composite materials[23,24] (Fig. 1a) or the evaporation process[25] (Fig. S1) but without homogenization of the acidic collagen solution. A gap of transparency was observed for both matrices after the fibrils precipitation (Fig. 1a and Fig. S1, arrows). Nevertheless, a slight difference in terms of opacity was observed between the two samples. Noticeably, the thicker material (*i.e.* 1 cm large) synthesized by injection/reverse dialysis was more opaque. The collagen concentration in the transparent domain was determined from quantifying the amount of hydroxyproline by titration. The same concentration was found whatever the process adopted (evaporation, continuous injection/reverse dialysis) which was around 45 mg/mL. Such gap of transparency found in the fibrillar collagen diagram appears quite counterintuitive since the increase in collagen concentration leads to an increase in fibrillar density and order: the isotropic/anisotropic transition occurring slightly above 40 mg/mL[26]. An increase in density and ordering are competing mechanisms that can lead to a suppression of scattering and the appearance of transparency beyond a given concentration threshold. But the recovery of opacity at even larger densities, and therefore the non-monotonic behaviour of the degree of transparency *versus* concentration, proves the crucial role of the ultrastructure on the optical properties.

A diluted soluble-acidic collagen (2 mg/mL) was concentrated by a slow evaporation[25,27] up to 45 mg/mL. This technique allows an accurate estimation of the concentration during evaporation by simple weighing. The fibrillar collagen matrix is shown in Figure 1b. A part of the collagen matrix has been removed locally (Area 1) to demonstrate the presence of a transparent matrix in the petri dish (Area 2). Area 3 shows a fibrillar collagen matrix where a shear stress was applied using a spatula before fibrillogenesis *in vitro*. This area becomes

127 opaque after the precipitation of the fibrils indicating a change in the material's properties.
128 The collagen concentration being above 40 mg/mL, this should be due to the destabilization
129 of the LC geometry. The phase diagram of collagen molecules has been extensively studied[28]
130 (Fig. 1c) and exhibits three arrangements: nematic (above 40 mg/mL) (N in Fig. 1c),
131 precholesteric (P in Fig. 1c) and cholesteric (above ~75 mg/mL)[26] (C in Fig. 1c). None of
132 them was described to lead to transparent collagen materials although thermotropic nematic
133 liquid crystals tend to be relatively translucent (LCDs).
134 The fact that the physical properties recorded on the transparent matrices were almost similar
135 whatever the source of collagen (the porcin clinical grade and the one extracted from rat tails
136 tendons, see Methods) ensured that the concentration protocols are *(i)* reproducible for
137 generating the transparency and *(ii)* that geometry, at a certain collagen concentration, is the
138 key factor for the matrix transparency. Previous work in the literature described the formation
139 of transparent but very thin collagen matrices[29,30] for which the transparency appears stable at
140 acidic pH (3.5) and is only related to a specific ionic strength thus rendering the comparison
141 with our work difficult.
142 Further investigations of the collagen phase diagram were done handling the solutions with
143 care. For this purpose, an acidic solution of collagen concentrated at 40 mg/mL was deposited
144 between slide and coverslip and studied by polarized light microscopy; the concentration of
145 collagen occurring at the air/solution interface through a slow evaporation of solvent. The
146 evaporation of solvent being not homogeneous over the drop, the precise concentrations
147 remain uncertain. As expected, first a nematic phase is observed where the molecules orient
148 themselves in the same direction (Fig. 1c, N). Second, when we slowly evaporated the
149 collagen solution reaching 44 mg/mL, a facetted pattern starts to appear (Fig. 1d) with the
150 presence of stripes in some domains (Fig. 1d', arrow). The facets are polydisperse in size and
151 organize mostly as a mosaic. Nevertheless, the bigger ones locally arrange in layers reminding

the fibrillar collagen arrangement in coelacanth scales[31]. The facetted organization of collagen molecules seems different from the « staggered dots » texture described for collagen since it was observed over the cholesteric phase[32] and not related to any optical property. Finally, controlling the sample thickness and the conditions of observations (temperature, humidity and time under the microscope light) slowed down its systematic transformation into precholesteric phase but did not avoid it (Fig. S2). However, another phase possessing some commonalities with a twist grain boundary phase in terms of colours and texture (filament) was sometimes observed[33] (Fig. 1c, TGB) but only with the highly purified collagen clinical grade (Fig. S3). The transition between the nematic and the precholesteric phases occurs around 46-47 mg/mL. The fact that the phase appears in a very narrow range of concentrations (~ 44-45 mg/mL) may explain why it was never observed before. Further investigations revealed that the collagen LC phase is birefringent but observed without polarizer, blue and brownish colours were observed remaining unchanged when the stage was rotated (Figs. 1e and e'). Interestingly, the blue phase is invariant in color upon rotation in polarized light[34] and consistently, is described as being a metastable intermediate phase between the isotropic and the cholesteric phases. Although blue phases are generally observed in highly chiral thermotropic liquid crystals[35,36], it was reported once with lyotropic DNA solutions[16]. The size of the biomacromolecules (DNA and collagen) is noticeably much longer than the thermotropic molecules. This difference in size is not incompatible with a blue phase organization of collagen fibrils as shown by the local arrangements of non-fluid analogues in annelid cuticle[37] and box-fish scutes[38]. It is worth mentioning that the cited examples reports on 3D fibrils order but do not demonstrate the existence of a LC state.

Corneal birefringence is known and varies within a single cornea. To improve our understanding of the origin of transparency in collagen structures, observations were performed on pig corneas without polarization (Fig. S4a). Birefringent domains are observed

under physical constraints (Fig. S4b) which at higher magnification appear as a layered texture (Fig. S4c). The fact that similar birefringence texture was observed in corneal stroma from mice[39] strengthens the analogy that may exist with a blue phase.

In summary, the presence of liquid crystalline blue phases appears compatible with collagen as also strengthened by an equilibrium double-twist model for the radial structure of collagen fibrils[40]. Nevertheless, we will refer to it as "blue phase-like" due to the lack of additional crystallographic evidence. To help identify the physico-chemical factors for the origins of the transparency, structural, optical and mechanical characterization are requisite.

Ultrastucture of transparent collagen matrices and analogy with cornea

Before samples preparation for Electron Microscopy observations, the synthetic and the biological materials were stored in a classical storage medium for cornea (*i.e*. Cornea cold, see Methods). Both were stable and remain transparent in the medium (Fig. 2a). This step allows a safe comparison of the materials in discarding any potential effect that would have been induced by different ionic forces, pH, *etc*) on the observed ultrastructure.

Scanning electron microscopy (SEM) observations were performed on a pig cornea (Fig. 2b, °) and compared to a transparent collagen matrix (~45 mg/mL) (Fig. 2b, *). Both exhibit dense network with thin collagen fibrils (≤ 100 nm). Transmission electron microscopy (TEM) investigations confirm the high similarity in appearance between the two samples (Fig. 2c). Higher magnification (inset in Fig. 2c) shows that fibrils are monodisperse in diameter, which is a main characteristic of biological tissues. The diameter is ~25-30 nm and classical for the corneal tissue [41]. The extrafibrillar space also appears in the same range of order (≤ 100 nm) in both samples. The lack of the other organic constituents (mainly proteoglycans) present in the corneal ECM may be the reason for the different aspects of the collagen. Collagen fibrils appear mostly aligned parallel (line) or perpendicular (dot) to the section

plane, reminding previous observations performed with clustered DNA bundles[16] although a periodic pattern is difficult to draw (Fig. S5). This is in fact also the case for cornea when the section plane is not perfectly performed perpendicular (Fig. S6a) avoiding the observation of the organized orthogonal plywood (Fig. S6b). This is quite intriguing since transparency of cornea is usually related to the arrangement of fibrils in a lattice with a high degree of order[5,6,7]. Although short-range order is certainly a key ingredient for transparency, the microstructure of cornea on a large scale appears to be more complex.

To improve our understanding on the correlation between the microstructure of the collagen material and its transparency, further investigations were performed on a material larger in size (cylinder ~0.5 x 1 cm^2) with a final concentration of ~45 mg/mL. Although the material is indeed transparent from the flat end (Fig. 2d, inset), a gradient of transparency forms going from opalescent to completely transparent when observed from the curve side as depicted in Figure 2d. This indicates a slight difference in concentration in the collagen material ($\Delta C \leq 1$). The ultrastructure was investigated by TEM revealing two other orthogonal arrangements of fibrils in the opalescent domain (Figs. 2e-f). Their spatial distribution appears heterogeneous over the domain but we cannot exclude that there is in fact a link between their position and a specific concentration. Both domains are denser in collagen fibrils.

One presents two types of bundles (of fibrils Fig. 2e), each showing a constant orientation, but abrupt angular changes at the transition from one bundle to the next one. Interestingly, this arrangement reminds that of the scutes of fish (Fig. S7a) where an analogy with a blue phase geometry is made[31,38]. This original architecture can also be compared to the arrangement found in ivory of the elephant[42] at higher scale. Noticeably, the orthogonal arrangement is due to the three-dimensional empty tubule *versus* collagen fibrillar network but remains optically transparent (Fig. S7b).

The other domain presents two types of layers of fibrils. Each layer shows a constant

orientation. As for the two other domains, the collagen fibrils are observed either in cross-section or in longitudinal section being systematically at approximate right angles to the surrounding layers. Thus the synthetic opalescent domain exhibits high similarities in terms of structure (*i.e.* orthogonal plywood of lamellae) and size (*i.e.* fibrils diameter, thickness of layers) with the corneal stroma (Fig. S6b). Although the orientation of the collagen fibrils in longitudinal section is perpendicular to the usual but very local observations found in the literature as discussed above, it is also found in cornea (Fig. S6a, rectangular).

In summary, three domains exhibit very thin and regular fibrils diameter with orthogonal arrangements (from single fibril to layers or bundles of fibrils). The domains coexist in the gap of transparency in the fibrillar collagen diagram. According to this noticeable difference in domains' size, it may be proposed that the ratio between the unit (whatever its nature, *e.g.* collagen fibril or empty tubule) and an associate orthogonal arrangement is the key for building transparent materials. To go further on the understanding of the structural-property relationship, the degree of transparency (optical thickness) was investigated on materials evolving from transparent to opaque, and compared to the cornea biological tissue. In addition, mechanical investigations were performed to help identify the physico-chemical parameters involved in the formation of such optical properties.

Correlation between the structure, mechanical and optical properties

A narrow range of collagen concentration was set around 45 mg/mL by using the slow evaporation process described above (see Methods). The concentrations are the following: ~40 mg/mL (curve 1), ~42 mg/mL (curve 2), ~43.5 mg/mL (curve 3), ~45 mg/mL (curve 5), ~47 mg/mL (curve 4) and ~48 mg/mL (curve 7). As a first experiment, the transmittance of hydrated fibrillar collagen matrices was studied by UV-vis spectroscopy and normalized as respect to pure water (see Methods). Figure 3a shows the optical transmittance of the matrices

between 370 and 1000 nm with thickness of ~2 mm. Increased transmittance regardless of the wavelength is obtained with the ~45 mg/mL matrix. Figure 3b shows the transmittance of the matrices at 700 nm. The transmittance reaches a maximum for fibrillar collagen matrices with a concentration of ~45 mg/mL. Above 45 mg/mL, the transmittance decreases. Transmittance spectra provide a qualitative support to the change in transparency. For a quantitative assessment of transparency, we measured the scattering mean free path ℓ using full-field Optical Coherence Tomography (OCT)[43] (Fig. 3). This characteristic length, defined as the average distance between two scattering events, measures the intrinsic scattering strength of a material. First, measurements were performed on an *ex vivo* pig cornea (Fig. 3c). A typical in-depth OCT cross-section (Fig. 3d) clearly shows the decreasing average OCT signal from which the value of ℓ is extracted (see Methods). Measurements in four different zones (indicated as square regions in Fig. 3c) are presented in a bar graph, showing an increased transparency in the center, consistent with the visual appearance of the cornea. Second, investigations were conducted on the matrix made with the broad gradient in collagen concentration (Fig. 1c). The scattering mean free path ℓ was measured in seven different zones (indicated in Fig. 3e), with decreasing concentration in collagen, resulting in the bar graph in Fig. 3e. Substantial changes, by almost a factor of two, are observed along the collagen concentration gradient, and thus by moving through different fibrillar structures. Larger values of ℓ at the centre indicate an increase in transparency, in agreement with visual appearance and the transmittance curves. This substantial change in ℓ is a signature of the crucial role of short-range order in disordered materials. Indeed, by simply changing the local degree of order, even at a given density of scattering centres (fibrils), it is known that ℓ can be changed towards smaller or larger values (stronger or weaker scattering)[44,45] up to transparency[46] . Interestingly, the value ℓ = 125.4 μm found in the centre of the pig cornea

(Fig. 3c) is on the order of the values $\ell \sim$ 120-140 μm measured at the edges of the transparency gap of the gradient matrix (zones 1 and 4 in Fig. 3e). This correspondence is supported qualitatively by the in-depth OCT cross-section images (Fig. 3f) of the 3D synthetic bulk (~45 mg/mL, Fig. 2d). Indeed, we observe that the collagen fibrils are parallel and superimposed in the opalescent part (corresponding to the edge of the transparency gap), reminding the structure of the corneal stroma (Fig. 3d). This strengthens the hypothesis that enhanced transparency at a concentration 45 ± 1 mg/mL is responsible for enhanced transparency. This also suggests that the structure of the real cornea may not correspond to a maximum of transparency, presumably since other properties (*e.g.* mechanical) also need to be optimized.

Based on the evidence of the crucial role of ultrastructure on the optical properties, the mechanical properties of the collagen matrices were also investigated. The transparent gel at ~45 mg/mL is tough and easy to handle (SI video 1). It remains transparent upon mechanical handling and shearing, suggesting that fibrillar rearrangements do not operate at the scale of visible wavelengths (from ~100 nm to – a few μm). However, gel stability is very sensitive to slight differences in concentration (Fig. S8). This suggests that the assumed improvement of mechanical properties of collagen fibrillar matrices with concentration described in the literature[29,47] does not necessarily apply around the concentration leading to transparency.

More quantitative assessment of the mechanical response of optically transparent materials with concentrations in the range ~43-45 mg/mL was obtained at large strains in tension, and compared to freshly extracted cornea. The general mechanical response of the matrices exhibits biomimetic mechanical behaviour. Tensile behaviour of the fibrillar matrices is strongly nonlinear (Fig 4), with extreme compliance at the lower stretches and hardening at intermediate strains, as expected for biological tissues[48,49,50] and more especially for cornea[51]. From this "J-shaped" mechanical response, elastic moduli were defined in the toe and linear

region, respectively.

Performing such large strain characterizations on hydrated materials is delicate due to their intrinsic softness and wetness that imply to prevent any slippage in the jaws and drying during the tests[52]. Besides, their potential drying can induce a collapse of the fibrillar collagen network dramatically enhancing the stiffness[53]. The elastic moduli in the linear region of the transparent collagen matrices in the range ~43-45 mg/mL (304±50 kPa) are consistent with the higher values found in the literature after the critical concentration threshold for anisotropic fibrillar arrangement[47,54]. However, the stiffness of the transparent matrices in the linear regime is about 4-fold lower than that of the pig cornea (1340±580 kPa).[29] These differences can be explained by the presence of other proteins and elements in the cornea that play an important role in ensuring the mechanical performance[53]. Furthermore, our process does not enable a precise spatial control of the anisotropy in 3D at the microscale, which increases the variability of the mechanical behaviour even in a narrow concentration range. Note that ultimate stages of the stress-strain curves were truncated when macroscopic damage (crack) appeared in the sample. Ultimate tensile stresses and strains at break were not investigated, as failure systematically occurred in the clamps. It is worth mentioning that a pre-treatment of collagen-based materials is quite systematically used in the literature to reinforce their mechanical properties by means of reticulant agents[55,56].

In conclusion, there is a strong correlation between the structure and the optical and mechanical properties of collagen. The gap in transparency found in the fibrillar collagen gradient appears to form thanks to spatial correlations between the collagen fibril units forming the final microstructure. The resulting architecture ensures the coexistence of transparency and biomimetic mechanical response. This is also indicative of morphogenetic processes based on liquid crystalline assembly principles. The very narrow concentration

range, less than a few mg/mL, within which the blue phase-like exists needs further improvement to be stabilized as it is studied for thermotropes[57].

The development of such matrices as corneal models, and more generally as biocompatible photonic materials, requires a deeper understanding of their three-dimensional organization and of their stability in a physiological medium (pH, ionic forces, composition) in order to determine an optimal environment for their conservation. Finally, to meet the expectations of the biomedical field, *in vitro* and *in vivo* investigations are required to ensure the non-toxicity, the integration and colonization of the keratocyte host cells.

Methods

Full details of the matrices synthesis and sample characterization techniques used are presented in the Supplementary Information.

References

1. Kerfoot, W. C. A question of taste: crypsis and warning coloration in freshwater zooplankton communities. *Ecology* **63**, 538–554 (1982).

2. Langsdale, J. R. M. Developmental changes in the opacity of larval herring, Clupea harengus, and their implications for vulnerability to predation. *J. Mar. Biol. Assoc. United Kingdom* **73**, 225–232 (1993).

3. Tsuda, A., Hiroaki, S. & Hirose, T. Effect of gut content on the vulnerability of copepods to visual predation. *Limnol. Oceanogr.* **43**, 1944–1947 (1998).

4. Meek, K. M. & Knupp, C. Corneal structure and transparency. *Prog. Retin. Eye Res.* **49**, 1–16 (2015).

5. Maurice, D. M. The structure and transparency of the cornea. *J. Physiol.* **136**, 263–286 (1957).

6. Hart, R. W. & Farrell, R. A. Light scattering in the cornea. *JOSA* **59**, 766–774 (1969).

7. Benedek, G. B. Theory of transparency of the eye. *Appl. Opt.* **10**, 459–473 (1971).

8. Freegard, T. J. The physical basis of transparency of the normal cornea. *Eye* **11**, 465 (1997).

9. Prockop, D. J. What holds us together? Why do some of us fall apart? What can we do about it? *Matrix Biol.* **16**, 519–528 (1998).

10. Giraud-Guille, M.-M. Cholesteric twist of collagen in vivo and in vitro. *Mol. Cryst. Liq. Cryst.* **153**, 15–30 (1987).

11. Weiner, S., Traub, W. & Wagner, H. D. Lamellar bone: structure–function relations. *J. Struct. Biol.* **126**, 241–255 (1999).

12. Mitov, M. & Dessaud, N. Going beyond the reflectance limit of cholesteric liquid crystals. *Nat. Mater.* **5**, 361 (2006).

13. Albéric, M., Gourrier, A., Wagermaier, W., Fratzl, P. & Reiche, I. The three-dimensional arrangement of the mineralized collagen fibers in elephant ivory and its relation to mechanical and optical properties. *Acta Biomater.* **72**, 342–351 (2018).

14. Velasco-Hogan, A. *et al.* On the Nature of the Transparent Teeth of the Deep-Sea Dragonfish, Aristostomias scintillans. *Matter* (2019).

15. Tidu, A. *et al.* Highly concentrated collagen solutions leading to transparent scaffolds of controlled three-dimensional organizations for corneal epithelial cell colonization. *Biomater. Sci.* **6**, 1492–1502 (2018).

16. Leforstier, A. & Livolant, F. DNA liquid crystalline blue phases. Electron microscopy evidence and biological implications. *Liq. Cryst.* **17**, 651–658 (1994).

17. Bouligand, Y. Twisted fibrous arrangements in biological materials and cholesteric mesophases. *Tissue Cell* **4**, 189–217 (1972).

18. Parenteau-Bareil, R., Gauvin, R. & Berthod, F. Collagen-based biomaterials for tissue engineering applications. *Materials (Basel).* **3**, 1863–1887 (2010).

19. Giraud-Guille, M. M., Nassif, N. & Fernandes, F. M. Collagen□based Materials for Tissue Repair, from Bioinspired to Biomimetic. in *Materials Design Inspired by Nature* 107–127 (2013).

20. Meek, K. M. Corneal collagen—its role in maintaining corneal shape and transparency. *Biophys. Rev.* **1**, 83–93 (2009).

21. Trelstad, R. L. & Coulombre, A. J. Morphogenesis of the collagenous stroma in the chick cornea. *J. Cell Biol.* **50**, 840–858 (1971).

22. Borderie, V. M. *et al.* Banding patterns: exploring a new feature in corneal stroma organization. in *ARVO Annual Meeting* **58**, 3906 (2017).

23. Wang, Y. *et al.* Controlled collagen assembly to build dense tissue-like materials for tissue engineering. *Soft Matter* **7**, 9659–9664 (2011).

24. Wang, Y. *et al.* The predominant role of collagen in the nucleation, growth, structure and orientation of bone apatite. *Nat. Mater.* **11**, 724–733 (2012).

25. Besseau, L., Coulomb, B., Lebreton-Decoster, C. & Giraud-Guille, M. M. Production of ordered collagen matrices for three-dimensional cell culture. *Biomaterials* **23**, 27–36 (2002).

26. Giraud-Guille, M. M. Liquid crystallinity in condensed type I collagen solutions: a clue

396 to the packing of collagen in extracellular matrices. *J. Mol. Biol.* **224**, 861–873 (1992).

397 27. Helary, C., Foucault-Bertaud, A., Godeau, G., Coulomb, B. & Giraud-Guille, M. M.
398 Fibroblast populated dense collagen matrices: cell migration, cell density and
399 metalloproteinases expression. *Biomaterials* **26**, 1533–1543 (2005).

400 28. Gobeaux, F. *et al.* Cooperative ordering of collagen triple helices in the dense state.
401 *Langmuir* **23**, 6411–6417 (2007).

402 29. Tidu, A. *et al.* Development of human corneal epithelium on organized fibrillated
403 transparent collagen matrices synthesized at high concentration. *Acta Biomater.* **22**, 50–
404 58 (2015).

405 30. Peixoto, P. D. S. *et al.* Achievement of cornea-like organizations in dense collagen I
406 solutions: clues to the physico-chemistry of cornea morphogenesis. *Soft Matter* **9**,
407 11241–11248 (2013).

408 31. Giraud, M. M., Castanet, J., Meunier, F. J. & Bouligand, Y. The fibrous structure of
409 coelacanth scales: a twisted 'plywood'. *Tissue Cell* **10**, 671–686 (1978).

410 32. Peixoto, P. D. S., Deniset-Besseau, A., Schanne-Klein, M. C. & Mosser, G.
411 Quantitative assessment of collagen I liquid crystal organizations: role of ionic force
412 and acidic solvent, and evidence of new phases. *Soft Matter* **7**, 11203–11210 (2011).

413 33. Dierking, I. Chiral liquid crystals: Structures, phases, effects. *Symmetry (Basel).* **6**,
414 444–472 (2014).

415 34. Lee, H. & Labes, M. M. Lyotropic Cholestebic Blue Phase. *Mol. Cryst. Liq. Cryst.* **82**,
416 355–359 (1983).

417 35. Murphy, A. Blue Phases in Liquid Crystals. (2011).

418 36. Bahr, C. & Kitzerow, H.-S. *Chirality in liquid crystals*. (Springer, 2001).

419 37. Lepescheux, L. Spatial organization of collagen in annelid cuticle: order and defects.
420 *Biol. Cell* **62**, 17–31 (1988).

421 38. Besseau, L. & Bouligand, Y. The twisted collagen network of the box-fish scutes.
422 *Tissue Cell* **30**, 251–260 (1998).

423 39. Aldrovani, M., Guaraldo, A. M. A. & Vidal, B. C. Optical anisotropies in corneal
424 stroma collagen fibers from diabetic spontaneous mice. *Vision Res.* **47**, 3229–3237
425 (2007).

426 40. Brown, A. I., Kreplak, L. & Rutenberg, A. D. An equilibrium double-twist model for
427 the radial structure of collagen fibrils. *Soft Matter* **10**, 8500–8511 (2014).

428 41. Komai, Y. & Ushiki, T. The three-dimensional organization of collagen fibrils in the
429 human cornea and sclera. *Invest. Ophthalmol. Vis. Sci.* **32**, 2244–2258 (1991).

430 42. Albéric, M. *et al.* Relation between the macroscopic pattern of elephant ivory and its
431 three-dimensional micro-tubular network. *PLoS One* **12**, e0166671 (2017).

432 43. Vabre, L., Dubois, A. & Boccara, A. C. Thermal-light full-field optical coherence
433 tomography. *Opt. Lett.* **27**, 530–532 (2002).

434 44. Rojas-Ochoa, L. F., Mendez-Alcaraz, J. M., Sáenz, J. J., Schurtenberger, P. &
435 Scheffold, F. Photonic properties of strongly correlated colloidal liquids. *Phys. Rev.*
436 *Lett.* **93**, 73903 (2004).

437 45. Vynck, K., Burresi, M., Riboli, F. & Wiersma, D. S. Photon management in two-
438 dimensional disordered media. *Nat. Mater.* **11**, 1017 (2012).

439 46. Leseur, O., Pierrat, R. & Carminati, R. High-density hyperuniform materials can be
440 transparent. *Optica* **3**, 763–767 (2016).

441 47. Ramtani, S., Takahashi-Iniguez, Y., Helary, C., Geiger, D. & Giraud-Guille, M. M.
442 Mechanical behavior under unconfined compression loadings of dense fibrillar
443 collagen matrices mimetic of living tissues. *J. Mech. Med. Biol.* **10**, 35–55 (2010).

444 48. Fung, Y. C. Elasticity of soft tissues in simple elongation. *Am. J. Physiol. Content* **213**,
445 1532–1544 (1967).

446 49. Humphrey, J. D. Continuum biomechanics of soft biological tissues. *Proc. R. Soc.*
447 *London. Ser. A Math. Phys. Eng. Sci.* **459**, 3–46 (2003).

448 50. Rose, S. *et al.* Nanoparticle solutions as adhesives for gels and biological tissues.
449 *Nature* **505**, 382 (2014).

450 51. Kling, S. & Hafezi, F. Corneal biomechanics–a review. *Ophthalmic Physiol. Opt.* **37**,

240–252 (2017).

52. Rose, S., Dizeux, A., Narita, T., Hourdet, D. & Marcellan, A. Time dependence of dissipative and recovery processes in nanohybrid hydrogels. *Macromolecules* **46**, 4095–4104 (2013).

53. Hoeltzel, D. A., Altman, P., Buzard, K. & Choe, K. Strip extensiometry for comparison of the mechanical response of bovine, rabbit, and human corneas. *J. Biomech. Eng.* **114**, 202–215 (1992).

54. Nassif, N. *et al.* Self-assembled collagen− apatite matrix with bone-like hierarchy. *Chem. Mater.* **22**, 3307–3309 (2010).

55. Khor, E. Methods for the treatment of collagenous tissues for bioprostheses. *Biomaterials* **18**, 95–105 (1997).

56. Nimni, M. E. Glutaraldehyde fixation revisited. *J. Long. Term. Eff. Med. Implants* **11**, (2001).

57. Kikuchi, H., Yokota, M., Hisakado, Y., Yang, H. & Kajiyama, T. Polymer-stabilized liquid crystal blue phases. *Nat. Mater.* **1**, 64 (2002).

Acknowledgements

Nadine Nassif thanks the Fondation Collège de France and Fondation EDF for the financial support and specially Marie Cheron for sharing opinions and her trust. We thank Josette Legagneux (Institut de Chirurgie, Paris) for providing pig cornea, Christophe Helary (LCMCP) for help with electrophoresis, Bernard Haye (LCMCP) for preparation of some TEM samples, Marie Albéric (MPI of Colloids and Interfaces, department Biomaterials, Potsdam) and Ina Reich (UMR8247, IRCP/C2RMF) for providing the photo of elephant's ivory.

Author contributions

C.S.[1], F.S., E.B., M.L., J.M.C., E.M., E.B., Y.Y., M.R., A.M., M.F. and N.N. performed the work; N.N. and C.S.[1,4] looked for financial support for the project; C.S.[1,], F.S, E.B. M.L. J.M.C., A.M., C.S.[1,4], M.M.G.G., M.F., R.C. and N.N. analysed data; all the authors discussed the results; F.S., M.M.G.G., and M.F. corrected the paper; C.S.[1], M.L., J.M.C., A.M., R.C. and N.N. wrote the paper; A.M., M.F. and R.C. designed and supervised the mechanical, transmittance and optical scattering studies, respectively;. N.N. wrote and supervised the project.

Additional information

The authors declare no conflict of interest. Current address of C.S.[1] : IEM (Institut Européen Des Membranes), UMR 5635 (CNRS-ENSCM-UM), Université Montpellier Place Eugène Bataillon, F-34095 Montpellier, France.

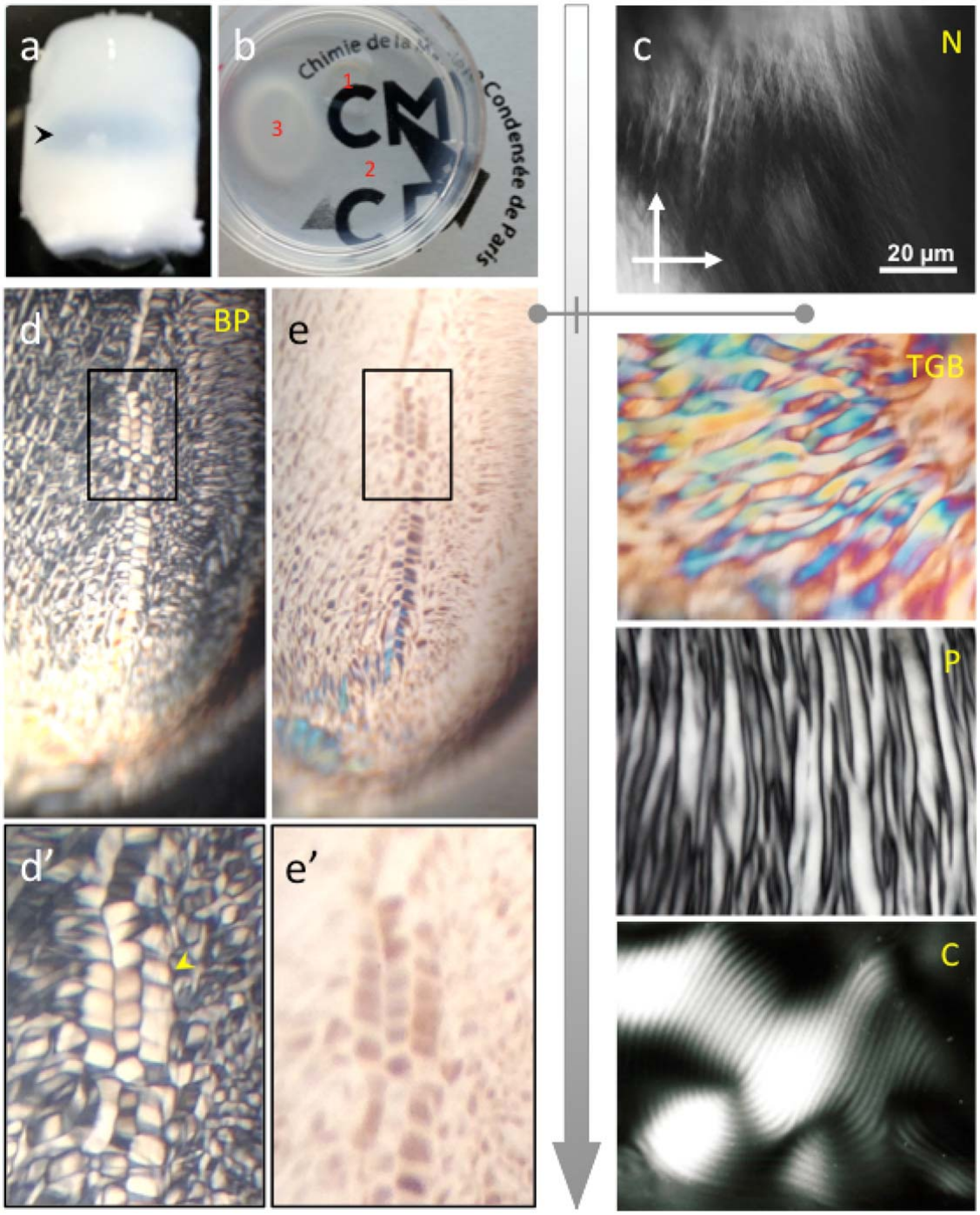

Figure 1 / Optical relationships between collagen fibrillar gradient and LC phase diagram. Images of a fibrillar collagen matrices (a-b). (a) is characterized by a gradient in concentration (20-50-100 mg/mL range) and exhibits a gap of transparency; (b) is fully transparent in a petri dish, the final concentration being about 45 mg/mL. 3 different areas are observed: 1 is completely transparent, 2 is opaque after shearing and area 3 is vacant. (c) Classical collagen phase diagram from nematic (N) to cholesteric (C) observed between crossed polarizers. It is implemented with two LC phases which possess some commonalities

499 with blue and twist grain boundaries (BP and TGB, respectively) phases that are not usually
500 observed with lyotropic molecules as collagen. The concentration is found around 45 mg/mL.
501 For the blue-like phase, the birefringent texture appears as cubic platelets (d and d'). This
502 faceted pattern is still observed without crossed polarizers as shown in e and e'. The
503 precholesteric phase (P) occurs by increasing the collagen concentration in the solution.

504

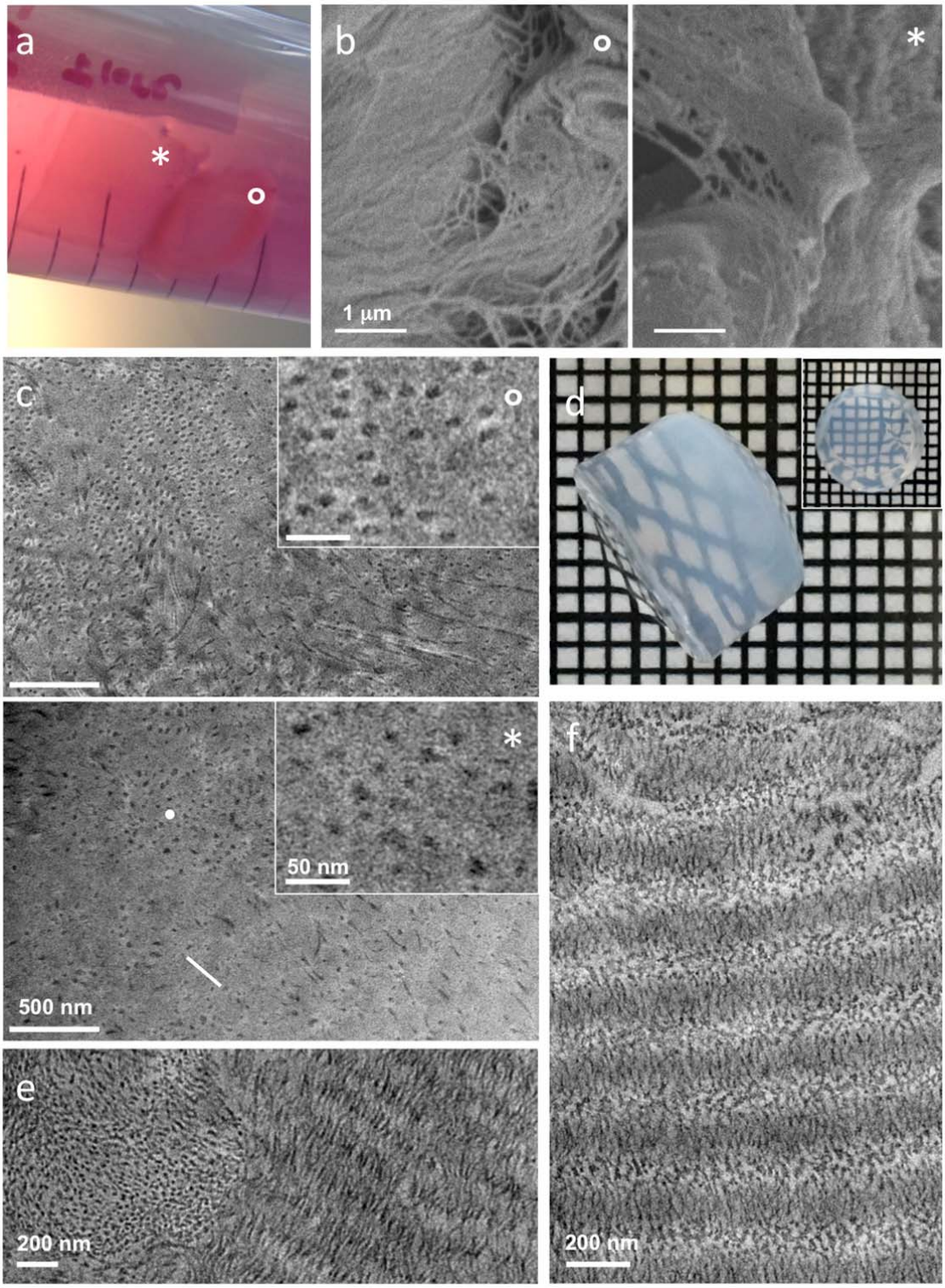

Figure 2 / Ultrastructure investigations of optically transparent collagen-based materials by electron microscopies. (a) The collagen matrix (*) and the cornea (°) stored in Cornea Cold as classical storage medium. Both samples remain transparent when stored in the medium. (b) SEM and (c) TEM images of the biological cornea (b°, c°) and the synthetic transparent collagen matrix (b*, c*). Insets in c are observations at higher magnification. The

fibrils lay parallel (white line) or perpendicular (white dot) to the section cut. (d) thick 3D fibrillar collagen matrix (1 cm in diameter) with a narrow gradient of concentration prepared by using the injection/reverse dialysis process to reach a final concentration around 45 mg/mL over the bulk. An optical gradient of transparency is observed going from opalescent (higher concentration) to transparent (lower concentration) from the curve side but is entirely transparent when observed from the flat end (inset). (e-f) TEM images of the opalescent collagen matrix showing orthogonal arrangements of the fibrils reminding that of the corneal stroma.

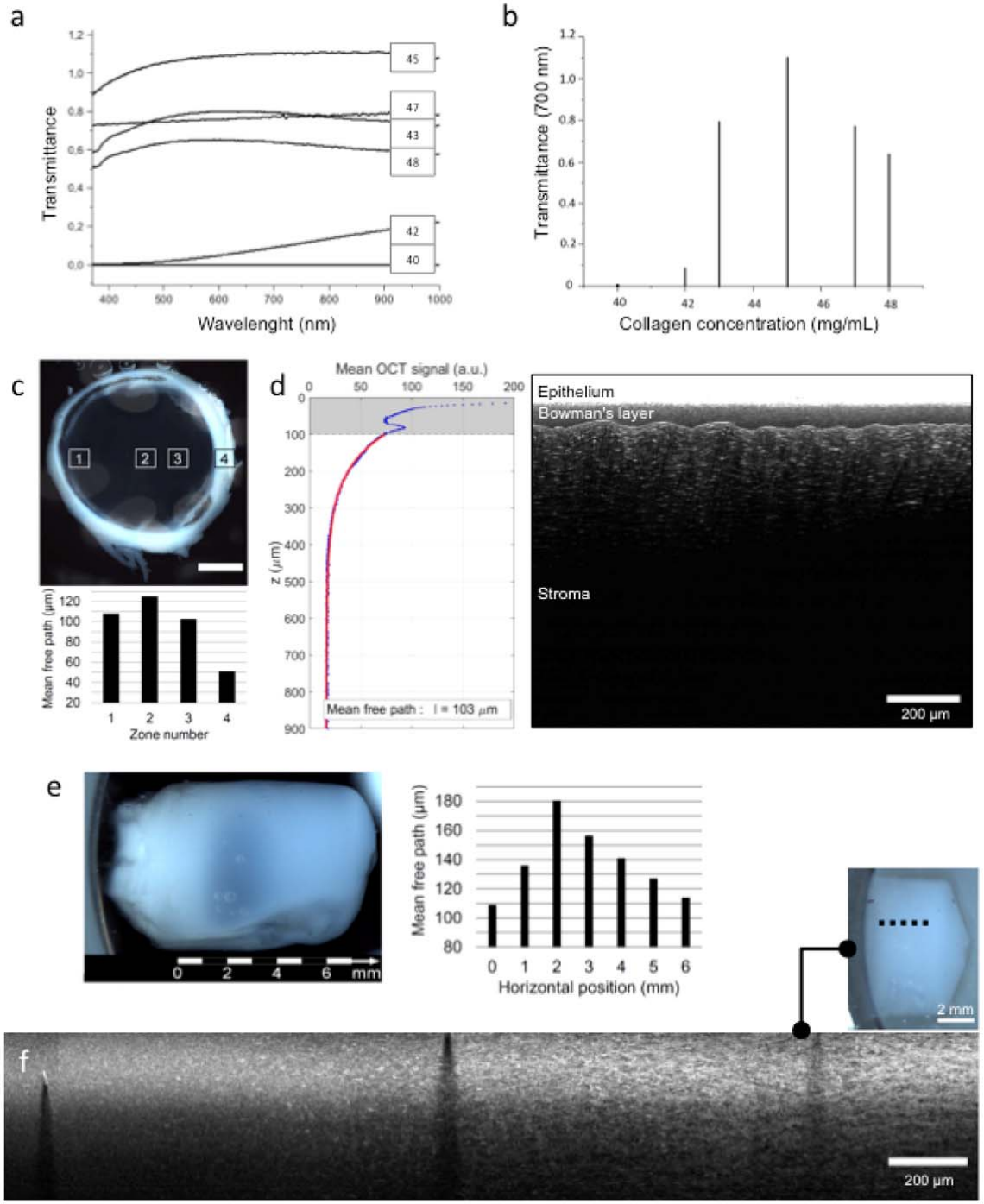

Figure 3 / Transparency of a freshly extracted pig cornea, and of collagen matrices, investigated by transmittance (a-b) and full-field OCT. (a) Transmittance spectra of collagen matrices for visible and near-IR wavelengths are provided for concentrations ranging from 40 to 48 mg/mL. Accordingly, (b) transmittance at 700 nm is shown for the same concentrations; (c) Pig cornea over the black background of the sample holder (top), and bar graph of the measured values of the scattering mean free path ℓ (bottom) in four 1.3x1.3 mm² zones in the stroma (zones 1 to 3) and in the sclera (zone 4). Larger values of ℓ correspond to

an increase in transparency. (d) In-depth OCT cross-section image in zone 3 (right) from which ℓ is extracted by fitting the average OCT signal versus the depth z (left, blue dots) with an exponential decay exp(-z/ℓ) (left, red curve – values in the grey zone are discarded in the fitting procedure). (e) Collagen matrix (characterized by a gradient in concentration (20-50-100 mg/mL range, *see* Fig 1a) over the black background of the sample holder (top), and measured values of ℓ (bottom) in seven 100x100 µm² zones, evenly spaced along a horizontal line, parallel to the collagen concentration gradient in the matrix. The general shape of the bar graph and the maximum value of ℓ measured in the third zone are consistent with the visual observation of maximum transparency in the center of the matrix. (f) Collagen matrix (with a narrow gradient of concentration around 45 mg/mL over the 1 cm bulk, *see* Fig. 2d) over the white background of the sample holder (top), and in-depth OCT cross-section image (bottom) along the collagen concentration gradient (dashed line). The change in the structural appearance of the matrix is clearly visible (from left to right in the OCT cross-section), with an increasing textured aspect.

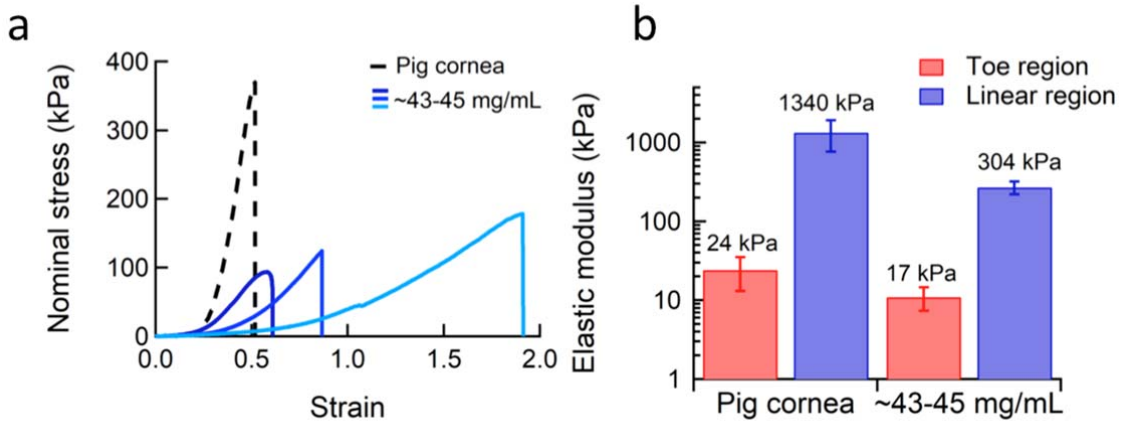

Figure 4 / Mechanical behaviour (tension mode) of transparent collagen matrices and of freshly extracted pig cornea. (a) The three fibrillar collagen gels prepared by injection/reverse dialysis approach at concentrations in the range ~43 to ~45mg/mL exhibit a "J-shaped" stress-strain response, as observed for biological tissues. As a guideline, the mechanical response of the pig cornea is given. No preconditioning was applied, *i.e.* curves correspond to the first loading. Note that the maximal stress value before rupture, usually defined as the Ultimate Tensile Strength (UTS), is only indicative since gel (as cornea) failure systematically occurred in the clamps, suggesting that clamps involve local premature damage. (b) Modulus increasing with extension, elastic moduli are given in the toe and linear region, respectively. Gel rigidities display moduli of same order of magnitude.

Structure-property correlations of stable transparent domain in fibrillar collagen gradient

Chrystelle Salameh[1†], Flore Salviat[1†], Elora Bessot[1], Miléna Lama,[1,3] Jean-Marie Chassot[2], Elodie Moulongui,[1] Yan Wang[1], Marc Robin[1], Alba Marcellan[3], Clément Sanchez[1,4], Marie-Madeleine Giraud-Guille[1], Marco Faustini[1], Rémi Carminati[2] and Nadine Nassif*[1,2]

† These authors contributed equally to this work.

Methods

Sample preparation

Collagen source

To ensure that the resulting transparency does not depend on the biological tissue source, two sources of collagen were investigated: (*i*) Type I collagen extracted from rat tail tendons, (*ii*) Type I collagen diluted in acetic acid 5 mg/mL purchased from Symatèse® (N°Baan : S2132380005). The extraction of type I collagen from rat tail tendons was performed following a classical procedure[1]. Fresh tendons were solubilized in 0.5 M acetic acid (glacial acetic acid Carlo Erba®, Purity >= 99.8%) after washing with a phosphate-buffered saline (PBS) solution. The raw solution was centrifuged and the supernatant was selectively precipitated with 0.7 M NaCl. Precipitated type I collagen was solubilized in 0.5 M acetic acid then desalted by dialysis against 0.5 M acetic acid. The concentration of type I collagen solutions was calculated by hydroxyproline titration[2], and found to be equal to ~2 mg/mL. By this procedure, all organic components and contaminants are removed giving rise to a pure diluted collagen solution.

Cornea source

Three Corneas were freshly removed from 3 months pigs. Under general anaesthesia and sterile conditions, the cornea at its junction with the sclera was cut on 360° and conserved firstly in Balanced Salt Solution (ophthalmic irrigation solution), secondly in Cornea Cold®. Scanning and transmission electron microscopies, mechanical tests and transparency measurements were performed on the extracted corneas.

Collagen gradient matrices synthesis

Evaporation procedure. Collagen matrices were synthesized by slow evaporation under a laminar flow hood. Typically 100 mL of collagen acid solution of a concentration comprised between 2 and 5 mg/ml were placed in a sterile 200 mL crystallizer previously weighed empty. The crystallizer is left open under a laminar flow hood for about 12 hours. Evaporation in a laminar hood allows the slow concentration of collagen to the desired concentration[3] by evaporation of the acetic acid/water present in the solution. This technique allows an accurate

estimation of the concentration during evaporation by simple weighing. The pH was then increased to a range of 9 to 10 by ammonia (Carlo Erba® 28-30%) gas diffusion for 2 days to induce collagen *in vitro* fibrillogenesis and stabilize the liquid crystalline organization into dense fibrillar matrices[4]. The matrices were then washed several times in PBS until neutralization. All the experiments were carried under sterile conditions and at room temperature (19 ± 2°C) in order to prevent collagen denaturation. The samples were then stored at low temperature.

***Injection/reverse dialysis*.** Collagen matrices were synthesized following a one step procedure (Ref. 23 in the main text) that combines injection[5] and reverse dialysis[6]. Collagen samples were cylinder-shaped with a thickness of ~3 mm and width of ~10 mm. A sterile syringe (20 mL) is filled with 15 mL of ~1 mg/mL soluble acidic collagen solution (0.5 mM acetic acid). The dialysis cell and the syringe are connected via a capillary, which will allow gradual injection of collagen. In order to make the system hermetic, a sterile cone is connected at one end to the syringe tip wrapped in Teflon, and at the other end to the capillary. The bottom of the chamber contained a dialysis membrane with a molecular weight cut off of 12-14 kDa. The flux of the collagen solution was controlled (1µL/min-15 mL/min for 8 days) to maintain the same pressure on each side of the dialysis membrane and avoid thus the « inflation » of the membrane. The reverse dialysis process was set against polyethylene glycol (PEG, 35 kDa, Fluka) dissolved in 0.5 M acetic acid up to respectively 20 mg/mL for 24h, 50 mg/mL for 72h, 100 mg/mL for 72h and 150 mg/mL for 36h (see Fig. 1a); the final concentration over the bulk being ~20-50-100 mg/mL. For the thick 3D fibrillar collagen matrix (1 cm in diameter) with a narrow gradient of concentration (final concentration around 45 mg/mL over the bulk) (see Fig. 2d), the reverse dialysis process was set against polyethylene glycol (PEG, 35 kDa, Fluka) dissolved in 0.5 M acetic acid up to respectively 20 mg/mL for 24h, 50 mg/mL for 72h, and 60 mg/mL for 36h. The homogeneity of the solution can be maintained by stirring. The continuous injection of this solution under dialysis allows the concentration of collagen within the matrix. The PEG solution was renewed each 2 days. The form and the size of the matrices depend solely on the mold which constitutes the dialysis cell into which the collagen solution is injected over time. The molds were adapted to the best configuration suitable for the characterization techniques. For instance, 3D thick cylinders were privileged for optical tomography, rectangular molds for the mechanical tests. Similarly to the evaporation dialysis protocol, the fibrillogenesis step is carried out by bringing the collagen matrix into contact with ammonia vapors. The operating conditions described above make it

possible to obtain a thick matrix of 1 cm^3 with a concentration gradient. These matrices were then removed from the dialysis chamber and washed several times in PBS solution to remove all the ammonia residues. They were then treated for characterization. All of the assembly is carried out under a laminar flow hood in order to keep the mixture in sterile conditions. The plugs and clips constituting the dialysis cell are previously sterilized by immersion in a beaker containing 90% ethanol for 30 minutes. The dialysis membranes are cut to approximately 5 cm in length (the optimum size) then rehydrated by immersion in boiling water and finally cooled in sterile water.

Collagen matrices storage and stability

Collagen matrices obtained by both processes (evaporation and injection/dialysis) derived from rat tails as well as clinical grade were stored for several months at 4 ° C in sterile ultrapure water, SBS and Cornea cold®, Eurobio, Les Ulis, France as a preservation medium dedicated to corneas without impairing transparency. The best preservation mediums were found to be SBS and Cornea cold® since the matrices remained without any alteration of transparence for more than a year. A film of salts can form on the surface when the matrices are stored in cold PBS in the case of "clinical grade" collagen, but it is possible to remove it. The precipitation of salts can be avoided and the storage time increased in a Cornea preservation medium (Cornea cold®) always at 4°C.

Sample characterization

For polarized light microscopy (PLM), collagen acid solutions (from rat tails and clinical grade) were left to slowly concentrate under a laminar hood up to ~39 mg/mL then a drop of each solution was placed between glass slides. Observations were made using a transmission Zeiss AxioImager A2 POL and performed on the drop, which slowly evaporate to reach concentrations between 40 and 48 mg/mL. The microscope is equipped with the standard accessories for examination of birefringent samples under polarized light (*i.e.* crossed polars) and an AxioCam CCD camera.

For scanning electron microscopy (SEM) investigations, the cornea as well as the synthetic collagen matrices at 45mg/mL were fixed in 2.5% glutaraldehyde and dehydrated through successive ethanol baths (30%, 50%, 70%, 80%, 90%, 95% and 100%) for the supercritical CO_2 drying process. The supercritical drying process was performed with a BAL-TEC 030.

Samples coated with a 10 nm layer of gold were analyzed with a Hitachi S-3400N SEM at an accelerating voltage of 10 kV.

For transmission electron microscopy (TEM), cornea and synthetic collagen matrices were fixed in 2.5% glutaraldehyde and dehydrated through successive ethanol baths (30%, 50%, 70%, 80%, 90%, 95% and 100%). After washing in a cacodylate/saccharose buffer solution (0.05 M/0.6 M, pH 7.4), the matrices were post-fixed with 2% osmium tetroxyde in the buffer solution for 1 h at 4°C, washed, dehydrated and embedded in araldite. Thin araldite sections (80 nm) were stained with uranyl acetate/lead citrate solutions and analyzed with a FEI TECMAI G2 Spirit Twin electron microscope operating at 120 kV.

Transmittance measurements were conducted by ellipsometry on the synthetic collagen matrices prepared by evaporation at different concentrations, ranging from 40 to 48 mg/mL. Transmission spectra are obtained using an Ellipsometer (Variable angle spectroscopic ellipsometry (VASE) M-2000U Woollam spectroscopic ellipsometer) between 370 and 1000 nm at an angle of incidence of 0°. In order to ensure the planarity of the surfaces, the ~2 mm thick hydrated collagen matrices are placed between two glass slides for microscopy. As reference for the determination of transmission, we use the same configuration but replacing the wet matrices with pure water between the two glass slides.

For mechanical characterization, tests were performed in tensile mode on an Instron tensile testing machine (model 5565) equipped with a 10 N load cell (with a relative accuracy of 0.5% from 0.1% to 100% of the full scale). The samples were placed in a home-made screw side action grip. Nominal strain was obtained from the cross-head displacement and defined as the ratio $(l\text{-}l_0)/l_0$, where l and l_0 are respectively the length during stretching and the initial length. Nominal stress, defined as engineering stress, was calculated from the tensile force and the initial cross section area, with respect to the dimensions of the samples. Samples dimensions were about 6mm x 3.5mm x 2mm. The tests were performed at room temperature at a nominal strain rate of 0.06 s^{-1}. Attention was payed to keep the samples hydrated in order to avoid the denaturation of collagen in the biological and synthetic materials.

For the characterization of the intrinsic degree of transparency, we used a Light-CT Scanner from LLTech SAS, Paris, France, to image the samples and evaluate their scattering mean free path ℓ on different locations. This instrument provides in-depth optical sectioning imaging system based on full-field Optical Coherence Tomography (FF-OCT)[7]. Standard *en face* reflection microscopy images are recorded in planes at different depths inside the material, the light backscattered from regions above and below the selected plane being rejected using an interferometric detection. From a set of images recorded at different depths,

2D or 3D numerical reconstructions are possible, resulting in images such as that in Figure 3d and 3f. The transverse resolution is FF-OCT is diffraction limited as in a usual optical microscope, unless optical aberrations from the sample are too significant. The axial (in depth) resolution depends on the spectral bandwidth of the illumination light[8]. The LLTech Light-CT Scanner, with its 10x NA 0.3 objectives and halogen illumination, achieves 1.5 µm lateral and 1 µm axial resolutions over a 1.3x1.3 mm² field of view. The inspected samples were placed in the cylindrical sample holder of the instrument, immersed in PBS, and covered with an appropriate glass plate. A piston enabled us to push and hold the sample close to or slightly in contact with the plate. For each inspected position of the samples, we performed a depth scan over several hundred micrometers, with a one micrometer step. We then used Fiji[9] and Matlab (The MathWorks, Inc., Natick, Massachusetts, United States) software to select a 100x100 µm² region of interest (ROI indicated in Figure 3c and 3e) and plot the mean FF-OCT signal over this ROI vs. the depth z. The signal was fitted with an exponentially decreasing function of the form $A \exp(-z/\ell) + B$, where A and B are constants needed to adjust the maximum and background signal, respectively. Note that, since the refraction index mismatch between the samples and the reference arm immersion medium (silicone oil, n = 1.41) introduces defocus in depth, blurring images and reducing the signal intensity, we used Light-CT tools to measure the mean refraction indices of the samples (n_s~1.34 to 1.36) and to compensate for defocus all along the axial displacement during the depth scans[10].

References

1. Gobeaux, F. *et al.* Cooperative ordering of collagen triple helices in the dense state. *Langmuir* **23,** 6411–6417 (2007).

2. Bergman, I. & Loxley, R. Two improved and simplified methods for the spectrophotometric determination of hydroxyproline. *Anal. Chem.* **35,** 1961–1965 (1963).

3. Helary, C., Foucault-Bertaud, A., Godeau, G., Coulomb, B. & Guille, M. M. G. Fibroblast populated dense collagen matrices: cell migration, cell density and metalloproteinases expression. *Biomaterials* **26,** 1533–1543 (2005).

4. Besseau, L. & Giraud-Guille, M.-M. Stabilization of fluid cholesteric phases of collagen to ordered gelated matrices. *J. Mol. Biol.* **251,** 197–202 (1995).

5. Mosser, G., Anglo, A., Helary, C., Bouligand, Y. & Giraud-Guille, M.-M. Dense tissue-like collagen matrices formed in cell-free conditions. *Matrix Biol.* **25,** 3–13 (2006).

6. Knight, D. P., Nash, L., Hu, X. W., Haffegee, J. & Ho, M. In vitro formation by reverse dialysis of collagen gels containing highly oriented arrays of fibrils. *J. Biomed. Mater. Res. An Off. J. Soc. Biomater. Japanese Soc. Biomater. Aust. Soc. Biomater.* **41,** 185–191 (1998).

7. Vabre, L., Dubois, A. & Boccara, A. C. Thermal-light full-field optical coherence tomography. *Opt. Lett.* **27,** 530–532 (2002).

8. Dubois, A. *et al.* Ultrahigh-resolution full-field optical coherence tomography. *Appl. Opt.* **43,** 2874–2883 (2004).

9. Schindelin, J. *et al.* Fiji: an open-source platform for biological-image analysis. *Nat. Methods* **9,** 676 (2012).

10. Labiau, S., David, G., Gigan, S. & Boccara, A. C. Defocus test and defocus correction in full-field optical coherence tomography. *Opt. Lett.* **34,** 1576–1578 (2009).

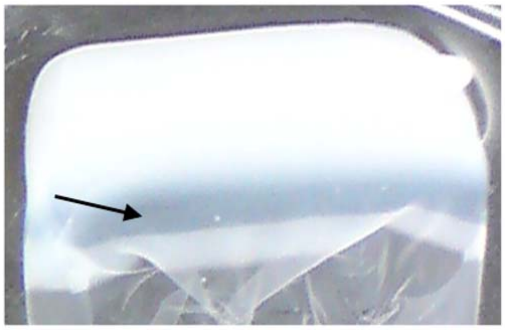

Figure S1/ Matrix with a gradient in collagen concentration synthesized by slow evaporation. From top to down, the collagen concentration is increasing from 10 reaching 100 mg/mL. A gap in transparency (arrow) is observed inside the matrix and found at ~45 mg/mL after hydroxyproline titration.

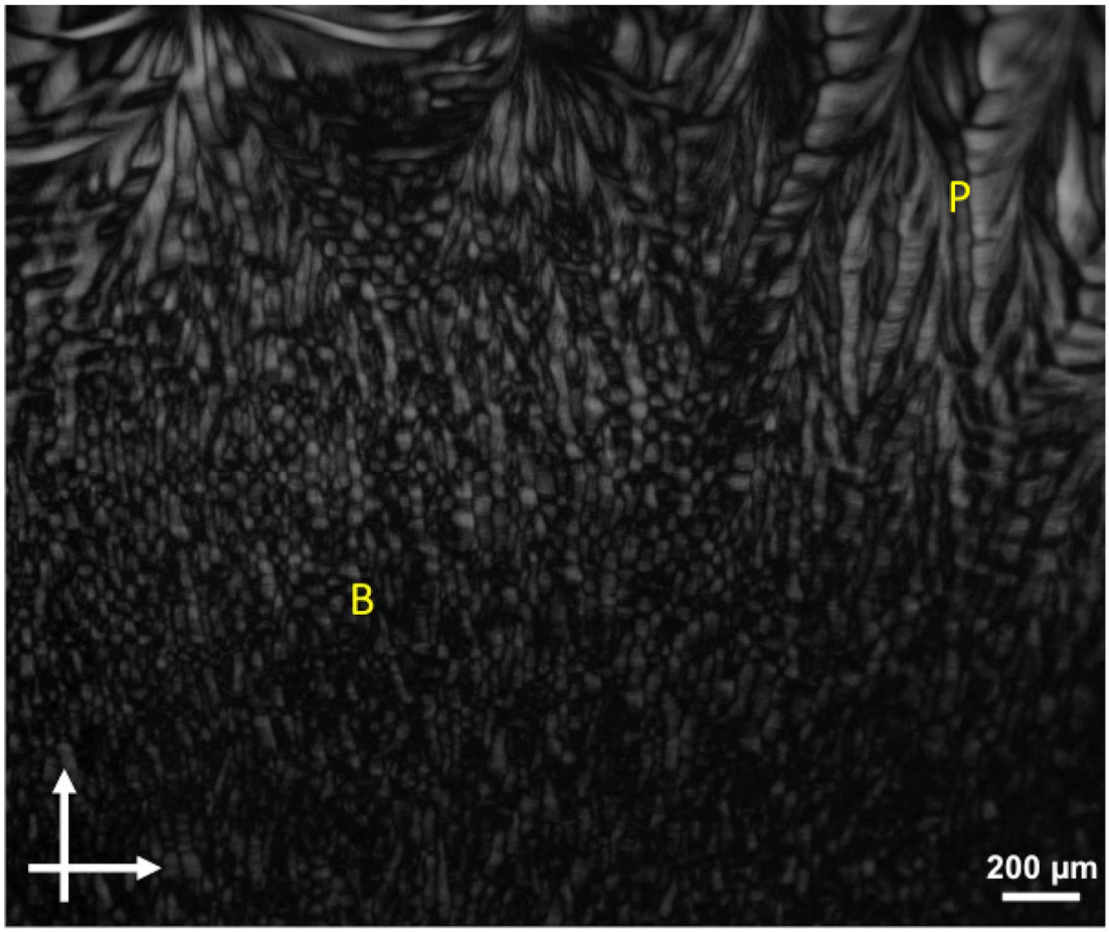

Figure S2/ Polarized light microscopy image of a collagen liquid-crystal solution observed between crossed-polars (90°). The transition between two birefringent textures is observed: the precholesteric banded-pattern (P) and the "staggered dots" reminding of a blue phase (B). The final concentration was determined by hydroxyproline titration and found ~48 mg/mL.

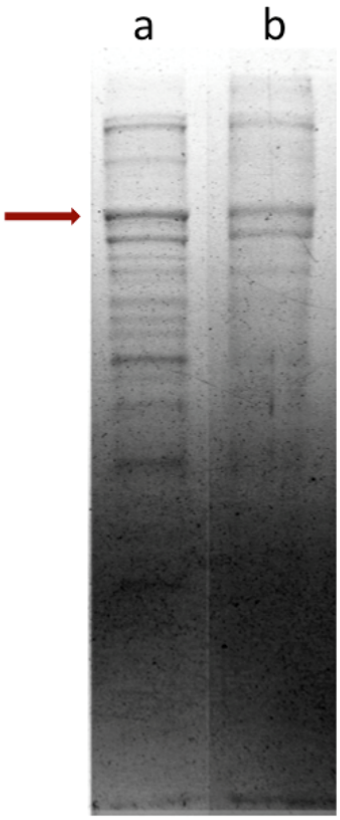

772

773 **Figure S3/ SDS-Polyacrylamide Gel Electrophoresis (SDS□PAGE) of type I Collagen**
774 extracted from (a) rat tails tendons and (b) porcin dermis (commercialized as clinical grade)
775 confirming the higher purity of this latter solution. The arrow shows the band corresponding
776 to the α chain of type I collagen (125.10^3 KDa).

777

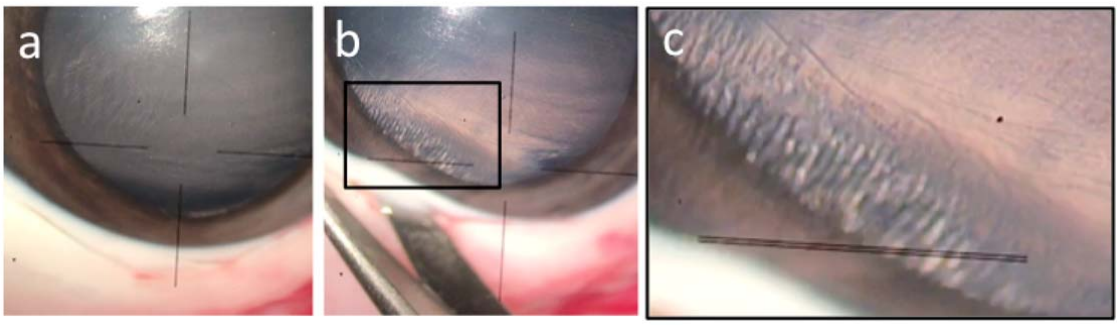

Figure S4/ Observations of pig cornea by light microscopy. (a) Freshly extracted cornea, (b) a birefringence texture is observed under mechanical constraint without the use of polarizers, (c) which appears layered at higher magnification.

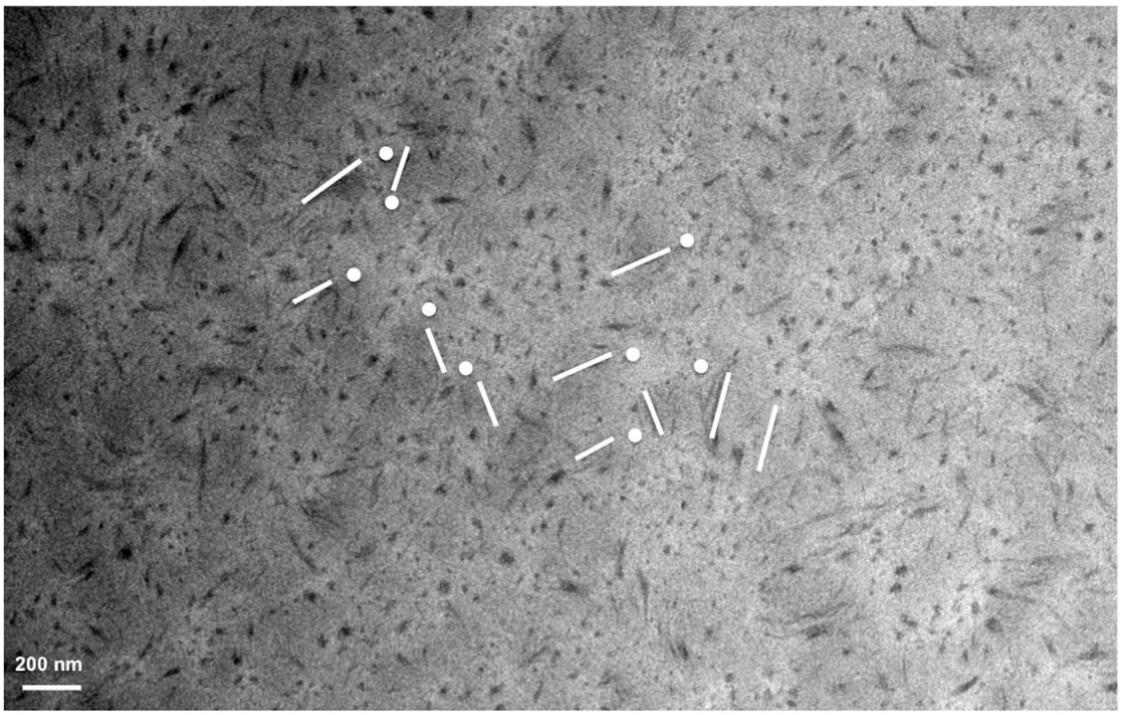

Figure S5/ TEM micrograph of a transparent collagen matrix (~45 mg/mL). Collagen fibrils are monodisperse in diameter (~25-30 nm). They appear aligned parallel or perpendicular to the section plane, as respectively underlined by lines and dots.

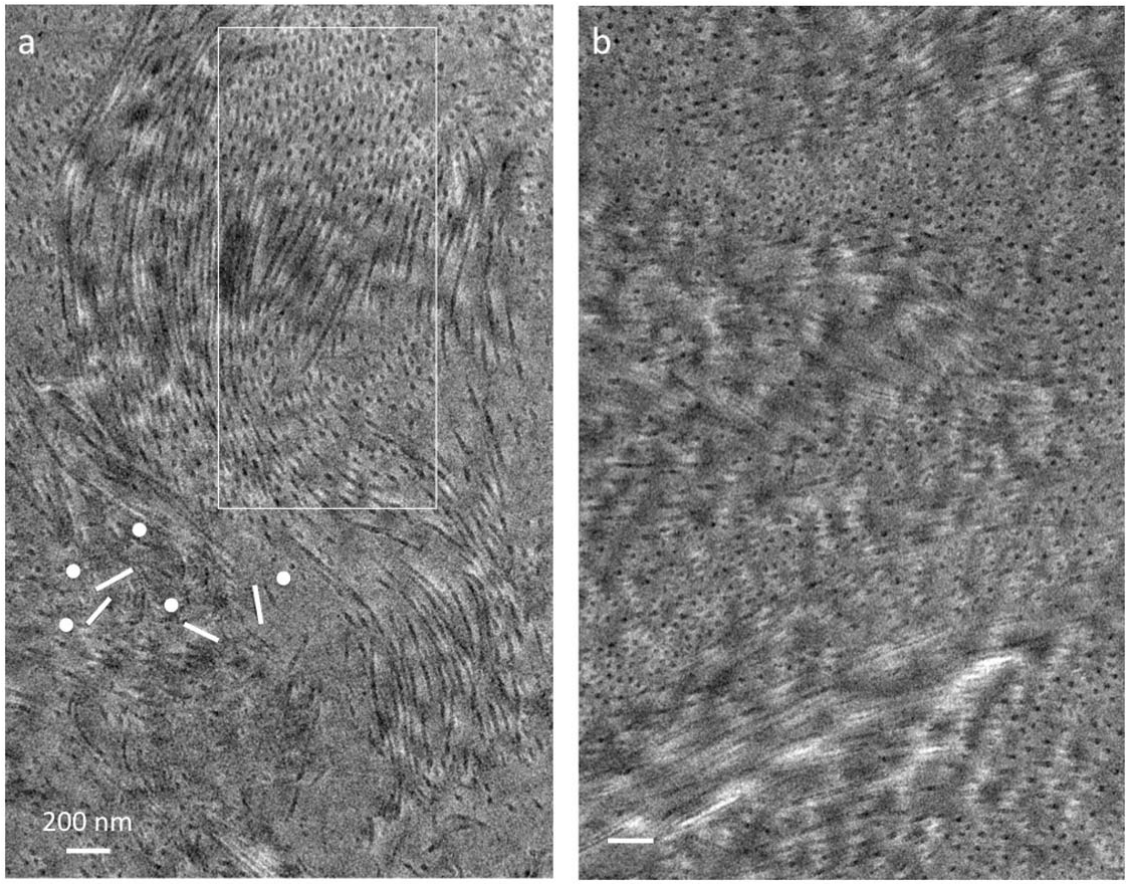

Figure S6/ TEM micrographs of corneal stroma (pig). Different sections orientations are shown (a-b). Fibrils are aligned parallel or perpendicular to the section plane, as respectively underlined by lines and dots in (a). The rectangular underlines a unusual illustration of the fibrils. (b) Transverse section performed on the orthogonal plywood showing the typical feature of the corneal architecture.

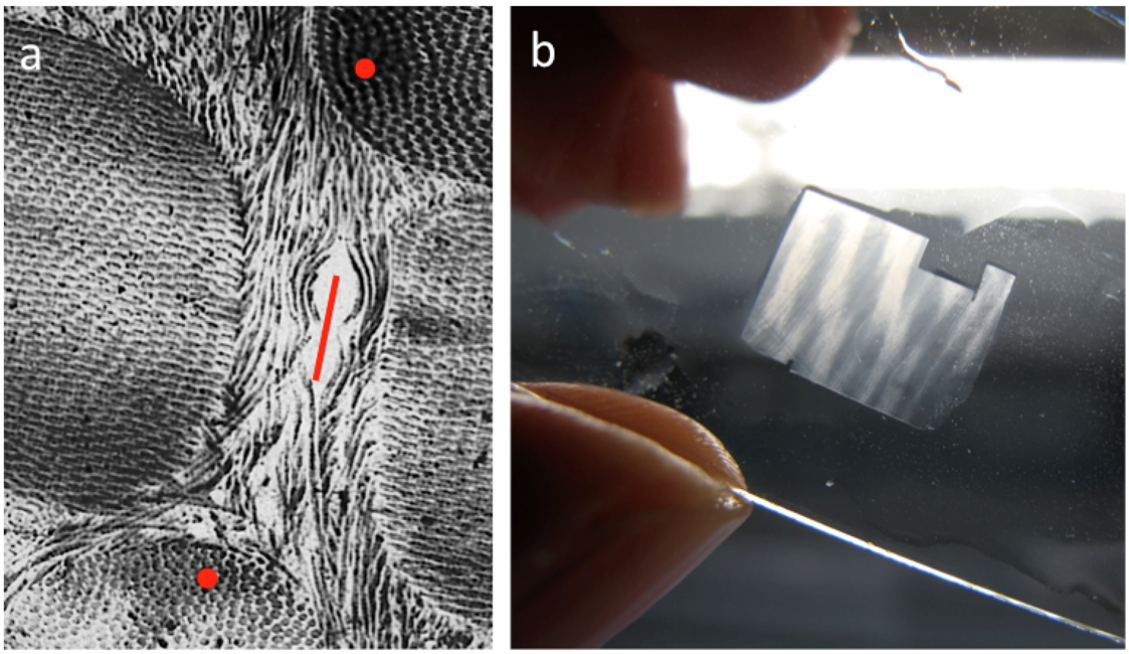

Figure S7/ Illustrations of transparent biological materials. a) TEM micrograph of a Fish scale showing that bundles of fibrils are aligned parallel or perpendicular to the fracture plane, as respectively underlined by red the line and dots; b) image of demineralized ivory revealing layered transparent/opalescent domains.

SI video 1/ showing a transparent gel at ~45 mg/mL which remains transparent upon mechanical handling. It is tough and easy to handle.

Figure S8/ Image of a transparent matrix synthesized by evaporation. When handling, its qualitative behaviour was very different although the concentration was slightly below 45 mg/mL. The gel exhibits extreme softness and weakness that preclude performing tensile mechanical characterization.

Miléna LAMA – Thèse de doctorat - 2019

Titre de la thèse

« Relation structure-propriétés de gels denses de collagène produits par injection de collagène séché par atomisation »

Résumé

Injecter des gels denses de collagène pour obtenir des matériaux 3D, biomimétiques en termes d'architecture et de propriétés mécaniques, est un enjeu pour la régénération tissulaire car cela pourrait éviter des chirurgies lourdes. Des solutions de collagène très concentrées ont la capacité de former des mésophases dont la géométrie mime celle des tissus biologiques. Ainsi, il est possible d'obtenir des gels de collagène en 3D possédant une meilleure tenue mécanique, sans utiliser de réticulant chimique qui peut induire des inflammations. Cependant, l'injection de solutions de collagène très concentrées est empêchée par l'augmentation drastique de leur viscosité.

Comment associer biomimétisme et injectabilité de gels denses de collagène ?

Nous proposons de concentrer des solutions acides de collagène par atomisation, produisant des billes denses de collagène. Une simple pesée de ces billes permet de déterminer la concentration des gels. Mélangées à un solvant aqueux, elles sont injectées dans un moule imitant un défaut tissulaire. La fibrillogénèse, induite *in vitro* dans les solutions de collagène, forme des gels rigides. Les microscopies optique et électroniques révèlent des organisations issues de l'auto-assemblage du collagène à l'échelle macroscopique, selon la concentration en collagène (de 3wt% à 8wt%). Le comportement mécanique des gels imite celui des tissus biologiques, et est fortement lié à l'ultrastructure des fibrilles de collagène. Cette étude ouvre des perspectives dans le domaine de la régénération tissulaire en dessinant le cadre d'une librairie tissulaire, contenant des matériaux en collagène biomimétiques, injectables et denses, permettant l'usage de procédures chirurgicales moins invasives.

Mots-clefs : Collagène dense ; biomimétisme ; auto-assemblage ; comportement mécanique ; séchage par atomisation ; biomatériau injectable

Abstract

Injection of dense collagen to obtain 3D biomimetic scaffolds in terms of structure and mechanical properties is challenging for regenerative medicine since it would avoid open-surgery. It is well-known that highly concentrated collagen solutions can form liquid crystal mesophases with tissue-like geometries. Thus, it is possible to obtain 3D collagen gels *in vitro* with better mechanical properties, without widely used chemical crosslinkers that may lead to inflammatory responses. Nevertheless, the injection of highly concentrated collagen solutions is unlikely due to their high viscosity.

How to combine biomimetism and injectability of dense collagen gels?

To achieve this goal we concentrate acidic collagen solutions by spray-drying, forming dense collagen beads. A simple weighing of the beads determines the concentration of the gels. Mixed with an aqueous solvent, the beads are injected into a mold mimicking a tissue defect. The fibrillogenesis *in vitro* is induced within the collagen solutions that transform into stiff gels. Electron and polarized light microscopies show organizations resulting from collagen self-assembly at macroscopic length scale depending on the collagen concentration *i.e.* from 3wt% to 8wt%. Mechanical tests results reveal tissue-like properties strongly linked to collagen fibrils ultrastructure. This study opens perspectives in tissue repair in setting the framework of a library made of biomimetic (anisotropic, dense and stiff) and injectable collagen gels, enabling minimally invasive procedures.

Keywords: Dense collagen; biomimetism; self-assembly; mechanical behavior; spray-drying; injectable biomaterial